Volume 129, Nos. 1—6

November—December, 1959

PROCEEDINGS OF THE ACADEMY OF SCIENCES

OF THE USSR

(DOKLADY AKADEMII NAUK SSSR)

Physical Chemistry Section

A publication of the Academy of Sciences of the USSR

IN ENGLISH TRANSLATION

Year and issue of first translation:
Vol. 112, Nos. 1-6 Jan.-Feb. 1957

Annual subscription	*$160.00*
Single issue	*35.00*

Copyright 1960
CONSULTANTS BUREAU ENTERPRISES, INC.
227 West 17th Street, New York, N. Y.

A complete copy of ***any*** *paper in this issue may be purchased from the publisher for $5.00*

Note: The sale of photostatic copies of any portion of this copyright translation is expressly prohibited by the copyright owners.

Printed in the United States of America

PROCEEDINGS OF THE ACADEMY OF SCIENCES OF THE USSR

Physical Chemistry Section

Volume 129, Numbers 1-6 November-December, 1959

CONTENTS

	PAGE	RUSS. ISSUE	RUSS. PAGE
The Influence of the Degree of Modification of a Silica Surface by Trimethylchlorosilane on the Adsorption Properties of the Surface. I. Yu. Babkin, V. S. Vasil'eva, I. V. Drogaleva, A. V. Kiselev, A. Ya. Korolev and K. D. Shcherbakova	893	1	131
The Study of the Bi_2Te_3 – Bi_2S_3 System. M. L. Beglaryan and N. Kh. Abrikosov.	897	1	135
Vacuum Gas Chromatography. D. A. Vyakhirev and P. F. Komissarov	901	1	138
The Mechanism of the Oxidation of Propylene to Acrolein on a Cuprous Oxide Catalyst. O. V. Isaev, L. Ya. Margolis and I. S. Sazonov	905	1	141
The Electron Paramagnetic Resonance Spectra of Certain Catalysts and Catalyst –Hydrocarbon Systems, and the Action of γ -Radiation on These. Yu. A. Kolbanovskii, I. M. Kustanovich, L. S. Polak and A. S. Shcherbakova	909	1	145
The Adhesion Between Polymers and Modified Glass Surfaces in Relation to the Charge-Reversal Phenomena Observed on Separation. N. A. Krotova, L. P. Morozova, and B. V. Deryagin.	913	1	149
The Theory of Stationary Combustion in Powders. A. G. Merzhanov and F. I. Dubovitskii.	917	1	153
The Theory of Low-Pressure Decomposition of Nitrous Oxide. E. E. Nikitin.	921	1	157
The Effect of Ultrasonic Vibrations on the Absorption of Carbon Dioxide by Water. V. Yu. Orlov and N. M. Zhavoronkov	925	1	161
Determination of "Unperturbed" Macromolecular Dimensions in Good Solvents. O. B. Ptitsyn	929	1	165
The Effects of Temperature and Laminary Velocity on the Rate of Turbulent Combustion. A. S. Sokolik and V. P. Karpov	933	1	168
The Effects of the Degree of Degassing on the Electron Work Function in Nickel. N. A. Shurmovskaya and R. Kh. Burshtein	937	1	172
The Energy of Adsorption of Hydrocarbons on Chemically Modified Silica. I. Yu. Babkin and A. V. Kiselev	939	2	357
An Electron Paramagnetic Resonance (Radiospectroscopic) Study of the Vulcanization of Rubber. G. A. Blokh	943	2	361
The Effect of Preliminary Irradiation on the Rate of Thermal Decomposition of Silver Oxalate Containing Cadmium. V. V. Boldyrev, Yu. A. Zakharov, V. I. Eroshkin and M. G. Sokolova	947	2	365
A Study of the Thermodynamic Properties of Solid Solutions in the Nickel–Chromium System. E. Z. Vintaikin	951	2	368

CONTENTS (continued)

	PAGE	RUSS. ISSUE	RUSS. PAGE
The Effect of the Surface Charge of Zinc Oxide on the Rate of Chemisorption of Oxygen. É. Kh. Enikeev, L. Ya. Margolis and S. Z. Roginskii	955	2	372
A New Type of Current Discontinuity in the Reduction of the BrO_3^- Anion at the Dropping Electrode. V. I. Zykov	959	2	376
A Determination of the Phase Diagrams of the Naphthalene – β-Cl-Naphthalene and 1, 8-Dinitronaphthalene – 1,5-Dinitronaphthalene Systems by the Method of Monocrystal Growth. A.I. Kitaigorodskii and R. M. Myasnikova	963	2	380
Kinetic Studies of Sorbent Structures: The Permeability of Active Charcoals with Partially Blocked Pores. D. P. Timofeev and I. T. Erashko	967	2	384
The Effect of Aging on the Structure, Elastic Recoil, Shear Strength, and Relaxation Time of Aluminum Naphthanate Gels. A. A. Trapeznikov	971	2	387
The Effect of γ-Irradiation on the Rate of Hydrogen Exchange between Water and Isoamylthiol. K. I. Sakodynskii and N. M. Zhavoronkov	975	2	391
The Temperature Dependence of the Radiational Oxidation of n-Heptane and n-Nonane. N. A. Bakh and T'ung T'ien-chen	979	3	604
The Relation between the Kinetic and Thermodynamic Isotopic Effects and the Molecularity of a Reaction. G. K. Boreskov	983	3	607
Kinetic Equations for the Polarography of Melts. Yu. K. Delimarskii and A. V. Gorodyskii	987	3	610
An Investigation of the Electrochemical Properties and Molecular form of the Copolymers of Ethylenesulfonic and Acrylic Acids. V. A. Kargin, S. Ya. Mirlina and A. D. Antipina	991	3	614
An Electronographic Study of Passive Films on Zinc. A. I. Levin, M. E. Prostakov and G. D. Susloparov	995	3	617
The Equation of the Phase Transition Curve. G. A. Martynov	999	3	620
The Electrode Processes on Germanium in Sulfuric Acid Solutions of Oxidizing Agents. E. N. Paleolog, A. Z. Fedotova and N. D. Tomashov	1003	3	623
The Problem of Evaluating the Reactivity of Explosives. A. I. Serbinov	1007	3	627
A Study of Graft Polymerization in Irradiated Teflon. Z. A. Sinitsyna, Yu. D. Tsvetkov, Kh. S. Bagdasar'yan and V. V. Voevodskii	1013	3	631
The Relation between the Kinetic Constants and the Rate of Flameless Combustion of Smokeless Powder. A. F. Belyaev	1017	3	635
The Mechanism of Hydrogen Peroxide Formation in the Corrosion of Metals. T. M. Abramova, I. L. Gankina, and A.S. Fomenko	1021	4	820
The Transport of Dispersed Particles in a Gaseous Stream During the Combustion of Powders. N. N. Bakhman	1025	4	824
Rectification at the Electrolyte–N-Type Semiconductor Contact. Yu. A. Vdovich, B. M. Grafov, and V. A. Myamlin	1029	4	827

CONTENTS (continued)

	PAGE	RUSS. ISSUE	RUSS. PAGE
The Formation of Porous Structure in Silica Gel in the Presence of Volatile Compounds. Z. Z. Vysotskii and M. V. Polyakov	1035	4	831
A Kinetic, an Adsorption, and an X-Ray Crystallographic Study of the Decomposition of Magnesium Carbonate. V. A. Gordeeva, G. M. Zhabrova and M. Ya. Kushnerev.	1039	4	835
Solid Solutions in the AlSb–InSb System. N. A. Goryunova and B. V. Baranov.	1043	4	839
The Electroplating of Copper and Cadmium on Solid Electrodes Using High Current Densities. G. A. Emel'yanenko and E. Ya. Baibarova	1045	4	841
Transition Temperatures in Synthetic Polymers with Rigid Chains. P. V. Kozlov, A. Endrykhovskaya, and V. A. Kargin	1049	4	844
A Mechanism for the Reduced Hydration Rate of Calcium Oxide Treated with Surface-Active Plasticizers. S. I. Kontorovich, E. E. Segalova, and P. A. Rebinder.	1053	4	847
Multiple Phase Inversion in Emulsions. L. Ya. Kremnev and L. A. Borodina.	1057	4	851
A Thermodynamic Study of the KBr–RbBr – H_2O System at 25°. L. L. Makarov and G. S. Popov	1061	4	854
A Comparative Study of Induced Conductivity and Free Radicals in the Radiolysis of Solid Paraffin. V. L. Tal'roze and E. L. Frankevich	1065	4	858
The Isotherm for the Adsorption of the Tetrabutylammonia Cation on Mercury. A. N. Frumkin and B. B. Damaskin	1069	4	862
The $I^{1/2}$ - Rules for the Action of Radiation on Solutions. B. V. Ershler	1073	4	866
A Mass-Spectrometric Determination of the Heat of Sublimation of Boron. P. A. Akishin, O. T. Nikitin, and L. N. Gorokhov	1077	5	1075
Limiting Cases of Combustion in Mixed Systems. N. N. Bakhman	1081	5	1079
A Study of the Electron Paramagnetic Resonance Spectra of the Negative Ions of Certain Aromatic and Heterocyclic Compounds. V. V. Voevodskii, S. P. Solodovnikov, and V. M. Chibrikin	1083	5	1082
An Infrared Absorption Study of the Complexes of Acetylene and Its Derivatives. E. A. Gastilovich, D. N. Shigorin, E. P. Gracheva, and M. F. Shostakovskii	1087	5	1085
A Universal Scale for the Effect of Solvents on the Electronic Spectra of Organic Compounds. I. A. Zhmyreva, V. V. Zelenskii, V. P. Kolobkov, and N. D. Krasnitskaya	1091	5	1089
The Solubility of Grafted Copolymers Derived from Polystyrene and Acrylic Acid. M. M. Iovleva, P. V. Kozlov, and V. A. Kargin	1095	5	1093
A Steady-State Theory for the Thermal Equilibrium in the Condensed Phases of Powders and Explosives. B. I. Plyukhin	1099	5	1096
The Effects of Inert Solvents on the Physicochemical Process in Solutions. E. S. Rudakov.	1105	5	1100

CONTENTS (continued)

	PAGE	RUSS. ISSUE	RUSS. PAGE
Electron Diffraction Study of the Structure of the Boron Sulfide Molecule. P. A. Akishin and V. P. Spiridonov	1109	6	1317
A Study of Electrode Processes on an Indium Amalgam Using Radioactive Tracers. G. M. Budov and V. V. Losev	1113	6	1321
The Dielectric Permeability and Dipole Moments of Certain Organosilicon Compounds. A. A. Gundyrev, N. S. Nametkin, G. M. Panchenkov and A. V. Topchiev	1119	6	1325
The Role of Diffusion in Electrokinetic Phenomena. The Diffusion Theory of the Dorn Effect (The Potential of Moving Particles). B.V.Deryagin, and S. S. Dukhin	1123	6	1328
The Viscosity of Certain Binary Hydrocarbon Mixtures and Gas Condensates in the Supercritical Range. S. L. Zaks and V. I. Sergeevich	1129	6	1332
A Study of the Oxidation Mechanism of Some Inorganic Substances by Persulfate. V. A. Lunenok-Burmakina and A. I. Brodskii	1133	6	1335
The Single Electrochemical Bond in Solid Electrolyte. S. F. Pal'guev, S. V. Karpachev, and L. D. Yushina	1137	6	1339
The Characteristic Features of Crystallization Structure Formation During the Hydration Hardening of Calcium Oxide. E. E. Segalova, S. I. Kontorovich and P. A. Rebinder	1141	6	1343
Double Bonds in Polyethylene Irradiated with Fast Electrons. N. A. Slovokhotova, A. T. Koritskii and N. Ya. Buben	1145	6	1347
The Reaction Capacity of the Anions of Certain Carboxylic Acids in the Acid-Catalyzed Enolization of Acetone. A. I. Tal'vik and V.A. Pal'm	1147	6	1349
The Electromagnetic Properties and Structural Diagram of the $FeO-SiO_2-ZnO$ System. D. M. Chizhikov, V. P. Schastlivyi, and L. I. Blokhina	1153	6	1353
Author Index, Vols. 124-129, 1959	1159		
Tables of Contents, Vols. 124-129, 1959	1162		
Erratum	1181		

THE INFLUENCE OF THE DEGREE OF MODIFICATION OF A SILICA SURFACE BY TRIMETHYLCHLOROSILANE ON THE ADSORPTION PROPERTIES OF THE SURFACE

I. Yu. Babkin, V. S. Vasil'eva, I. V. Drogaleva, A. V. Kiselev, A. Ya. Korolev and K. D. Shcherbakova*

(M. V. Lomonosov State University, Moscow; All-Union Scientific Research Institute for Aviation Materials)

(Presented by Academician M. M. Dubinin, June 13, 1959).

The nature of the surface and its chemical modification have a considerable influence, not only on the behavior of highly dispersed solids, such as adsorbents and catalysts, but also on the properties of filling materials based on polymers. We have shown [1-6] that the modification of highly dispersed materials ("blacks", silica) by surface chemical reactions permits control of the nature of the surface and of its physical and chemical properties over wide limits.** Such modification, for example, can alter the adsorption of vapor, for example, water vapor on silica*** and "blacks", by factors of from ten to several hundred.

The present work is devoted to a study of the influence of the degree of modification of the surface of highly dispersed, nonporous specimens of silica (aerosil), by reaction with trimethylchlorosilane, on the adsorption properties of the silica. The surface of the original aerosil was not completely hydrated, so that the reaction with trimethylchlorosilane led only to partial modification, since the dehydrated part of the surface did not react. The dehydrated part of the surface is hydrophobic [4, 8], and the modified part, which is covered with $Si(CH_3)_3$ groups, is also hydrophobic, so that the original specimen after modification adsorbs water vapor only very weakly [1]. The aim of the present work was to reduce the adsorption of the vapor of other substances, in particular saturated hydrocarbons, whose behavior at a silica surface is only very slightly affected by dehydration [4, 9]. This made it necessary to increase the degree of covering of the surface by the $Si(CH_3)_3$ groups to such an extent that the part remaining uncovered might be inaccessible to the molecules of organic substances. Since an increase in the degree of covering by $Si(CH_3)_3$ groups could only be expected for a more extensively hydrated surface, we subjected the original aerosil to a hydrothermal treatment before the treatment with trimethylchlorosilane. The present work therefore describes the study of the following four silica specimens: 1) the original aerosil [1] – specimen A1, 2) the original aerosil modified in trimethylchlorosilane vapor [1] – specimen A1M, 3) the aerosil hydrated in an autoclave – specimen A1H, and 4) the aerosil hydrated in an autoclave and then modified in trimethylchlorosilane vapor – specimen A1HM.

The quantity of trimethylsilyl groups linked to the silica surface was determined from the increase in weight of the specimen and by microanalysis.

The specific surface of the specimens s, the analysis data, the average trimethylsilyl group concentrations $\alpha_{Si(CH_3)_3}$, and the average degree of covering of the surface by these groups θ $Si(CH_3)_3$ are shown in Table 1.

---

*L. I. Doroshina, M. G. Kuz'mina, G. M. Lyulina and L. F. Pavlova took part in the work.

**See references cited in [1] for details.

***The influence of the hydrophobic properties of aerosil on the adsorption of water is dealt with in [7].

The value of θ $Si(CH_3)_3$ was determined using the fact that the Van der Waal's dimensions of this group correspond to an area $\omega^0 Si(CH_3)_3 = 42$ Å^2 or concentration $\alpha m Si(CH_3)_3 = 2.3_5$ $Si(CH_3)_3$ groups per 100 Å^2. In actual fact, these groups, as a result of the complex relief of the aerosil surface, are not arranged in such regular fashion, so that the possible limiting $Si(CH_3)_3$ group concentration on the aerosil surface for the most favorable distribution may differ slightly from the indicated value of $\alpha m Si(CH_3)_3 = 2.3_5$ groups per 100 Å^2. For an approximate estimate of the average degree of covering of the aerosil surface by $Si(CH_3)_3$ groups, however, we may accept this value of the limiting concentration. From this, θ $Si(CH_3)_3 = \alpha Si(CH_3)_3 / 2.3_5$. The $Si(CH_3)_3$ groups, as a result of their large size, can screen part of the hydroxyl groups on the silica surface. It should also be noted that the reaction with $ClSi(CH_3)_3$, even for a fully hydrated silica surface, cannot lead to an absolutely compact arrangement of these groups, since in the chemisorption processes there are usually formed small "gaps" between the attached molecules of adsorbed material, and new molecules of such large size cannot enter these gaps. This leads to a mosaic-like structure for the chemically modified surface, and allows molecules of smaller size to penetrate into the gaps.

TABLE 1

Specific Surface, Microanalysis Results and Degree of Covering of the Surface with $Si(CH_3)_3$ Groups

Silica specimens		Specific surface s, m^2/g	Carbon content, %	Quantity of chemisorbed $Si(CH_3)_3$ groups per 100 A	Average degree of covering of surface θ $Si(CH_3)_3$
symbol	characteristics				
A1	Original	170	0	0	0
A1M	Treated in trimethylchlorosilane vapor	170	1,28 } 1,28 1,29 }	1,38	~0,58
A1H	Hydrated at 350° for 19.5 hours	50*	0	0	0
A1HM	Hydrated at 350° for 19.5 hours and then treated with trimethylchlorosilane vapor	50	0,61 } 0,65 0,70 }	2,21	~0,93

*Prolonged or severe hydrothermal treatment leads to a reduction in the surface of silica and alumina – silica specimens.

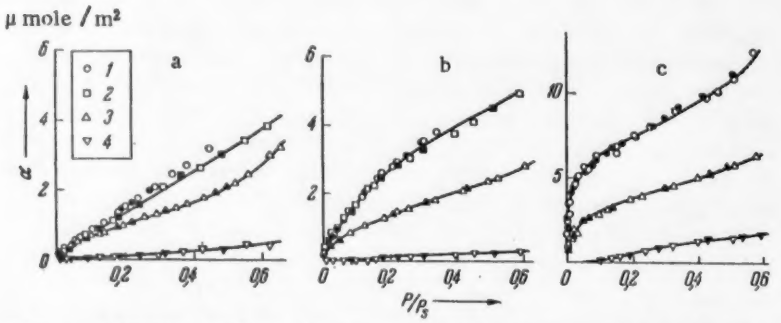

Fig. 1. Adsorption isotherms for the vapor of (a) n-hexane, (b) benzene and (c) methanol on aerosil specimens: 1) original A1, 2) hydrated A1H, 3) modified A1M and 4) modified after hydration A1HM.

We have studied the adsorption isotherms for hexane, benzene, methanol and water vapor, for all four silica specimens. Before the experiments the specimens were degassed in a vacuum adsorption apparatus at 150°.

Figure 1 gives the adsorption isotherms obtained for n-hexane, benzene, and methanol vapor. Modification leads to a decrease in the adsorption of all three substances. In the case of hexane (Fig. 1, a), the change from the hydrated surface to the surface modified to an extent of approximately 58% at first brings about only a slight

decrease in the adsorption. In the range of relative vapor pressure p/p_s from 0 to 0.1, the adsorption isotherm for the modified original material A1M is practically identical with that of the original and hydrated specimens A1 and A1H. This is probably related to the fact that in the case of the A1 specimen, the hexane is adsorbed predominantly in the dehydrated parts of the surface not covered by $Si(CH_3)_3$ groups (the behavior of hexane is little affected by decrease in the concentration of hydroxyl groups on the adsorbent surface [4-9]). On a surface modified to the much greater extent of 93%, however, the adsorption of hexane is considerably reduced (by a factor of 15 at $p/p_s = 0.1$). The surface of the A1HM specimen modified to an extent of approximately 93% is evidently covered by $Si(CH_3)_3$ groups in such a compact fashion that the free "gaps" on the surface are inaccessible to the large hexane molecules. The trimethylsilyl groups separating the adsorbing surface from the silica skeleton of the aerosil weaken the dispersion interaction with the surface, which leads to a considerable decrease in the adsorption of hexane on the aerosil which is modified to an extent of 93%, by comparison with the original and hydrated specimens and the specimens modified to an extent of only 58%.

The adsorption of benzene is even more sensitive to change in the extent to which the surface is covered with $Si(CH_3)_3$ groups. Figure 1, b shows that the adsorption at $p/p_s = 0.1$ on the A1M aerosil modified to an extent of approximately 58% is less than that on the original (A1) and hydrated (A1H) aerosil by a factor of 1.8, whereas on the A1HM specimen for which the degree of covering is approximately 93% the adsorption at $p/p_s = 0.1$ is smaller than in the hydrated specimen by a factor of 65.This sharp decrease in the adsorption of benzene results not only from the weakening of the dispersion interaction, but also to a considerable extent from the weakening of the electrostatic interaction of its molecules with the hydroxyl groups of the surface [4, 11]. This electrostatic interaction is extremely sensitive to the removal of the hydroxyl groups from the aerosil surface when they are replaced by nonpolar groups. In the case of a surface modified to an extent of approximately 58%, part of the de hydrated silica surface remains accessible to the benzene molecules, and the dispersion interaction is similar to that for the hydrated surface, as in the case of the adsorption of hexane. In this case the adsorption of benzene is decreased for the most part as a result of the weakening of the electrostatic interaction with the hydroxyl groups, which are replaced or screened by $Si(CH_3)_3$ groups. In the case of the A1HM aerosil modified to an extent of 93%, however, the layer of $Si(CH_3)_3$ groups on the surface is much more compact. Thus, whereas the A1M aerosil modified to an extent of 58% still has dehydrated regions on the silica surface between the $Si(CH_3)_3$ groups, so that the large benzene molecules can arrange themselves in these gaps, the A1HM aerosil has no such gaps. The benzene is adsorbed on this surface only on the layer of $Si(CH_3)_3$ groups and the dispersion interaction is weakened considerably. The extremely weak interaction between adsorbent and adsorbed material in this case is shown by the concave shape of the benzene adsorption isotherm.

Comparison of the methanol adsorption isotherms (Figure 1, c) showed that on going from the hydrated surface to the surface covered with $Si(CH_3)_3$ groups to an extent of 55%, the methanol adsorption decreases by a factor of approximately two. The change to the surface covered to an extent of 93% (specimens A1HM) however, reduces the methanol adsorption at $p/p_s = 0.1$ by a factor of 16. The methanol adsorption isotherm becomes slightly concave, which at very low adsorption values is characteristic of extremely weak interaction between adsorbent and adsorbed material. The reason for this is evidently the same as for the case of the adsorption of benzene.

Figure 2 gives the water-vapor adsorption isotherms. Water is adsorbed on the original A1 aerosil to a slightly smaller extent than on the hydrated A1H specimen, and this is related to the fact that the degree of hydration is less for the original specimen. The lowest water adsorption was obtained for the A1M specimen with the surface covered by $Si(CH_3)_3$ groups to an extent of only 58%, and on the more completely modified (to an extent of 93%) A1HM specimen the adsorption of water was found to be slightly higher. This is related to the fact that in the first case the region of the silica surface still available for adsorption of water is dehydrated, whereas in the second case the extensively hydrated part of the silica surface which remains uncovered by $Si(CH_3)_3$ groups is still accessible to water molecules, which have the smallest dimensions of all the adsorbed substances studied in the present work. For this reason, although the total surface not covered by $Si(CH_3)_3$ groups has been reduced, its ability to adsorb water has increased.

This comparison shows that the decrease in the adsorption of methanol, benzene and hexane caused by modification of the surface to an extent of 58% is less than the corresponding decrease in the adsorption of water, whereas more complete modification leads to a sharp decrease in the adsorption, particularly that of benzene. The sharp decrease in the adsorption of hydrocarbons is of considerable interest in connection with the chromatographic separation of hydrocarbon mixtures by the gas-adsorption method, which is normally used only for the

separation of lower hydrocarbons, because the heavier hydrocarbons are too strongly adsorbed. In the case of extensively modified silica, in the first place, the adsorption of the heavier hydrocarbons is considerably reduced, while, in the second place, the isotherm becomes almost linear. This makes it possible to shift the boundary between the gas-adsorption and gas-liquid methods towards the heavier hydrocarbons, while retaining the advantages of the high chemical and thermal stability of the surface. When, as is necessary, the mosaic character of the modified layer has been eliminated, it will be possible to combine the advantages of the adsorption and distribution methods of gas chromatography.

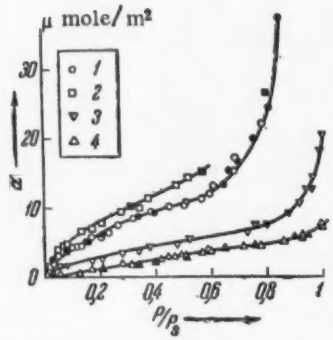

Fig. 2. Adsorption isotherm for water vapor on aerosil specimens: 1) A1, 2) A1H, 3) A1M and 4) A1HM.

LITERATURE CITED

[1] A. V. Kiselev, N. V. Kovaleva, et al., Dokl. Akad. Nauk, 124, 617 (1959).*

[2] A. Ya. Korolev, "Chetvertaya Vsesoyuzn. Konfer. po Kolloidnoi Khimii, Referaty Doklady" (Abstract of Reports from the Fourth Conference on Colloid Chemistry), Izd. Akad. Nauk SSSR, 1958. [In Russian].

[3] A. V. Kiselev, Vestn. Akad. Nauk SSSR, No.10, 43 (1957).

[4] A. V. Kiselev, in the collection "The Structure and Properties of Porous Materials", London, 1958, p. 257.

[5] A. V. Kiselev, A. Ya. Korolev and K. D. Shcherbakova, "VIII Mendeleevskii S'ezd, Referaty Dokladov" (Abstract of Reports from the VIII Mendeleev Congress), Izd. Akad. Nauk SSSR, 1959, p. 129. [In Russian].

[6] A. Ya. Korolev, T. N. Malova, V. I. Romanova, Poligrafich. Proizvodstvo, 7, 25 (1957).

[7] G. J. Young, and J. J. Chessick, J. Coll. Sci., 13, 358 (1958).

[8] A. V. Kiselev, and G. G. Muttik, Koll. Zhur, 19, 562 (1957).

[9] A. A. Isirikyan and A. V. Kiselev, Dokl. Akad. Nauk SSSR, 115, 343 (1957); L. D. Belyakova and A. V. Kiselev, Dokl. Akad. Nauk SSSR, 119, 298 (1958).*

[10] A. V. Kiselev, E. A. Leont'ev et al., Zhur. Fiz. Khim., 30, 2149 (1956).

[11] A. V. Kiselev and A. D. Poshkus, Dokl. Akad. Nauk SSSR, 120, 834 (1958).*

Received June 11, 1959

*Original Russian pagination. See C. B. translation.

Card + photo cats

THE STUDY OF THE $Bi_2Te_3 - Bi_2S_3$ SYSTEM

M. L. Beglaryan and N. Kh. Abrikosov

(A.A.Baikov Institute of Metallurgy, USSR Academy of Sciences)

(Presented by Academician I. V. Tananaev, June 20, 1959).

At the present time the study of systems of three or more components with a view to finding new semiconducting materials is of considerable interest. Certain chalcogenides of the elements of the fifth group of the Mendeleev Periodic Table, and solid solutions based on these compounds, have already found application in thermoelectric and photoelectric technology. Thus, for example, bismuth sulfide is used as a photoresistor [1]. A temperature decrease of 40° has been obtained by the use of bismuth telluride in thermoelectric refrigerators [2].

It is known that the efficiency of thermal cells is proportional to the ratio of the electrical conductivity to the thermal conductivity in the branches of the thermocouple. A. F. Ioffe [3] has shown that this ratio can be increased by using multicomponent systems containing heavy atoms. In practice, when bismuth telluride is replaced by solid solutions formed in the systems $Bi_2Te_3 - Bi_2Se_3$ and $Bi_2Te_3 - Sb_2Te_3$, the decrease in the thermal conductivity of the lattice makes possible a considerable increase in the efficiency of the thermal cells [4, 5]. The thermoelectric properties of alloys of the Bi_2Te_3–Bi_2S_3 system have not been studied.

Work has been carried out [6] on the mobility of electrons and "holes" in the region adjoining bismuth telluride and extending up to a concentration of 30 mole % Bi_2S_3. The authors of the work cited suggest that a solid solution exists in the range from bismuth telluride to the compound Bi_2Te_2S, which have identical crystal structures.

An earlier work [7] described the construction of the phase diagram for the Bi_2Te_3–Bi_2S_3 system (Fig.1). According to the data of the authors, this system contains the single compound $Bi_2Te_3 \cdot Bi_2S_3$, which forms a eutectic with bismuth telluride. It should be noted that in the work cited the studies were carried out on specimens which had not been annealed, and which therefore had not reached equilibrium. The formation of the compound Bi_2Te_2S, corresponding in composition to the natural mineral tetradymite, was denied by the authors of the work cited.

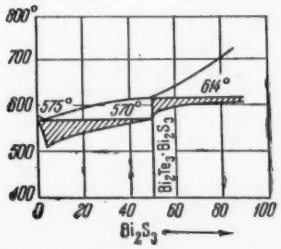

Fig.1. Phase diagram for the Bi_2Te_3–Bi_2S_3 system, according to the data of M. Amadori.

The crystal structure of the mineral tetradymite has been studied in detail by D. Harker [8] who showed that the mineral has a rhombohedral structure with parameters a = 11.31 A and $\alpha = 24° 10'$. A characteristic feature of the tetradymite structure is the layer arrangement of the bismuth, tellurium and sulfur atoms in the order Te–Bi–S–Bi–Te–Te–Bi–S. . .,etc. Work has also been done on the nature of the bonds between the atoms within the layers and between the atoms of different layers [9].

The aim of the present work was to check the phase diagram of the Bi_2Te_3–Bi_2S_3 system using equilibrium alloys, and also to study certain physical properties of the alloys.

The specimens studied were prepared by fusing together bismuth, tellurium and sulfur in the required proportions in evacuated quartz ampoules

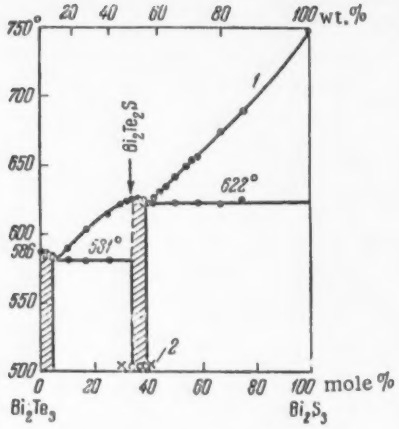

Fig. 2. Phase diagram for the Bi_2Te_3 – Bi_2S_3 system, according to our data: 1) halts on the thermograms, 2) two-phase alloys; open circles – single-phase alloys.

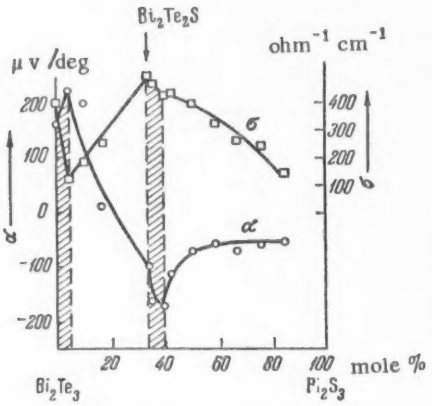

Fig. 3. Electrical properties of alloys in the Bi_2Te_3 – Bi_2S_3 system.

The tellurium and sulfur were purified by distilling twice in vacuo. Spectral analysis showed that the bismuth contained less than 0.0005 % Ag and Sb, less than 0.001% Fe, Si, Cu and As, and 0.015% Mg and Pb; the tellurium less than 0.0001% Cu, Ag, As, Bi and Sb; and the sulfur less than 0.0001% Al and Fe, less than 0.001% Mg and less than 0.01% As. The alloys obtained were subjected to prolonged annealing to bring them to the equilibrium state. The annealing temperature chosen was 530° for the alloys rich in bismuth telluride and 580° for the alloys containing more than 50 mole % Bi_2S_3. The alloys were hardened in air after annealing.

The thermal analysis was carried out using an N. S. Kurnakov pyrometer. The standard used for the differential thermocouple consisted of a solid solution containing 80 mole % SnTe and 20 mole % GeTe. The liquidus was constructed from the results obtained by recording the cooling curves and the solidus from the heating curves for the equilibrium alloys. The phase diagram for the Bi_2Te_3 – Bi_2S_3 system is given in Figure 2. The system shows one intermediate phase, which at 530° extends from the composition corresponding to the compound Bi_2Te_2S (33.3 mole % Bi_2S_3) to 39 mole % Bi_2S_3, as shown by microstructural analysis. This phase melts with an open maximum at a temperature of 625.5°. The composition of the maximum shows a slight deviation from the stoichiometric composition of the compound Bi_2Te_2S towards higher Bi_2S_3 concentrations, and, according to the thermal analysis data, corresponds to the composition of an alloy with 35 mole % Bi_2S_3. The deviation of the maximum on the fusion diagram from the composition of the compound Bi_2Te_2S was confirmed by microstructural studies. A cast alloy corresponding in composition to the compound Bi_2Te_2S was found to contain two phases. The structure of this alloy consisted of the first-formed crystals of the phase lying in the central part of the system, and a eutectic formed by this phase with a solid solution based on the compound Bi_2Te_3. After prolonged annealing at 530° this alloy became single-phased. The solid solution based on the compound Bi_2Te_2S forms two eutectics: one with the solid solution based on bismuth telluride and one with bismuth sulfide. The first eutectic lies at a concentration of 6 mole % Bi_2S_3 and melts at a temperature of 581°; the second eutectic is very close to the single-phase region of the solid solution based on the compound Bi_2Te_2S, namely 40 mole % Bi_2S_3, and melts at a temperature of 622°. The solid solution based on bismuth telluride extends to 4 mole % Bi_2S_3 at 530°. The results of our studies therefore have not confirmed the formation of a solid solution between the compounds Bi_2Te_3 and Bi_2Te_2S, as suggested by Harker [8].

No solid solution based on bismuth sulfide was detected. The alloys studied, however, extended only as far as a concentration of 98 mole % Bi_2S_3. This alloy, in both cast and annealed states, contained two phases. The first-formed crystals of the Bi_2S_3 phase did not show dendrite liquation, which indicates either the absence or the presence in very low concentration of solid solution based on bismuth sulfide.

Measurements were made of the electrical conductivity and thermo-emf of the alloys after annealing (Fig.3). In the solid solutions based on the compounds Bi_2Te_3 and Bi_2Te_2S, the electrical conductivity decreases with increase in the bismuth sulfide concentration. The absolute value of the thermo-emf shows a corresponding increase. The solid solution based on the compound Bi_2Te_3 has the positive type of conductivity, and that based on the compound Bi_2Te_2S, the negative type. The decrease in the electrical conductivity and the

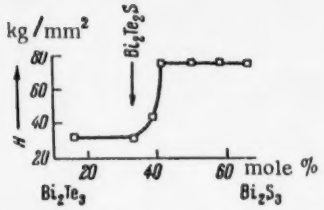

Fig. 4. Microhardness of alloys in the Bi_2Te_3 – Bi_2S_3 system.

corresponding increase in the thermo-emf with increase in the bismuth sulfide content of the solid solutions based on the compounds Bi_2Te_3 and Bi_2Te_2S is apparently due to the decrease in the mobility of the current carriers when the composition of the alloys deviates from the stoichiometric composition.

The curve showing the relationship between the microhardness of the alloys and their composition, given in Fig.4, also reveals the solid solution boundaries in the central part of the system. The alloy corresponding to the composition Bi_2Te_2S has a minimum hardness, which confirms the existence of the compound Bi_2Te_2S.

An x-ray structural analysis of the compound Bi_2Te_2S was carried out.

The x-ray diagrams were recorded using a Debye – Scherrer camera with iron radiation. The values obtained for the lattice parameters a = 10.1 A and α = 24° 8', and the intensities of the lines show good agreement with the literature data for the mineral tetradymite [8].

LITERATURE CITED

[1] B. T. Kolomiets, Zhur. Tekh. Fiz., 19, 1, 126 (1949).

[2] H. J. Goldschmid, J. Electronics, 1, 2, 218 (1955).

[3] A. F. Ioffe, S. V. Airapetyants, et al., Dokl. Akad. Nauk, 106, No.6, 981 (1956).

[4] S. S. Sinani and G .N. Gordyakova, Zhur. Tekh. Fiz., 26, No.10, 2399 (1956).

[5] E. A. Kolenko and L.S. Stilbans, Sborn. Poluprovodniki v Nauke i Tekhnike" (Coll. Semiconductors in Science and Technology), 2, Izd. Akad. Nauk SSSR, 1958, p. 233 [In Russian].

[6] S. V. Airapetyants, B. A. Efimova, et al., Zhur. Tekh. Fiz., 27, No.9, 2167 (1957).

[7] M. Amadori, Gazz. chim. Ital., 48, Parte II, 42 (1918).

[8] D. Harker, Zs. Kristallogr., 89, 175 (1934).

[9] S. V. Airapetyants, B. A. Efimova, et al., Zhur. Tekh. Fiz., 28, No.8, 1768 (1958).

Received June 20, 1959.

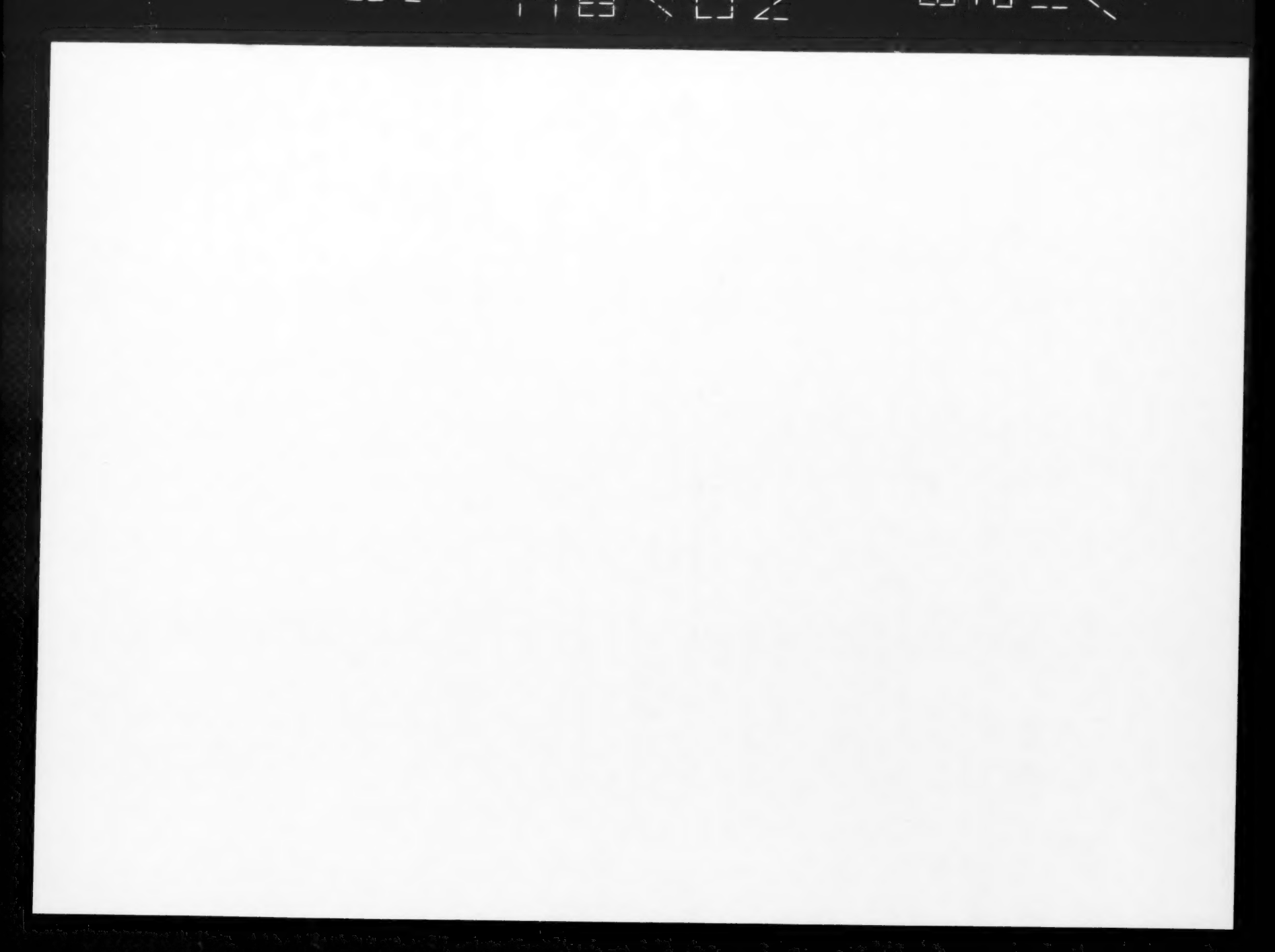

VACUUM GAS CHROMATOGRAPHY

D.A. Vyakhirev and P. F. Komissarov*

(Scientific Research Institute of Chemistry, N. I. Lobachevskii State University, Gor'kii)

(Presented by Academician M. M. Dubinin, June 16, 1959).

Published works on gas chromatography [1, 2] recommend that the gas outlet from the chromatographic column be connected to a vacuum to produce the pressure gradient necessary to overcome the resistance of the sorbent layer to the flow of carrier gas, and also (in the separation of high-boiling substances) to prevent condensation of the desorbed substances in the recording apparatus. The necessity to establish a pressure gradient across the ends of the column is very frequently encountered in distribution chromatography, which requires the use of long narrow columns and highly dispersed sorbents. The pressure difference is usually created by increasing the pressure of the carrier gas at the point of entry to the column, or, less frequently, at the outlet. In the works cited above, attention is paid to the necessity to introduce corrections for the change in retention volume caused by this pressure difference, as given by the formula of James and Martin [3], but no conclusions were reached regarding the influence of the absolute value of the pressure inside the column on the retention volume or on the height and width of the peak on the eluate curve. Our studies have shown that this influence may be considerable, and this may be regarded as an advantage, since a reduction in the pressure in the column leads to a marked reduction in the time required for the separation process, while at the same time the efficiency is increased.

EXPERIMENTAL

A constant temperature was maintained in the column (Fig. 1) by passing water from a thermostat through the surrounding jacket. The test gas was passed from a gas holder via the tap of the gas-measuring apparatus (4) into the spiral copper tube of the gas-measuring apparatus, whose volume had previously been accurately measured, and from there to a trap containing dry ice in acetone (not shown in Figure 1). The taps were then turned through 180° and the test sample taken to the column by the current of carrier gas (nitrogen) The gas-measuring apparatus was kept at the same temperature as the column by means of a thermostat. The rate of flow of the nitrogen at the inlet and outlet was established beforehand by means of the flow-meters shown, using a simple manostat and a special Cartesian manostat operating only at reduced pressures. The necessary pressure level in the column and the zero position of the recorder pen were established beforehand. As the test gas reached the column, the process of chromatogram development started, under the given experimental conditions of temperature, rate of nitrogen flow, pressure and volume of test gas sample: the chromatograms were reproduced on a recording potentiometer at different pressures inside the column, the other experimental parameters remaining constant. The readings on the recorder were converted to concentrations by means of a calibration graph.

RESULTS

Figures 2 and 3 give the eluate curves obtained for n-butane at different pressures, with coordinates C, $\underline{t}$ and C, V, where C is the eluate concentration, $\underline{t}$ is the time and V is the volume of nitrogen passed through the column in time $\underline{t}$. The constant parameters of the experiment are: adsorbent – eMSK silica gel, with particle diameter 0.25-0.5 mm; column 2 · 40 cm; rate of flow at outlet 20 ml/min; temperature of column and gas-

*L.G. Levkov took part in the initial experimental work.

measuring apparatus (thermostat) 70 ± 0.01°, and volume of butane sample passed to column from gas-measuring apparatus approximately 2 ml. Figures 2 and 3 show the considerable decrease in the time required for the butane to leave the column, and the increase in the eluate concentration as the pressure inside the column is decreased.

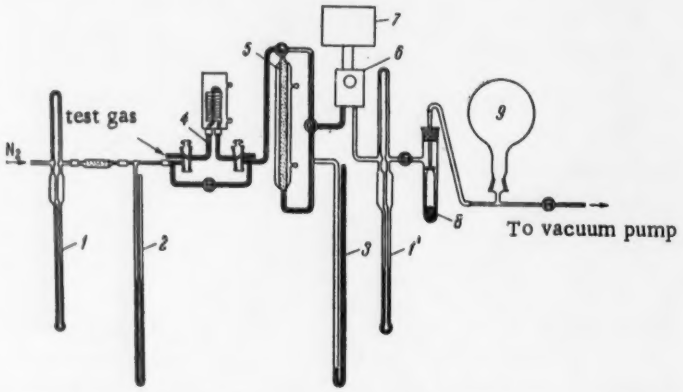

Fig. 1. Chromatographic apparatus for the elution analysis of gases at reduced pressures: 1, 1') flow-meters; 2,3) manometers; 4) gas-measuring apparatus bypass; 5) chromatographic column with surrounding jacket; 6) thermal conductivity recording apparatus, type GEUK-21; 7) recording potentiometer, type KVT/1; 8) Cartesian manostat; 9) pressure bulb.

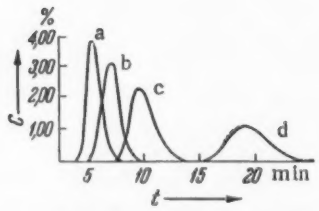

Fig. 2. The influence of decrease in the pressure inside the column on the n-butane output; coordinates C, t. a) P = 176 mm; b) 237 mm, c) 351 mm, d) 768 mm.

A similar effect was obtained using a number of gaseous and liquid mixtures.

Figure 4 gives the eluate curves for a mixture of n-butane and β-butylene at reduced pressure and at atmospheric pressure inside the column. The parameters are the same as those of the experiments of Figures 2 and 3. The increase in the yield of adsorbed material with decrease in the pressure has been explained by the resultant expansion of the carrier gas inside the column, and consequent increase in the rate of flow of the carrier gas through the sorbent layer, which can be observed directly from the increase in the readings on the flow-meter 1', which measures the rate of flow inside the column (or at the outlet).

The measurement of this rate α_2 at different pressures inside the column P_2, and constant rate of flow α_1 and pressure P_1 at the inlet showed that the quantities are inversely proportional to one another, as follows from the Boyle–Mariotte law:

$$\frac{\alpha_1}{\alpha_2} = \frac{P_2}{P_1} \qquad (1)$$

or

$$\alpha_2 = \frac{K}{P_2}. \qquad (2)$$

It is known that the rate of movement of the adsorption zone is determined from the equation [7,8]:

$$W = \frac{L}{t} = \frac{\alpha}{\Gamma}, \qquad (3)$$

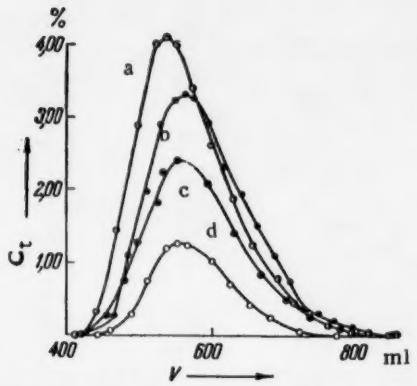

Fig. 3. The influence of decrease in the pressure inside the column on the n-butane output, coordinates C, V. Curve symbols the same as for Fig.2.

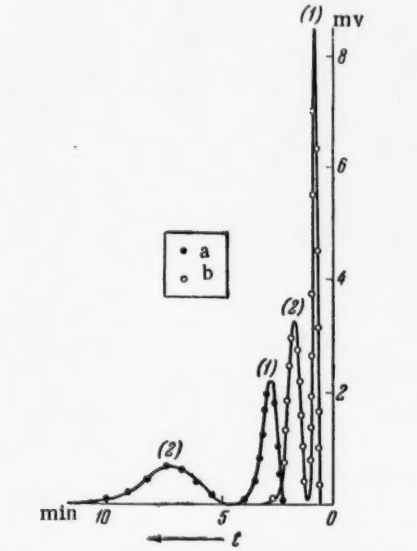

Fig. 4. Eluate curves for a mixture of n-butane (1) and β-butylene (2) at reduced pressure and at atmospheric pressure inside the column. Rate of flow at inlet 45 ml/min. Ratio of components in mixture 1:1.

where W is the rate of movement of the zone through the sorbent layer, Γ is the adsorption coefficient, L is the length of the layer, and t is the time taken for the zone to pass through the whole layer, i.e., the time of the experiment or the output time.

Substituting in this equation the value of α^2 from formula (2), we find the output time t:

$$t = \frac{\Gamma L}{K} P_2. \qquad (4)$$

The value of Γ is proportional to the retention volume V_{max}, as follows from equation (3):

$$\Gamma = \frac{\alpha_2 t}{L} = \frac{V_{max}}{L}. \qquad (5)$$

Figures 2 and 3 show, however, that the retention volume changes only very slightly with decrease in the pressure. As expected, therefore, the value of Γ is practically independent of the pressure. As a result, the term Γ L/K in equation (4) is constant, and the output time t is directly proportional to the pressure P_2. The eluate curves in Figure 2 also show that as the pressure in the column is decreased within the range 768-176 mm, the half-width of the butane peak $\Delta V_{1/2}$ (at the half-height), expressed in volume units ($\Delta V_{1/2} = \alpha_2 \Delta t$), remains practically unchanged, whereas the eluate concentration C_t increases considerably.

In view of the lack of experimental material, it is as yet difficult to give a sufficiently rigorous theoretical explanation of this phenomenon. The fact that the band width is constant is evidently related to the fact that the ratio of the lengthwise diffusion coefficient D to the rate of flow α_2 is constant [9] with change in temperature within the range indicated. As far as the increase in the eluate concentration C_t is concerned, we may assume that since the half-width does not change, the increase in C_t does not result from compression of the chromatographic zone, which is very sharp in the case of increase in the temperature. It is quite possible that the concentration increases as a result of decrease in the mole fraction of the carrier gas on rarefaction at the moment when the adsorbed substance is desorbed from the column (see [4], p. 27).

LITERATURE CITED

[1] N. H. Ray, J. Appl. Chem., 4, 21 (1954).

[2] F. R. Cropper, and A. H. Heywood, Nature, 172,1102 (1953); 1063 (1954).

[3] A. T. James and A. J. P. Martin, Biochem. J., 52, 679 (1952).

[4] C. S. G. Phillips, Gas Chromatography, Butterworth Scient. Publ., London, 1956.

[5] D. A. Vyakhirev and A. I. Bruk, Zhur. Fiz. Khim., 31, 1713 (1957).

[6] R. Gillmant, Analyt. Chem., 23, 157 (1951).

[7] N. A. Shilov, L. K. Lepin', and S. A. Voskresenskii, Zhur. Russ. Khim. Obshch., 51, 1107 (1929).

[8] Don de Vault, J. Am. Chem. Soc., 65, 532 (1943).

[9] N. M. Turkel 'taub, and A. A. Zhukhovitskii, Zav. Lab., 23, 1023 (1957).

Received June 15, 1959.

THE MECHANISM OF THE OXIDATION OF PROPYLENE TO ACROLEIN ON A CUPROUS OXIDE CATALYST

O. V. Isaev, L. Ya. Margolis and I. S. Sazonova

(Institute of Physical Chemistry, USSR Academy of Sciences)

(Presented by Academician P. A. Rebinder, June 19, 1959).

In recent years the tracer-atom method has been used to examine the stepwise mechanism of certain reactions involved in the catalytic oxidation of hydrocarbons [1]. It has been shown that in the oxidation of ethylene to ethylene oxide on silver, and of propylene to aldehydes (acetaldehyde and formaldehyde) on vanadium pentoxide, the reactions involved in the formation of the aldehydes, ethylene oxide and carbon dioxide take place by independent simultaneous routes via unstable intermediate products. Acrolein is a more reactive compound than saturated aldehydes or ethylene oxide. Under oxidizing conditions, therefore, the acrolein can be readily oxidized and may play an important part in the formation of carbon dioxide.

There are no papers in the literature devoted to the study of the mechanism of the oxidation of propylene to acrolein. We have earlier suggested that this reaction takes place by a parallel – successive mechanism, since this is indicated by the kinetic measurements [2]. The aim of the present study was to establish the accuracy of this suggestion using a tracer-atom method.

Propylene labeled with radiocarbon was prepared by dehydration of isopropyl alcohol on alumina at 400° with subsequent purification from traces of aldehydes, ethers and unreacted alcohol. The labeled propylene was mixed with acrolein, nitrogen and oxygen in the ratio 17% C_3H_6, 3.5-5% acrolein and 8.5% O_2.

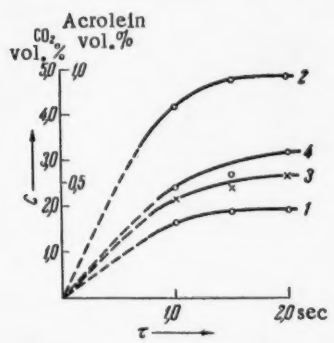

Fig. 1. Graphs showing how the CO_2 and acrolein concentrations in the gas (vol.%) vary with time of contact for the oxidation of a mixture of propylene, oxygen and nitrogen (at 396°): acrolein (1) and CO_2 (2) on catalyst containing 1.0% Cu on SiC; acrolein (3) and CO_2 (4) on a catalyst containing 0.1% Cu on SiC.

The oxidation process was studied in a flow-through apparatus [2] at atmospheric pressure on two catalyst specimens (0.1% Cu on SiC and 1.0% Cu on SiC). The reaction products were analyzed to determine the acrolein concentration by the bromide – bromate method, and the propylene and carbon dioxide contents using a VTI gas-analysis apparatus. The radioactivity of the carbon dioxide and propylene oxidized to CO_2 was determined by measurements on the barium carbonate produced, using an end-face counter with mica window, while the radioactivity of the acrolein was determined by examining the precipitated 2,4-dinitrophenylhydrazone. The specific activity (imp/min · mg) of the precipitates was calculated, taking account of the self-absorption in the layer, from calibration curves for $BaCO_3$ and acrolein hydrazone. The specific activities of the acrolein hydrazones ($\alpha'_{acr.}$) were expressed in terms of the specific activity of the $BaCO_3$ ($\alpha_{acr.}$) using the relationship: $\alpha_{acr.} = \alpha'_{acr.} M_{hydrazone}/3M_{BaCO_3}$, where M is the molecular weight.

Figure 1 gives curves showing the yield of acrolein and carbon dioxide for different times of contact on catalysts containing 0.1 and 1% copper on carborundum, obtained in the oxidation

of a mixture of the following composition: 17% C_3H_6, 8.5% O_2 and 74.5% N_2.

Figure 1 shows that with increase in the contact time up to 2 seconds, the yields of acrolein and carbon dioxide increase simultaneously, which indicates that the reactions involved in their formation proceed in parallel. The relationship between the kinetic curves for the formation of acrolein and carbon dioxide depends on the composition of the catalyst: increase in the concentration of copper on the carrier leads to a decrease in the yield of acrolein, while the yield of carbon dioxide increases, indicating the further oxidation of acrolein to carbon dioxide.

Figure 2 gives the kinetic curves for the oxidation of a mixture of propylene, acrolein, oxygen and nitrogen on the same catalyst specimens. As the time of contact increases, the acrolein concentration decreases, while the carbon dioxide concentration increases. In the oxidation of the propylene–acrolein mixture, increase in the concentration of copper on the carrier leads on the one hand to an increase in the yield of carbon dioxide (as in the case of the oxidation of pure propylene) but, on the other hand, has no influence on the rate of conversion of the acrolein.

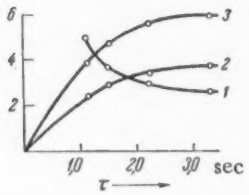

Fig.2. Graphs showing how the concentrations of CO_2 and acrolein in the gas vary with change in the time of contact for the oxidation of a mixture of propylene, acrolein, oxygen and nitrogen (at 396°): 1) acrolein on a catalyst containing 0.1 and 1.0% Cu on SiC, 2) CO_2 on a catalyst containing 0.1% Cu on SiC, 3) CO_2 on a catalyst containing 1.0 % Cu on SiC.

Figure 3 shows the relationship between the specific activities of acrolein and carbon dioxide and the time of contact on a catalyst containing 0.1% Cu on carborundum. The specific activities of the acrolein and CO_2 increase with increase in the time of contact. The specific activity of the carbon dioxide is greater than the corresponding value of the specific activity of the acrolein, but less than that of the propylene (Fig.3). If the carbon dioxide and acrolein were formed from propylene independently, then the specific activity of the CO_2 would be equal to that of the propylene. The intermediate value proves the accuracy of the previously proposed parallel–successive mechanism for the oxidation of propylene on Cu_2O. The data given in Figure 3 also indicate that the successive process predominates over the parallel process, since

$$\frac{\alpha_{C_3H_6}}{\alpha_{CO_2}} > \frac{\alpha_{CO_2}}{\alpha_{acr}}.$$

It was considered of interest to compare the rates of formation and decomposition of acrolein during the process. For this purpose we used a kinetic isotope method [3] to calculate the rate of formation (W_1) and decomposition (W_2) of acrolein, and also the rates of formation of CO_2 from propylene (W_4) and from acrolein (W_3) using the following equations:

$$\frac{d\alpha_{C_3H_4O}}{dt} = \frac{(\alpha_{C_3H_6} - \alpha_{C_3H_4O})\,W_1}{[C_3H_4O]};$$

$$\frac{d[C_3H_4O]}{dt} = W_1 - W_2; \quad \frac{d\alpha_{CO_2}}{dt} = \frac{(\alpha_{C_3H_4O} - \alpha_{CO_2})\,W_3}{[CO_2]} + \frac{(\alpha_{C_3H_6} - \alpha_{CO_2})\,W_4}{[CO_2]}.$$

Table 1 (Columns 5 and 6) gives the results of the calculation of the rates of formation and decomposition of acrolein. If the acrolein were only oxidized to CO_2 under the conditions of the process, then the rate of formation of carbon dioxide from acrolein (W_3) should be equal to the rate of decomposition of the acrolein (W_2). The data (Column 9) show that $W_2 > W_3$, so that the disappearance of the acrolein from the catalyst surface is not entirely the result of its subsequent oxidation to carbon dioxide. There are reports in the literature [4] on the adsorption of aldehydes and ethylene oxide on the surface of various oxidizing catalysts (silver and vanadium pentoxide) leading to the formation of an organic film which is slowly oxidized at the temperatures of the catalytic process. In addition, it has been shown by electron diffraction that a polymer film is formed on the surface of cuprous oxide catalyst during the adsorption of acrolein in the presence of oxygen. If a similar organic film is formed on the catalyst surface in the oxidation of the mixture (C_3H_6, C_3H_4O, O_2 and N_2) then it should be detectable by tracer-atom methods. We therefore carried out the following experiments.

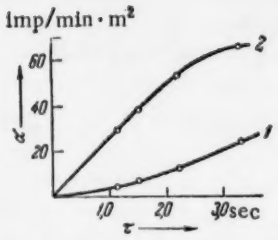

Fig. 3. Relationship between the specific activities of acrolein (1) and carbon dioxide (2) and the time of contact on a catalyst containing 0.1% Cu on SiC.

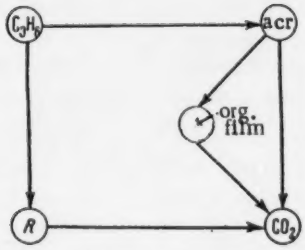

Fig.4. Diagram illustrating the oxidation of propylene on a copper catalyst. R represents the intermediate product, which was not isolated.

TABLE 1

Rates of the Different Reactions in the Oxidation of Propylene on a Copper Catalyst at 396°

Time of contact τ, sec	Composition of orig. mixture: C_3H_6	O_2	acr.	Concentration in yield, vol. % of gas: CO_2	acr.	Specific activities: C_3H_6	CO_2	acr.	Rates of conversion of propylene and acrolein in arbitrary units: formation of acrolein, W_1	decomp. of acrolein, W_2	formation of CO_2 from acrolein, W_3	formation of CO_2 from propylene, W_4	formation of organic film, $W_2 - W_3 = W_5$	ratio of rates W_3 / W_4
1	2			3		4			5	6	7	8	9	10
Catalyst containing 0.1% Cu on SiC														
1,15	17,3	8,7	5,0	2,4	4,8	320	29	4	8,8	4,5	1,4	0,3	3,1	4,7
1,5	17,3	8,7	4,4	2,9	3,8	320	39	7	4,5	2,6	0,95	0,3	1,6	3,2
2,2	17,3	8,7	4,2	3,4	3,0	320	53	13	2,4	1,5	0,4	0,25	1,1	1,7
3,3	17,3	8,7	3,5	3,75	2,5	320	65	24	1,0	0,8	—	—	—	—
Catalyst containing 1.0% Cu on SiC														
1,15	17,3	8,7	5,0	3,9	5,2	320	35	6	8,8	4,5	2,0	0,48	2,5	4,2
1,5	17,3	8,7	4,4	4,7	3,6	320	42	10	4,5	2,6	1,6	0,48	1,0	3,3
2,2	17,3	8,7	4,2	5,6	3,0	320	55	15	2,4	1,5	0,55	0,36	0,9	1,5
3,3	17,3	8,7	3,5	6,0	2,75	320	68	20	1,0	0,8	—	—	—	—

1. After the oxidation of the mixture of propylene (labeled with C^{14}) acrolein, oxygen and nitrogen over a catalyst containing 1% Cu on SiC, air purified from CO_2 was passed through the apparatus at 400°. The carbon dioxide formed as a result of the combustion of the organic film was converted to $BaCO_3$. The specific activity of the CO_2 was equal to 35 imp/min· mg, which is comparable to that of the acrolein obtained under the same conditions.

2. A mixture of (inactive) acrolein and nitrogen was first passed over a catalyst (0.1% Cu on SiC) at 400°, after which a mixture of labeled propylene, oxygen and nitrogen was passed through at the same temperature for the same time of contact (2 seconds). The specific activity of the carbon dioxide amounted to 70 imp/min· · mg. The organic layer formed on the catalyst surface in the adsorption of the acrolein has therefore taken part in the process of carbon dioxide formation, since otherwise its activity would be equal to that of the original propylene, i.e., 320 imp/min · mg.

The calculations (Table 1, Column 9) show that the organic film is more stable on the catalyst containing 0.1% Cu on SiC than on the catalyst containing 1.0% Cu on SiC. This is in accordance with the experimental data: the increased yield of CO_2 on the catalyst containing 1% Cu is probably due to the subsequent oxidation of the organic film.

The change in the relationship between the rate of formation of carbon dioxide from acrolein (W_3) and propylene (W_4) with time of contact (Table 1, Column 10) indicates a difference in the laws governing the degree of oxidation of the propylene and acrolein. Increase in the concentration of copper in the carrier leads to an increase in the absolute rates of the reactions involving the formation of CO_2 from acrolein and propylene, but does not change their relative values, i.e.,the laws governing the oxidations are preserved.

The present work using the tracer-atom method has thus confirmed the parallel–successive mechanism of the oxidation of propylene to acrolein. It has been shown that the catalyst surface (copper on carborundum) becomes covered with an organic film formed chiefly from acrolein. With change in the conditions under which the process is carried out (composition of original mixture, nature of carrier, etc.)the ratio of the rates of the separate stages of the process may evidently also vary.

LITERATURE CITED

[1] L. Ya. Margolis, Uspekhi Khim., 28, No.5, 615 (1959).

[2] O. V. Isaev, L. Ya. Margolis and S. Z. Roginskii, Zhur. Obshch. Khim., No.5 (1959).*

[3] M. B. Neiman, and A. F. Lukovnikov, "Tsepnye Reaktsii Okisleniya Uglevodorodov v Gazovoi Faze" (Chain Reactions of Hydrocarbon Oxidation in the Vapor Phase), Izd. Akad. Nauk SSSR, 1955, p. 140.

[4] L. Ya. Margolis and S. Z. Roginskii, Problemy Kinetiki i Kataliza, 9, 107 (1957).

[5] O. V. Isaev, M. Ya. Kushnerev, Dokl. Akad. Nauk, 124, 858 (1959).*

Received June 15, 1959.

* Original Russian pagination. See C. B. translation.

THE ELECTRON PARAMAGNETIC RESONANCE SPECTRA OF CERTAIN CATALYSTS AND CATALYST–HYDROCARBON SYSTEMS, AND THE ACTION OF γ-RADIATION ON THEM

Yu. A. Kolbanovskii, I. M. Kustanovich, L. S. Polak and A. S. Shcherbakova

(Institute for the Synthesis of Petroleum Chemicals, USSR Academy of Sciences)

(Presented by Academician A. V. Topchiev, June 8, 1959)

The study of the electron paramagnetic resonance (e.p.r.) spectra of catalysts and catalyst – hydrocarbon systems provides a new method for the examination of catalysts and the processes involved in chemisorption and catalysis. The results published here were obtained with the typical oxide catalysts used in the processes of cracking, dehydrogenation, hydrogenation, dehydrocyclization and desulfurization, and with representatives of the chief classes of hydrocarbon. The data obtained in the study of the effect of γ-radiation forms part of our studies on the radiolysis of hydrocarbons in heterogeneous systems.

EXPERIMENTAL METHOD

1. The catalysts were: I) industrial chromatographic alumina; II) industrial spherical aluminosilicate cracking catalyst; III) microspherical alumina – molybdenum oxide catalyst formed by mixing the gels, which were prepared separately [1] (composition: MoO_3 10%, Al_2O_3 90%); IV) alumina – molybdenum oxide catalyst prepared by impregnating catalyst I with ammonium molybdate followed by ignition in a current of air at 500° for 3 hours (composition: MoO_3 10%, Al_2O_3 90%); V) catalyst IV reduced with hydrogen at 450° for 1.5 hours; VI) industrial cobalt oxide – alumina – molybdenum oxide catalyst (composition: CoO 5.5%, MoO_3 15.5%, Al_2O_3 79%); VII) industrial alumina – chromic oxide catalyst promoted with potassium oxide (composition: Cr_2O_3 8%, K_2O 2.0%, Al_2O_3 90%); VIII) industrial molybdenum disulfide (in tablet form). The catalysts were given a preliminary treatment at a pressure of $1 \cdot 10^{-4}$ mm mercury and $\underline{t} \sim 200°$, until no more gas was evolved: this corresponds approximately to the treatment usually given.

2. The hydrocarbons n-heptane, n-heptene-1, cyclohexane and benzene were purified, and their constants and spectra corresponded to the literature data. The hydrocarbons were freed from dissolved air [2] and were then transferred to an ampoule with the prepared catalyst. The ratio of the weight of hydrocarbon to the weight of catalyst lay between 0.15 and 0.2.

3. The irradiation was carried out in Pyrex ampoules using Co^{60} sources with different dose rates, determined by ferrous sulfate and cerium dosimetry. Dosimetry cannot be regarded as completely developed for heterogeneous systems in general, and for surfaces in particular. It is therefore impossible to give absolute values for the integral doses and radiochemical yields for these systems. The irradiation was carried out at +20°, and in a number of cases at -78 and -196°.

4. The e.p.r. spectra were recorded on an apparatus giving direct absorption spectra. The apparatus operates in the 3 cm range and has a half-wave rectangular resonator of the reflection type. The maximum modulation depth was ~ 1000 gauss, so that wider signals were not recorded. The comparatively large particle size of the catalysts studied made it necessary to use ampoules with an outer diameter of 5 mm, which resulted in a sharp decrease in the sensitivity of the apparatus: the minimum detectable number of unpaired spins (US) in a volume of 0.15 cm^3 filled with catalyst amounted to $\sim 10^{16}$ at room temperature and $\sim 10^{15}$ when the resonator

and ampoules were cooled with liquid nitrogen. The signals corresponding to these and lower concentrations were not recorded and were noted as being weak. The width of the lines was measured with an error of ± 3 gauss, and the spectroscopic splitting factor g = ± 0.002. The measurement of the number of US in the volume indicated (N) was carried out according to DFPG, with a probable relative error of ± 15%. The apparatus was graduated for each temperature at which the spectra were recorded.

5. The procedure was as follows: the e.p.r. spectra of the catalyst was recorded before and after irradiation, after which the spectrogram of the catalyst and adsorbed hydrocarbon was recorded before and after irradiation. The spectra of all the specimens were recorded at two temperatures (+20° and -196°) and in some cases at -78°.

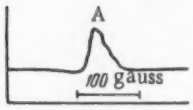

Fig. 1.

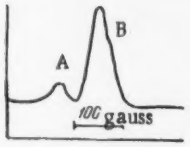

Fig. 2.

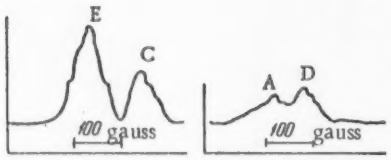

Fig. 3.

EXPERIMENTAL RESULTS

Catalyst I is the main component of most oxide catalysts, and was therefore studied first. Nonirradiated catalyst I, with or without any of the hydrocarbons, gives a weak signal at values of t_s equal to +20° and -196°.* After irradiation with a dose of 9 Mr, the e.p.r. spectrum has the shape A (Fig.1) with factor g = 2.013, value of $\Delta g = g - 2.0023 > 0$, signal width $\Delta H = 71$ gauss and $N = 1.4 \cdot 10^{18}$; when irradiated together with the hydrocarbons ($t_{irr.}$** = 20°) the catalyst gives the same signal (t_s = + 20° and -196°). When catalyst I is irradiated together with n-heptane at $t_{irr.}$ = -196°, , the e.p.r. spectrum (t_s = -196°) shows a signal corresponding in position, width and structure to that of the heptyl radical, but signal A is not detected. This heptyl radical signal is characteristic for heterogeneous radiolysis at -196° [3] and disappears when the temperature is raised. It is evidently related to the presence in the system of nonadsorbed hydrocarbon (Fig. 3), Signal D). Catalyst II behaves in the same way as catalyst I, as shown in studies with n-heptane and n-heptene-1 (signal of type A).

Catalyst III, before irradiation with or without any of the hydrocarbons adsorbed on it, gives a weak signal. After irradiation, catalyst III gives an e.p.r. spectrum of type A. When the dose is increased from 6 to 120 Mr, no change in the intensity of the signal is observed. With the same irradiation, catalyst III with adsorbed heptane shows a spectrum (t_s = +20° and -196°) (Fig.2) consisting of two signals: the one on the left is of type A (the characteristic signal of the catalyst itself) and the one on the right handis of type B, for which g = 1.964, $\Delta g < 0$ and ΔH = 121 gauss. The intensity of B increases with increase in the dose, but reaches saturation before 30 Mr (at $N = 1.1 \cdot 10^{19}$). The opened ampoules (catalyst III + n-heptane) after irradiation show a marked decrease in the intensity of both the left-hand and right-hand signals. When a sealed irradiated ampoule is heated to +200° (catalyst III + n-heptane), there is an irreversible increase in the intensity of the right-hand signal (t_s = + 20° and -196°).

Irradiation of catalyst III + n-heptane at $t_{irr.}$ = -196° gives an e.p.r. spectrum of type C (Figure 3). The signal D, as in the case of catalyst I, corresponds to the heptyl radical. Signal C has g = 1.943, $\Delta g < 0$ and ΔH = 110 gauss. Both signals disappear when the temperature is raised to -78°. Irradiation ($t_{irr.}$ = +20°) of catalyst III with n-heptene-1 and cyclohexane using a dose of 6 Mr gives an e.p.r. spectrum of type A and B at t_s = 20°. At t_s = -196°, this spectrum shows a decrease in the intensity of the right-hand signal relative to the left-hand signal, which remains unchanged. Irradiation of catalyst III with benzene using a dose of 6 Mr ($t_{irr.}$ = +20°) gives an e.p.r. spectrum of the type A + B at t_s = +20° and -196°, although B is very weak. Catalyst IV, with and without n-heptane, before and after irradiation with a dose of 30 Mr at $t_{irr.}$ = +20°, gives the same e.p.r. spectrum as catalyst III. Catalyst V, before irradiation at t_s = + 20° and -196°, gives a very wide (more then 1000 gauss) and intense signal corresponding to the formation of a new phase. The adsorption of n-heptane suppresses this signal. Catalyst VI gives a wide weak signal in the e.p.r. spectrum before irradiation, at t_s = +20° and -196°. Irradiation of catalyst VI

* t_s is the temperature of the specimen while the e.p.r. spectrum was being recorded.
** $t_{irr.}$ is the irradiation temperature.

with a dose of 6 Mr ($t_{irr.}$ = +20°) leads to the production of signal A. Catalyst VI, with any of the adsorbed hydrocarbons, gives a weak signal before irradiation, and a signal of type A + B after irradiation; in this case B is weaker than in the case of catalyst III. As in the case of catalyst III, there is an increase in the intensity of the right-hand signal when the dose is increased from 6 to 30 Mr.

Before irradiation, catalyst VII at t_s = +20° and -196° gives an e.p.r. spectrum of type D (Fig.3) with g = 1.975, $\Delta g < 0$ and ΔH = 70 gauss. The adsorption of hydrocarbons does not change this picture, but in the case of n-heptene-1 the intensity of the signal increases appreciably. Irradiation of catalyst VII with a dose of 9 Mr ($t_{irr.}$ = +20°) leads to the appearance of a second signal A in the e.p.r. spectrum. Irradiation of catalyst VII with n-heptane, n-heptene-1 or cyclohexane at $t_{irr.}$ = + 20° using doses of 6 and 30 Mr leads to the appearance of two intense, incompletely resolved signals in the e.p.r. spectrum (Fig.4, a), with g = 2.013 and 1.985. In the case of the adsorption of benzene, the intensity of these two signals decreases by approximately one order of magnitude. Irradiation of catalyst VII with n-heptane ($t_{irr.}$ = -196°) using a dose of 30 Mr leads to the appearance of two incompletely resolved signals in the e.p.r. spectrum (t_s = -196°) (Fig.4, b) with g = 2.007 and 1.991. When the temperature of this system is raised to -78°, the signals disappear, but the signal D corresponding to the non-irradiated specimen becomes quite distinct.

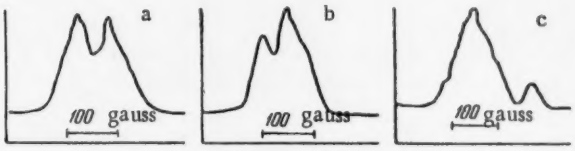

Fig. 4.

Catalyst VIII, with and without adsorbed hydrocarbons, before and after irradiation ($t_{irr.}$ = +20°), gives a weak signal at t_s = + 20°. At t_s = -196°, before and after irradiation with any of the hydrocarbons, the spectrum illustrated in Fig. 4, c is obtained. For these signals g = 2.022 and $\Delta g > 0$ (left-hand signal) or g = 1.952 and $\Delta g < 0$ (right-hand signal); $N = 3.3 \cdot 10^{18}$. These signals are not observed at t_s = -78°, either before or after irradiation.

The adsorption of hydrocarbons on alumina and aluminosilicate catalyst is thus reflected only to a very slight extent in the e.p.r. spectrum, irrespective of the effects of radiation. It is interesting to note the rapid saturation (with respect to concentration) of the U S carriers during the irradiation of catalyst III (dose < 6 Mr) and the hydrocarbons adsorbed on it (dose < 30 Mr), which is not typical of the homogeneous radiolysis of hydrocarbons. On alumina–molybdenum oxide and alumina–chromic oxide catalysts with adsorbed hydrocarbons, irradiation brings about a sharp change in the appearance of the spectrum. The change in the concentration of US carriers with change in the temperature at which the system is heated shows the existence of activation barriers. The most remarkable temperature effects are the absence of signal A when the catalysts are irradiated at $t_{irr.}$ = -196° and the intense signals for the adsorption of all the hydrocarbons on nonirradiated MoS_2 at t_s = -196° and the intense signals for the adsorption of all the hydrocarbons on nonirradiated MoS_2 at t_s = -196°, but not at t_s = -78°. Most of the e.p.r. spectra studied do not have a superfine structure. The latter is observed in the case of the irradiation of catalyst II with heptane and heptene.

LITERATURE CITED

[1] Ya. R. Katsobashvili, N. S. Kurkova, V. S. Likhobabenko, and É. A. Levitskii, "Otchet za 1958 g., Fondy Instituta Neftekhimicheskogo Sinteza Akad. Nauk SSSR" (Report for 1958, Institute for the Synthesis of Petroleum Chemicals, USSR Academy of Sciences).

[2] A. M. Brodskii, Yu. A. Kolbanovskii, et al., Dokl. Akad. Nauk, 122, 1035 (1958).*

[3] N. Ya. Chernyak, N. N. Bubnov, et al., Dokl. Akad. Nauk, 120, 346 (1958).*

*Original Russian pagination. See C. B. translation.

Received June 2, 1959.

THE ADHESION BETWEEN POLYMERS AND MODIFIED GLASS SURFACES IN RELATION TO THE CHARGE REVERSAL PHEOMENA OBSERVED ON SEPARATION*

N. A. Krotova, L. P. Morozova, and Corresponding Member Acad. Sci. USSR B. V. Deryagin

Institute of Physical Chemistry of the Academy of Sciences USSR

In a previous communication [1] we noted that the charge of a polymer torn apart from a glass is reversed after the surface of the latter has been chemically modified. This phenomenon has a strong effect on the adhesion of polymers, while the charge reversal occurs in a region which corresponds to the minimum adhesive force.

The purpose of this work was to carry out a more thorough and concurrent study of the mechanical and electrical adhesion characteristics after the chemical nature of the backing surface has been modified. The backing surface (glass) was treated with organosilicon compounds of the type $(CH_3)_{4-n}SiCl_n$, where n = 1,2,3,4. The principal reagents used were: CH_3SiCl_3 (methyltrichlorosilane), $(CH_3)_2SiCl_2$ (dimethyldichlorosilane) and $(CH_3)_3SiCl$ (trimethylchlorosilane). Before the treatment with alkylchlorosilanes the glass was purified by exposure to a glow discharge [2]. The glass thus treated becomes coated with a thin layer of organosilicon compound, while the HCl evolved during this treatment is removed from the surface by repeated washing and heating at 100°. The glass was modified in such a way that within a series of surfaces thus treated the relative number of methyl groups on the surface increased, while the number of hydroxyls decreased. Each glass surface, after being treated in the above-described manner, was coated with a polymer film in the manner described in [3]; the following polymers were studied: cellulose esters (nitro-, benzyl-, and ethylcellulose), polyvinyl alcohol, gutta-percha, perchlorovinyl, and carboxylate rubbers, copolymers of BSR (Buna-S rubber) with methacrylic acid, with varying carboxyl group content. The polymers were purified by repeated reprecipitation. In each set of experiments the adhesive force between one of the above-listed polymers and a series of modified surfaces was studied. In this way the effects of shrinking stresses on the adhesion work were eliminated. Adhesion was determined from the maximum tearing work at a high rate of tearing (v = 1 cm/sec).

The experiments recorded distinct differences between the various polymers examined. While perchlorovinyl, nitrocellulose, and ethylcellulose exhibit identical adhesive force with respect to a series of modified glasses, the other polymers studied by us exhibit a definite minimum on the glasses treated with dimethyldichlorosilane (Table 1). An aqueous solution of polyvinyl alcohol will readily wet glass surfaces purified in glow discharge, but over surfaces rendered hydrophobic it can only be spread mechanically, and with considerable effort. The force of adhesion, after the film of polyvinyl alcohol was dried, is less by 1-2 orders of magnitude than the force observed on clean glass.

In all the cases where the polymer was torn apart from clean glass the charge on the polymeric surface, as determined by means of a vacuum-tube electrometer [4], was negative. When polymers like perchlorovinyl and nitrocellulose, which exhibit no sharp variations in the adhesion to a series of glasses treated with organosilicon compounds, are torn apart from their respective backings, their charge sign remains the same, whereas other investigated polymers reverse their charge from negative to positive.

*The glass surfaces were chemically modified by A. Ya. Korolev and co-workers in their laboratory.

TABLE 1

Mechanical and Electrical Characteristics of Polymeric Adhesion on Modified Glass Surfaces

Polymer	Organosilicon compound used for treatment of the backing (glass)	Adhesive work A_0 at v = 1 cm/sec, (erg/cm^2)	Charge on the polymer after tearing
Ethylcellulose	Clean glass	$2 \cdot 10^3$	Negative
	CH_3SiCl_3	$4 \cdot 10^3$	Positive
	$(CH_3)_2SiCl_2$	$4 \cdot 10^3$	"
	$(CH_3)_3SiCl$	$4 \cdot 10^3$	"
Gutta-percha	Clean glass	$6{,}3 \cdot 10^3$	Negative
	CH_3SiCl_3	$9 \cdot 10^4$	"
	$(CH_3)_2SiCl_2$	$3 \cdot 10^2$	Positive
	$(CH_3)_3SiCl$	$2{,}8 \cdot 10^4$	"
Polyvinyl alcohol	Clean glass	$1 \cdot 10^5$	Negative
	CH_3SiCl_3	$4 \cdot 10^3$	Positive
	$(CH_3)_2SiCl_2$	$2{,}8 \cdot 10^2$	"
	$(CH_3)_3SiCl$	$1{,}6 \cdot 10^4$	"
Perchlorovinyl	$SiCl_4$	$2 \cdot 10^2$	Negative
	CH_3SiCl_3	$1 \cdot 10^2$	"
	$(CH_3)_2SiCl_2$	$1 \cdot 10^2$	"
	$(CH_3)_3SiCl$	$1 \cdot 10^2$	"
Nitrocellulose	CH_3SiCl_3	$8 \cdot 10^1$	Negative
	$(CH_3)_2SiCl_2$	$8 \cdot 10^1$	"
	$(CH_3)_3SiCl$	$8 \cdot 10^1$	"

TABLE 2

Molar Ratios between the Components of the Tetrachlorosilane – Alkylchlorosilane Mixtures Used for Treating the Glass Surfaces

Sample No.	CH_3SiCl_3	$SiCl_4$	Sample No.	CH_3SiCl_3	$(CH_3)_2SiCl_2$
1	0,0	10,0	11	10,0	0,0
2	0,75	9,25	12	8,0	2,0
3	1,75	8,25	13	6,0	4,0
4	2,5	7,5	14	5,0	5,0
5	3	7	15	4,0	6,0
6	3,75	6,25	16	3,0	7,0
7	4,5	5,5	17	2,0	8,0
8	5,0	5	18	1,5	9,5
9	7,5	2,5	19	1,0	9,0
10	10,0	0,0	20	0,0	10,0

In the experiments described in this work we examined the adhesion of polymers on five types of backing: glass treated with $SiCl_4$, which introduced no new types of groups on the backing surface, glass purified in glow discharge, and glass treated with the three above-described alkylchlorosilanes.

It seemed also interesting to examine the variations in the adhesive forces, as a function of the chemical composition of surfaces which had been treated by various combinations of chloro-substituted silanes in such a manner that within any investigated series of modified surfaces the number of methyl groups increases monotonically. At the same time the study was confronted by the problem of finding the region in which the charge

between the two separated surfaces is reversed and finding if it corresponds to any sharp changes in the adhesive forces. In Table 2 we have listed the compositions of the mixtures used for preparing a series of modified glass surfaces in such a manner that the number of methyl groups steadily increased while the number of hydroxyl groups steadily decreased. We prepared a total of twenty different modified surfaces and studied the adhesion between them and three distinct polymers, all of which exhibited charge-transfer phenomena in our exploratory experiments; these were: benzylcellulose and two representative copolymers between BSR and methacrylic acid, in which the latter constituted 0.3% and 20%, respectively, of the total copolymer weight.

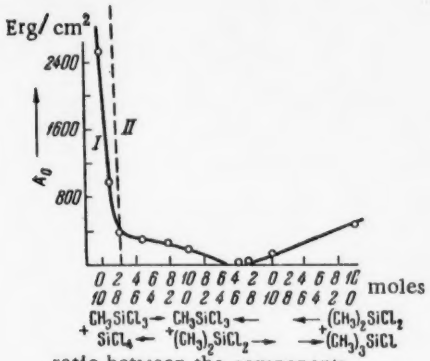
Erg/cm²
2400
1600
800
A₀
I
II
0 2 4 6 8 10 8 6 4 2 0 2 4 6 8 10 8 6 4 2 0
moles
CH₃SiCl₃ → CH₃SiCl₃ ← ← (CH₃)₂SiCl₂
+ SiCl₄ ← + (CH₃)₂SiCl₂ → → (CH₃)₃SiCl
ratio between the components of the modifying mixture.

Fig. 1. Adhesion between benzylcellulose and modified glass surfaces. I) Negatively charged polymer film; II) positively charged polymer film.

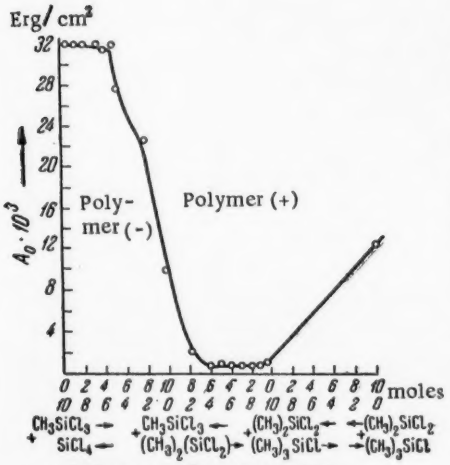

Fig. 2. Adhesive force between BSR-30—methacrylic acid (0.03%) copolymers and modified glass surfaces.

Benzylcellulose gave the most interesting results; its adhesion towards a series of modified glasses (see Table 2, Nos.1-4) sharply declined over a range of values corresponding to a negatively charged polymer film (Fig. 1, I). In the region between samples 4 and 6 the charge is reversed, while further on in region II the surface of the detached polymer film becomes positively charged. The adhesive force in region II changes smoothly, attaining a zero value on samples 13 and 14, then begins to increase relatively fast.

Similar behavior was observed in the case of adhesion between the BSR — methacrylic acid copolymer and modified glass (Fig. 2 and 3). Moreover, in this case the force of adhesion does not decrease to zero, but to a certain minimum value (710 erg/cm² in Fig.2 and 1780 erg/cm² in Fig.3). There is a corresponding decline in the adhesive force by 2 to 3 orders of magnitude from the force on glass treated with $SiCl_4$. The region of negatively charged film covers the contacts with samples 1-10, while the positively charged film appears on samples 10-20. Thus, to reverse the charge of the above-mentioned polymers one requires backings with a higher methyl-group content than in the case of benzylcellulose. The adhesive force (just as in the case of benzylcellulose) rapidly declines and a minimum is observed near the region of charge reversal (samples 12-16).

Hence, the following conclusions can be made concerning the adhesion properties of the polymers studied by us. Depending on the chemical composition of the surface the signs of the two detached surfaces will be reversed. When any one particular polymer is coated on a backing, then torn apart, one observes a region of minimum adhesion (between the two), which is near the region of charge reversal, and in some cases there may even arise a repulsion. Consequently a direct relationship is established between the mechanical and electrical properties of adhesion.

The fact that the observed properties became apparent as a result of chemical changes on the surface indicates the fundamental role of chemical factors in the formation of electrical double layers. Therefore, if, in accordance with the electrical adhesion theory, we assume that the charge on the surfaces torn apart is the resulting charge of the separated electrical double-layer backings, then the reversal in the charges of the separated surfaces seems to indicate a reversal in the charges of the static condenser. Consequently, the untreated surface, which acts as an electron donor in the formation of a double layer, becomes an acceptor due to modification. This change occurs when a certain number of methyl groups become accumulated on the surface, or more precisely, when a certain ratio between the methyl and hydroxyl groups on the backing surface is attained. Most probably the charge on the contact surfaces (i.e., condenser backing) represents the statistical sum of the effects

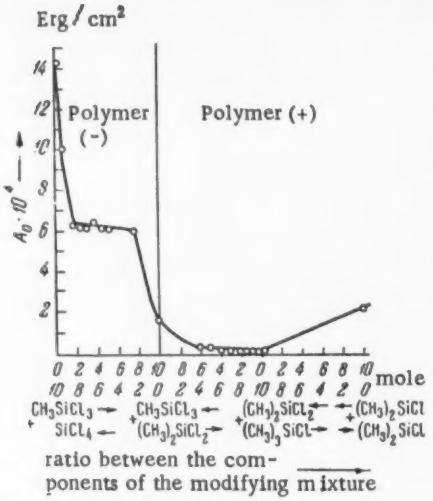
Erg / cm²
Polymer (-)
Polymer (+)
A₀ · 10⁴
mole
CH₃SiCl₃ → + SiCl₄ →
← CH₃SiCl₃ + ← (CH₃)₂SiCl₂ →
← (CH₃)₂SiCl₂ + ← (CH₃)₃SiCl →
← (CH₃)₃SiCl + ← (CH₃)₂SiCl
ratio between the components of the modifying mixture

Fig. 3. Adhesive forces between the copolymer of BSR-30 with methacrylic acid (20%) and modified glass surfaces.

resulting from the interaction between individual molecular groups on the adhering surfaces. When a film is deposited on a modified backing and an electrical double layer arises, the surface charge density declines within the series to the point of charge reversal, after which point the donor-surface becomes an acceptor-surface and the double-layer formation on members of the series becomes a qualitatively different process.

In concluding, the authors wish to express their gratitude to A. Ya. Korolev, in whose laboratory the glass surfaces were modified.

LITERATURE CITED

[1] L. P. Morozova, and N. A. Krotova, Colloid J. 20, 59 (1958).*

[2] V. V. Karasev and G. I. Izmailova, J. Tech. Phys. 24, 871 (1954).

[3] N. A. Krotova, V. V. Karasev and Yu. M. Kirillova, Trans. Inst. Phys. Chem., Acad. Sci. USSR, No.6, New Methods in Physicochemical Research, Izd AN SSSR, 111 (1957).

[4] N. A. Krotova and L. P. Morozova, Proc. Acad. Sci. USSR, No.1 (1959).*

Received July 2, 1959

*Original Russian pagination. See C. B. translation.

THE THEORY OF STATIONARY COMBUSTION IN POWDERS

A. G. Merzhanov and F. I. Dubovitskii

Institute of Chemical Physics of the Academy of Sciences USSR

(Presented by Academician N. N. Semenov, June 13, 1959)

According to the theory of Ya. B. Zel'dovich [1], the combustion of solid powders is accompanied by endothermic or slightly exothermic reactions, the products of which burn in the gas phase evolving the main amount of heat produced. The gas-phase reaction is responsible for, and determines, the course of combustion. Variations in the amount of heat conducted to the powder surface affect the evaporation rate and control the rate of the gas-phase reaction. Zel'dovich set up a mathematical equation for the rate of combustion as a function of the gas-phase parameters.

In the present work the combustion of powders is examined from the standpoint of processes taking place in the solid phase, and equations are derived connecting the temperature gradient in the powder and the combustion rate to the thermokinetic characteristics of solid-phase reactions and to the thermal flux from the gas phase.

Designations: T = temperature, T_s = temperature on the surface of the burning powder; T_0 = temperature away from the combustion zone; x = coordinates of distance (cm); x_r = width of the chemical reaction zone (cm); x_t = thickness of the hot layer (cm); u = combustion rate (cm/sec); q = thermal flux ($cal/cm^2 \cdot sec$); Q_t = heat content (cal/cm^2); p = pressure (kg/cm^2); a = temperature coefficient (cm^2/sec); c = specific heat ($cal/g \cdot deg$); ρ = density (g/cm^3); λ = thermal conductivity ($cal/cm \cdot sec \cdot deg$); Q = heat of the solid phase reactions (cal/cm^3); k_0 = frequency factor (sec^{-1}); E = activation energy (cal/mole); θ = reduced temperature; ξ = reduced coordinate; ω = reduced combustion rate.

The most important and general assumptions made in deriving the equations were: that the reactions are exothermic* ($Q > 0$) and that the reaction rate $\omega = k_0 e^{-E/RT}$. The specificity of solid-phase processes was neglected.

The starting system of equations, with the usual combustion theory approximations, looks as follows:

$$a \frac{d^2T}{dx^2} + u \frac{dT}{dx} + \frac{Q}{c\rho} k_0 e^{-E/RT} = 0, \tag{1}$$

$$u = \int_0^\infty k_0 e^{-E/RT(x,\,u)}\, dx \tag{2}$$

with the boundary conditions: $x = 0$, $T = T_s$; $x = \infty$, $T = T_0$.

Equation (1) is a thermal conductivity equation in which the source of heat is continuously distributed and the coordinate system is with reference to the solid phase (Fig. 1). The combustion rate in this equation

*An experimental investigation, carried out by Pokhil [2], showed that the over-all processes taking place in the solid phase of a burning powder are exothermic.

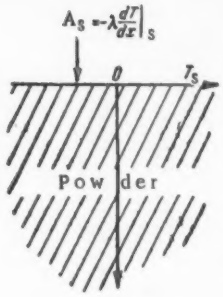

Fig. 1.

appears as a constant. Equation (2) relates the combustion rate (rate at which the solid phase is consumed) to the temperature gradient in the powder. Equations (1) and (2) are solved in the following manner: From Equation (1) the temperature gradient T(x,u) is determined and substituted in Eq. (2). In order to solve Equation (2) for u, one has to solve a system of integral equations, which will give the desired combustion rates as a function of parameters determined by the type of system and boundary conditions. The first solution of the thermal conductivity equation, with Equation (2) and boundary conditions considered,

$$q_s + Qu = c\rho u (T_s - T_0) \tag{3}$$

represents the net heat content of the solid phase and relates the thermal flux and the combustion rate to the surface temperature. Equation (3) can be used to find out what fraction of the heat used for heating the cold layers of the powder is liberated from the solid phase:

$$\alpha = \frac{Q}{c\rho (T_s - T_0)} . \tag{4}$$

Equations (1) and (2) are conveniently transformed into a dimensionless form *:

$$\frac{d^2\theta}{d\xi^2} + \frac{d\theta}{d\xi} - \frac{1}{\gamma\omega^2} e^{-\theta} = 0; \tag{5}$$

$$\omega^2 = \int_0^\infty e^{-\theta(\xi, \omega)} d\xi; \tag{6}$$

$$\xi = 0, \quad \theta = 0, \quad \frac{d\theta}{d\xi} = \theta_0 - \frac{1}{\gamma};$$

$$\theta = \frac{E}{RT_s^2}(T_s - T), \quad \xi = \frac{ux}{a};$$

$$\theta_0 = \frac{E}{RT_s^2}(T_s - T_0), \quad \gamma = \frac{c\rho}{Q}\frac{RT_s^2}{E},$$

$$\omega^2 = \frac{u^2}{k_0 e^{-E/RT_s} a}.$$

The solution of this system of equations has the general form:

$$\theta = \theta(\xi, \gamma, \theta_0 - \frac{1}{\gamma}); \quad \omega = \omega(\gamma, \theta_0 - \frac{1}{\gamma}).$$

We can get an approximate solution by neglecting (see Ya. B. Zel'dovich [4]) the heat used for heating the powder in the reaction zone, i.e., by assuming that all the heat evolved in the reaction zone is conducted away.

The approximate system of equations:

$$\frac{d^2\theta}{d\xi^2} - \frac{1}{\gamma\omega^3} e^{-\theta} = 0; \qquad \omega^2 = \int_0^\infty e^{-\theta(\xi, \omega)} d\xi;$$

$$\xi = 0, \qquad \theta = 0, \qquad \frac{d\theta}{d\xi} = \theta_0 - \frac{1}{\gamma}$$

*In the transformation into dimensionless variables we used the series expansion of exponential functions developed by Frank-Kamenetskii [3] while the boundary condition for ∞ was replaced by an appropriate equation [3].

is solved analytically, and the expression for the rate assumes the simple form:

$$\omega^2 = \frac{1}{\theta_0 - 1/2\gamma}, \tag{7}$$

or in dimensional variables:

$$u^2 = ak_0 e^{-E/RT_s} \frac{RT_s^2/E}{T_s - T_0 - \frac{1}{2}\frac{Q}{c\rho}}. \tag{8}$$

Using this approximation it is also possible to estimate the width of the chemical reaction zone*:

$$\xi_r = \omega \sqrt{\frac{\gamma}{2}}\, \varphi(b),$$

$$\varphi(b) = \frac{1}{\sqrt{b}} \left\{ \ln \frac{\sqrt{b} - \sqrt{b-1}}{\sqrt{b} + \sqrt{b-1}} - \ln \frac{\sqrt{b} - \sqrt{b - \frac{1}{e}}}{\sqrt{b} + \sqrt{b - \frac{1}{e}}} \right\}, \tag{9}$$

$$b = 1 + \frac{\gamma\omega^2}{2}\left(\theta_0 - \frac{1}{\gamma}\right)^2.$$

Essentially, the heat content and the thickness of the hot layer are related by a Michelson distribution, and have the form:

$$q_t = \frac{uQ_t}{\lambda(T_s - T_0)} = 1 \qquad \text{(Leipunskii's equation, [5])} \tag{10}$$

$$\xi_t = 1. \tag{11}$$

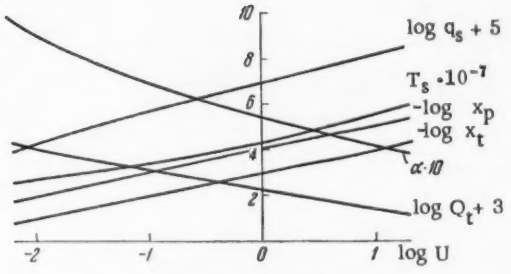

Fig. 2. The fundamental combustion characteristics of a pyroxylene powder as a function of the combustion rate.

TABLE 1

	ω	ξ_r	q_t	ξ_t
Numerical integration	0,362	0,135	1,045	2,28
Approximate calculation	0,329	0,114	1,0	1,0
Deviation, in %	9,1	15,5	4,3	21,8

In order to verify our approximate equations we numerically integrated Equations (5) - (6) (substituting large parameters $1/\gamma = 15.5$; $\theta_0 = 17.0$). The calculated results are presented in Table 1.

As may be seen in Table 1 the approximate equations are entirely satisfactory.

*By the term "width" we mean the distance across which the chemical reaction rate declines by a factor of $\underline{e}$.

It is interesting to note that for the limiting case $\gamma \to \infty$, where the amount of heat produced in the solid phase can be neglected in comparison with the heat absorbed from the gas phase, Equations (5) - (6) have an analytical solution, and the rate expression becomes:

$$\omega^2 = e^{-\theta_s} \mathrm{Ei}(\theta_0),$$

where $\mathrm{Ei}(\theta_0) = \int_{-\infty}^{\theta_s} \frac{e^x}{x}\,dx$ is an exponential integral function.

TABLE 2

p, kg/cm².	u, cm/sec.	α	T_s °C	q_s, cal/cm² · sec	Q_t, cal/cm².	x_t, cm.	x_r, cm.
1	0,07	0,73	330	3,2	2,4	$1{,}6\cdot10^{-2}$	$1{,}4\cdot10^{-2}$
40	1,0	0,55	440	$1\cdot10^{2}$	$2{,}2\cdot10^{-1}$	$1\cdot10^{-3}$	$8\cdot10^{-5}$
800	10,8	0,42	560	$1{,}6\cdot10^{3}$	$2{,}8\cdot10^{-2}$	$1\cdot10^{-4}$	$8\cdot10^{-6}$

From the derived Equations (3), (4), (8) - (11) we obtained numerical solutions for pyroxylene powder. The initial values used in our calculations were: $a = 1\cdot10^{-3}$ cm²/sec; $c = 0.35$ cal/g · deg; $\rho = 1.6$ g/cm³; $Q/\rho = 80$ cal/g [2]; $k_0 = 10^{17.8}$ sec^{-1}, and $E = 44600$ cal/mole (Samsonov's values for pyroxylene No.1 [6]), $T_0 = 20°$.

The calculated results are presented in Fig. 2 and partially in Table 2. Due to a lack of satisfactory values for the heat evolution kinetics and for the function Q (P), these results have to be considered solely as rough approximations.

LITERATURE CITED

[1] Ya. B. Zel'dovich, J. Exptl. Theoret. Phys. 12, 498 (1942).

[2] P. F. Pokhil, Doct. Dissert., Moscow, 1954.

[3] D. A. Frank-Kamenetskii, J. Phys. Chem. 13, 738 (1939).

[4] Ya. B. Zel'dovich and D. A. Frank-Kamenetskii, J. Phys. Chem. 12, 100 (1938).

[5] Z. I. Aristova and O. I. Leipunskii, Proc. Acad. Sci. 54, 507 (1946).

[6] K. K. Andreev, Thermal Decomposition and Combustion of Explosives, Moscow, 1957.

Received June 10, 1959.

THE THEORY OF LOW-PRESSURE DECOMPOSITION OF OF NITROUS OXIDE

E. E. Nikitin

Institute of Chemical Physics of the Academy of Sciences USSR

(Presented by Academician V. N. Kondrat'ev, June 15, 1959)

The thermal decomposition of nitrous oxide constitutes one of the most thoroughly investigated reactions, and many papers have been devoted to its examination (see for example [1]). Recently Gill and Laidler [2], have attempted to calculate the rate constants for the decomposition of N_2O from the standpoint of the Cassell-Slater theory on the basis of the available experimental data, and concluded that at low pressures this constant may be computed from the Cassell equation by assuming two effective degrees of freedom, and that deformation vibrations do not contribute to the decomposition rate constant $\underline{k}$. This interpretation of the decomposition does not take into account, however, the following two facts.

First, according to Kassel's theory, only the degrees of freedom with the energy exchange time much smaller than the time interval between successive molecular collisions, $\tau_0 = 1/Z$ (Z is the number of molecular collisions per unit time), will affect the dissociation. It can be easily demonstrated that in the case of N_2O decomposition, the condition $\tau \ll \tau_0$ holds for all the degrees of freedom. In fact, the bimolecular decomposition kinetics were studied under pressures of $p \approx 10^2$ mm [2,3]; under these conditions $Z = 10^9$ sec^{-1}. The maximum value of τ can be approximated by analyzing the energy exchange between the normal vibrations of N_2O molecules. The exchange rate is proportional to the coefficient of vibrational anharmonicity and is determined from the parameters for the triple interaction between bonds and angles in the series expansion of the potential energy (with reference to the real coordinates). We can, therefore, write $1/\tau \approx \omega\gamma$ where ω is the vibrational frequency and γ the coefficient of anharmonicity. The value of γ can be determined by two methods: either from the ratio between the overtones and the fundamental frequencies, or from the relative frequency shift of the first vibrational transition relative to the frequency of small (purely harmonic) vibrations. As is well known, the relative intensity of the overtones is about 10^{-2} [4]; the relative frequency shift gives the same value. The latter can be obtained, for example, from analysis of the CO_2 molecular spectrum [5], the electronic structure and the fundamental frequencies of which are very similar to the structure and frequencies of N_2O. If we accept the value of γ given above and assume an $\omega = 10^{14}$ sec^{-1}, then we will get a τ of the order of 10^{-12} sec. Thus the condition that $\tau \ll \tau_0$ is fulfilled. Since the relative importance of anharmonicity increases with increasing vibrational energy, for the case under consideration (a vibrationally excited molecule), this inequality will become greater. Consequently, within the framework of Kassel's theory, one should take into account four instead of two vibrational degrees of freedom.

Second, the decomposition rate at low pressures depends on the activation rate, i.e., on the vibrational excitation rate of the decomposing molecules near the dissociation boundaries. Kassel's theory assumes that this rate is equal to the collision frequency Z. According to the collision theory such a large excitation effectiveness could only be explained by assuming that the vibrational quanta near the dissociation boundary are small and that the collisions are nonadiabatic [6]. This, however, is not the case in the thermal decomposition of N_2O, because the process involves a change in the multiplicity:

$$N_2O\,(^1\Sigma) \rightarrow N_2O\,(^3\Sigma) \rightarrow N_2\,(^1\Sigma) + O\,(^3P). \qquad (1)$$

The point of intersection between the singlet, 1Σ, and triplet, 3Σ, potential curves, which defines the activation energy (E_{act} = 60 kcal/mole), falls where the lower potential curve changes its direction abruptly, so that the vibrational quanta are not appreciably reduced near the dissociation boundary. If the molecule N_2O is to decompose, its total vibrational energy must exceed the activation energy, E_{act}; at the same time the decomposition will occur within a time interval $1/\omega P$, where P denotes the probability of a singlet→triplet transition. The probability P, determined from the experimental rate constants for the monomolecular decomposition of N_2O, is of the order of 10^{-1} to 10^{-2} [2]. Since the minimum amount of energy, ΔE, which can be transferred during a collision should be close to the quanta of deformation vibrations (~600 cm^{-1}), then according to the general collision theory the effectiveness of vibrational excitation should be smaller than Z by several orders of magnitude [7].

The above-noted features of the decomposition theory can be taken into account simultaneously if we apply the variation of the bimolecular decomposition theory in which a perturbed Boltzman distribution is assumed [6]. According to the results reported in [6] the decomposition rate constant depends on the value of $\mu_0 = \mu_0(\Delta E)$, averaged over all the vibrational and electronic states of the dissociating molecule. The rate constant for the decomposition of a nonrotating diatomic molecule can be calculated from the equation:

$$\mu_0 = Z \Big/ \left[\frac{1}{x_n^{(0)} P_\infty} + \sum_{n=0}^{n_0-1} \frac{1}{x_n^{(0)}} P_{n,\,n+1} \right], \qquad (2)$$

where $x_n^{(0)}$ is the normalized equilibrium vibrational distribution function, $P_{n,\,n+1}$ the probability of a one-quantum vibrational excitation, and P_∞ the probability of transitions into the dissociated state. Equation (2), which was derived for diatomic molecules, can be extended to polyatomic molecules. To do this, one simply has to consider the increased vibrational statistical weight, g_{vib}, of all the energy levels with $E \simeq E_{act}$. This is easily accomplished if we remember that the dissociation occurs as a result of antisymmetric vibrations, ω_3, of the N_2O molecule (since the N_2O molecule is not symmetrical, the term antisymmetric vibrations simply means that the displacements of the nitrogen and oxygen atoms from the equilibrium position are out of phase). The remaining vibrations (symmetrical bond vibration ω_1 and two deformation vibrations ω_2) act as an energy pool. Hence we find that

$$g_{vib} \approx (E_{act}/\hbar\omega_1)(E_{act}/\hbar\omega_2)^2/Q \cdot 3!, \qquad (3)$$

where Q is the sum of all the energy states in three oscillators, one with a frequency ω_1 and two with doubly degenerate frequencies ω_2. If we assume that $\omega_1 = \omega_2$, then we will get a well-known expression for the degree of degeneracy of a $E = E_{act}$ level in a system composed of four harmonic oscillators. Equation (3) is only an approximation, since it does not take into account the decrease in frequency caused by anharmonicity. The probable error resulting from this omission may increase g_{vib} by a factor of 2-3.

In our case the transition into a dissociated state corresponds to a transition from a group of uppermost layers, which are located below the intersection point of the singlet and triplet potential curves, into the nearest layers just above this intersection point. Let us denote the probability of such a transition by $P(\Delta E)$. Since the excitation energy ΔE, which denotes an energy difference between two groups of closely packed levels, changes very little near the dissociation boundary, while the function $1/x_n^{(0)}$ rapidly decreases with decreasing energy, the substitution $P_{n,n+1} = P_\infty = P(\Delta E)$ is permissible in summation (2); this yields the equation:

$$\mu_0 = Z g_{vib} P(\Delta E) \exp(-E_{act}/kT). \qquad (4)$$

When this expression is averaged over the rotational and electronic states, two additional coefficients, g_{rot} and g_{el}, appear. A simple calculation, similar to that shown in [6], gives $g_{rot} = 2$. As far as g_{el} is concerned, it was found that the electronic state $^1\Sigma_u^+$ of the N_2O molecule, spectroscopically combined with the ground state, lies above the dissociation boundary (~3000A). On the basis of qualitative graphs, plotted by Walsh [8], one can conclude that there also exist terms $^1\Delta_u$ and $^1\Sigma_g^+$ between the ground state $^1\Sigma_g^+$ and $^1\Sigma_u^+$, so that the possible value of g_{el} is in the range of 1-3. Substituting into Eq. (4): $g_{rot} = 2$, $g_{el} = 1$, E_{act} = 60 kcal/mole, T= 888° K, $Z = 2 \cdot 10^{14}$ cm^3/mole · sec, $\omega_1 = 1284$ cm^{-1}, $\omega_2 = 588$ cm^{-1}, and $\omega_3 = 2238$ cm^{-1}, we get:

$$k \approx P(\Delta E) \cdot 2 \cdot 10^4 \ \text{cm}^3/\text{mole} \cdot \text{sec}. \tag{5}$$

The probability of the vibrational excitation P (ΔE) can be calculated from the Schwartz-Herzfeld equation [7]:

$$P(\Delta E) \approx |(\alpha \Delta q)_n^{n+1}|^2 (\pi \Delta E / \varepsilon_0)^2 \chi^{1/2} \exp[-3\chi - \Delta E / 2kT], \qquad \chi = [\pi (\Delta E)^2 / 4\varepsilon_0 kT]^{1/2}, \ \varepsilon_0 = \hbar^2 \alpha^2 / 2m. \tag{6}$$

Here Δq denotes the vibration amplitude, α^{-1} the range of exchange forces, m the reduced mass of two colliding molecules. In our case, the vibration amplitude of the vibrationally excited molecule is approximately equal to the radius in which exchange forces operate, and hence we assume that $(\alpha \Delta q)_n^{n+1} \approx 1$. For α, we will pick its usual value in the expression $\alpha^2 = 5 \cdot 10^{16} \text{cm}^{-1}$. Since the probability P(ΔE) rapidly decreases with increasing transition energies (ΔE), its value will be determined by the smallest quantum. We should, therefore, only consider the deformation vibration frequencies, taking into account the anharmonicity produced before dissociation. The appropriate calculations yield $\Delta E \approx 550 \ \text{cm}^{-1}$. Substituting these parameters into Eq. (6) we get:

$$P(\Delta E) = 4 \cdot 10^{-4}, \tag{7}$$

so that we finally get the decomposition rate constant:

$$k \approx 10 \ \text{cm}^3/\text{mole} \cdot \text{sec}. \tag{8}$$

The value of k obtained by Gill and Laidler [2], who extrapolated the experimental data to zero pressure (at the same temperature, T =888°K), is:

$$k_{\text{extrap.}} = 14 \ \text{cm}^3/\text{mole} \cdot \text{sec}. \tag{9}$$

It is obvious that the satisfactory agreement obtained between the calculated and experimental rate constants is only true within the accuracy of an order of magnitude. It is essential, however, to note that if the deformation vibrations are not taken into account at all, but the small effectiveness of vibrational excitation is considered, the calculated decomposition rate constants are smaller than the experimental by two to three orders of magnitude.

The basic conclusions of this work can also be extended to nonadiabatic decompositions of other molecules; the rates of nonadiabatic thermal decompositions of molecules, which in the case of monomolecular decompositions depend on the transition rate from one potential curve to another and are accompanied by a change in multiplicity, will be limited by the vibrational activation rates in the case of bimolecular decompositions. The latter fact is connected with the relatively large values of the vibrational quanta near the intersection point of two potential curves with varying multiplicities.

We wish to express our gratitude to Prof. N. D. Sokolov for a discussion of this work.

LITERATURE CITED

[1] V. N. Kondrat'ev, Kinetics of Chemical Gas Reactions, Izd AN SSR 1958 [In Russian].

[2] E. K. Gill and K. J. Laidler, Canad. J. Chem., 36, 1570 (1958).

[3] H. S. Johnston, J. Chem. Phys., 19, 663 (1951).

[4] G. Herzberg, The Structure and Spectra of Diatomic Molecules (IL, 1949) [Russian translation].

[5] T. Wentink, J. Chem. Phys., 30, 105 (1959).

[6] E. E. Nikitin, Proc. Acad. Sci. 119, 527 (1958).*

[7] R. N. Schwartz and K. F. Herzfeld, J. Chem. Phys., 22, 767 (1954).

[8] A. D. Walsh, J. Chem. Soc., 1953, 2266.

Received June 12, 1959.

*Original Russian pagination. See C. B. translation.

THE EFFECT OF ULTRASONIC VIBRATIONS ON THE ABSORPTION OF CARBON DIOXIDE BY WATER

V. Yu. Orlov and Corr. Member Acad. Sci. USSR

N. M. Zhavoronkov

L. Ya. Karpov Physicochemical Scientific Research Institute

In studying the effects of ultrasonic vibrations on absorption it is important to select conditions where the rate-determining step is the diffusion into the liquid phase. In this work we studied the effect of ultrasonic vibrations on the absorption (solution) rate of carbon dioxide in water; as is well known, in this case the mass transport depends on the drag in solution [1].

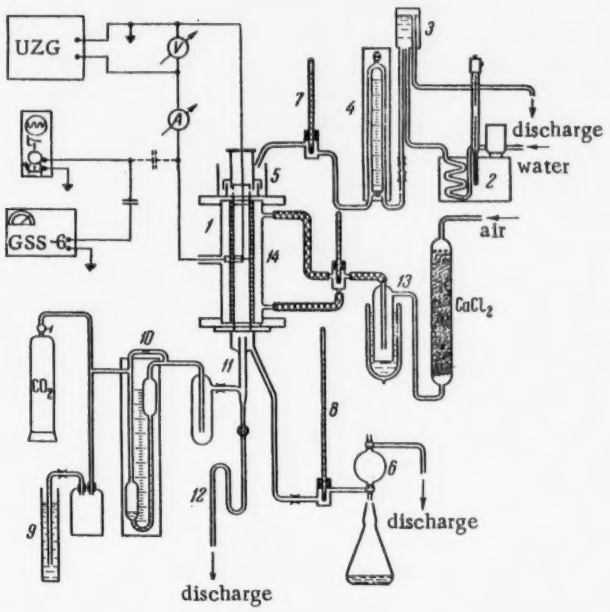

Fig. 1. Experimental set-up.

Preliminary experiments were carried out in a beaker which was filled with water and exposed to pure CO_2; ultrasonic vibrations with a frequency of 800 kcycles/sec and an intensity of several watts per cm^2 were introduced through the bottom of the beaker. It was found that ultrasonic vibrations (which produced a water spout) increased the absorption rate by a factor of 100, as compared to the usual diffusion rate, and by one order of magnitude in comparison with the absorption rate observed when a four-blade stirrer was used at 800-1800 rpm.

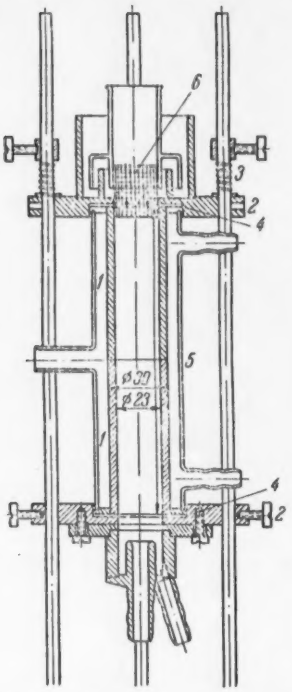

Fig. 2. Design of the ultrasonic column: 1) barium titanate cylinders; 2) plexiglas flanges; 3) springs; 4) rubber washers; 5) glass jacket; 6) a mesh to ensure an even distribution of the film.

Such an increase in the absorption rate could be attributed to a greatly increased area of phase contact, with the contact rapidly renewed due to the formation of spray and mist, and also due to the vigorous stirring of the solution. It should be noted that despite strong cavitation, no degassing of solution was observed; within several minutes after the beginning of the experiment the concentration of CO_2 in water attained its equilibrium value for the given temperature.

The experiments* designed to study the continuous absorption of CO_2 were carried out in two medium-size ultrasonic film columns, using open barium titanate cylinders as emitters.

The use of radially (across the wall thickness) polarized barium titanate cylinders is particularly suited to this experiment, since, first of all, the emitter itself can be used as a film absorption column, and second, each emitter has two characteristic vibration frequencies (perpendicular to the line of film flow) — one across the wall width, another around the circumference. This makes it possible to study the effect of ultrasonic frequencies on absorption, without changing any other conditions.

The apparatus is shown diagramatically in Fig. 1. Column 1 is supplied with a high-frequency voltage from the generator UZG; the oscillograph ÉO-7 and generator GSS-6 permit a determination of the vibrational frequency. Conductivity water is passed through thermostat 2, manostat 3, rheometer 4, and trap 5 into the upper end of the column; a large portion of the water running out of the column passes through receiver 6, from which 50 ml samples are removed for analysis. The temperatures t_1 and t_2, at the entrance and the exit of the column, respectively, are measured with thermometers 7 and 8, respectively; the intensity of ultrasonic vibrations can be estimated from the difference between t_1 and t_2.

Carbon dioxide, the delivery of which is regulated by manostat 9 and measured by rheometer 10, is fed into the column from below through tube 11 and emerges above through a narrow opening left for the grounding wire; seal 12 helps maintain a slightly positive pressure. The cylinders are cooled externally with air; the latter is passed through trap 13, which is submerged in liquid air, and through jacket 14, and consequently, there is no need to apply a polarizing voltage to the barium titanate.

A detailed drawing of one of the columns is shown in Fig. 2. The cylinders (1) are compressed between the flanges (2) by means of springs (3). The net (6) distributes the liquid evenly over the entire wetted surface. The column characteristics are listed in Table 1.

Generators GU-3 and RFT-602 were used to induce vibrations in the cylinders. A high frequency, 150 volt, current was superimposed on each emitter; the ultrasonic waves penetrating into the columns and the film had an intensity of several watts per cm^2. The intensity was calculated from the equation:

$$I = 4{,}18 \frac{v}{S_{\text{emit}}} (t_2 - t_1),$$

where V is the volume of water wetting the column. Since the cylinders were not maintained sufficiently cold, the resulting values of I might be slightly too high. The mass transport in our columns, in the absence of ultrasonic vibrations and under a series of temperatures and water flow rates corresponding to our experimental

*R. A. Ivanova participated in these experiments.

conditions (Table 3), was calculated by the method developed by Higbie [2]. The relative concentration of the dissolved gas in the water which had run down the column is:

$$C/C_{eq} = 200S/v\sqrt{D/\pi\tau},$$

TABLE 1

Some Dimensions and Properties of Ultrasonic Columns

Column characteristics	Column 1	Column 2
Barium titanate cylinders*	Nos. 1,2	Nos. 3,4
The total length of two cylinders, mm.	135	153,4
External diameter, mm.	18,5	30,0
Internal diameter, mm.	12,2	23,0
Internal surface of emitters, cm^2	51.3	111
Cylinder surface	Silvered	Silvered, covered with glass
Electrode contacts	Locked	Soldered
Vibration frequency f_t (transverse), kcs.	800	780
Vibration frequency f_d (diametrical), kcs.	100	50

*Cylinders Nos. 1 and 2 were made in the State Electroceramics Institute, Nos. 3 and 4 in the Acoustical Institute of the Acad. Sci. USSR.

TABLE 2

Column 1, h - 14 cm, S ≃ 53 cm^2			Column 2, h = 16 cm, S ≃ 116 cm^2.		
t, °C	C/Ceq, %	C/Ceq, %	t, °C	τ, sec	C/Ceq, %
v = ml/min, w = cm^2/sec.			v = 500 ml/min, w = 1,15 cm^2/sec.		
10	0,48	14,9	5	0,35	8,8
15	0,46	16,0	10	0,33	9,6
20	0,44	17,1	15	0,32	10,4
25	0,42	18,3	—	—	—
v = 200 ml/min, w = 0,88 cm^2/sec			v = 560 ml/min, w = 1.29 cm^2/sec		
5	0,36	9,9	—	—	—
10	0,35	10,8	10	0,31	8,9
15	0,33	11,6	15	0,29	9,6
20	0,32	12,4	20	0,28	10,3
25	0,31	13,3	25	0,27	11,0
30	0,30	14,0	30	0,26	11,6

where C is the concentration of CO_2, C_{eq} the equilibrium concentration at the given temperature, S the absorption surface, D the diffusion coefficient for CO_2 in water, and τ the duration of absorption. The calculated results are valid if the condition:

$$Dh/w\delta \leqslant 0{,}02,$$

is fulfilled [3]; this condition was satisfied for all the calculated points. In this equation h is the height of the absorption column, w the wetting density per unit circumference length, and δ the thickness of the film.

The variation of C/C_{eq} with temperature can be described by an equation of the type $C/C_{eq} = a(1+0.02t)$, as seen in Table 2. Thus, the absorption of CO_2 is increased by about 2% for an increase of one degree centigrade. Our experimental values of C/C_{eq} are in good agreement with the calculated.

Our experimental conditions are presented in Table 3. Introduction of ultrasonic vibrations produced a substantial change in the flow pattern of the liquid in the column. Whereas in the absence of ultrasonic vibrations the water runs down as a smooth (or occasionally slightly rippled) film, in the presence of ultrasonic vibrations there arises a system of glittering, transverse, standing waves. In experiments carried out using column 1 the waves were usually circumferential and regularly spaced at 3 mm intervals at an 800 kcs frequency, or at 1 cm intervals at a 100 kcs frequency. Experiments carried out in column 2 gave short, irregular, rippled waves at both frequencies. When a 50 kcs frequency was used, there also appeared cavitation of the film in the form of two bonds facing towards the middle of the cylinder (lengthwise). The band width extended over 20 to 100% of the cylinder height, depending on the intensity of ultrasonic vibrations. A small amount of spray, which was formed at this frequency, also enabled us to observe the standing waves in the gas phase, since the spray particles were retained within vibrational angles in the form of three concentric rings (in one plane) around the cylinder axis.

In Fig. 3 we have plotted the increase of the relative concentration of CO_2 in water as a function of ultrasonic vibration frequency. The coordinate is in units of:

$$Q = \frac{(C/C\,eq)usv}{(C/C_{eq})no\ usv}.$$

TABLE 3

Experimental Conditions.

Column No.	Experiment No.	Frequency, f, kcs.	Flow rate of water, v, ml/min.	Wetting density w, cm²/sec.	Temp. of entering water t_1, °C.	Max. temp. drop t_2-t_1, °C.	Max. increase of relative conc., Q_{max}.
1	1	800	123	0,54	15	11	2
	2	800	200	0,88	15	7	2,4
	3	800	200	0,88	15	15	2,6
	4	800	200	0,88	6—9	12	2,5
	5	800	200	0,88	8	12	2,5
	6	100	200	0,88	6	5	1,9
2	2′	49	500	1,15	4	5	3,0
	3′	51	560	1,29	20	9	3,7
	4	790	560	1,29	20	4	1,7
	5′	770	500	1,15	4—5	7	2,2

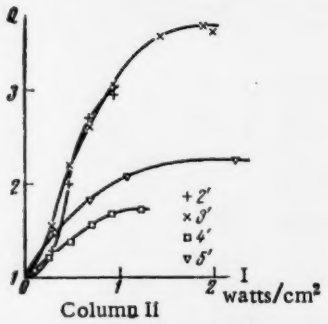

Column II

Fig. 3. Increased absorption rate resulting from ultrasonic vibrations-column No.2.

The equilibrium concentration C_{eq} was chosen as that at the average column temperature, $t_{av}=\frac{t_1+t_2}{2}$.

The maximum values of Q attained in each experiment are also listed in Table 3. As may be seen from the Figure and the Table, the absorption rate is considerably increased by ultrasonic vibrations. The frequency of 50 kcs was most effective. With an intensity of 1-2 watt/cm² the relative concentration increased almost four times; the same intensity at 800 kcs gave only 2 to 2.5-fold increase. The effects of 100 kcs vibrations were no different from the 800 kcs.

On the basis of visual observations, it seems that the increased interphase contact area, resulting from the wave formation, was not large enough to account for the observed increase in the absorption rate. The calculations shown above indicate that any increase in the mass transfer on account of the temperature rise (caused by ultrasonic vibrations) was also insignificant. For example, in experiment No.3 this factor could only account for a 16% increase in C/C_{eq} – the observed amount is 160%. It seems that the increased absorption rate was mainly connected with the film turbulence caused by ultrasonic vibrations; evidently, at 50 kcs the turbulence was also helped by cavitation.

Unfortunately, when the ultrasonic vibration intensity was increased above 2-3 watt/cm², the film of the thickness used in our experiments usually dried out partially, with dry spots appearing on the column surface. This phenomenon arose not only due to the increased heating of the cylinders, but also on account of a less uniform distribution of the liquid along the circumference of the tube, also caused by ultrasonic vibrations.

In concluding the authors wish to express their gratitude to B. I. Konobeev for a discussion of this work.

LITERATURE CITED

[1] N. M. Zhavoronkov, V. A. Malyusov and N. A. Malafeev, Chem. Ind. No.8, 240 (1951).

[2] R. Higbie, Trans. Am. Inst. Chem. Eng., 31, 325 (1935).

[3] V. V. Vyazovov, J. Tech. Phys. 10, 1519 (1940).

Received July 6, 1959.

DETERMINATION OF "UNPERTURBED" MACROMOLECULAR DIMENSIONS IN GOOD SOLVENTS

O. B. Ptitsyn

Institute of High-Molecular Compounds of the Academy of Sciences

(Presented by Academician V. A. Kargin, June 11, 1959)

As is well known, by studying the dimensions of polymeric molecules in solution one can get some idea about their chain flexibility and stereochemical configuration [1-5]. To do this, however, it is necessary to carry out the measurements at Flory's θ-temperature [2], temperature at which the solution behaves ideally, or, in other words, under conditions where the second virial coefficient A_2 in the series expansion of the osmotic pressure (with concentration as the variable) is zero. In good solvents the macromolecular dimensions depend to a large extent on higher-order interactions between chain segments and between chains and solvent molecules. Current theories of higher-order interactions have established a relationship between the "swelling coefficient" of a macromolecule which is transferred from the θ-point to a good solvent and the thermodynamic physical constants characterizing the corresponding polymer – solvent system [6].

Since the second virial coefficient can also be expressed in terms of these thermodynamic constants, it is possible to derive a theory which would interconnect the macromolecular dimensions in a given solvent, the second virial coefficient, and the molecular weight of the polymer, with the macromolecular dimensions (unperturbed by higher-order interactions [6]) in the θ-solvent. Such a theory would permit the determination of unperturbed macromolecular dimensions by means of experiments carried out in good solvents, without resorting to measurements at the θ-point. This would be particularly important in the case of crystallizable polymers, the solutions of which are metastable with respect to the crystalline state at temperatures below their melting point, since in transition to poorer solvents the polymer precipitates before point-θ is attained (in case the latter lies below the melting point). Hence, for polymers with a regular structure, and other polymers with a high melting point, the θ-point measurements have to be carried out at high temperatures, which obviously presents considerable experimental difficulties.

The theoretical treatment of the second virial coefficient developed by Flory, Krigbaum, and Orofino [2,6,7] does not provide a satisfactory agreement with the experimental data, particularly in poor solvents, near the θ-point. The improved theory of A_2, developed by Casassa and Markovitz [8], gives a good agreement with the experimental data in the vicinity of the θ-point, but in good solvents it yields values of A_2 which are substantially different from the experimental ones. Recently, the author and Yu. E. Eizner [9], by working within the framework of the Casassa-Markovitz theory and calculating more rigorously the effects of intermolecular forces on A_2, have obtained results which agreed well (in the range of experimental errors) with the experimental data in both poor and good solvents. This justifies the use of the Ptitsyn-Eizner theory for the determination of unperturbed macromolecular dimensions from their dimensions in good solvents, A_2, and their molecular weight.

This theory may be formulated as follows:

$$A_2 = 4\pi^{3/2} N_A \frac{(\overline{R^2})^{3/2}}{M^2} \Psi(\alpha), \qquad (1)$$

where $\overline{R}^2$ is the mean square radius of inertia of the molecule, M the molecular weight, $\alpha = (\overline{R}^2/\overline{R}_0^2)^{1/2}$ ($\overline{R}_0^2$ is the mean-square radius of inertia of the chain at the θ -point).

$$\Psi(\alpha) \simeq \frac{1}{5{,}68} \cdot \frac{\alpha_{eff}^3}{\alpha^3}\left(1 - e^{-5{,}68z/\alpha^3_{eff}}\right), \qquad (2)$$

while z and α_{eff} are related to α through the equations $\alpha^2_{eff} = 1 + 2.93 \cdot z/\alpha^3_{eff}$, $\alpha^5_{eff} - \alpha^3_{eff} = 1.04\,z$ and $\alpha^5 - \alpha^3 = (4z/3)(\alpha^3/\alpha^3_{eff})$ [9, 10]. In Fig. 1 we have plotted the Ψ (α) function given in Eq. 2. As was shown elsewhere [9], the experimental points fall pretty well along the curve drawn in Fig. 1.

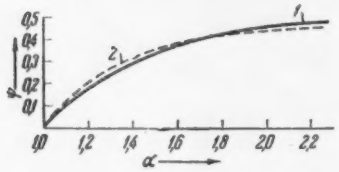

Fig.1. The function $\Psi(\alpha) = (^1/_4\,\pi^{3/2}\,N_A)\,A_2M^2/(\overline{R}^3/_2)$ plotted against $\alpha = (\overline{R}^2/\overline{R}_0^2)^{1/2}$. 1) Theoretical curve [9] (Equation 2); 2) Krigbaum's empirical equation [16] (Equation 4).

Having determined (from light scattering or hydrodynamic properties) the $\overline{R}^2$ of the macromolecule in any solvent, and using known values of A_2 and M, we can calculate Ψ (α) from Equation (1); subsequently by using the curve shown in Fig.1 we can determine α and $(\overline{R}_0^2)^{1/2} = (\overline{R}^2)^{1/2}/\alpha$ (the unperturbed chain dimensions). In Table 1 we have tabulated the values of $(\overline{h}_0^2/M)^{1/2}$ ($\overline{h}_0^2 = 6\overline{R}_0^2$ – the mean square distance between chain ends (at the θ -point), which we determined for various polymers by the above-described method. As is well known, the $\overline{h}_0^2/M$ function is independent of M and is used as a measure of the chain flexibility. The values of α, listed in Column 4, were obtained from the curve in Fig. 1. The calculated values of $(\overline{h}_0^2/M)^{1/2}$ practically coincide with the corresponding values determined experimentally in θ -solvents; for polystyrene, polyisobutene, and polyvinylacetate they are: $70 \cdot 10^{-10}$ cm [14], $79.5 \cdot 10^{-10}$ cm [2], and 78.10^{-10} cm [15], respectively. Thus, by using the previously described theory [9], it is possible to determine the unperturbed chain dimensions in good solvents with practically the same degree of accuracy as in θ -solvents. It should, however, be emphasized that any polydispersion of the investigated samples may alter considerably the experimental results (particularly if R^2 is determined by light scattering), so that it is advisable to carry out measurements on narrow polymeric fractions.

The determination of unperturbed macromolecular dimensions through measurements in good solvents has also been proposed by Krigbaum [16]; by combining the equations for $\overline{R}^2$ and A_2, which are valid only in the vicinity of the θ -point, he derived the equation:

$$(\overline{R}^2)^{5/2} = (\overline{R}_0^2)^{5/2} + 3\frac{134}{105}\frac{1}{(4\pi)^{5/2}} A_2 \frac{M^2}{N_A}. \qquad (3)$$

TABLE 1

Polymer	Solvent	$M \cdot 10^3$	α	$(\overline{h}_0^2/M)^{\frac{1}{2}} \cdot 10^{10}$ cm	Lit. ref.
Polystyrene	Toluene	31—612	1,24—1,38	71 (±2)	(11–13)
Polystyrene	Cyclohexane (T ≠ θ)	3200	1,05—1,21	69 (±0,5)	(14)
Polyisobutylene	Cyclohexane	38—721	1,23—1,47	82 (±2)	(11)
Polyvinylacetate	Methylethylmethane	860—3460	1,43—1,60	78 (±3)	(15)

Equation (3), as is obvious from its derivation, is only valid provided all higher-order interactions are insignificantly small, so that from a theoretical standpoint it is not applicable to good solvents. Nevertheless, due to an accidental compensation among the various factors not considered in the derivation, the equation has proven

quite useful, since by means of it the correct values of $\bar{R}_0^2$ can be calculated from $\bar{R}^2$, A_2, and M [12]. As a matter of fact, Equation (3) can be rewritten in a form similar to Equation (1), and if we disregard the small difference between $\bar{h}^2/\bar{h}_0^2$ and $\bar{R}^2/\bar{R}_0^2$, we will get:

$$\Psi(\alpha) = \frac{1}{2}(1 - 1/\alpha^3). \tag{4}$$

The function represented by Equation (4) was also plotted in Fig. 1; the Figure shows that Krigbaum's equation, which in good solvents is essentially empirical, is in good agreement with the theoretical results obtained by the author and Yu. E. Eizner. Hence, instead of Equations (1) and (2),one can use the empirical Equation (3) to calculate $\bar{R}_0^2$.

In paper [17] Equation (3) was used for the determination of the $\bar{R}_0^2$ of isotactic polystyrene. The authors of that paper also concluded that although in good solvents the molecular dimensions of the isotactic and atactic polystyrenes are the same for a given M, the unperturbed dimensions of an isotactic polystyrene are somewhat larger (since for a given M the isotactic polystyrene has a smaller A_2). In view of the extensive polydispersion of the sample studied in paper [17], the results require a further verification.This is the more so,since we didn't confirm the ideas presented in paper [17], when we used in our calculations some recent data of Trossarelli, Campi, and Saini [18], who studied the viscosity and light-scattering of isotactic polystyrene in toluene. The problem evidently requires a further investigation by the use of the narrowest fractions possible.

LITERATURE CITED

[1] M. V. Vol'kenshtein, Configuration Statistics of Polymeric Chains, Izd AN SSR, 1959, [In Russian].

[2] P. Flory, Principles of Polymer Chemistry, N. Y., 1953,

[3] T. M. Birshtein and O. B. Ptitsyn, J. Phys. Chem. 28, 213 (1954).

[4] O. B. Ptitsyn and Yu.A.Sharonov,J.Tech. Phys. 27, 2744, 2762 (1957).

[5] T. M. Birshtein and O. B. Ptitsyn, J. Tech. Phys. 29, 1075 (1959).

[6] T. Orofino and P. Flory, J. Chem. Phys., 26, 1067 (1957).

[7] P. Flory and W. Krigbaum, J. Chem. Phys., 18, 1086 (1950).

[8] E. Casassa and H. Markovitz,J. Chem. Phys., 29, 493 (1958).

[9] O. B. Ptitsyn, and Yu. E. Éizner, High-molecular Compounds, 1, No.8 (1959).

[10] O. B. Ptitsyn, High-molecular Compounds, 1, No.4 (1959).

[11] W. Krigbaum and P. Flory, J. Am. Chem. Soc., 75, 1775 (1953).

[12] W. Krigbaum, J. Polymer Sci., 28, 213 (1958).

[13] D. Carpenter and W. Krigbaum, J. Chem. Phys., 24, 1041 (1956).

[14] W. Krigbaum and D. Carpenter, J. Phys. Chem., 59, 1166 (1956).

[15] A. Shultz, J. Am.Chem. Soc., 76, 3422 (1954).

[16] W. Krigbaum, J. Polymer Sci., 18, 315 (1955).

[17] W. Krigbaum, D. Carpenter and S. Newman, J. Phys. Chem., 62, 1586 (1958).

[18] L. Trossarelli, E. Campi and G. Saini, J. Polymer Sci., 35, 205 (1959).

Received June 11, 1959.

THE EFFECTS OF TEMPERATURE AND LAMINARY VELOCITY ON THE RATE OF TURBULENT COMBUSTION

A. S. Sokolik and V. P. Karpov

Institute of Chemical Physics of the Academy of Sciences USSSR

(Presented by Academician V. N. Kondrat'ev, June 15, 1959).

There currently exist two apparently alternate points of view concerning the mechanism of turbulent combustion; the one proposed first is called the laminary-surface combustion model [1-4], the other, proposed in 1955, treats turbulent flame as the propagation of a three-dimensional pulsating reaction [5-7]. Although several observations concerning the variations in the order at which certain types of light are emitted and the great difference in the time intervals between emissions in laminary and turbulent flames throw some doubt on the laminary-surface model, they at the same time fail to present any adequate evidence in support of the other, three-dimensional turbulent flame model. It seems that one first has to establish whether there is any connection between the propagation velocities of turbulent and laminary flames. The solution of this problem became feasible due to the development of an essentially physical method of measuring turbulent combustion velocities [8]; in the current paper an attempt is made to present this solution. The example presented in Fig.1 shows the usual effects of mixture composition (β represents the ratio between the true and the stoichiometric fuel concentrations) on the laminary combustion velocity U_c and on the corresponding flame temperature T_c, as well as the turbulent combustion velocity U_t under static bomb conditions, where turbulence intensity is constant; the data are given for air + propane mixtures (Fig. 1a). In these and in subsequent experiments, by using stirring motors, we maintained a constant turbulence intensity, which, as was demonstrated in calibration experiments, corresponds to having constant $|\overline{U'}|$ and $\sqrt{\overline{u'^2}}$ while the physical properties of mixtures are varied; in this case $|\overline{U'}|$ and $\sqrt{\overline{u'^2}}$ are the average absolute turbulence intensity and the variable component of the instantaneous recorded velocity, respectively [8]. The fact that any change in U_c is accompanied by a change in U_t has also been frequently observed when U_t was measured by propagation methods in turbulent stabilized flames, and the fact was invariably regarded as a proof for the direct relationship between turbulent and laminary velocities. However, the fact that a change in U_t is also accompanied by a change in T_c was entirely ignored.

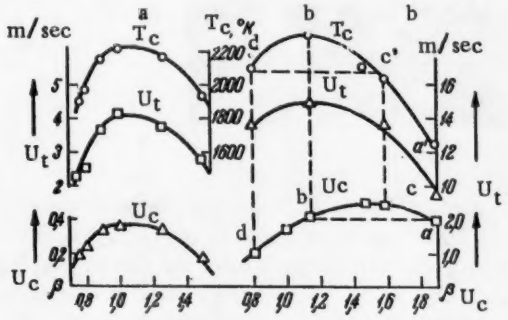

Fig. 1.

In order to separate the two factors, U_t was determined in hydrogen + air flames (Fig. 1b); these mixtures can be varied in such a manner that U_c remains constant while the combustion temperature T_c is varied (Expt. 1, points a, b, and a', b', in Fig. 1), or T_c can be kept constant while U_c is varied (Expt. 2, points c, d, and c', d' in Fig. 1). The air - hydrogen mixtures exhibit these properties as a result of the great dependence of thermal conductivity on the ratio of hydrogen to air. As the data in Expt. 2 show, when U_c is increased by a factor of 2, while T_c is maintained constant, U_t remains practically unchanged.

In Experiment 1, where T_c was varied from 1650 to 2300°K, while U_c remained constant, the value of U_t increased from about 9.5 to 14.5 m/sec. The above-described

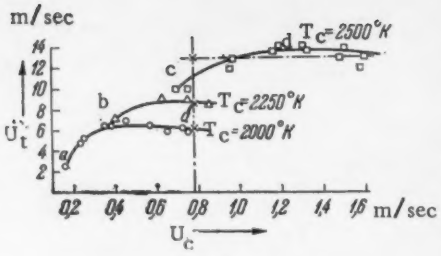

Fig. 2.

conditions were also reproduced by using mixtures of the composition : $2H_2 + O_2 + M$, where M = N_2, Ar, or He; the concentration of the inert gas was chosen in such a manner as to give a constant U_c (200 ± 7 cm/sec), while the combustion temperature was varied from 2000 to 2400°K (see the data in [9]). As T_c was raised within the above-mentioned range, at a constant U_c (the latter was carefully controlled), U_t increased from 10 to 16.8 m/sec. Finally, we studied the relationship between U_t, U_c, and T_c by using ternary mixtures of $CH_4 + nO_2 + M$, with the concentrations of O_2 and of the dilutant(N_2, Ar, He) chosen so as to maintain a constant T_c over a wide range of U_c values; in order to be consistent with our previous work [10], the temperatures: 2000, 2250, and 2500°K, respectively, were used in each series of experiments. As can be seen from Fig. 2, when T_c is maintained constant U_t remains practically unchanged over a wide range of U_c values; the values of U_t at the three combustion temperatures were 6.2, 8.8, and 13 m/sec, respectively. Only when U_c is decreased below a certain value, specific for each temperature, does one observe a sharp decrease in U_t. As will be shown later on, this phenomenon is connected with an actual change in the nature of the flame itself. Now, though, on the basis of the experimental results one can conclude that the turbulent combustion velocity is independent of the laminary combustion velocity when T_c is constant, but increases with increasing combustion temperature.

An examination of several film frames, representing an example of flame propagation (Fig. 3), reveals a substantial difference between the types of turbulent flame propagation present in the region of constant U_t (Fig. 2, point d, and Fig. 3,d)and on the declining branch of the curve, for example, at points a, b, c in Fig. 2 (corresponding to Fig. 3a, b, c).

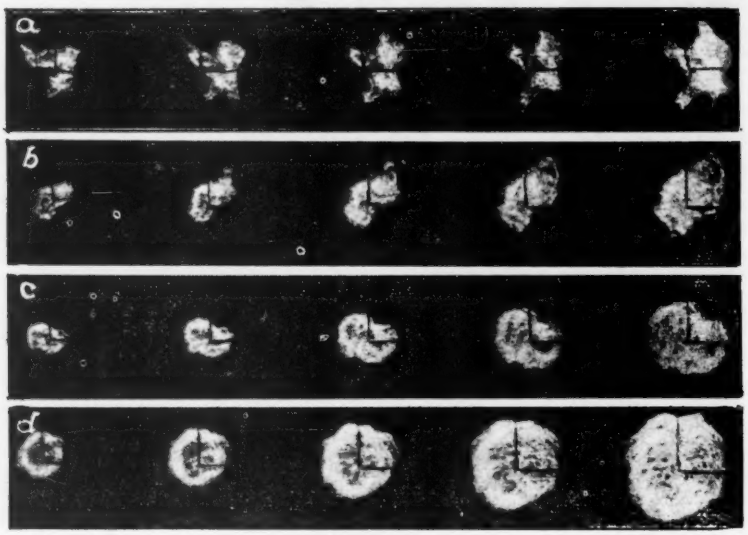

Fig.3.

It is evident that along the downward portion of the U_t curve the flame is not spreading uniformly over the entire space but encompasses individual, sometimes several, zones (particularly obvious in Fig. 3a). When the normal observable velocity of individual ejections is conserved, the less uniformly filled the flame sphere, the smaller will be the rate of increase in the reduced radius, dR/dt. Hence, the decreased turbulent combustion velocity at a constant T_c may be attributed to the increased probability of extinction as the boundary of turbulent flame propagation is approached. A comparison between Fig. 2 and Fig. 3 indicates that the propagation

boundary of the turbulent flame advances at a constant adiabatic combustion temperature and not when T_c is decreased, as happens in the case of a laminary flame. The turbulent combustion is directly hampered under these conditions (at a constant T_c) by the reduced reaction rate, which results from the altered composition of the ternary mixture. This boundary property of turbulent flame propagation will be the object of a further study.

Since the laminary-surface model is completely incompatible with the experimental results, one should represent turbulent combustion as a propagation of pulsating ignitions, caused by a turbulent mixing of fresh and burning gases. Using this approach, the turbulent combustion velocity should depend on the ratio of the path along which the fresh and burning gases undergo turbulent mixing $\sqrt{\overline{x^2}}$ to the induction period of the combustion, τ_i. For small periods:

$$\sqrt{\overline{X^2}} = U'_\Sigma \cdot t_0, \tag{1}$$

where $t_0 = \int_0^\infty R dt$, the characteristic diffusion time. From this we get:

$$U_t = \sqrt{\overline{X^2}}/\tau_i = (U'_\Sigma \cdot t_0)/\tau_i = aU'_\Sigma. \tag{2}$$

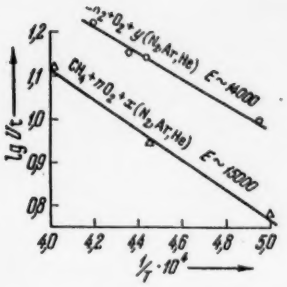

Fig.4.

The maximum value of τ_i for which the propagation of combustion is possible is $\tau_i = t_0$, which corresponds to the minimum value of $U_t = U'_\Sigma$. With decreasing τ_i, for example, as T_c is increased, U_t increases, while U'_Σ remains constant; this has previously been pointed out as an increase in the coefficient a (see Equation (3) in [8]).

The representation of turbulent combustion as a pulsating ignition caused by the mixing of fresh and burning gases also explains the observed order of emission in turbulent flames: CH → CO_2 → CC [7].

The relationship $U_t \sim 1/\tau_i$ can be used to estimate the effective activation energy, E_{eff}, from the equation:

$$U_t \sim \exp(-E_{eff}/RT_c). \tag{3}$$

In Fig. 4 we have plotted U_t against combustion temperature for mixtures of H_2 and CH_4, which is equivalent to having a constant U_c. We already discussed the sequence in which these functions were selected for ternary mixtures of $2H_2 + O_2 + M$. For methane we used the values given in Fig. 2; moreover, in order to get comparable values of U_t, which were outside the turbulent combustion limits of the three temperatures, the values of U_t at 2500°K were obtained by extrapolating the horizontal segment of the curve. The values of E_{eff} found in both cases were close to the activation energy for the reaction: $H + O_2 \rightarrow OH + O$ (E = 15 kcal) [11], which is the principal chain propagation step in combustion reactions proceeding via OH and H radicals.

LITERATURE CITED

[1] G. Damkohler, Zs. phys. chem., B-46, No.11, 601 (1940).

[2] K. I. Shchelkin, J. Tech. Phys. 13, No.9, 520 (1943).

[3] B. Karlovitz, D. W. Denniston,Jr., and F. E. Wells, J. Chem. Phys., 19, No.5, 541 (1951).

[4] A. C. Scurlock, and J. H. Grover, Fourth Symposium on Combustion, 1953, p.645.

[5] M. Summerfield and S. H. Reiter,et al., Jet Propuls., 25, No.8, 377 (1955).

[6] E. S. Shchetinkov, Coll. Papers on Turbulent Combustion of Homogeneous Mixtures, Moscow,1956, p.50. [In Russian].

[7] K. Wohl, Zs. phys. Chem., Neue Folge, 16, 387 (1958).

[8] V.N. Karpov, E. S. Semenov, A. S. Sokolik, Proc. Acad. Sci. 128, No.6 (1959).*

*Original Russian pagination. See C. B. translation.

[9] G. Morgan and W. Kane, Fourth Symposium on Combustion, 1953, p.313.

[10] S. Weil, E. Searight and R. Ellington, Ind. and Eng. Chem., 50, No.7, 1101 (1958).

[11] L. V. Karmilova, A. B. Nalbandyan, and N. N. Semenov, J. Phys. Chem. 32, No.6, 1193 (1958).

Received June 5, 1959.

THE EFFECTS OF THE DEGREE OF DEGASSING ON THE ELECTRON WORK FUNCTION IN NICKEL

N. A. Shurmovskaya and R. Kh. Burshtein

(Presented by Academician A. N. Frumkin, June 23, 1959)

In the preceding communication [1], which dealt with the effects of adsorbed oxygen on the electron work function in nickel, we showed that the contact potential difference depends on the conditions under which nickel and oxygen are allowed to react, which indicates that different types of bonds are formed between the metal and the adsorbed gas. These results were similar to those previously obtained by R. Kh. Burshtein and co-workers, who studied the adsorption of oxygen on iron [2] and platinum [3]. In papers [2] and [3] they described how the metals were repeatedly reduced with hydrogen at 400° and subsequently degassed in vacuo under pressures as low as 10^{-7} mm and temperatures as high as 900-1000° (using high-frequency current for heating).

However, certain literature data indicate that a metal surface degassed at 10^{-7} mm is not entirely free of adsorbed gases. To obtain a pure metallic surface a vacuum of the order of 10^{-9}-10^{-10} mm of Hg is required. Becker [4] has demonstrated that at a pressure of 10^{-6} mm a single layer of nitrogen is adsorbed on a tungsten surface within one second, while at 10^{-8} mm the same process requires 100 seconds. Oxygen, hydrogen, and water vapor behave similarly. On the basis of these facts Becker expressed his doubts concerning the accuracy of most of the literature data on the adsorption on metals, since in his opinion the adsorption was studied on surfaces which were already covered with an indeterminate amount of adsorbed gases. As is already known, the determination of the potential difference at the point of contact between a pure metal and a metal which has absorbed some gas provides a clue to the adsorption mechanism of gases and constitutes one of the most sensitive methods of studying the physical and chemical state of a surface.

It was accordingly interesting to see what effect would the degassing of a metal surface at pressures between 10^{-7} and 10^{-10} mm have on the contact potential difference between a "pure" metal and the same metal with some absorbed gas. We selected for our investigation the nickel – oxygen system; though this system has previously been studied by us [1], the surface was never degassed at pressures below 10^{-7} mm. For the sake of comparison with previous results, we determined the contact potential difference between pure nickel, which had been repeatedly reduced with hydrogen at 400° and thoroughly degassed at 900° in vacuo at pressures of 10^{-9} - 10^{-10} mm, and nickel which was allowed to absorb oxygen at various temperatures. During degassing the nickel was heated by a high-frequency current. Partial vaporization of nickel was already observed at 900°. A thermoelectronic method was used for measuring contact potential differences. Measurements were carried out in an apparatus which consisted of a diode containing a tungsten wire cathode and a movable anode. The anode consisted of a 6 cm^2 plate made of spectroscopically pure nickel ("Hilger" brand). During the preliminary work the anode and the cathode were kept relatively far apart, but they could be brought together to within 1 mm, by means of an electromagnetic device, when volt-ampere characteristics were to be recorded. The conditions necessary for a complete purification of the tungsten wire surface were established by carrying out special experiments in an apparatus with separate anode and cathode compartments. The ultrahigh vacuum was obtained by using a manometer designed by Alpert [5]. The measuring portion of the system was detached from the vacuum assembly with the help of a tin seal designed by I. I. Tret'yakov [6].

The results obtained in this work are compared with our previous work in Fig. 1. The curves show the temperature dependence of the contact potential differences between nickel degassed in vacuo at 10^{-7} mm (1), as well as nickel degassed at 10^{-9} -10^{-10} mm (2), and nickel which had absorbed oxygen (at various temperatures)

to the extent of $1.3 \cdot 10^{15}$ O_2 molecules per 1 cm^2 of actual surface. In nickel which had been degassed in ultra-high vacuum the work function decreases by 0.27 v when oxygen is absorbed at 60° and by 0.41 v when the nickel plate is heated at 100°.

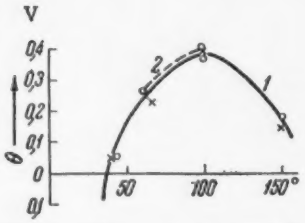

Fig. 1. The contact potential difference on nickel which was degassed in vacuo as a function of the oxygen-absorption temperature: 1) degassed at 10^{-7} mm; 2) at 10^{-9} mm.

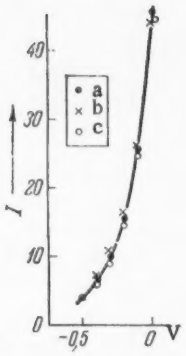

Fig.2. The effects of the extent of degassing on the current-voltage characteristics of Ni at various pressures of residual gases: a) 10^{-9} mm; b) 10^{-7} mm; and c) at 10^{-7} mm of oxygen.

Hence, as can be seen in Fig.1, measurements carried out in ultrahigh vacuum gave the same results as those obtained when nickel was degassed at pressures above 10^{-7} mm [1]. In order to verify these results we recorded a series of volt-ampere characteristics using nickel degassed at 10^{-9} mm (Fig.2). After that, the pressure in the measuring portion of the system increased to 10^{-7} mm due to residual gases, or was increased by introducing oxygen. The results clearly indicate that the volt-ampere characteristics for both types of degassing practically coincide, which means that the work function remains the same.

Our results are in full agreement with those obtained by Clarke and Farnsworth [7], who showed that the contact potential differences on silver are independent of the residual gas pressure in the range from 10^{-6} to 10^{-8} mm. Culner, Pritchard, and Tompkins [8] have established that no adsorption of oxygen is observed at 10^{-6} mm pressure on finely powdered films of gold, silver, and copper.

Thus, the results obtained by the contact potential-difference method are not consistent with the electron emission studies [4,9]. The reason for this is not clear, but it is quite possible that the indicated difference is related to the existence of an electric field in the emission microscope.

LITERATURE CITED

[1] N. A. Shurmovskaya and R. Kh. Burshtein, J. Phys.Chem. 31, 1150 (1957).

[2] R. Kh. Burshtein and M.D.Surova, Proc.Acad. Sci. 61,75 (1948); R. Kh. Burshtein, M. D. Surova and I. I. Zaidenman, J. Phys. Chem. 24, 214 (1950).

[3] T. V. Kalish and R. Kh. Burshtein, Proc. Acad.Sci.81, 1093 (1951).

[4] J. A. Becker, Advances in Catalysis, 7, 135 (1955).

[5] D. Alpert, J. Appl. Phys., 24, 860 (1953).

[6] I. I. Tret'yakov, Factory Labs. No.3, 362 (1956).

[7] E. N. Clarke and H. E. Farnsworth, Phys. Rev., 85,484 (1952).

[8] R. Culner, J. Pritchard and F. C. Tompkins, Intern.Congress of Surface Activity, 3, 243 (1957).

[9] S. Z. Roginskii, I. I.Tret'yakov, Proc. Acad. Sci. 105, 112 (1955); J. Phys. Chem. 30, 2539 (1956); I. I. Tret'yakov, Chem. Sci. and Industry, 2, 181 (1957).

Received June 22, 1959.

THE ENERGY OF ADSORPTION OF HYDROCARBONS ON CHEMICALLY MODIFIED SILICA

I. Yu. Babkin and A. V. Kiselev

The M. V. Lomonosov State University, Moscow

(Presented by Academician M. M. Dubinin June 24, 1959)

The modification of a silica surface by chemical bonding with trimethylsilyl groups [1] to approximately 93% coverage results in a marked diminution in the adsorption of various substances, this effect being especially pronounced in the case of the hydrocarbons [2].

Absolute isotherms for the adsorption of n-hexane and benzene on a silica surface (aerosil) which is hydrated or 93% covered with chemically bound trimethylsilyl groups are given in Figure 1. This Figure shows that such modification reduces the hydrocarbon adsorption sharply even though it does lead to the formation of an "organophilic" film of methyl groups on the surface, the reduction being particularly pronounced for benzene vapors. Interest attaches to an interpretation of this effect in the theory of adsorptional forces, with an evaluation of the energies of adsorption of these hydrocarbons on a modified silica surface.

The lack of exact information on the distribution of force centers on the surface and in the body of amorphous silica complicates the problem of evaluating the energy of adsorption here [3]. Much significance therefore attaches to the selection of a model adsorbent in which there is a regular periodic ordering of these force centers in both the modifying surface layer of the silica and in the body. The silicon atoms of trimethylsilane add on to the silica lattice during chemical modification of the latter's surface by the reaction

$$-\overset{|}{\underset{|}{\mathrm{Si}}}-\mathrm{OH}+\mathrm{ClSi(CH_3)_3}\rightarrow-\overset{|}{\underset{|}{\mathrm{Si}}}-\mathrm{O}-\mathrm{Si(CH_3)_3}+\mathrm{HCl}$$

and they, together with the methyl groups, form a structured layer (Fig.2a) which will have a depth of 3.5 A if these groups are of van der Waals' dimensions. The acceptance of this simplified model of modified silica is justified, in view of the fact that the surface is almost fully covered by the $Si(CH_3)_3$ groups [2] with only 7% departure from maximum packing density, while the effect of the adsorbed molecules on the underlying silica lattice is slight because of the rather considerable depth of the layer of methyl groups.

The model adopted for the layer of methyl groups was a plane with maximum packing density (Fig.2b), whereas the silica was assumed to have a tridymite structure (Fig.2c) with a (1000) plane oriented toward the methyl group layer. This spatial distribution of the silicate tetrahedrons is especially suitable for the purposes of calculation, the oxygen atoms, the principal force centers, being arranged in parallel planes. The tridymite structure was chosen because its density (2.3 g/cm^3) approximates that of silica gel (about 2.2 g/cm^3). A defect of this model is that the (1000) plane of tridymite cannot assure the maximum density of coverage by the trimethylsilyl groups in the reaction with $ClSi(CH_3)_3$. A coverage which approached this density would in actuality demand that the silica surface entering into the reaction be covered with hydroxyl groups at maximum density [2]. It has been pointed out above, however, that this model is acceptable because of the smallness of the contribution which the silica lattice makes to the energy of adsorption on the modified surface.

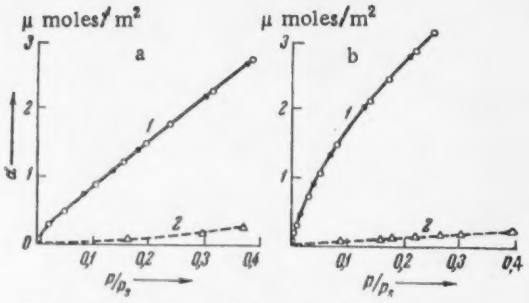

Fig.1. Adsorption isotherms for n-hexane vapors (a) and for benzene vapors (b) on a hydrated silica surface (1) and on a trimethylsilyl-covered surface (2).

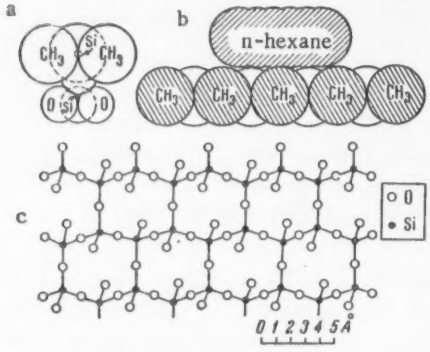

Fig.2. One possibility for bonding between a trimethylsilyl group and a silicate tetrahedron (a); a model of a dense-packed layer of methyl groups with an adsorbed n-hexane molecule shown above (b); and the tridymite structure (c).

TABLE 1

Values of the Constant for Dispersional Attraction, the Polarizability, and the Magnetic Susceptibility

	$\alpha \cdot 10^{24}$, cm³	$-\chi \cdot 10^{29}$, cm³	$C \cdot 10^{58}$, (kcal/mole)·cm⁶		
			CH_3	O	Si
O	1,69 (5)	10 (5)			
Si	0,04 (6)	1,66 (7)			
CH_3	2,26 (5)	23,6 (5)	1,86	1,02	0,05
CH_2	1,82 (5)	18,9 (5)	1,50	0,82	0,04
CH arom.	1,72 (5)	15,3 (5)	1,31	0,73	0,03

Only the dispersional component of the adsorption potential has been evaluated here since the induction effect is principally due to hydroxyls which have not been fully replaced and are screened by the $Si(CH_3)_3$ groups; the electrical field is nonuniform, however, and falls off rapidly with increasing distance so that this effect would be small [4]. The interaction of the adsorbate molecule with the force centers of this model is composed additively of: 1) an interaction with the methyl-group layer, and 2) an interaction with the tridymite lattice. The CH_3 groups and the O and Si atoms are considered as the centers of dispersional interaction in the adsorbent, the CH_3, CH_2, and aromatic CH groups filling this role in the adsorbate.

The interaction with the CH_3 groups of the modifying layer was evaluated separately through the equation [3]

$$\Phi \approx -C\Sigma r_{ij}^{-6} + B\Sigma r_{ij}^{-12}, \qquad (1)$$

r_{ij} being the distance from the i-th unit in the adsorbate molecule to the j-th methyl group of the modifying layer, C, the constant for dispersional attraction and B, the repulsive constant. This equation represents only the contribution from the first dipole-dipole member in the expression for the energy of dispersional attraction, more complete calculations [3, 5] having shown that the contribution from subsequent members can be allowed for by the introduction of a small correction term. Summation was carried out over the 64 nearest CH_3 groups. The constant C was determined from the Kirkwood-Muller Equation [3].

$$C = -6mc^2 \frac{\alpha_1\alpha_2}{\alpha_1/\chi_1 + \alpha_2/\chi_2}, \qquad (2)$$

in which m is the mass of the electron, c is the velocity of light and α, χ_1, α_2, χ_2 are, respectively, the polarizability and magnetic susceptibility of the centers of the adsorbent and the adsorbate.

The values of α and χ which were employed in these calculations are shown in Table 1 together with the corresponding values of the constant, C, of dispersional attraction. The value of the constant B was obtained from the condition that the energy of interaction be at a minimum at the equilibrium distance of separation, z_0, of the adsorbed molecule from the modifying layer

$$\left(\frac{\partial\Phi}{\partial z}\right)_{z_0} = 0. \qquad (3)$$

The equilibrium distance, z_0, was fixed as the sum of the van der Waals' radius of the methyl group (2.0 A) and the van der Waals' half-width of the adsorbate molecule [3, 5, 8]. Only the attraction potential was taken

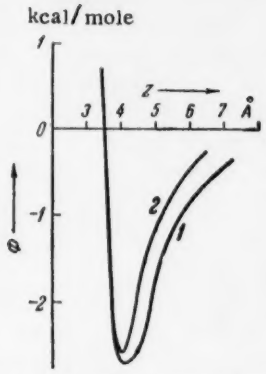

Fig. 3. Potential curves for the adsorption of n-hexane (1) and benzene (2) on the surface of a layer of methyl groups [see model of (Fig. 2)].

TABLE 2

Calculated Values of the Energy of Adsorption of Individual Molecules of n-Hexane and Benzene on the Surface of the Chemically Modified Model of Silica

Type of interaction	Energy of adsorption in kcal/mole	
	n-hexane	benzene
With the modifying layer of methyl groups	2,7	2,6
With the tridymite lattice	1,2	1,0
Correction for quadrapole-dipole and quadrapole-quadrapole interactions	0,4	0,4
Total	4,3	4,0

into account in evaluating the second component which arises from interaction with the tridymite lattice, the repulsion being negligibly small at such large distances. For this reason the attraction potential between a molecule of the adsorbate and the tridymite lattice was calculated at a distance of 5.5 A (the sum of the half-width of the n-hexane molecule and the distance from the surface of the modifying layer to the plane of centers of the first layer of (1000) oxygen atoms of the tridymite), using the equation:

$$\Phi \approx -C_O(\Sigma r_{ij}^{-6} + J_j) - C_{Si}(\Sigma r_{ik}^{-6} + J_k), \quad (4)$$

in which Φ is the attraction potential, C_o and C_{Si} are, respectively, the constants for dispersional attraction in interaction with oxygen and silicon atoms, J_j and J_k are, respectively, integrals [8] representing the interaction with those lattice centers which are not covered in the summation, and r_{ij} and r_{ik} are, respectively, the distance from the i-th unit of the adsorbate molecule to the lattice center of type j or k. Summation was carried out over the 220 nearest centers of the tridymite lattice*. Potential curves for the interaction of molecules of n-hexane and benzene with the methyl-group layer are shown in Figure 3. The value of Φ corresponding to the minimum on the potential-energy curve was increased by 10% to correct for dipole - quadrapole and quadrapole -quadrapole dispersive interaction, as has been suggested by more complete calculation [3,5,8]. The results of these calculations are presented in Table 2.

No essential difference is to be expected in the adsorption of n-hexane and benzene on highly modified specimens such as these, since the modifying layer of methyl groups markedly weakens the electric field of the adsorbant and adsorption is principally due to the dispersive forces. The adsorption (see Fig.1) and the energy of adsorption of n-hexane on the modified silica prove to be higher than adsorption and the energy of adsorption of benzene, this being in distinction to the case for adsorption on a hydrated surface [4], but in line with the adsorption on graphite [3] and magnesium oxide [5].

The resultant values of the energy of adsorption of n-hexane and benzene are small and make up about 50% of the respective values of the heat of condensation, L, so that the values of the true heat of adsorption, Φ - L, are negative and equal to -3.3 kcal/mole for n-hexane and -4.1 kcal/mole for benzene. This fact is responsible for low adsorbability of these hydrocarbons on the surface of a 93% modified aerosil [2] (see Fig. 1) and for the concavity of the adsorption isotherm. It is true, of course, that these results are valid only for the chosen model. It has already been noted that the density of distribution of the methyl groups is not actually so uniform and that these groups do not fall entirely in a single plane, but this could not alter the fundamental conclusion that there is a marked diminution in the energy of adsorption of the hydrocarbons as the result of this type of modification of the silica surface.

*Such a detailed evaluation of the interaction with the tridymite lattice is not required for the present purposes; use was made of the results obtained in an evaluation of the energy of adsorption on silica [9].

Thus the sharp reduction in the potential of the dispersonal attractive forces resulting from the displacement of the external modifying layer of methyl groups away from the silica lattice is the principal cause of the marked diminution in the adsorption of hydrocarbons and other vapors when the silica surface is almost fully modified by reaction with trimethylsilane (or by alkylation [10]). There is an added effect in the case of molecules with a pronounced nonuniformity in the density distribution within the electron cloud (benzene, in the present instance); this arises from elimination of the electrostatic interaction with the hydroxyl groups and leads to a sharp reduction in the adsorption, with the adsorption of n-hexane falling to 1/15th and that of benzene, to 1/65th, of the original value at a relative pressure of 0.1 [2]. It is hoped that a comparison of the heats of adsorption can be made in a future communication.

LITERATURE CITED

[1] A. V. Kiselev, N. V. Kovaleva, et al, Proc. Acad. Sci. USSR, 124, 617 (1959).*

[2] I. Yu. Babkin, V. S. Vasil'eva, et al, Proc. Acad. Sci. USSR, 129, No.1 (1959). *

[3] N. N. Avgul', A. A. Isirikyan, et al, Bull. Acad. Sci. USSR, Div. Chem. Sci., 1957, 1314. *

[4] A. V. Kiselev and D. P. Poshkus, Proc. Acad. Sci. USSR, 120, 834 (1958).*

[5] A. V. Kiselev and D. P. Poshkus, J. Phys. Chem., 32, 2824 (1958) [USSR].

[6] H. Landolt and R. Bornstein, Phys. chem. Tabellen, 6. Auflage, 1, T.1, 401, 1950.

[7] P. Selwood, Magnetochemistry, Foreign Lit. Press, 1958, p.89. [Russian translation].

[8] N. N. Avgul', A. V. Kiselev, et al, Bull. Acad. Sci. USSR, Div. Chem. Sci., 1959, 1196.*

[9] I. Yu. Babkin, Diploma Work, Moscow, 1959.

[10] O. M. Dzhigit, A. V. Kiselev, et al, Proc. Acad. Sci. USSR, 70, 441 (1950).

Received June 23, 1959.

*Original Russian pagination. See C. B. translation.

AN ELECTRON PARAMAGNETIC RESONANCE (RADIOSPECTROSCOPIC) STUDY OF THE VULCANIZATION OF RUBBER

G. A. Blokh

The Dnepropetrovsk Institute of Chemical Technology

(Presented by Academician P. A. Rebinder May 18, 1959)

The methods of modern physical chemistry are now being used to study the most important technological problems of the rubber industry. The use of radioactive isotopes has made it possible to obtain new insight into the complex process of rubber vulcanization and the mechanism of the action of organic accelerators [1]. Ionizing radiations have been employed to effect the so-called radiational vulcanization [2,3].

New, wide perspectives are opened by the application of electron paramagnetic resonance (radiospectroscopy) to the study of the chemical reactions which are involved in rubber vulcanization. It is well known that the molecules in a chemical reaction must usually pass through an active state, forming free radicals with unpaired electron spins and magnetic moments. The production and consumption of free radicals in a chemical reaction can be followed by studying the paramagnetic resonance adsorption of these particles. The degree of dissociation of a compound into free radicals can be estimated from a measurement of its magnetic susceptibility.

Thus, it is quite important that electron paramagnetic resonance be used in attacking the problem of the nature of the vulcanization reactions. The electron paramagnetic spectra should show whether vulcanization is actually a radical reaction, or not.

All of the present studies were carried out [5, 6] on a radiospectrometer which had been constructed in the laboratories of S. E. Bresler and had a high sensitivity of $2 \cdot 10^{-12}$ moles of diphenylpicrylhydrazyl, the substance generally employed in such sensitivity calibrations [4]. Investigation was made of the vulcanization of natural rubber by tetramethylthiuramdisulfide in the presence of zinc oxide and stearic acid. Parallel studies were carried out on similar systems in which the natural rubber had been replaced by polyisobutylene. Thus, the investigated systems differed in respect to the double bonds in the polymer structure. Electron paramagnetic spectra were studied for mixtures of the compositions shown in Table 1.

TABLE 1

Mixture composition	Specimen No.							
	1	2	3	4	5	6	7	8
Natural rubber	100	100	100	100	—	—	—	—
Polyisobutylene	—	—	—	—	100	100	100	100
Tetramethylthiuram-disulfide (thiuram)	3,0	3,0	3,0	—	3,0	3,0	3,0	—
Zinc oxide	—	5,0	5,0	—	—	5,0	5,0	—
Stearic acid	—	—	2,0	—	—	—	2,0	—
Sulfur	—	—	—	3,0	—	—	—	3,0

The rubber mixtures were made up and loaded into ampules of high-quality quartz glass which was free of paramagnetic contaminants; these ampules were then partially evacuated and sealed. The ampules were placed into the resonator and heated from 20 to 220° at a fixed rate. Parallel observations were made on the paramagnetic spectra of rubber which had been plasticized, without an additive, between rollers for 30 minutes. A paramagnetic spectrum was not shown by the unplasticized natural rubber (clear crepe). The plasticized rubber showed a single characteristic spectral line, and it was obvious that peroxide radicals had been produced by the oxidation processes in the rubber (Fig.1). This spectral line was subsequently

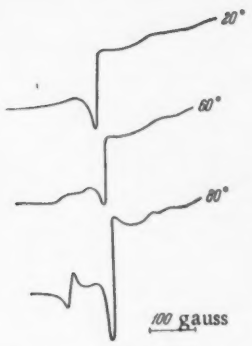

Fig. 1. The formation of polymeric radicals during heating of natural rubber with 3% tetramethylthiuramdisulfide at 20-80°.

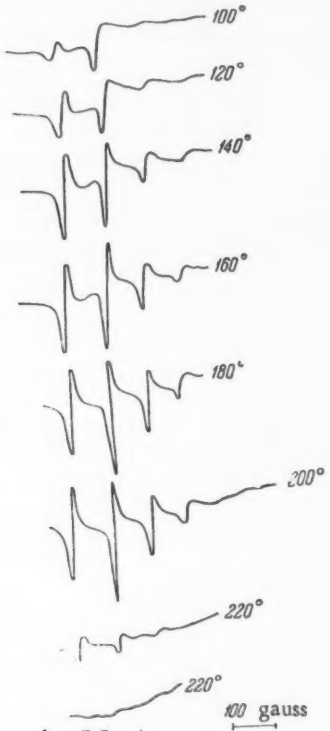

Fig. 2. The kinetics of the formation of polymeric radicals during the vulcanization of natural rubber with 3% tetramethylthiuramdisulfide at 100-220°.

observed in mixtures containing rubber and thiuram, or other ingredients, as these mixtures were carried up to vulcanization. Increasing the temperature of vulcanization of rubber by the tetramethylthiuramdisulfide resulted in an almost instantaneous increase in the complexity of the paramagnetic spectrum, this change taking place in less than a minute. There was a deformation of the spectral line at 60°; two lines were observed at 80°, three at 120°, and four at 140-160° [5,6]. An increase in the intensity of the paramagnetic spectrum with subsequent extinction was observed 10-20 minutes after the temperature has reached 200° in the course of a further heating to 180- 200 - 220°. The reverse change was observed in the paramagnetic spectrum 20 minutes after the beginning of heating at 200°, or 5 - 7 minutes after the beginning of heating at 220°; eventually, only three of the four lines remained as an intermediate triplet state, and two of these gradually disappeared with cooling to leave the original single peak (Figs. 2 and 3). These experiments showed that the presence of zinc oxide or stearic acid in the mixture did not essentially alter the paramagnetic spectrum.

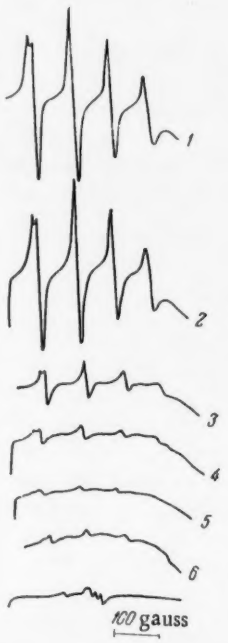

Fig. 3. The kinetics of the formation of polymeric radicals in the vulcanization of natural rubber with 3% tetramethylthiuramdisulfide at 200°: 1)after 5 min; 2) 10 min; 3) 16 min; 4) 22 min; 5) 27 min; 6) after 32 min; 7)after cooling until the following day.

A second heating of the vulcanizate resulted in a paramagnetic spectrum of almost the same intensity. The electron paramagnetic resonance observed during the heating of natural rubber (clear crepe) with tetramethylthiuramdisulfide, zinc oxide, and stearic acid gave clear proof of the fact that the vulcanization of such mixtures is a radical reaction. On the other hand, no paramagnetic spectrum was observed when similar mixtures in which the natural rubber had been replaced by polyisobutylene were heated to any one of the test temperatures. This illustrates clearly the role played by the polymer double bonds; polyisobutylene contained no such bonds, and neither vulcanized nor showed a paramagnetic resonance spectrum.

The vulcanization of natural rubber by sulfur (without tetramethylthiuramdisulfide) also failed to give rise to a paramagnetic resonance spectrum. The observed paramagnetic spectra indicated that polymeric radicals were formed in the vulcanization of natural rubber by tetramethylthiuramdisulfide, since any low-molecular radicals which might have resulted from the dissociation of this compound would have readily recombined at the vulcanization temperatures of 140-200°, where the diffusion coefficient is quite high. The polymeric radicals were clearly rather long-lived at the experimental temperatures. A second heating led to the formation of a new chain of polymeric radicals which recombined as heating was continued; these were consumed in the formation of spatial structures. Preliminary calculations showed that the concentration of polymeric radicals in these vulcanization experiments was $4 \cdot 10^{-7}$ moles/g. The observed spectra are undoubtedly quite complex since their various parts appeared and disappeared at different times. It is possible that an analysis of these spectra could be had through further studies on model systems with isotopic replacement of the various elements in the tetramethylthiuramdisulfide and the polymer. The following scheme for the dissociation of tetramethylthiuramdisulfide into radicals and the production of polymeric radicals with recombination into spatial structures (vulcanization) can be set up on the basis of the experimental data of various investigators:

1. The dissociation of tetramethylthiuramdisulfide into radicals:

a) $$(CH_3)_2N-\overset{\overset{S}{\|}}{C}-S-S-\overset{\overset{S}{\|}}{C}-N(CH_3)_2 \rightleftarrows 2\,(CH_3)_2-N-\overset{\overset{S}{\|}}{C}^{\bullet} + {}^{\bullet}S-S^{\bullet},$$

b) $$(CH_3)_2N-\overset{\overset{S}{\|}}{C}-S-S-\overset{\overset{S}{\|}}{C}-N(CH_3)_2 \rightleftarrows 2\,(CH_3)_2N-\overset{\overset{S}{\|}}{C}-S^{\bullet},$$

c) $$(CH_3)_2N-\overset{\overset{S}{\|}}{C}-S-S-\overset{\overset{S}{\|}}{C}-N(CH_3)_2 \rightleftarrows (CH_3)_2N-\overset{\overset{S}{\|}}{C}^{\bullet} + {}^{\bullet}S-S-\overset{\overset{S}{\|}}{C}N(CH_3)_2,$$

2. The formation of polymeric radicals:

$$(CH_3)_2N-\overset{\overset{S}{\|}}{C}-S^{\bullet} + \sim CH_2-\overset{\overset{CH_3}{|}}{C}=CH-CH_2\sim \xrightarrow{t} (CH_3)_2N-\overset{\overset{S}{\|}}{C}SN + \sim CH_2-\overset{\overset{CH_3}{|}}{C}=CH-CH\sim$$
$$\sim CH_2-\overset{\overset{CH_3}{|}}{\dot{C}}-CH=CH\sim$$

3. The recombination of the polymeric radicals with the formation of spatial structures and the entry of the thiuram radicals into the rubber structure:

a) $$\sim CH_2-\overset{\overset{CH_3}{|}}{C}=CH-\dot{C}H\sim + \sim CH_2-\overset{\overset{CH_3}{|}}{\dot{C}}-CH=CH\sim \rightarrow CH_2-\overset{\overset{CH_3}{|}}{C}-CH=CH\sim$$
$$\sim CH-CH=\overset{\overset{CH_3}{|}}{C}-CH_2\sim$$

b) $$\sim CH_2-\overset{\overset{CH_3}{|}}{C}=CH-CH_2\sim + \dot{S}-\overset{\overset{S}{\|}}{C}-N(CH_3)_2 \rightarrow \sim CH_2-\overset{\overset{CH_3}{|}}{\dot{C}}-CH-CH_2\sim,$$
$$S=\overset{\overset{S}{|}}{C}-N(CH_3)_2$$

c)

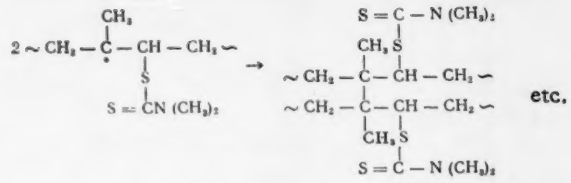

etc.

The possibility of the formation of the dimethyldithiocarbamate of zinc during vulcanization is not to be excluded and this compound could facilitate the passage of the rubber into a spatial structure by accepting hydrogen from its α-methyl groups:

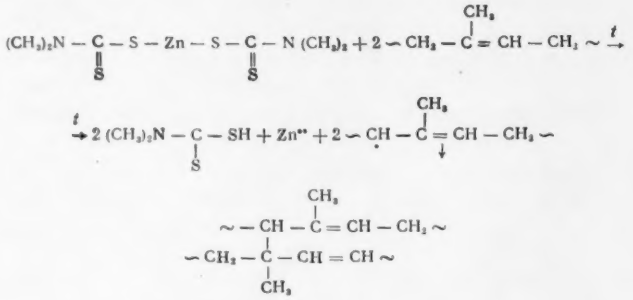

The vulcanization with tetramethylthiuramdisulfide and sulfur in the presence of accelerators is essentially different, as was brought out by the fact that no paramagnetic spectra were observed when rubber was vulcanized by sulfur with diphenylguanidine at 100-160°. Thus, the observed electron paramagnetic spectra gives experimental proof that radical reactions are involved in the vulcanization of rubber by tetramethylthiuramdisulfide.

I wish to express my deep appreciation to Professor S. E. Bresler, E. M. Saminskii, and É. N. Kazbekov for their considerable help in the course of this investigation.

LITERATURE CITED

[1] G. A. Blokh, Chem. Ind., 2, 14 (1956) [USSR].

[2] A. S. Kuz'minskii, T. Nikitina and V. Karpov, Atomic Energy, 3, 137 (1956) [USSR].

[3] Z. Tarasova, M. Kaplunov, B. Dogadkin, V. Karpov and A. Breger, Caoutchouc and Rubber, 5, 14 (1958) [USSR].

[4] S. E. Bresler, E. M. Saminskii and É. N. Kazbekov, J. Tech. Phys. 27, 2 (1958) [USSR].

[5] G. A. Blokh, Session, Acad. Sci. UkSSR, November 17–22, 1958, Kiev, 1958.

[6] G. A. Blokh, Mezhvuzovsk Scientific-Technological Conference on New Polymers, November 25 – 27, 1958, Dnepropetrovsk, 1958.

[7] B. A. Dolgoplosk, et al, Collected Reports, Conference on Chemical Kinetics and Reactivity, Acad. Sci. USSR Press, 1955, p.303.

[8] S. E. Bresler, V. I. Pryadilova and V. Ya. Khainman, J. Tech. Phys. 24, 4, 577 (1954) [USSR].

[9] W. Scheele, O. Lorenz and W. Dummer, Kautschuk und Gummi, 2, 27 (1955).

Received February 20, 1959.

THE EFFECT OF PRELIMINARY IRRADIATION ON THE RATE OF THERMAL DECOMPOSITION OF SILVER OXALATE CONTAINING CADMIUM

V. V. Boldyrev, Yu. A. Zakharov, V. I. Eroshkin and M. G. Sokolova

The S. M. Kirov Polytechnic Institute, Tomsk

(Presented by Academician M. M. Dubinin June 22, 1959).

There is indication in the literature that the thermal decomposition of silver oxalate can be accelerated by preliminary irradiation with visible or ultraviolet light [1-6], or with x-rays [7]. The present work has aimed at elucidating the effect of irradiation with ultraviolet light or with Co^{60} γ-radiation on the rate of thermal decomposition of silver oxalate containing 5 mole percent of added Cd.

The preparation of the working materials has already been described in [8]. The thermal decomposition was studied by a weight method, working at 158° and using quartz spring balances. A 1 mg alteration in mass corresponded to a 13.88 mm screen displacement of the end of the spring. Gaseous reaction products were continuously evacuated. A PRK-4 quartz mercury lamp was used for ultraviolet irradiation. The charge was loaded into a quartz tube which was placed at a distance of 5 cm from the lamp. A Warren motor kept this tube in continuous rotation at 60 rev/min. A source containing a Co^{60} preparation was used for γ-ray irradiation. Kinetic analysis of the experimental results was carried out through the equation $1-\alpha=\exp(-kt^n)$ [9] with subsequent evaluation of the rate constants from $K=nk^{1/n}$ [10].

Our results agree with the data of the literature in showing that preliminary ultraviolet irradiation will accelerate a subsequent thermal decomposition. Preliminary irradiation with γ-rays also leads to a marked acceleration of the thermal decomposition of silver oxalate. Figure 1 gives results from a kinetic analysis of our data on the effect of ultraviolet irradiation on the thermal decomposition of pure silver oxalate and silver oxalate containing added Cd. This figure shows that the velocity constants increase, at first rapidly and then more slowly, as the time of irradiation is extended. The constant n of the topokinetic equation diminishes, this effect being especially marked in the first hour of irradiation.

It has been shown in [2,5,7] that the activating action of a preliminary irradiation involves the production of metallic silver particles in the oxalate lattice through capture of photoelectrons from the conduction band by anion vacancies or other capture centers. These silver particles serve as centers for initiating the subsequent thermal decomposition. Thermal decomposition proceeds more rapidly in a radiated preparation than in one which has not been radiated because of the increase in the number of initiating centers for the reaction. The proportion of the surface involved in the basic reaction increases with the radiation-induced increase in the number of initiating centers and this leads, in turn, to a diminution in the exponent n of the topokinetic equation, a quantity which has been shown to characterize the extent of localization of the topochemical process [10]. The action of ultraviolet light is limited to the surface of the oxalate crystal, while the nonirradiated portion of the surface steadily diminishes as the time of irradiation increases, so that the rate of increase of the velocity constant falls and the effect of preliminary ultraviolet irradiation is thus most pronounced at the beginning of thermal dissociation.

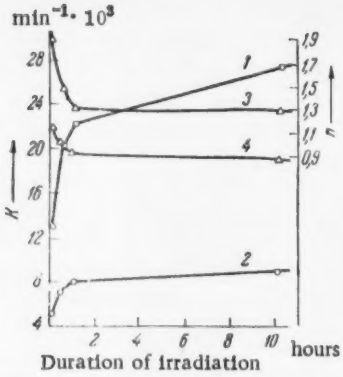

Fig. 1. The effect of ultraviolet irradiation on the kinetic parameters for the thermal decomposition of silver oxalate: 1) the variation in the rate constant for thermal decomposition of pure silver oxalate; 2) the same, for silver oxalate containing added Cd; 3) the variation of the exponent n for thermal decomposition of pure silver oxalate; 4) the same, for silver oxalate containing added Cd.

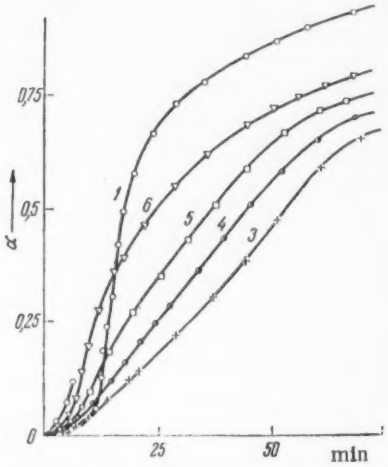

Fig. 2. The effect of γ -irradiation from Co^{60} on the thermal decomposition of silver oxalate at 158°: 1) nonirradiated specimen of pure silver oxalate; 2) the same, irradiated at a dose of $43 \cdot 10^3$ r; 3) nonirradiated specimen of silver oxalate containing added cadmium; 4) the same, irradiated at a dose of $43 \cdot 10^3$ r; 5) the same, irradiated at a dose of $240 \cdot 10^3$ r; 6) the same, irradiated at a dose of $300 \cdot 10^3$ r.

The addition of Cd reduces the rate of thermal decomposition and diminishes the effect of preliminary irradiation on the rate. The action of the added Cd is particularly pronounced at the longer exposure times (Fig. 1). In an earlier paper [8] on the effect of additives on the rate of thermal decomposition of silver oxalate, we have expressed the opinion that the retarding action of added Cd arises from the fact that the cation vacancies associate with the Cd ions entering into the lattice and capture positive holes which must then be removed from the crystal in the course of the thermal decomposition. It is also possible that the rate of the thermal decomposition diminishes because of recombination of interstitial Ag ions with cation vacancies (Frenkel defects) in cases where these ions are involved in the initial stages of the process. The added Cd thus decreases the number of active centers from which the thermal decomposition can be initiated on the surface of the oxalate crystal. A similar mechanism can be set up for the effect of added Cd on ultraviolet irradiation of the oxalate if it is supposed that photolysis proceeds through the same elementary steps as thermal decomposition.

Irradiation with the γ -rays from Co^{60} (a substance which is known to emit γ -quanta of energies 1.17 and 1.33 mev [11]) results in a marked acceleration of the subsequent thermal decomposition of the silver oxalate. The results of experiments on the rate of thermal decomposition of pure silver oxalate and silver oxalate containing added cadmium after irradiation with the γ -rays from Co^{60} are shown in Figure 2, the coordinates being α, the the fraction of material reacted and t, the time. Irradiation at each dose strength in the range from 43 to 300 thousand roentgens results in the thermal decomposition of the silver oxalate becoming explosive 6-8 minutes after beginning an experiment. The thermal decomposition of silver oxalate containing added cadmium is also accelerated by irradiation, but to a considerably smaller extent. The higher the irradiation dosage, the greater the increase in the rate. Figure 3 shows the results of a kinetic analysis of data on the decomposition of silver oxalate which had undergone a preliminary γ -ray irradiation. These data indicate that an increase in the dosage of the preliminary irradiation results in an increase in the rate constant and a diminution in the exponent n. The exponent n alters during the entire time of γ -irradiation and not merely during the initial period, as is the case in the irradiation of the silver oxalate with ultraviolet light.

The photoelectric absorption of γ -quanta and the Compton scattering are the most significant of the processes which might conceivably be involved in this interaction of the γ -radiation with the solid [12]. The energy of the γ -quantum is many times greater than that required for ejecting an electron and carrying it into the conduction band, so that an electron which has interacted with a

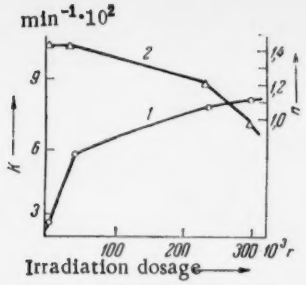

Fig. 3. The effect of irradiation with the γ -rays from Co^{60} on the kinetic parameters for the thermal decomposition of silver oxalate containing added cadmium: 1) alteration in the velocity constant; 2) alteration in the exponent n of the topokinetic equation.

quantum in photoelectric absorption should possess sufficient energy for dislogding secondary electrons. In the final analysis, the Compton scattering should also result in the appearance of additional free electrons in the solid body. These free electrons could, in any case, be captured by anion vacancies or other capture centers, either in the body of the crystal or on the surface, to form initiating centers for subsequent thermal decomposition. It can thus be supposed that the formation of initiating centers under γ -ray irradiation follows the same mechanism as that applying to the action of ultraviolet light. The difference is found in the fact that the action of the ultraviolet light is limited to the crystal surface so that the principal effect appears in the initial stage of the thermal decomposition whereas γ -ray irradiation gives rise to active centers throughout the body of the crystal and thus affects not only the initial stage of the thermal decomposition but the entire course of this reaction throughout the material.

In this case the effectiveness of preliminary γ -irradiation on the rate of thermal decomposition of the silver oxalate is diminished because of the formation of additional cation vacancies which can capture positive holes or silver cations from the lattice interstices.

LITERATURE CITED

[1] A. Benton and J. Cuningham, J. Am. Chem. Soc., 57, 2230 (1935).

[2] F. Tompkins, Trans. Farad. Soc., 44, 206 (1948).

[3] S. Sheppard and W. Vanselow, J. Am. Chem. Soc., 52, 3467 (1930) .

[4] Z. Szabo and E. Biro-Sugar, Zs. Elektrochem., 60, 871 (1956).

[5] A. Finch, P. Jacobs and F. Tompkins, J. Chem. Soc., 1954, 2054.

[6] L. Suchow and S. Hersh, J. Phys. Chem., 57, 438 (1953).

[7] V. V. Sviridov, "An Investigation of the Effect of Preliminary Irradiation on the Thermal Decomposition of Solid Substances", Avtoref. Dissertation, Minsk, 1955.

[8] V. V. Boldyrev, V. I. Eroshkin and Yu. A. Zakharov, Scientific Reports, Higher Schools, chem. and chem. tech. series., No. 3 (1959).

[9] B. V. Erofeev, Proc. Acad. Sci. USSR, 52, 575 (1946).

[10] G. V. Sakovich, Annals, Tomsk University, 26, 103 (1955).

[11] N. G. Gusev, V. P. Mashkovich and G. V. Obvintsev, Gamma Irradiation of Radioactive Isotopes and Fission Products (in Russian), Moscow, 1958.

[12] V.F lyuarty*,The Chemical Action of High-energy Radiations, Foreign Lit. Press, 1949.[Russian transl.].

Received June 19, 1959.

*Transliteration from the Russian.

A STUDY OF THE THERMODYNAMIC PROPERTIES OF SOLID SOLUTIONS IN THE NICKEL – CHROMIUM SYSTEM

E. Z. Vintaikin

The Central Scientific-Research Institute for Ferrous Metallurgy

(Presented by Academician G. V. Kurdyumov July 7, 1959).

A study of the thermodynamic properties of the solid solutions in the nickel – chromium system should be of interest for a variety of reasons. In particular, this study should lead to a deeper understanding of the processes which occur in such heat-resistant alloys as Nimonik,* a material which is widely employed in industry. A separation or coagulation of the consolidating phase is known to take place in these alloys during their operation and preliminary thermal treatment, this process being fixed by the rate of chemical diffusion of the alloying components. Data on the partial thermodynamic potentials of the components are indispensable to a study of chemical diffusion. A knowledge of the thermodynamic characteristics of the phases which are present in an alloy would also make it possible to independently determine the conditions required for the existence of these phases and the miscibility limits of the components. A thermodynamic study of commercial heat resistant alloys is difficult because of the large number of components which are present in these materials. Thus a study of the nickel – chromium system would be a first step toward investigating the thermodynamic properties of such heat resistant alloys as Nimonik.

The thermodynamic properties of the nickel –chromium system have been treated in [1,2]. Data on the oxidation of chromium in nickel – chromium alloys has been used by Grube and Flad [1] in determining partial and integral enthalpies and free energies at 1100 and 1200°. These data show that nickel – chromium alloys are characterized by negative values of the heat and entropy of mixing, and by negative departures from ideality over the entire concentration range.

Meijering [3] has analyzed Grube's results and has shown that they are not in conformity with the phase diagram for the nickel – chromium system. He considers that the results of [1] are in error, that equilibrium was not reached in the nickel-rich alloys, and that the method employed was of low precision in the case of the chromium-rich alloys. Measurements on the emf of concentration cells were used in [2] for determining the activity of chromium in nickel – chromium alloys at 750°. It was shown that the deviations from ideality are negative at the lower chromium concentrations and become positive as this concentration is increased. These authors were unable to obtain the temperature dependence of the activity because of the lack of reproducibility in the results.

The present work has aimed at a determination of the free energy, heat, and enthalpy of mixing in the case of nickel-rich solid solutions from the nickel –chromium system. This has involved a determination of the equilibrium pressures of chromium vapors above alloys of various concentrations and development of more precise data on pure chromium. The experimental technique was a combination of the method of radioactive isotopes and the Knudsen procedure for the determination of vapor pressures [4]. Vapor pressures were obtained for pure chromium and for alloys containing 3.5, 7.85, 20.3, 27.4, and 41.6 atomic percent of chromium over the temperature interval from 1100 to 1300°. The experimental data on the chromium vapor pressures are shown in Fig. 1, the pressures being expressed in dynes/cm^2. The following equations give the temperature variation of these pressures:

* Transliteration of the Russian-Publisher's note.

$$\lg p = -\frac{19760}{T} + 11{,}18 \quad \text{for} \quad 3{,}5 \text{ at.\% chromium}$$

$$\lg p = -\frac{20250}{T} + 11{,}93 \quad \text{for} \quad 7{,}85 \text{ at. \% chromium}$$

$$\lg p = -\frac{19770}{T} + 12{,}26 \quad \text{for} \quad 20{,}3 \text{ at. \% chromium}$$

$$\lg p = -\frac{19010}{T} + 12{,}03 \quad \text{for} \quad 27{,}4 \text{ at. \% chromium}$$

$$\lg p = -\frac{19060}{T} + 12{,}37 \quad \text{for} \quad 41{,}6 \text{ at. \% chromium}$$

$$\lg p = -\frac{19810}{T} + 13{,}02 \quad \text{for pure chromium}$$

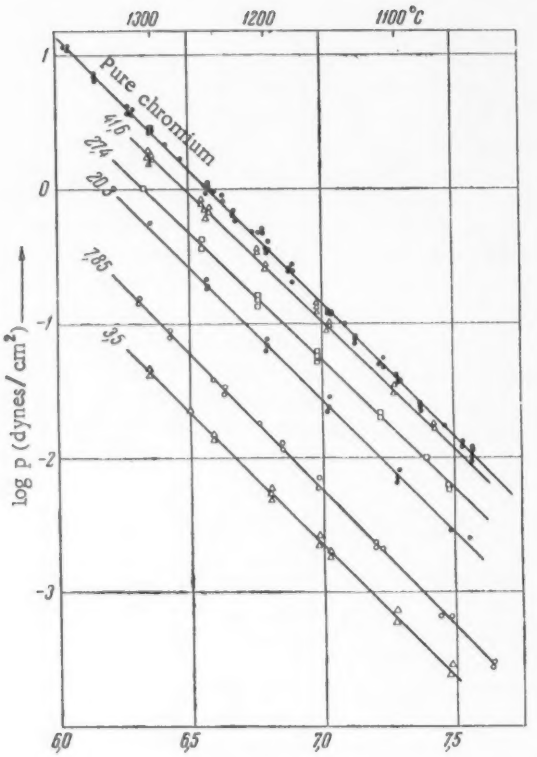

Fig. 1. The pressure of chromium vapors (dynes/cm²) above nickel – chromium alloys.

The thermodynamic activity of chromium at 1200° was determined from the equilibrium chromium vapor pressures and the activity of nickel then calculated through the Gibbs-Duhem Equation. These data are shown in Figure 2. The heat of solution of the chromium is clearly best calculated from the activity data of [2]. The error would be much less in this case since the data cover a wider temperature range (750-1200°). Figure 3 gives heats of solution of chromium and nickel as determined from the Gibbs-Duhem Equation.

Values of the relative integral thermodynamic functions, i.e., the heat content, $\Delta H = X_{Cr}\,\Delta\bar{H}_{Cr} + X_{Ni}\Delta\bar{H}_{Ni}$, and the thermodynamic potential, $\Delta F = RT\,(X_{Cr}\ln a_{Cr} + X_{Ni}\ln a_{Ni})$, were obtained from the data on the thermodynamic activities and the partial heats of solution. The entropy was evaluated from the well-known equation: $\Delta S = (\Delta H - \Delta F)/T$. The thermodynamic functions for the Ni-Cr systems are presented in Fig. 4.

It is to be seen from Figure 2 that the thermodynamic activity of chromium is characterized by negative departures from ideality at low concentrations and by positive departures at the higher concentrations. The heat of solution of chromium (Fig.3) is negative when the chromium concentration is low and becomes positive as the solubility limit is approached. The data indicate that a chromium atom is more firmly bound to the lattice of pure nickel than to the lattice of the solid solution. Certain conclusions of [5] (in which it was shown that the activation energy for the diffusion of chromium in pure nickel is less than for diffusion in an alloy containing 20% chromium) must be corrected in the light of the present results. It is clear that the assertion, given there, to the effect that the chromium atom is more firmly bound to the lattice of the solid solution, is to be taken in the kinetic sense, the chromium atom on a lattice point in the solid solution being more highly localized and having a higher potential barrier to overcome in order to undergo an elementary act of diffusion.

Figure 4 gives the concentration dependence of the free energy, entropy, and heat of mixing at 1200°. This figure shows that the free-energy excess is negative for nickel – chromium alloys lying in the 0-40 atomic % Cr concentration range; above 40 atomic % Cr this excess is clearly positive. The heat of mixing is negative

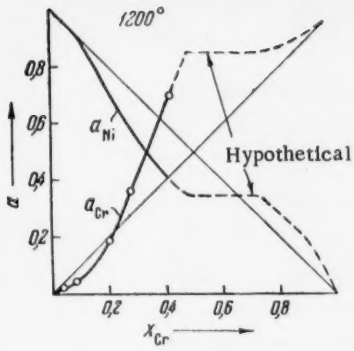

Fig. 2. The thermodynamic activity of chromium (1), and nickel (2), in nickel–chromium alloys.

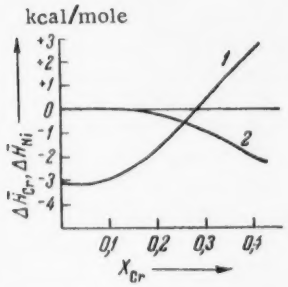

Fig. 3. The heat of solution of chromium (1), and nickel (2), in nickel – chromium alloys.

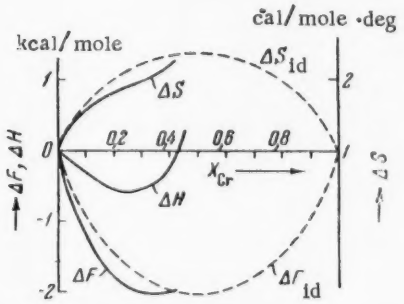

Fig. 4. The free energy,(1), heat, and entropy of mixing in nickel – chromium alloys.

for solid solutions falling in the interval of concentrations from 0 to 43 atomic % chromium, so that there is an evolution of heat when these alloys are formed from the pure components. This indicates that the energy of bonding rises as chromium is added to pure nickel. It has been shown in [6] that the bond strength also rises when chromium is added to nickel. Thus there is a certain parallelism between the energy of bonding and the bond strength in the nickel–chromium system.

It is clear from Figure 4 that the entropy of mixing is much less than that for the ideal case, the maximum negative departure being met at a concentration corresponding to Ni_2Cr. The observed negative value of the entropy excess obviously points either to local ordering or to nonadditivity in the heat capacity of the alloy.

Some interest attaches to a discussion of these results from the point of view of quasichemical theory. An interpretation of these data on the assumption that the energy of the solid solution is the sum of the energies of interaction of pairs of neighboring atoms leads to the conclusion that the bonding between unlike atoms is stronger than the bonding between atoms of the same kind. And the heat of solution of the chromium actually has its largest negative value in dilute solutions where each chromium atom is completely surrounded by nickel atoms. The heat of solution becomes more positive as the chromium concentration is increased and less tightly bound Cr–Cr pairs are formed. Nickel is principally bound to nickel in solutions in which the chromium atom concentration is low. The heat of dilution becomes negative when the chromium concentration is increased and the number of more tightly bound Nr – Cr pairs rises. Thus quasichemical theory would predict local ordering with preferential formation of unlike atom pairs on the basis of our data. It is interesting to note that the Ni_2Cr superstructure which was observed in [7, 8] is also characterized by a larger number of unlike atom pairs than would correspond to a random distribution.

LITERATURE CITED

[1] G. Grube and M. Flad, Zs. Electrochem., 48, No. 7 (1942).

[2] M. B. Panish, R. F. Newton, et al., J. Phys. Chem., 62, No.8 (1958).

[3] J. L. Meijering, Philips Res. Rep., 3, 281 (1948).

[4] E. Z. Vintaikin, Proc. Acad. Sci. USSR, 118, No.4 (1958).*

[5] P. L. Gruzin and G. B. Fedorov, Proc. Acad. Sci. USSR, 105, No.2 (1955).

[6] G. V. Kurdyumov and N. T. Travina, Problems of Metallography and the Physics of Metals, 4, 402 (1955).

*Original Russian pagination. See C. B. translation.

[7] G. Baer, Naturwiss., 43, No.13 (1956).

[8] Yu. A. Bagaryatskii and Yu. D. Tyapkin, Proc. Acad. Sci. USSR, 122, No. 5 (1958).*

Received June 29, 1959.

*Original Russian pagination. See C. B. translation.

THE EFFECT OF THE SURFACE CHARGE OF ZINC OXIDE ON THE RATE OF CHEMISORPTION OF OXYGEN

É. Kh. Enikeev, L. Ya. Margolis and S. Z. Roginskii,

Corresponding Member, Acad. Sci. USSR

The Institute of Physical Chemistry of the Academy of Sciences of the USSR

The effect of the surface charge on the kinetics of chemisorption on a semiconductor has been considered by a number of authors [1-4]. One of the authors of the present work has recently shown [5] that the energy of charging of a semiconducting surface with respect to the underlying body is one of the components of the observed activation energy, E, for a chemical process which proceeds through charged transition complexes on this surface, i.e.:

$$\Delta E^{\pm} = \mp e\Delta V_{\Sigma},$$

where V_{Σ} is the total potential difference between the surface and the body of the semiconductor.

The introduction of an additive into a semiconductor will affect the value of E_{chem} by displacing the Fermi level and altering its distance from the band edges in the body of this material. The change in the activation energy, $\Delta E^{\mp}_{chem}$, will be almost identical with the band bending if the Fermi level is fixed in the body of the semiconductor. The controlling band undergoes continual displacement as the coverage rises during chemisorption on a nonuniform surface, the observed value of $\Delta E^{\pm}$ for this adsorption (at fixed initial E) being represented by a sum

$$\Delta E^{\pm}_{obs} = \Delta E_{\rho} + \Delta E_{v},$$

in which ΔE_{ρ} is the change resulting from a shift over the distribution, and ΔE_{V} is the distortion in the distribution arising from the surface charge. Such superposition of effects is not met in catalytic processes, but it is one of the principal complicating factors in determining the charge effect in the mechanism of chemisorption on actual adsorbents and catalysts which are always nonuniform. The experimentally observed alteration in the work function, $\Delta\varphi$, can serve as a measure of the energy band bending, ΔV_{D}, on the semiconducting surface when molecules of low dipole moment are irreversibly captured by this surface,

The initial surface potential must be varied over wide limits in order to develop the relation between the charge and the rate of chemisorption. The impregnation of ZnO with dissolved $ZnSO_4$ with subsequent heating to 450° will increase the work function, φ, by 0.5 ev with respect to its value for pure ZnO. G. M. Zhabrova has used tagged S^{35} to show that this $ZnSO_4$ is firmly bound to the ZnO surface. The value of φ can be reduced considerably by introducing Li_2O into the ZnO.

The Deryagin filtration method was used here to measure the specific surfaces of ZnO specimens containing various additives and led to the results shown in Table 1.

The alteration in the work function of the ZnO was obtained by using the vibrating condenser method [6] to measure the difference of contact potentials. Adsorbed oxygen was removed from the surface of each specimen by heating to 350 –400° in an atmosphere of carbon monoxide with subsequent evacuation to 10^{-6} mm of Hg.

TABLE 1

The Specific Surface of Adsorbents

Preparation no.	Adsorbent	Specific surface (m^2/g)
1	ZnO	7,5
2	ZnO + 8% Li_2O	11,0
3	ZnO + 0,1% $ZnSO_4$	7,5
4	ZnO + 15% $ZnSO_4$	22,6

TABLE 2

Preparation no.	Catalyst	Contact potential relative to gold
1	ZnO	+0,75
2	ZnO + 8% Li_2O	—0,05
3	ZnO + 0,1% $ZnSO_4$	+0,95
4	ZnO + 15% $ZnSO_4$	+1,30

TABLE 3

The Alteration in the Activation Energy for Oxygen Adsorption and the Surface Charge of Pure Zinc Oxide and Modified Zinc Oxide

Preparation no.	Catalyst	Alteration in work function, $\Delta\varphi$		Activation energy, kcal/mole			Alteration in the activation energy, kcal/mole
		ev	kcal	from initial rate	from the Zel'dovich-Roginskii Equation with q = 0	to a coverage of $5 \cdot 10^{-5}$ ml/m^2	
1	ZnO	0	0	26	19	25	—
2	ZnO + 8% Li_2O	—0,80	—18	7	7,9	10	—19
3	ZnO + 0,1% $ZnSO_4$	+0,20	+ 4,5	30	—	—	+ 4
4	ZnO + 15% $ZnSO_4$	+0,55	12,5	38	35	—	+12

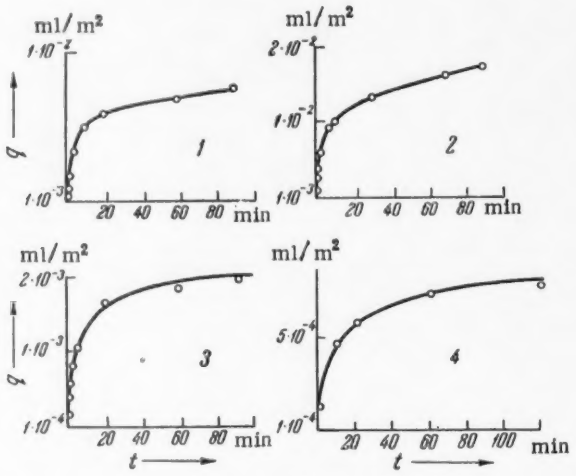

Fig. 1. Kinetic isotherms for the 342° adsorption of oxygen: 1) on ZnO, 2) on ZnO + 8% Li_2O; 3) on ZnO + 0.1% $ZnSO_4$; 4) on ZnO + 15% $ZnSO_4$.

The difference in the contact potentials of the specimen and a gold reference electrode was measured to within ± 0.01 volt at room temperature. The measured values were reproducible to within 0.05 volts. Table 2 gives values of the contact potentials (or the alteration in the work function, φ) for pure ZnO and for ZnO which had been modified by additives. The value of the work function relative to pure ZnO was increased by the addition of $ZnSO_4$ and diminished by the addition of Li_2O.

Figure 1 gives the 342° kinetic isotherms for the adsorption of oxygen on pure ZnO and on modified ZnO. This figure shows that the chemisorption of oxygen was accelerated by Li^+ and retarded by SO_4^{2}.

Kinetic isotherms were developed at 242, 300, and 430°, and from these energy of adsorption was determined. Table 3 gives values of the activation energy for the adsorption of oxygen on pure ZnO and on ZnO containing additives. The activation energy for chemisorption was determined from the initial rate (at the end of 3 minutes) using the equation $W = W_0 e^{-\alpha q}$, with $q = 0$, and from the isothermal rates.

The alteration of the activation energy for oxygen adsorption on ZnO containing added Li_2O or $ZnSO_4$ is compared with the alteration in the value of φ in Figure 2. The relation between ΔE and $\Delta\varphi$ is linear to within approximately 2 kcal, the limit of experimental error. This straight line has a slope of almost exactly 45°. It is to be noted that the rate of adsorption altered only insignificantly (~ 100 fold. in this case) although the energy of activation was greatly affected by the change in φ. This is to be explained by the existence of a compensating effect which will be reported on separately.

The rate of adsorption fell and the value of φ increased as the surface was progressively covered with the adsorbed O_2, the effect being the same as that resulting from an increase of the potential barrier by irreversible introduction of an additive. The maximum change of φ in the adsorption of oxygen on ZnO or on ZnO + 8% Li_2O was about 0.2-0.4 ev (4.5-9 kcal) in these experiments, the associated increase in the activation energy being 5-9 kcal.

We have shown earlier [7] that the φ value for ZnO increases linearly with the oxygen coverage when the latter is less than .1%, i.e., that $\Delta\varphi = \gamma q$, where q is the amount of adsorbed O_2 per 1 cm^2, and that $\Delta\varphi = \gamma \log q$ for ZnO + 8 Li_2O at high coverage. Assuming that the oxygen adsorption occurs exclusively on the surface and introducing these $\Delta\varphi$, coverage relations into the equation for the adsorption rate

$$\frac{dq}{dt} = A \exp\left(\frac{-\Delta\varphi}{kT}\right)$$

gave the Zel'dovich-Roginskii Equation [8]

$$W_i = \frac{dq}{dt} = A \exp\left(\frac{-\gamma q}{kT}\right), \tag{1}$$

for the case $\Delta\varphi = \gamma q$, and the Benkhem Equation [9]

$$W_i = \frac{dq}{dt} = A \exp\left(\frac{-\gamma \lg q}{kT}\right). \tag{2}$$

for the case $\Delta\varphi = \gamma \log q$.

Figure 3 gives kinetic isotherms for the adsorption of oxygen on ZnO containing added Li_2O or $ZnSO_4$. The surface potential of ZnO + $ZnSO_4$ varied linearly with the oxygen coverage so that the adsorption kinetics for this material follow the Zel'dovich-Roginskii Equation. The work function for ZnO containing Li_2O was logarithmically related to the oxygen coverage and the adsorption kinetics follow the Benkhem* Equation. This indicates that the kinetic isotherm is fixed by the surface charge at which the oxygen adsorption takes place.

The time dependence of the potential in adsorption could be had by substituting for q in Equation (1) to obtain

$$\Delta\varphi \cong \gamma \lg (t + t_0).$$

A similar substitution into Equation (2) led to

$$\Delta\varphi = \gamma' \lg (t + t_0).$$

*Transliteration from the Russian.

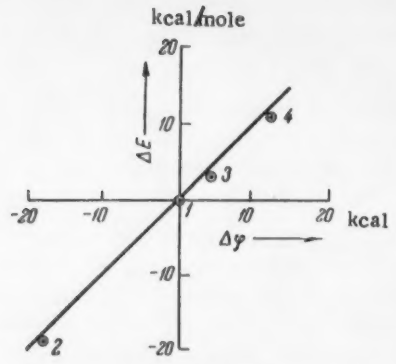

Fig. 2. The relation between the alteration in the activation energy for the chemisorption of oxygen as calculated from the initial rate and the alteration in the work function for ZnO (1), and for ZnO with 8% Li_2O (2); 0.1% $ZnSO_4$ (3); or 15% $ZnSO_4$ (4).

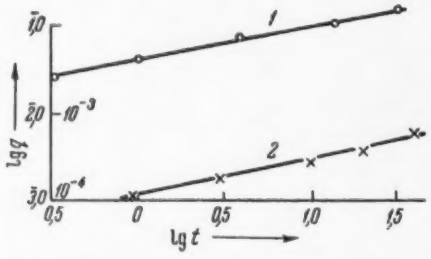

Fig. 3. Kinetic isotherms for the adsorption of oxygen on ZnO + 8% Li_2O (1) in the co-ordinates log q vs log t, and for adsorption on ZnO + 15% $ZnSO_4$ (2) in the coordinates q vs log t.

These relations are actually observed to hold for ZnO and for ZnO containing 8% Li_2O.

These results show that there is a simple relation between $\Delta\varphi$ and ΔE in the kinetics of chemisorption. It should be noted that this relation is dependent on the type of additive and the method of its introduction into the semiconductor, whether this be by adsorption, by surface capture, or by the formation of a bulk solid solution.

The fact that this relation is valid in the area of ZnO containing bulk-dissolved Li_2O indicates that the work function is a determining factor in fixing the kinetics of chemisorption. The surface charge in oxygen adsorption, or in $ZnSO_4$ capture from solution, will affect the adsorption kinetics in so far as it alters the experimentally measured value of the work function. The adsorption of a mixture of one donor and one acceptor gas (such adsorption is frequently met in catalysis, an instance being the catalytic oxidation of CO by oxygen on NiO) results in the adsorption of one of these gases being accelerated by the adsorption of the other. This can possibly be explained by the fact that the catalytic reaction sometimes proceeds more rapidly than the adsorption of either of the gases.

In conclusion, the authors wish to express their thanks to G. M. Zhabrova for furnishing the specimens of zinc oxide containing the additives and to M. Ya. Kushnerev for x-ray and electronographic analyses of these specimens.

LITERATURE CITED

[1] K. Hauffe and H. J. Engel, Zs. Elecktrochem., 56, 366 (1952); 57, 762 (1953).

[2] P. Aigrain and C. Dugas, Zs. Elektrochem., 56, 363 (1952).

[3] S. Roy Morrison, Advance in Catal., 7, 259 (1955).

[4] F. F. Vol'kenshtein, Prog. Chem., 27, 1304 (1955). [USSR].

[5] S. Z. Roginskii, Problems of Kinetics and Catalysis No.10 (1959); Proc. Acad. Sci. USSR, 126, No.4 (1959).*

[6] V. F. Bogolyubov, Radiotechnology and Electronics, 1, 527 (1957).

[7] É. Kh. Enikeev, L. Ya. Margolis and S. Z. Roginskii, Proc. Acad. Sci. USSR, 124, 606 (1959);* É. Kh. Enikeev, Problems of Kinetics and Catalysis, No.10 (1959).

[8] S. Z. Roginskii and Ya. B. Zel'dovich, Acta Physico-Chim., 1, 139 (1954).

[9] S. Z. Roginskii, Adsorption and Catalysis on Nonuniform Surfaces (in Russian), Acad. Sci. USSR Press, 1949.

Received June 25, 1959.

*Original Russian pagination. See C. B. translation.

A NEW TYPE OF CURRENT DISCONTINUITY IN THE REDUCTION OF THE BrO_3^- ANION AT THE DROPPING ELECTRODE

V. I. Zykov

The All-Union Scientific Research Institute for Aviation Materials

(Presented by Academician A. N. Frumkin May 29, 1959)

The literature [1-7] has described a certain current discontinuity on the polarization curves for reduction of various oxygen-containing anions of the XO_3^- type which occurs at fixed potential as the result of autocatalysis of the electrode reaction. An indispensable condition for the appearance of such discontinuity in unbuffered electrolytes is the presence of tri-, or tetra-, valent cations such as those of lanthanum or cerium.

This discontinuous increase in the current can also be observed when the bromate anion is reduced against a background of doubly charged cations under certain definite conditions (Fig. 1). These conditions can be realized by adding increasing amounts of the $(C_4H_9)_4N^+$ cation to a $BaCl_2$ solution containing BrO_3^- (Fig.1, curve 2). The present experiments were carried out with a dropping mercury electrode which had a capillary of circular cross-section. This electrode had the following characteristics: rate of mercury flow with a 300 mm mercury column, m = 1.96 mg/sec; drop period measured in 1.0 M KCl at 25°, with η = -0.46 volts and a pressure of 300 mm of Hg, τ = 3.1 sec. Potentials were measured against a saturated calomel electrode.

The first signs of an anomalous current, potential relation are met at tetrabutylammonia concentrations of the order of 10^{-4} M (Fig.1, curve 3). The curvature of the initial wave segment at first markedly increases, and at the same time the wave is displaced in the direction of more negative potentials. Displacement continues in the negative direction with increasing curvature of the initial segment of the polarization curve as the tetrabutylammonia concentration rises (Fig.1, curves 4,5). A current discontinuity appears on the steep portion of the wave (up to its merging with Curve 1) when the additive concentration is in excess of $9 \cdot 10^{-4}$ M (Fig.1, curves 6-9). The potential of this current discontinuity moves in the negative direction as the tetrabutylammonia concentration is increased. Figure 2 shows, however, that the rate of increase of this movement sharply diminishes as the additive concentration rises.

An increase in the bromate ion concentration at fixed concentrations of background and added $(C_4H_9)_4N^+$ leads to a proportionate increase in the value of the saturation current, the position of the wave with respect to the potential axis remaining unaltered. The i_{sat}, $\sqrt{P_{Hg}}$ relation indicates that the saturation current on the bromate wave is a diffusional current, regardless of the concentration of the added $(C_4H_9)_4N^+$. There is no hysteresis loop when the polarization curve is developed in the opposite direction, working from the more negative to the more positive potentials. Current discontinuities of this type are not met when the doubly charged cations of the background are replaced by alkali metal ions.

It is interesting to compare the above results with the data of Figures 3 and 4* on the effect of tetrabutylammonia on the reduction of BrO_3^- and IO_3^- against a $LaCl_3$ background. The $(C_4H_9)_4N^+$ concentration for curve 6, Fig. 1, is less by several factors than the concentration for curve 5, Fig.3 and curve 13, Fig.4, but these latter curves show only an brupt rise in the current with no discontinuity.

*The observations on the reduction of iodate anions against a $LaCl_3$ background in the presence of $(C_4H_9)_4N^+$ are of interest in themselves and we propose to consider them in detail in a separate communication.

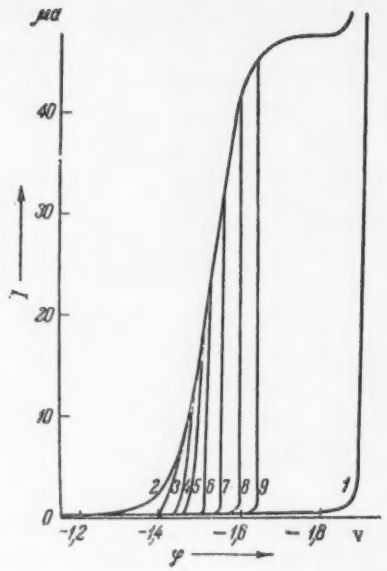

Fig. 1. The reduction of BrO_3^- on a $BaCl_2$ background with added tetrabutylammonia. Solution compositions: 1) 0.1 M $BaCl_2$ background; 2) 0.1 M $BaCl_2$ + $1.96 \cdot 10^{-3}$ M $KBrO_3$; 3) the same + + $1.57 \cdot 10^{-4}$; 4) the same + $3.14 \cdot 10^{-4}$; 5) the same + $4.70 \cdot 10^{-4}$; 6) the same + $9.23 \cdot 10^{-4}$; 7) the same + $2.40 \cdot 10^{-3}$; 8) the same + $3.62 \cdot 10^{-3}$; 9) the same + $1.20 \cdot 10^{-2}$ M $(C_4H_9)_4NI$.

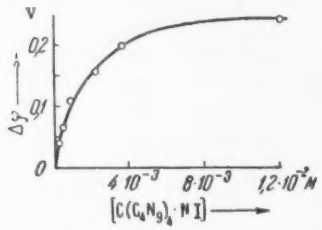

Fig. 2. The relation between the displacement of the potential corresponding to the current discontinuity in the reduction of BrO_3^- on a $BaCl_2$ background and the concentration of added tetrabutylammonia.

In this connection it is worth noting that the potential for the current discontinuity in the case of curve 6, Fig. 1, is more negative than the $\varphi_{1/2}$ value for the reduction of BrO_3^- (Fig. 3, curve 5) or IO_3^- (Fig. 4, curve 13) against a lanthanum chloride background.

The following conclusions can be drawn from this experimental material:

1. The current discontinuity in the reduction of the bromate anion against a background of alkali metal cations in the presence of $(C_4H_9)_4N^+$ arises through a mechanism which is different from that met in autocatalytic discontinuities; 2) the discontinuous alteration in the current results from an alteration in the double-layer structure as a consequence of an abrupt desorption of the tetrabutylammonia cations at fixed potential [10]. For this reason, the discontinuities which are described in the present work could be designated as desorption discontinuities.

The study of the mechanism of this effect can follow the same bath as has been marked out in investigating the kinetics of the bromate-ion reduction and its dependence on the nature and charge of the cations of the indifferent electrolyte [8,9]. The starting point here is found in the assumption that a mobile equilibrium is established between the reducing BrO_3^- anions and the M^+ cations which are adsorbed on the electrode surface

$$M^{z+} + BrO_3^- \rightleftarrows [M^{z+} \cdots BrO_3^-]^{(z-1)+}, \qquad (1)$$

ion pairs being formed with those BrO_3^- anions which participate in the reaction.

From this point of view, the retarding effect of adding $(C_4H_9)_4N^+$ cations to solution is the result of a reduction of the surface concentration of the reacting particles due to displacement of Equilibrium (1) to the left. A comparison of the adsorbabilities and ionic radii of the $(C_5H_9)_4N^+$ and M^+ cations will make this understandable. The M^+ cations will be displaced from the double layer and replaced by the specifically adsorbing $(C_4H_9)_4N^+$ cations when the latter are added to the solution. The probability that a BrO_3^- will form an ionic pair with so large a cation as a $(C_4H_9)_4N^+$ is less than the probability for the formation of a pair with an M^+ cation, so that the concentration of particles in the layer adjacent to the cathode will fall, the rate of reaction at given potential will diminish, and the wave will be displaced in the negative direction. The normal structure of the double layer is abruptly reestablished at the desorption potential for the tetrabutylammonia and the current sharply increases, going from essentially zero to the value corresponding to the desorption potential in the absence of $(C_4H_9)_4N^+$. Further alteration in the current strength with increasing negative potential of the cathode is the result of diminishing energy of activation, just as in the absence of the tetrabutylammonia, and it is for this reason that Curves 3-9 of Fig. 1 coincide with Curve 2 at potentials more negative than the desorption potential. The displacement of the discontinuity potential in the negative direction with increasing concentration of the added $(C_4H_9)_4N^+$ is tied up with the displacement of the desorption potential of these latter ions.

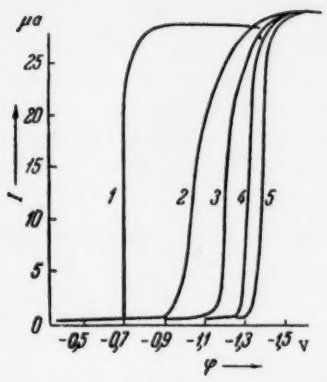

Fig.3. The reduction of BrO_3^- on a $LaCl_3$ background with added tetrabutylammonia. Solution compositions: 1) $1.28 \cdot 10^{-2}$ M $LaCl_3$ + $1.27 \cdot 10^{-3}$ M $KBrO_3$; 2) the same + $4.0 \cdot 10^{-4}$; 3) the same + $8.0 \cdot 10^{-4}$; 4) the same + $1.56 \cdot 10^{-3}$; 5) the same + $3.43 \cdot 10^{-3}$ M $(C_4H_9)NBr$.

The lack of a current discontinuity on curves 5 and 13 of Figures 3 and 4 for the reduction of BrO_3^- or IO_3^- on a La^{3+} cation background in the presence of tetrabutylammonia is clearly due to the fact that the reduction of these anions begins here at potentials under which the $(C_4H_9)_4N^+$ cations are not yet desorbed, the desorption potential being reached at the saturation value of the current. There is also the possibility that tetrabutylammonia desorption in the presence of La^{3+} cations takes place gradually, over a certain potential interval, rather than abruptly, at fixed potential, but this is a point which needs further experimental checking.

It is to be understood that the kinetics of BrO_3^- reduction on a background of alkali metal cations need not be affected by addition of tetrabutylammonia, since the reaction is taking place here at potentials (-1.85 v in 0.1 M KCl) under which the $(C_4H_9)_4N^+$ is not yet adsorbed. The BrO_3^- wave does not appear at all on a background of $(C_2H_5)_4N^+$ and $(C_4H_9)_4N^+$ which does not contain alkali metal cations. This fact can be explained by extensive displacement of Equilibrium (1) to the left.

This is not the only point of view which can be adopted in interpreting the mechanism of the retarding action of adsorbed organic R_4N^+ cations on the reduction of anions of the type XO_3^-.

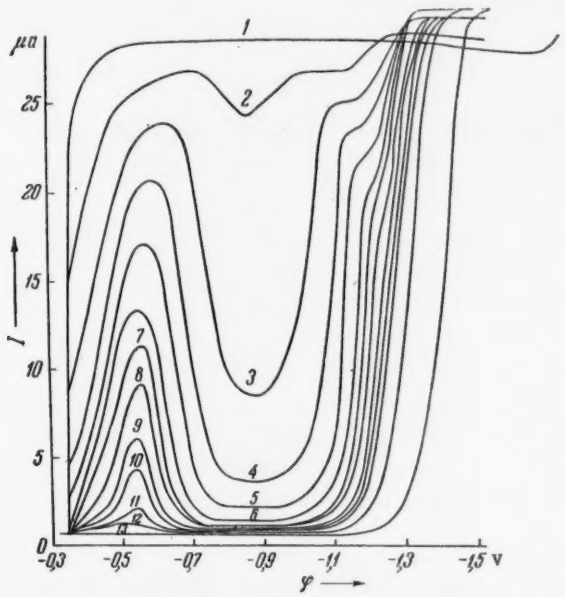

Fig. 4. The reduction of IO_3^- on a $LaCl_3$ background in the presence of added tetrabutylammonia. Solution composition: 1) 0.1 M $LaCl_3$ + $1.5 \cdot 10^{-3}$ M KIO_3; 2) the same + $6.9 \cdot 10^{-5}$; 3) the same + $1.03 \cdot 10^{-4}$; 4) the same + $1.38 \cdot 10^{-4}$; 5) the same + $1.72 \cdot 10^{-4}$; 6) the same + $2.07 \cdot 10^{-4}$; 7) the same + $2.41 \cdot 10^{-4}$; 8) the same + $2.76 \cdot 10^{-4}$; 9) the same + $3.45 \cdot 10^{-4}$; 10) the same + $4.14 \cdot 10^{-4}$; 11) the same + $2.52 \cdot 10^{-4}$; 12) the same + $8.97 \cdot 10^{-4}$; 13) the same + $4.20 \cdot 10^{-3}$ M $(C_4H_9)NBr$.

A. N. Frumkin has shown that this retardation can also be explained by taking account of the alteration in the local φ_1 -potential at the point where the reducing anion is located during adsorption of the R_4N^+ [9, 10]. The mean φ_1 -potential is displaced in the positive direction, but it is still possible that the local φ_1 -potential would move in the negative direction and thereby bring about a retardation in the process.

An effect which is similar, but of opposite sign, has been observed in the reduction of the persulfate anion in the presence of tetrabutylammonia [10, 11]. Direct measurements of the potential dependence of the differential capacity of the mercury electrode have shown that the accelerating effect of the $(C_4H_9)_4N^+$ cation on this reaction diminishes at the desorption potential of these ions, the current falling sharply to the value which is observed without the tetrabutylammonia.

I wish to express my deep thanks to Academician A. N. Frumkin for his valuable advice and for discussion of this work.

LITERATURE CITED

[1] J. Mašek, Chem. listy, 46, 683 (1952).

[2] M. Tokuoka, Coll. Czech. Chem. Comm., 4, 444 (1932).

[3] M. Tokuoka and J. Ruzicka, Coll. Czech. Chem. Comm.,6, 339 (1932).

[4] J. Kolthoff, W. E. Horris and G. Matsujama, J. Am. Chem. Soc., 66,1782(1944).

[5] A. N. Frumkin and S. I. Zhdanov, Proc. Acad. Sci. USSR, 92, 629 (1953).

[6] S. I. Zhdanov, Dissertation, Moscow, 1954.

[7] V. I. Zykov and S. I. Zhdanov, J. Phys. Chem., 32, 644 (1958) [USSR].

[8] V. I. Zykov and S. I. Zhdanov, J. Phys. Chem., 32, 791 (1958) [USSR].

[9] A. Frumkin, Trans. Farad. Soc., 55, 156 (1959).

[10] A. N. Frumkin and N. V. Nikolaeva-Fedorovich, Herald, Moscow University, phys.chem.series, 4,169 (1957).

[11] N. V. Nikolaeva-Fedorovich and B. B. Damaskin, Proc., Conference on the Effect of Surface Active Substances on the Electrodeposition of Metals, Vilna, 1957, page 33.

Received March 26, 1959.

A DETERMINATION OF THE PHASE DIAGRAMS OF THE NAPHTHALENE–β-Cl-NAPHTHALENE AND 1, 8-DINITRONAPHTHALENE – 1, 5-DINITRONAPHTHALENE SYSTEMS BY THE METHOD OF MONOCRYSTAL GROWTH

A. I. Kitaigorodskii and R. M. Myasnikova

The Institute for Elementoorganic Compounds of the Academy of Sciences of the USSR

(Presented by Academician N. V. Belov June 12, 1959)

The conditions which are required for forming solid solutions of organic compounds, and the requirements for complete miscibility of such substances, were formulated in 1956 - 1957 [1]. The data reported in the literature on many systems which had been studied by the thermographic method are not consistent with this theory and it has been shown that the phase diagrams for these systems are probably in error. A systematic program for establishing correct phase diagrams for these systems has been carried out in this laboratory.

The Determination of Phase Diagrams by the Method of Monocrystal Growth

It is known that the low sensitivity of the thermographic method is especially significant in developing phase diagrams for organic systems [2] for there is a pronounced tendency toward supercooling in these systems and the heats of phase transition are low. It often happens that an organic eutectic, even one in the interior of the diagram, can only be made to crystallize by the introduction of "seeds" into an intensively agitated, strongly supercooled melt, while many eutectics in the fields adjacent to the pure components will not crystallize at all under the conditions which prevail during the recording of the cooling curves. All of this has forced us to seek other methods for testing those reported phase diagrams which clearly fail to conform to the theory.

A method for developing phase diagrams under conditions giving maximum approach to reversible melt crystallization has been worked out in this laboratory [3,4]. A tube crystallizer closed by a stopper carrying a thin sharpened wire of low thermal conductivity was placed into a thermostat which had transparent walls. Monocrystals of the components, or of solid solutions of these components, grew from the end of this wire in the crystallizer. With a thermostat of high stability (the temperature variation did not exceed 0.05° in the present case) and minimum supercooling of the melt (by 0.1-0.2°) it was possible to grow several reasonably uniform monocrystals (about 10 mg, total) from 3-4 g of a given melt in 8-10 hours. The liquidus curve was constructed from the melting points of these crystals in the melt (it has already been pointed out that the melting temperature, t_1, is higher than the crystallization temperature, t_2, by 0.1-0.2), the number of phases being determined either by x-ray analysis or by visual observation of the form of the growing crystal.

The crystals were removed from the melt and used for determining the solidus curve. The solidus curve could be located readily from microanalyses of the crystals for an element which was present in only one of the components. A method based on the exact knowledge of the liquidus curve was used in those cases in which the two components had the same composition. The composition of the monocrystals of the solid solution is different from that of the solution in which these crystals are growing and these crystals will therefore melt over a different temperature interval. These crystals were introduced into a wide capillary (D ≈ 2 mm) which was then sealed, placed in a thermostat and heated; first signs of a "rarefraction" in the capillary appeared at the temperature t_1 of the point on the liquidus which corresponded to the melt out of which these crystals were grown.

TABLE 1

Melt composition mole %		Temperature*, C		External form of crystals	Solid phase composition, mole %	
naphthalene	β-Cl-naphthalene	t_1	t_2		naphthalene	β-Cl-naphthalene
100	0	80,0	79,9	plates	100	0
90	10	76,2	76,1	same	—	—
80	20	68,4	68,2	same	93,49	6,51
70	30	61,9	—	fibers - grow	—	—
60	40	51,2	—	same	—	—
55	45	49,3	—	same	—	—
50	50	49,7	49,6	petals	43,9	56,1
40	60	50,3	50,1	same	32,5	67,5
20	80	53,7	53,6	same	14,0	86,0
0	100	57,3	57,2	same	0	100

* t_1 is the melting temperature for fusion of the crystals into the melt and t_2 is the temperature of crystal growth.

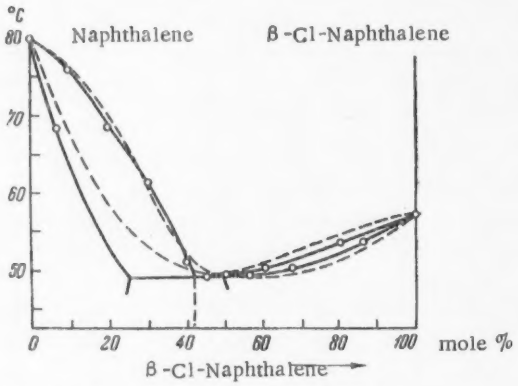

Fig. 1. Phase diagram for the naphthalene – β-Cl-naphthalene system (the diagram represented by the dashed curves was developed from the data of the literature).

The temperature t_3 at which the last "solid" grain melted into the liquid could be fixed satisfactorily by raising the temperature so slowly that equilibrium was always maintained between the liquid and solid phases in the capillary. The foot of a perpendicular dropped onto the axis of abscissas from the point of intersection of the t_3 horizontal with the already-known liquidus curve gave the crystal composition, and the intersection of this perpendicular with the t_1 -horizontal fixed a point on the solidus curve. This method was tested on the acridine – –anthracene and naphthalene– β-Cl-naphthalene systems for which the liquidus curves had been located by microanalysis, and gave satisfactory results.

Phase Diagrams for the Naphthalene –β-Cl-Naphthalene and the 1, 8-Dinitronaphthalene – 1, 5-Dinitronaphthalene Systems.

The thermographic data of the literature on the naphthalene – β-Cl-naphthalene [5] and the 1, 8-dinitronaphthalene – 1, 5-dinitronaphthalene systems [6] point to complete miscibility in the solid state with a minimum (Roozeboom's Type III). Our theory shows that it is impossible to have complete miscibility in these systems. Results from a study of the naphthalene– β-Cl -naphthalene system are given in Table 1.

Figure 1 (the diagram represented by the dashed curves has been described earlier in [5]) shows that there is only limited solid state miscibility in the naphthalene – β-Cl-naphthalene system (Roozeboom's Type V). Monocrystals could not be grown from mixtures falling in the interval of concentrations from 30 to 45% β-Cl-naphthalene; here points on the liquidus curve were located from the melting of the polycrystalline fibers which grew on the wire and the boundaries of the region of limited solubility were fixed by the beginning of "softening" of the solidified melts (this softening occurs at 49.3-49.5° in the interval from 30 to 50% β-Cl-naphthalene). The eutectic point was located at 49.3° and 41.5% β-Cl-naphthalene by extrapolation of the two liquidus curves. X-ray structure diagrams were used in deciding whether monocrystals belonged to the naphthalene or the β-Cl-naphthalene phase, even though these substances have different crystalline forms. The solidus line was located from microanalyses for the chlorine content of the monocrystals.

TABLE 2

Melt composition, mole %		Temperature *, °C			External form of crystal
1,8-$C_{10}H_6(NO_2)_2$	1,5-$C_{10}H_6(NO_2)_2$	t_1	t_2	t_3	
100,0	0	169,0	168,8	169,0	Rhombohedra
85,0	15,0	155,9	155,8	168,8	same
77,9	22,1	148,3	148,2	168,0	same
76,7	23,3	147,3	147,2	—	Rhombohedra and needles
75,0	25,0	149,9	149,8	—	Needles
70,0	30,0	157,2	157,1	211,4	same
60,0	40,0	169,9	169,8	212,6	same
50,0	50,0	180,4	180,3	212,7	same
40,0	60,0	188,3	188,2	212,7	same
30,0	70,0	194,9	194,8	212,8	same
15,0	85,0	204,0	203,9	212,8	same
5,0	95,0	210,4	210,3	212,9	same
0	100,0	213,0	212,9	212,9	same

* t_1 is the melting temperature for fusion of the crystals into the melt, t_2 is the temperature of crystal growth, and t_3 is the temperature at the end of melting in the capillary.

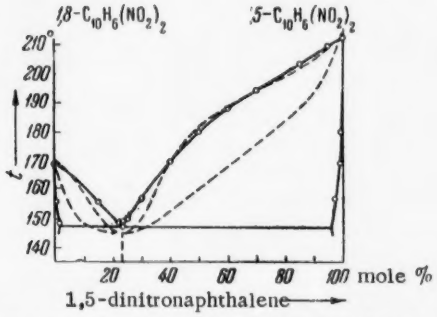

Fig. 2. Phase diagram for the 1, 8-dinitronaphthalene – 1, 5-dinitronaphthalene system (the diagram represented by the dashed curves was developed from the data of the literature).

The results from our study of the 1, 8-dinitronaphthalene – 1, 5-dinitronaphthalene system are shown in Table 2 and Figure 2 (the diagram represented by the dashed curves was constructed from the data of Pascal [6]).

This system also showed only limited miscibility in the solid phase. It differed from the preceding system in that good rhombohedral crystals (1,8-dinitronaphthalene phase) or needles (1, 5-dinitronaphthalene phase) could be grown at all concentrations. Extrapolation of the two liquidus curves gave a eutectic point at 147.3° and 23.3% 1, 5-dinitronaphthalene in the melt; rhombohedral crystals and needles grow simultaneously from a melt of this composition at 147.2° (see Table 2). The solidus line was located by observation of the melting of crystals taken out of the melt. The extension of the eutectic line from 2 to 95% 1, 5-dinitronaphthalene was also based on visual observations; a liquid phase appeared when solidified melts lying in this concentration range were heated to 147.3-147.5°, with final melting at the liquidus curve.

It is to be noted that the rhombohedral crystals of 1,-8-dinitronaphthalene and its solid solutions decompose on cooling. Optical measurements showed that these crystals should be classified as having monoclinic syngony, whereas crystals of 1, 8-dinitronaphthalene grown from alcoholic solution at room temperature have the form of right prisms and possess rhombohedral syngony. It is clear that 1, 8-dinitronaphthalene has two enantiotropic modifications.

LITERATURE CITED

[1] A. I. Kitaigorodskii, Proc. Acad. Sci. USSR, 113, No.3, 604 (1957).*

[2] V. Ya. Ansov and S. A. Pogodin, Principles of Physicochemical Analysis, (in Russian), Acad. Sci. USSR Press, 1947.

*Original Russian pagination. See C. B. translation.

[3] R. M. Myasnikova and A. I. Kitaigorodskii, Crystallography, 3, vol. 2, 160 (1958).

[4] N. Ya. Kolosov, Crystallography, 3, vol. 6, 700 (1958).

[5] L. Klem, W. Klem and G. Schiemann, Zs. Phys. Chem., 165, 379 (1933).

[6] M. Pascal, Bull. Soc. chim. France, 4, 27, 388 (1920).

Received June 11, 1959.

KINETIC STUDIES OF SORBENT STRUCTURES
THE PERMEABILITY OF ACTIVE CHARCOALS WITH PARTIALLY BLOCKED PORES

D. P. Timofeev and I. T. Erashko

The Institute of Physical Chemistry of the Academy of Sciences of the USSR

(Presented by Academician M.M. Dubinin July 7, 1959)

Active charcoals will in general show three types of pore: micro, intermediate, and macro. The methods which have been developed for studying the porosity of sorbents (sorption methods, mercury porometry, electron microscopy, etc.) have made it possible to determine satisfactorily the dimensions and volumes of each of these pore types, the distribution of pore volumes over dimensions, and (to a certain degree) the interconnection between the intermediate pores and the micropores (electron microscopy). It has not been possible to establish the existence of connections between the micropores and the other types of pores through electron-microscopic studies. The problem of the connection between the various types of pores is of fundamental interest to the study of material transfer in porous sorbents.

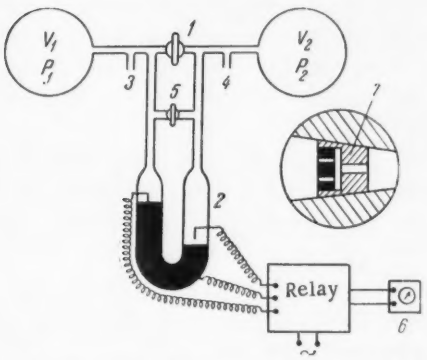

Fig. 1. Diagram of apparatus: 1) stopcock with grains of charcoal; 2) differential manometer; 3, 4) connections to manometer section and vacuum pump; 5) stopcock; 6) timer; 7) ground metallic insert in opening of stopcock.

Dubinin, Zhuk, and Zaverina [1] have studied the interconnection of the various types of pores in charcoal by using the thermal decomposition of benzene vapors at 900° to progressively deposit nonporous, crystalline carbon on the grain surface and in the pore volumes. Investigation of the resulting charcoal specimens confirmed the theory of the ramified porous structure of active charcoal which had been advanced earlier by these authors; this theory considers the micropores to be offshoots of the intermediate pores and the latter to be offshoots of the macropores. Wicke has adopted a similar view concerning the porous structure of active charcoals in [2].

Plachenov [3] has expressed the opinion that the micropores are interconnected to form an independent transport system. This conclusion was reached on the basis of sorption kinetic studies and discharge curves for charcoals whose coarse pores had been filled with mercury. These two papers [1, 3] essentially exhaust the attempts which have been made to develop experimentally the interconnection of the various types of pores and even their results are not completely concordant.

We have continued the study of this problem by measuring the permeability of active charcoals with partially blocked pores. The essence of this method is as follows. The permeability of the charcoal was first determined with respect to helium and nonadsorbing gas. Vapors of isopropyl alcohol were then adsorbed onto the charcoal at a pressure corresponding to filled micropores (these pores are filled at a relative benzene pressure

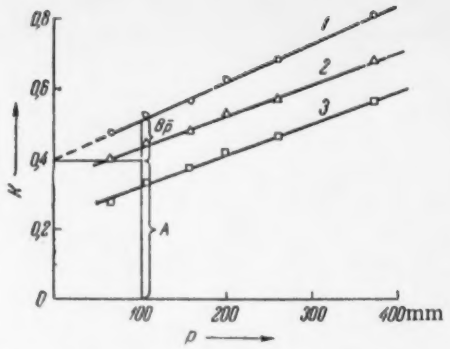

Fig. 2. Permeability of charcoal I to helium: 1) charcoal in initial state; 2) with filled micropores; 3) with filled micropores and intermediate pores.

TABLE 1

Brief Characterization of the Charcoals

Charcoal	Pore volume, cm^3/g			Granule diameter, mm	Granule length, mm
	micro	intermediate	macro		
I	0,33	0,10	0,25	3	5—6
II	0,38	0,05	0,31	1,6	3—3,5

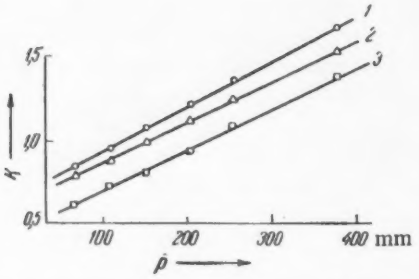

Fig. 3. Permeability of Charcoal II to helium: 1) charcoal in initial state; 2) with filled micropores; 3) with filled micropores and intermediate pores.

of $p/p_s = 0.17$, according to Dubinin [4], and the corresponding pressure of isopropyl alcohol is $p/p_s = 0.22$) and the permeability once more determined. The intermediate pores of this same specimen were then filled at saturated vapor pressure and experiments once more carried out. Desorption of the alcohol from the charcoal was avoided in these last two cases by using helium - alcohol vapor mixtures of requisite concentration instead of pure helium in determining the permeability.

The essentials of the apparatus which was used in these experiments are sketched in Figure 1. The volumes V_1 and V_2 were joined by the special stopcock 1 which contained one or several grains of charcoal. The structure of this cock and the method of inserting the grains in it are shown in the figure. Piciene, Wood's alloy, and paraffin were used as lubricants in order to assure vacuum-tight attachment of the grains. The system was evacuated to high vacuum with cocks 1 and 5 open, after which these cocks were closed, and the working gas pressures, p_1 and p_2, were established in the volumes V_1 and V_2. The initial pressure difference was 60 mm of Hg. The apparatus being in readiness for the experiment, cock 1 was opened and the gas allowed to flow through the grain from one volume into the other. The timer was turned on automatically as soon as the pressure had fallen to 40 mm of Hg and the time of flow was recorded. The permeability of the charcoal was evaluated from the equation

$$K = \frac{V_1' V_2'}{(V_1' + V_2')\, t} \cdot \frac{l}{F} \ln \frac{p_1^0 - p_2^0}{p_1 - p_2}, \qquad (1)$$

in which V_1^1 and V_2^1 are the system volumes with correction for the volume change in the manometers, p_1^0 and p_2^0 are the initial gas pressures, p_1 and p_2 are the pressures, p_1 and p_2 are the pressures at the time t, and l and F are, respectively, the length and cross-sectional area of the charcoal granule.

These experiments were carried out with granulated charcoals which had been obtained from anthracite coal or paper pulp tar by the water-gas method at laboratory conditions. A brief characterization of these charcoals is given in Table 1.

The experiments were performed at 20°. The results are shown in Figures 2 and 3 where the permeability is given as a function of the mean pressure

$$\bar{p} = \frac{p_1 + p_2}{2}.$$

It is clear from these figures that the permeability diminished when the micropores and intermediate pores were filled. Similar observations were made in each of the experiments, although the diminution in the permeability varied from grain to grain because of nonuniformity in the charcoal. The data are well described by the Adzumi Equation [5].

$$K = A + B\bar{p} \qquad (2)$$

in which A and B are constants whose values depend on the structure of the sorbent and the nature of the gas.

The terms A and $B\bar{p}$ can be looked on as the contributions to the permeability arising from molecular flow and from viscous flow, respectively.

Active charcoal contains pores of various diameters, and molecular and viscous flow can occur simultaneously over a wide interval of pressures.

The data of Dubinin [4] indicate that the most probable values of the radii of the micropores, intermediate pores, and macropores are: $r_{mi} = 8 \cdot 10^{-8}$ cm; $r_i = 4 \cdot 10^{-7} - 2 \cdot 10^{-6}$ cm, and $r_{ma} = 2 \cdot 10^{-4} - 5 \cdot 10^{-5}$ cm. The mean free path of the helium molecule at the working pressures is $r_{ma} = 2.6 \cdot 10^{-5} - 1.2 \cdot 10^{-4}$ cm. Thus molecular flow will occur in the micropores and in the intermediate pores, whereas the flow in the macropores will be viscous. The preceding graphs indicate that A exceeds actually $B\bar{p}$, whereas the Hagen-Poisielle and Knudsen Equations show that the permeability for viscous flow, $B\bar{p}$, at a mean pressure of 100 mm must be ten times greater than A if the pores in any one group are identical, independent cylindrical capillaries. From this it follows that the micropores and intermediate pores do not make up an independent transport system. This conclusion remains unaltered even when allowance is made for the convolutions and noncylindrical form of the capillaries, and other corrections are introduced. The marked diminution of the charcoal permeability which results from filling the micropores and the intermediate pores can be explained only if it is assumed that there are macropores which are joined through micropores, and macropores which are joined through intermediate pores.

If molecular flow were limited to these porosities it could also be expected that A would fall almost to zero when the micropores and intermediate pores were filled. Thus it must be further supposed that there will be molecular gas flow in certain of the smaller macropores. The same considerations as were outlined above would indicate that these latter pores are only connecting links for still coarser pores. Thus these studies of specimens of active charcoal have also disclosed several variants of pore interconnection.

LITERATURE CITED

[1] M. M. Dubinin, G. S. Zhuk, and E. D. Zaverina, J. Phys. Chem., 31, 1126 (1957) [USSR].

[2] E. Wicke, Koll. Zs., 93, 129 (1940).

[3] T. G. Plachenov, Reports, Scientific-Technologic Conference on Sorbents, Leningrad, 1957.

[4] M. M. Dubinin, Prog. Chem., 24, 3 (1955) [USSR].

[5] A. Adzumi, Bull. Chem. Soc. Japan, 12, 304 (1937).

Received July 4, 1959.

THE EFFECT OF AGING ON THE STRUCTURE, ELASTIC RECOIL, SHEAR STRENGTH, AND RELAXATION TIME OF ALUMINUM NAPHTHANATE GELS

A. A. Trapeznikov

The Institute of Physical Chemistry of the Academy of Sciences of the USSR

(Presented by Academician S. I. Vol'fkovich June 19, 1959)

The gradual aging of aluminum soap gels leads to alterations in the maximum high-elastic deformation (maximum elastic recoil), structural strength, and relaxation time for deformation, which are of considerable interest for an understanding of the nature of gels and their rheological properties. Aging and maturing are preliminary steps in the swelling and partial dissolution of the soap granules.

The present investigations were carried out on low-concentration gels which showed a very rapid and clear-cut aging. A powder of the aluminum naphthanate soap (Batch No.24) was ground in a mortar until the granule dimensions fell below 0.5 mm, after which it was poured into decalin and stirred until setting took place, i.e., until a compact structure was formed throughout the body of the solvent. The resulting semiliquid mass was then introduced into the cylinder of an elastorelaxometer [1], and curves showing the relation between the elastic recoil, ϵ_e, the shear stress, P, and the deformation ϵ, were plotted one hour later at $\dot{\epsilon} \approx 100\ \text{sec}^{-1}$. Determinations of ϵ_e were made for each new value of ϵ at one minute intervals, even though this was insufficient time for a complete thixotropic regeneration of the P-determining structure, the aim being to keep the time involved in obtaining a curve (20 - 30 minutes) short in comparison with the rather rapid aging process. All of this was practically without effect on the magnitude of ϵ_e [2].

The alterations which aging produces in the $\epsilon_e(\epsilon)$ and $P(\epsilon)$ curves which are given in Figure 1, curves a, b, for the 2% naphthanate gel are quite characteristic. Each $\epsilon_e(\epsilon)$ curve obtained at the beginning of aging has a sharp discontinuity at a point $\epsilon = \epsilon_L$ where the $\epsilon_e = \epsilon$ relation breaks down, the value of ϵ_e remaining essentially constant as ϵ is increased beyond this point.

As aging progresses, each $\epsilon_e(\epsilon)$ curve gradually diverges from the $\epsilon_e = \epsilon$ line as it approaches the point $\epsilon = \epsilon_L$ (which is undergoing displacement toward larger ϵ values) and passes through a more and more pronounced maximum at ϵ_{emax} which is associated with $\epsilon = \epsilon_m$ [3].

Each of the $P(\epsilon)$ curves has a clear-cut maximum, $P = P_r$* at $\epsilon = \epsilon_L$ at the beginning of aging; the P maximum at $\epsilon + \epsilon_r$ moves toward higher ϵ values as aging progresses and approaches $\epsilon = \epsilon_m$ although it once more falls at $\epsilon_r < \epsilon_m$ when τ_{ag} becomes very high.

Figure 2 applies to the relaxation of deformation, $\log \epsilon_e = f(\tau_{ag})$, in a 2% naphthanate gel at various values of τ_{ag}, the data being presented in the form of curves $\log \theta_e = f(\tau_{ag})$, $\epsilon_e = \dfrac{2\theta_e R_2^2}{R_2^2 - R_1^2}$, for $\epsilon_e = \epsilon$ = 9.6, 20.3 and 28.7 (mean values for each curve). Each of these $\epsilon_e < \epsilon_L$ values satisfies the relation $\epsilon_e = \epsilon$. Each curve is composed of a linear segment and a more or less sharply falling curved segment. The slope at any

*The P_r value obtained by this method is somewhat low because of partial structural breakdown and the corresponding point, $\epsilon = \epsilon_r$, is displaced toward a lower value which is identical with ϵ_L.

point of the curve, $\frac{d\tau}{d \ln \epsilon_e}$, gives the relaxation time, $\vartheta^{\dot{\epsilon}} = f(\epsilon_e, \dot{\epsilon})$. The curves for $\dot{\epsilon} = 20.9$ and 28.7 show that aging diminishes the inclination of each of these curve segments at low values of τ_{ag}, although the slope of the linear portion quickly begins to increase. From this it follows that aging increases the number of long structural elements and diminishes the number of those short elements which fix the value of $\vartheta^{\dot{\epsilon}}$ at low ϵ_e. The slope of each curve segment steadily increases under very extended aging while $\vartheta^{\dot{\epsilon}}$ falls over the entire curve, the indication being that the number of bonds in the system is being reduced.

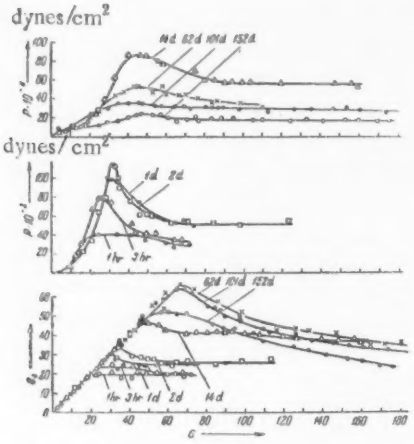

Fig. 1.

Figure 3 gives $\vartheta^{\dot{\epsilon}}(\tau_{ag})$ curves which have been plotted by using $\vartheta^{\dot{\epsilon}}$ values that were obtained from the linear segments of the curves of Figure 2. The maximum in $\vartheta^{\dot{\epsilon}}$ is at τ_{ag} = 4 days and the maximum on the $P_r(\tau_{ag})$ curve is located at this same point (see below).

The curves of Figure 4 show the relation between the maximum elastic recoil, $\epsilon_{e\,max}$, the strength, P_r, and τ_{ag}, for 1%, 1.5% and 2% naphthanate gels. All of these curves pass through maxima, but $(\epsilon_{e\,max})_{max}$ fall at different points. The strength goes through its maximum value at 0.3-4 days and then diminishes, whereas the elastic recoil increases over a longer period, reaching a maximum only at 1,7 and 62 days. The higher the gel concentration, the more gradual is the aging. It might be supposed that $\epsilon_{e\,max}$ falls below $(\epsilon_{e\,max})_{max}$ only because of a fictitious effect arising from the increased ease of relaxation in deforming the system. On the other hand, $\epsilon_{e\,max}(\tau_{ag})$ and $P_r(\tau_{ag})$ curves which have been obtained for a 1 % gel at $\dot{\epsilon} = 711$ sec^{-1} show a maximum at τ_{ag} = 1 day just as do similar curves which were developed at $\dot{\epsilon} \approx 100$ sec^{-1}. Thus the maxima on the aging curves are actually related to structural alterations in the system, reflecting the limiting deformation in its elements.

The characteristics of the viscous aluminum naphthanate gels are due to their network structures [4].The high-elastic properties, strength, viscosity, and thixotropy of such systems are all determined by the number of contacts and network branch points, the length and flexibility of the intermediate chain sections, the solvent viscosity, and by the other substances which may be present.

The fact that the $\epsilon_e(\epsilon)$ curves are horizontal beyond ϵ_L in the initial stages of aging of the gel indicates that the structure which fixes the $\epsilon_{el} = \epsilon_L$ relation is almost instantly regenerated in the $\epsilon > \epsilon_L$ interval. Colloidal systems of this kind behave at $\dot{\epsilon} \approx 100$ sec^{-1} as plastic solid bodies in which the deformation remains constant beyond the elastic limit. The properties of such bodies are probably due to the presence of relatively compact particles which aggregate rapidly but relax rather slowly over the time required for reaching a given value of ϵ in the $\epsilon, > \epsilon_L$ interval. These particles undergo partial straightening and microswelling as a result of the solvation of the radicals of the organic naphthenic acids which occurs during the aging of the system. More and more long, thin, flexible, highly mobile, rapidly relaxing, elements appear in the structure. The properties of the system become more and more nearly those of an elastic plastic fluid. The presence of a clear-cut maximum, $\epsilon_{e\,max}$, on the $\epsilon_e(\epsilon)$ curve is to be explained by the fact that the comparatively long structural elements rupture when the system passes through ϵ_m and then contract rapidly as deformation is continued beyond ϵ_m. Thus the coiling of the particles in such a system is more extensive after passing into stationary flow than it was at the point of structural rupture, ϵ_m, provided $\dot{\epsilon}$ is not too high.

The increase in the structural strength at the beginning of aging is the result of an increase in the total number of branch points in the network. The simultaneous lengthening of the structural elements leads to an increase in $(\epsilon_{e\,max})_{\dot{\epsilon}}$. The decrease in P_r which accompanies extended aging (passage through $P_{r\,max}$) is clearly to be explained by a decrease in the number of network junctions which leads, in turn, to a further lengthening of the flexible intermediate chain segments. This also results in an additional increase in $\epsilon_{e\,max}$. A reduction in the number of junctions is equivalent, in a certain sense, to a reduction in the concentration of

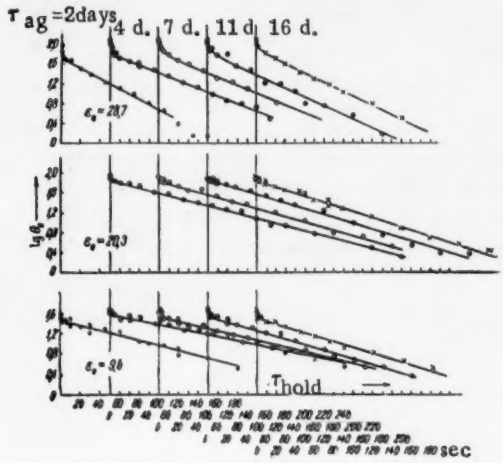

Fig. 2.

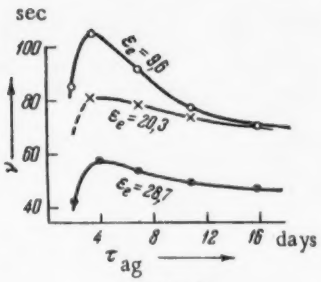

Fig.3.

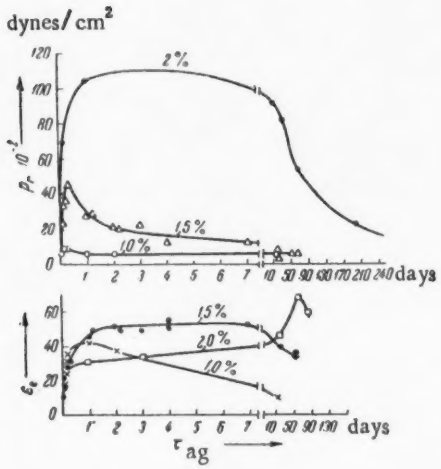

Fig. 4.

the system, although Figure 4 shows that $(\epsilon_{e\ max})_{max}$ will also diminish if C is reduced too far. Thus the system reaches maximum elasticity (deformability) during either aging or concentration change, not when the strength is at maximum, but when it has a comparatively low value with the longest possible chain segments between the branch points and a branch-point concentration which is not too high.

Earlier data [2, 4] indicate that the completed ϵ_{rm} (C) and $\epsilon_{e\ max}$ (C) curves will have maxima at relatively low C values which are associated with a loose network.

The diminution in $\epsilon_{e\ max}$ and ϵ_{rm} in the concentration region beyond the maximum on the $(\epsilon_{e\ max})_{max} = f(C)$ curve is due to a marked increase in the number of branch points and intertwinings, which shortens the intermediate chains. The fact that $\epsilon_{e\ max}$ and ϵ_{rm} fall below the respective maxima as C diminishes is to be related to an excessive decrease in the number of those branch points and intertwinings which function as supporting points for the extended chains. The particles remain isolated and probably slip over one another in a weakly distended condition so that the value $\epsilon_{e\ max}$ cannot become very large, even if there is a marked increase in the deformation rate. It is clear that the particles in such low-concentration systems can be stretched in purely hydrodynamic, stationary flow at very high velocities, but this will not assure elastic deformation of the system because the particles are not interconnected. Mutual penetration of the rod-shaped molecules occurs more frequently as the concentration C increases and the number of support points (branch points, interternings) begins to rise, i.e., a more or less stable network, capable of supporting reversible deformations which are large in the initial stage but diminish as stationary flow is approached, is formed.

The low values of $(\epsilon_{e\ max})_{max}$ for aluminum soaps in the low C interval can be explained in terms of a decrease in the chain length resulting from a depolymerization of the chain-like particles, which is similar to the decrease in the molecular weight of aluminum laurate that has been postulated by McBain and Working [5] from osmotic pressure data. It is obvious that this factor would not come into play in solutions of those polymers which have stable chemical bonds in their chains.

Reversible depolymerization of aluminum soap gels might result from rupture of those weak coordination Al. . . O − Al bonds which can be presumed to exist in the chain along with the stable covalent Al −O−Al bonds.

The decrease which extended aging produces in $\epsilon_{e\ max}$ is probably related to the crystallization and separation of [6] the $Al(OH)_3$ of the nuclei which arise from precipitation of the aluminum soap or of the $Al(OH)_3$ which comes from such breakdown of the soap chain and would result from transfering a hydrogen atom from a hydroxyl to an acid radical to form a stable covalent bond from a coordination bond $\overset{R}{Al} \ldots \ldots \overset{H}{O} \rightarrow Al{-}O{-}+RH$.

The chains of aluminum naphthanate gels are highly flexible in such low-viscosity solvents as decalin, so that large high-elastic deformations ϵ_e can develop or disappear rapidly; this points, in turn, to free spatial movement of the gel chains and to the presence of univalent bonds which assure free rotation of the chain segments. The recently proposed [7] chain structure in which the oxygen atoms of the carboxyl group coordinate, not only with one another, but also with the neighboring aluminum atoms, is not realistic since it would result in a rigid chain. The Gray model [8] is more acceptable.

The author would like to conclude by expressing his deep thanks to L. S. Meshcheryakova for having made the measurements.

LITERATURE CITED

[1] A. A. Trapeznikov, Colloid J. 21, 108 (1959).

[2] A. A. Trapeznikov, Colloid J. 20, 476 (1958).

[3] A. A. Trapeznikov and T. G. Shalopalkina, Proc. Acad. Sci. USSR, 111, 380 (1956)*.

[4] A. A. Trapeznikov and V. A. Fedotova, Proc. Acad. Sci. USSR, 81, 1101 (1951); 82, 97 (1952); V. A. Fedotova and A. A. Trapeznikov, 120, 841 (1958).

[5] J. W. McBain, and E. B. Working, J. Phys. and Coll. Chem., 51, 974, 1947.

[6] G. V. Belugina and A. A. Trazpeznikov, Colloid. J., 20, 3 (1958).

[7] W. O. Ludke, S. E. Wiberley, et al., J. Phys. Chem., 59, 222 (1955).

[8] V. R. Gray, Trans. Farad. Soc., 42 B, 196 (1946).

Received June 2, 1959.

*Original Russian pagination. See C. B. translation.

THE EFFECT OF γ-IRRADIATION ON THE RATE OF HYDROGEN EXCHANGE BETWEEN WATER AND ISOAMYLTHIOL

K. I. Sakodynskii and N. M. Zhavoronkov,

Corresponding Member, Acad. Sci. USSR

The L. Ya. Karpov Institute of Physical Chemistry

Thus far, only very little work has been done on the effect of irradiation on hydrogen exchange. Bardwell and Dyne [1] have found that there is an increase in the rate of isotopic exchange between water and gaseous hydrogen under irradiation and that the distribution coefficient is then equal to unity. It is not clear, however, whether this results from the fact that the reaction follows an atomic mechanism in the radiation field, or whether it is due to some change in equilibrium distribution of the deuterium itself. Varshavskii, Karpov, et al, [2], have observed hydrogen exchange in the heterogeneous system gaseous deuterium – solid polymer. Such exchange will not occur at all without irradiation.

We have studied the effect of γ-irradiation on the isotopic exchange between water and isoamylthiol in a heterogeneous liquid – liquid system. Measured amounts of water, deuterium enriched to 3-5% (approximately 1 g), and isoamylthiol (4-5 g) were loaded into ampules. These ampules were so placed in the field of γ-irradiation from a cobalt source that the radiation intensity was 90 r/sec in one case and 180 r/sec in the other. Each ampule was broken open immediately after irradiation and its contents transferred to a separatory funnel. The water layer was separated off after long standing and freed from traces of the thiol by a preliminary distillation. The specimen of water was then subjected to the type of purification which generally precedes isotopic analysis; the specimen was vaporized, the vapors passed over copper oxide heated to 700° in a current of oxygen, condensed and subjected to microdistillation under vacuum. The drop method of analysis [3] was used in determining the isotopic composition of the water. The degree of exchange was calculated from the equation:

$$F = \left(1 - \frac{X_0 - X_\tau}{X_0 - X_\infty}\right) 100\%,$$

in which X_0 is the concentration of deuterium originally present in the water, X_τ is the concentration of deuterium in the water τ hours after beginning the exchange and X_∞ is the theoretical equilibrium concentration of deuterium in the water under the experimental conditions.

All of these concentrations are expressed in mole percentages. The concentration X_∞ was calculated from the experimental data by using the following equation, which is based on the expression for the distribution coefficient of the deuterium [4]:

$$X_\infty = \frac{B \pm \sqrt{B^2 - 4AC}}{2A},$$

$$A = 2\lambda(\alpha - 1),$$
$$B = 1 + 2\alpha\lambda + y_0(\alpha - 1) + AX_0,$$
$$C = dy_0 + 2\alpha\lambda X_0,$$

here λ is the mole ratio of the amounts of exchanging water and isoamylthiol, α is the distribution coefficient between water and isoamylthiol which has the value 2.14 according to [5], and y_0 is the concentration of deuterium originally present in the isoamylthiol.

The conditions under which the kinetics of isotopic exchange were studied with and without irradiation, and the results obtained from this study are presented in Table 1. The effect of γ-irradiation on the rate of isotopic exchange between water and isoamylthiol is shown in Figure 1. These data indicate that γ-irradiation markedly increases the rate of isotopic exchange, the effect being most pronounced in the initial period. The deuterium distribution itself is unchanged by γ-irradiation in this case.

TABLE 1

Experimental Results on the Effect of γ-Irradiation on the Rate of Hydrogen Exchange.

Time of irradiation, τ, hours	Molar ratio of the amounts of water and thiol, λ	Initial concentration of D in H_2O, X_0, mole	Concentration of D in H_2O after irradiation, X_τ, mole %	Theoretical equilibrium concentration of D, X_∞, mole %	Degree of exchange, F, %
		Without irradiation			
2	0,9655	4,37	4,25	3,51	14
6	1,3098	4,37	4,12	3,70	37
48	1,0278	4,57	3,91	3,72	78
		Intensity of radiation 90 r/sec			
0,5	0,9244	4,61	4,48	3,67	14
1	0,9660	4,57	4,29	3,67	31
1	1,2645	5,39	5,11	4,53	32
2	0,9647	4,57	4,25	3,67	35
2	0,6375	3,94	3,53	2,88	39
3	1,0093	3,94	3,55	3,19	52
4	1,0558	4,57	3,97	3,73	70
6	0,9427	4,57	3,91	3,66	72
12	0,8520	4,61	3,78	3,61	83
22	1,1389	5,39	4,58	4,46	87
24	1,3863	3,94	3,40	3,37	95
34	0,8073	4,57	3,52	3,54	102
		Intensity of radiation 180 r/sec			
0,5	0,9632	4,57	4,29	3,67	31
2	0,9515	4,57	4,10	3,66	52
6	0,9506	4,57	3,83	3,66	81
12	1,0263	4,57	3,90	3,75	83

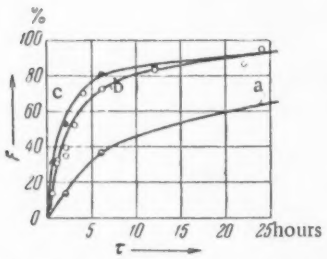

Fig. 1. The effect of γ-irradiation on the rate of isotopic exchange between water and isoamylthiol a) without irradiation; b) intensity of radiation, 90 r/ sec; c) intensity of radiation, 180 r/sec.

It was found that irradiation accelerates the hydrogen exchange only in the S - H group. This conclusion was confirmed by carrying out experiments on the effect on the isotopic exchange between water and isopentane of irradiation with γ-rays for the same period. In no case was there any observable alteration in the isotopic composition of the water. The exchange did not exceed 100%, a fact which indicates that γ-irradiation did not bring about a redistribution of the deuterium within the isoamylthiol molecule. The considerable increase in the quantity of tarry products in the final isoamylthiol distillation points to a partial formation of disulfides during isotopic exchange under irradiation.

It is impossible to set up an exhaustive explanation of the observed acceleration of isotopic exchange under irradiation in terms of exceptional ionization effects (radiolysis of water and isoamylthiol with a subsequent exchange of hydrogen ions) in the present case. The mutual solubility of water and isoamylthiol is low [6], and the exchange

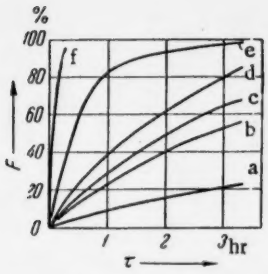

Fig. 2. The effect of agitation and temperature on the rate of isotopic exchange between water and isoamylthiol: a) without agitation, b) agitated by shaking at 100 vibrations per minute; c) agitated by a paddle operating at 250 rev/min; d)agitated by shaking at 136 vibrations per minute; e) agitated by shaking at 136 vibrations per minute at 80°; f)supersonically agitated.

thus takes place between two immiscible phases. There is a great deal of data indicating that isotopic exchange is controlled by diffusional factors. Thus an alteration of the conditions of agitation is of great significance to the rate at which equilibrium is approached in the exchange reaction; the effect of temperature on the rate of approach of equilibrium is typical of a diffusional process, the activation energy for exchange under comparable conditions with fixed interfacial surface area being 4.2 kcal/mole. Figure 2 presents the data on the effect of temperature and agitation on the rate of isotopic exchange. Finally, our measurements on the isotopic exchange between water and isoamylthiol in which [4] an inert solvent was used to eliminate diffusional resistance have shown that the rate of exchange is rather high, just as predicted by A. I. Brodskii [7].

A comparison of these data on the acceleration of isotopic exchange between water and isoamylthiol under γ -irradiation with the recorded data on the course of this reaction in the diffusion region shows that such irradiation can effect diffusional processes.

LITERATURE CITED

[1] Bardwell and P. Dyne, Cand. J. Chem., 35, 82 (1957). P. Harteck, Nucleonics, 14, No.9, 37 (1956).

[2] Ya. M. Varshavskii, G. Ya. Vasil'ev, et al, Proc. Acad. Sci. USSR, 118, 315 (1956).*

[3] A. I. Shatenshtein et al, The Isotopic Analysis of Water (in Russian), Acad. Sci. USSR, Press,1957.

[4] K. I. Sakodynskii and N. M. Zhavoronkov, Scientific Reports, Higher Schools, Chem.and Chem. Tech., 2, No.2, 256 (1959).

[5] K. I. Sakodynskii, S. I. Babkov,and N. M. Zhavoronkov, Proc. Acad. Sci. USSR, 121, No.4, 681 (1958).*

[6] K. I. Sakodynskii and S. I. Babkov, Chem. Sci. and Indus., 4, No.1, 135 (1959).

[7] A. I. Brodskii, Bull. Acad. Sci. USSR, Div. Chem. Sci., 1949, 1, 3. Problems of Chemical Kinetics, Catalysis and Reactivity (in Russian), Acad. Sci. USSR, Press, 1955, page 13.

Received July 25, 1959.

*Original Russian pagination. See C. B. translation.

THE TEMPERATURE DEPENDENCE OF THE RADIATIONAL OXIDATION OF n-HEPTANE AND n-NONANE

N. A. Bakh and T'ung T'ien-chen

The Institute of Electrochemistry of the Academy of Sciences of the USSR

(Presented by Academician A. N. Frumkin July 10, 1959)

Data obtained earlier in our laboratory have indicated that radiational oxidation of hydrocarbons proceeds through a non-chain radical mechanism at ordinary temperatures [1]. It has been shown, however, that chain - oxidation reactions can be initiated by γ -irradiation of these systems at elevated temperatures [2] and can even occur at ordinary temperatures in cases such as that of isopropylbenzene [3]. It is of both theoretical and practical interest to draw a line of demarcation between these mechanisms, and this can be done through a study of the relation between the reaction kinetics, the temperature and the radiation intensity.

Investigation has been made of the formation of liquid products in the oxidation of n-heptane and n-nonane under x-ray irradiation, working over the temperature interval from -80 to + 130° and at dose strengths ranging from $1 \cdot 10^{14}$ to $8 \cdot 10^{15}$ ev/cm^3 · sec. Oxidation was carried out under a continuous flow of oxygen when working in the region from 0 to 130°, and in cells which were sealed after saturation with oxygen when working in the low temperature region. The test hydrocarbons were carefully freed from unsaturated compounds and from traces of peroxides and other oxidation products. The peroxides in the irradiated liquids were determined by an iodometric method which gave the sum of the hydro - peroxides and the dialkylperoxides; the carbonyl compounds and alcohols were determined spectrophotometrically as dinitrophenylhydrazones and alkyl nitrites, respectively, and the acids estimated by titration with sodium methylates in a nonaqueous medium. Details of the techniques of irradiation, dosing, and analysis will be presented elsewhere.

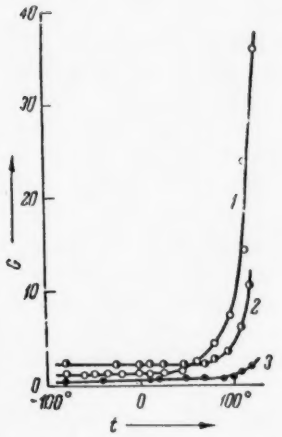

Fig.1. The relation between the temperature and the yield from radiational oxidation: 1) peroxides, 2) carbonyl compounds, 3) acids .

The accumulation of reaction products under increasing dosage was studied at each temperature. It has been noted earlier [1] that all of these oxygen-containing compounds are formed simultaneously with zero induction period. The radiational yield, G, was obtained from the slope of the initial linear segment of the characteristic curve showing increase in concentration as a function of the dose in the radiational oxidation reaction.

Figure 1 shows yields of peroxides, carbonyl compounds, and acids from irradiation of n-heptane and n-nonane at dose strengths in the $7\text{-}8 \cdot 10^{15}$ ev/cm^9 · sec range. The n-nonane was treated at temperatures above 70°; the yield from oxidation under fixed conditions was the same in both of these hydrocarbons. It is to be seen that each product showed one region within which the G value was low (~ 1-2 molecules per 100 ev) and independent of the temperature, and another region in which the yield increased rapidly with rising temperature, reaching 30-40 molecules per 100 ev in the case of the peroxides.

The temperature-independent yields must be associated with reactions which do not require an activation energy, or with reactions which proceed because of an excess energy inherent in one of the reacting particles. The generally accepted scheme of oxidation processes leads to the following as the simplest possible path for the formation of the observed reaction products:

$$\dot{R} + O_2 \rightarrow R\dot{O}_2; \quad (1)$$

$$R\dot{O}_2 + R\dot{O}_2 \rightarrow ROOR + O_2 \quad \text{or} \quad R\dot{O}_2 + \dot{R} \rightarrow ROOR; \quad (2)$$

$$R\dot{O}_2 + RH \rightarrow ROOH + \dot{R}; \quad (3)$$

$$R_1R_2HC\dot{O}_2 \rightarrow R_1R_2CO + \dot{O}H \quad \text{or} \quad R_1R_2HC\dot{O}_2 \rightarrow R_1CHO + \dot{O}R_2; \quad (4)$$

$$R\dot{C}H\dot{O}_2 \rightarrow RC\begin{matrix}H\\ \\O\end{matrix}\!\!\begin{matrix}O\\|\\O\end{matrix} \rightarrow RC\begin{matrix}O\\ \\OH.\end{matrix} \quad (5)$$

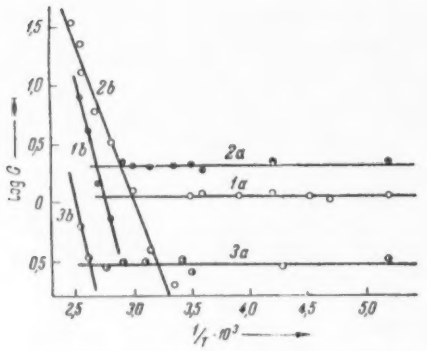

Fig. 2. The relation between the logarithm of the yield of oxidation products and the reciprocal temperature: 1) peroxides, 2) carbonyl compounds; 3) acids.

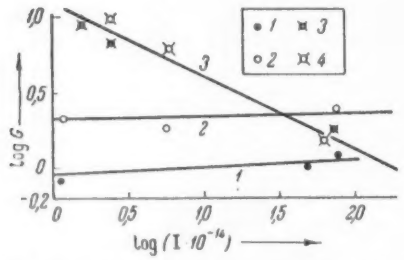

Fig. 3. The relation between the yield of oxidation products and the dose strength: 1) peroxides at -80°, 2) carbonyl compounds at + 10°, 3) peroxides at + 70°, 4) carbonyl compounds at + 95°.

Only the first two of these reactions require an activation energy. From the fact that the yield of dialkyl peroxides is independent of the temperature and that the same is also true of the yield of hydroperoxides, carbonyl compounds, and acids, it can be concluded that it is the excess energy of the peroxide radicals which is responsible for the formation of these compounds through replacement or isomerization reactions; this excess can be due to the retention of a certain energy when the "hot" free radicals produced in the ionization excitation and interaction of the irradiated liquid combine with oxygen, or it can be due to a redistribution of energy.

The yield of each of these reactions should be limited and constant over any given temperature interval since the number of primary, chemically active particles is fixed by the number of acts of ionization, which does not exceed several units per 100 ev and is independent of the temperature. Chain development becomes possible at sufficiently elevated temperatures [3]. This process will not interfere with the non-chain radical reactions, but will be simply superposed on them. The energy of activation for Reaction (2) can be determined from the true yield of the temperature-dependent reaction, which is the difference between the observed yield and that part of the yield which is independent of the temperature. The data of Figure 1 have been plotted in the coordinates log G, 1/T in Figure 2, the b branches being developed from the true temperature dependent yields. The fact that log G and 1/T are linearly related within the range of the temperature variation of G shows each product to be associated with two independent superposed mechanisms.

Increase in the yield of peroxides begins at ~40°, whereas the yield of carbonyl compounds begins to increase only at ~ 70° and the yield of the acids, only at ~100°. This leads to the conclusion that additional carbonyl compounds are formed from the hydroperoxides when these are formed with sufficient rapidity, and that additional acids are formed, in turn, from these carbonyl compounds, even though induction periods are not observed. The relation between the activation energies also justifies such a conclusion, the respective values for the hydroperoxides, carbonyl compounds, and

acids being 15, 20 and 20 kcal/ mole, plus or minus 2-3 kcal/mole. A similar sequence of reactions is met in thermal oxidation [4]. This does not indicate, however, that the mechanisms are the same in the two cases, since the product radicals from radiolysis can be expected to participate in the radiational oxidation. The question remains open as to whether the products from a chain reaction under irradiation are identical with the products obtained from this same chain reaction in the absence of radiation. Data on methyl oleate indicate complete identity here [5], whereas work on the oxidation of n-cetane points to considerable differences [6].

Nonradiational oxidation caused no complications in our experiments since such oxidation could scarcely begin in the time of irradiation needed for a determination of the radiational yield, even at 130°.

The yield of the alcohols was approximately the same as that of the carbonyl compounds and also showed two different characteristic temperature intervals. It differed from the yield of the other products by being temperature dependent over both of these intervals; the energy of activation is ~ 2 kcal/mole from -75 to + 90° and ~ 18 kcal/mole above + 90°. It can be supposed that the alcohols are not formed directly from the primary peroxide radicals over the first of these intervals.

The rate of a radiational chain reaction is in general related to the radiation intensity, I, by $dc/dt = aI^n$ or $G = \frac{dc}{I\,dt} = aI^{n-1}$; $n = 1/2$ for second-power chain rupture and then $G\ a/\sqrt{I}$. Data for the peroxides and carbonyl compounds over the range from $1.1 \cdot 10^{14}$ to $7.8 \cdot 10^{15}$ ev/cm^3 · sec are presented in Figure 3. The yield is independent of the dose strength (lines 1 and 2) when the conditions are such that it is also independent of the temperature (at -80° for the peroxides and at + 10° for the carbonyl compounds). On the other hand, the yield does vary with the dose strength in the region where it is temperature dependent. The observed yields lead to n = 0.33 in the case of the peroxides at + 77° and to n = 0.37 for the carbonyl compounds at + 95°. Both results would approximate to n = 1/2 if account were taken of the yield from non-chain temperature-independent processes (Fig. 3, curve 3).

Thus the dose relation also confirms the fact that the radiational oxidation of the n-alkanes can involve the superposition of chain reactions on non-chain radical reactions. The possibility of a combination of these two mechanisms is a general property of radiational oxidations but the temperature at which chain processes appear will vary with the irradiated compound.

LITERATURE CITED

[1] N. A. Bakh and V. V. Saraeva, J. Phys. Chem., 32, 209 (1958).

[2] N. M. Émanuél', Proc. Acad. Sci. USSR, 111, 1286 (1956);* M. A. Proskurnin, Yu. P. Khmel'nitskii, et al, Proc. Acad. Sci. USSR, 112, 886 (1957).*

[3] M. Durup, Actions chimiques et biologiques des radiations, 4 ser., Paris, 1958, p.18.

[4] A. G. Knorre, Z. K. Maizus, et al, Prog. Chem., 26, 416 (1957).

[5] M. T. Slover and L. R. Dugan, J. Am. Oil Chem. Soc., 34, 333 (1957).

[6] Yu. P. Khmel'nitskii, M. A. Proskurnin, et al, Proc., First Conference on Radiation Chemistry, Acad. Sci. USSR, Press, 1958, page 240.

Received July 7, 1959.

*Original Russian pagination. See C. B. translation.

THE RELATION BETWEEN THE KINETIC AND THERMODYNAMIC ISOTOPIC EFFECTS AND THE MOLECULARITY OF A REACTION

G. K. Boreskov, Corresponding Member, Acad. Sci. USSR

The following relations in the kinetic parameters of the forward and reverse reactions have been developed [1] for the reversible chemical process:

$$\frac{k_2}{k_1} = K^{M_A}; \tag{1}$$

$$E_2 - E_1 = M_A q, \tag{2}$$

k_1 is here the rate constant for the forward reaction, k_2 is the rate constant for the reverse reaction, K is the equilibrium constant for the stoichiometric reaction involving one molecule of the substance A, E_1 is the activation energy for the forward reaction, E_2 is the activation energy for the reverse reaction, q is the heat of reaction per mole of A, and M_A is the molecularity of the reaction with respect to A, or the number of molecules of A which enter into reaction with one active complex.

An analogous quantity, the stoichiometric number, ν_r, was introduced by J. Horiuchi in treating the reactions at the hydrogen electrode [2] and later used in a general study of the kinetics of chemical processes [3]. The stoichiometric number indicates how many times the rate-determining step must occur in order that the reactant molecules, shown in the stoichiometric equation, enter into reaction. The relation

$$\nu_r = \frac{1}{M}.$$

will apply when the stoichiometric equation is written for one molecule of the reactant A.

The molecularity of a chemical process is fixed by the mechanism, and a determination of its value is essential for a decision as to the limiting step in a complex reaction.

It is not always possible to carry out the separate determinations of the rates of the forward and reverse reactions, which are needed if the molecularity is to be calculated through Equations (1) and (2). Horiuti [4] has proposed a more general method which is based on the relation:

$$M = \frac{V}{\vec{V}} \frac{\Delta\mu}{RT},$$

in which V is the observed reaction rate, $\vec{V}$ is the rate of the forward reaction, $\Delta\mu$ is the free energy change accompanying passage of the reacting system into equilibrium, R is the molar gas constant, and T is the absolute temperature.

The weak point in this method is the necessity of measuring the reaction rate in the neighborhood of the equilibrium state. The molecularity can be determined from the relation between the kinetic and the thermodynamic isotopic effects.

We will consider the example of the process:

$$A_m B + \frac{m}{n} C_n D \underset{\overleftarrow{k_1}}{\overset{\overrightarrow{k_1}}{\rightleftharpoons}} C_m B + \frac{m}{n} A_n D, \tag{3}$$

in which $\overrightarrow{k_1}$ and $\overleftarrow{k_1}$ are the rate constants for the forward and the reverse reactions.

The rate constants for the forward and the reverse reactions diminish to $\overrightarrow{k_2}$ and $\overleftarrow{k_2}$ when the A atom is replaced by its heavier isotope A*:

$$A^*_m B + \frac{m}{n} C_n D \underset{\overleftarrow{k_2}}{\overset{\overrightarrow{k_2}}{\rightleftharpoons}} C_m B + \frac{m}{n} A^*_n D, \tag{4}$$

According to (1)

$$\frac{\overrightarrow{k_1}}{\overleftarrow{k_1}} = K_1^M \tag{5}$$

and

$$\frac{\overrightarrow{k_2}}{\overleftarrow{k_2}} = K_2^M, \tag{6}$$

K_1 and K_2 being the equilibrium constants for Reactions (3) and (4).

Dividing (5) by (6) leads to:

$$\frac{\overrightarrow{k_1}\overleftarrow{k_2}}{\overrightarrow{k_2}\overleftarrow{k_1}} = \left(\frac{K_1}{K_2}\right)^M. \tag{7}$$

$K_1/K_2 = \alpha$ is, on the other hand, the equilibrium constant for the isotopic exchange reaction:

$$A_m B + \frac{m}{n} A^*_n D \rightleftharpoons A^*_m B + \frac{m}{n} A_n D \tag{8}$$

or the separation coefficient of the A and A* isotopes when the isotopic exchange reaction is carried into equilibrium (the thermodynamic isotopic effect). This coefficient can be either greater or less than unity. We will choose the forward direction of the reaction to be that for which α is greater than 1.

The separation coefficient α can be determined experimentally, or it can be calculated with high precision from the vibrational frequencies of the molecules entering into the equation, using the methods of statistical thermodynamics [8]. The kinetic isotopic effect for the forward reaction, $\frac{\overrightarrow{k_1}}{\overrightarrow{k_2}} = \overrightarrow{\beta}$, expresses the increase in the rate of reaction resulting from a replacement of the heavy isotope by the light isotope. The factor $\frac{\overleftarrow{k_1}}{\overleftarrow{k_2}} = \beta$ fulfills the same role for the reverse reaction. Equation (7) then gives $\frac{\overrightarrow{\beta}}{\overleftarrow{\beta}} = \alpha^M$, i.e., the ratio between the kinetic isotopic effects for the forward and the reverse reactions is equal to the separation coefficient for the isotopes (the thermodynamic isotopic effect) raised to the power of the molecularity of the reaction.

Thus the molecularity of the reaction can be calculated from measurements on the isotopic effects of the forward and the reverse reactions. The inequality $\overrightarrow{\beta} > \alpha^M$ is always valid since $\overleftarrow{\beta} > 1$.

This makes it possible to fix a maximum value of the molecularity from which a choice between various reaction mechanisms can be made in individual cases.

LITERATURE CITED

[1] G. K. Boreskov, J. Phys. Chem., 19, 92 (1945).

[2] J. Horiuchi and M. Ikushima, Proc. Imp. Acad., 15, 39 (1939).

[3] J. Horiuchi, Proc. Japan Acad., 29, 160 (1953).

[4] J. Horiuchi, J. Res. Inst. Catalysis, 5, No.1, 1 (1957).

Received July 18, 1959.

KINETIC EQUATIONS FOR THE POLAROGRAPHY OF MELTS

Yu. K. Delimarskii, Academician, Acad. Sci. UkSSR,

and A. V. Gorodyskii

Institute of General and Inorganic Chemistry, Academy of Sciences, USSR

The literature of electrochemistry contains various kinetic equations which have been developed for the polarography of melts:

$$\varphi = \text{const} - \frac{RT}{(n-m)F} \ln \frac{i}{i_d - i} \quad ([1,2]); \tag{1}$$

$$\varphi = \text{const} + \frac{RT}{(n-m)F} \ln (i_d - i) \quad ([3,4]); \tag{2}$$

$$\varphi = \text{const} - \frac{RT}{\alpha (n-m)F} \ln \frac{i}{i_d - i} \quad ([5]), \tag{3}$$

φ is here the electrode potential, i is the current, i_d is the saturation current, R is the molar gas constant, T is the absolute temperature, F is the faradays, (n - m) is the change in the charge of the reacting substance, and α is a coefficient.

This apparent contradiction can be eliminated by applying the usual concepts of the kinetics of electrode processes.

Ionic discharge on the electrode can be considered as involving three consecutive reactions:

1) the transport of ions to the electrode

$$M^{n+}(a_0') \underset{k_2}{\overset{k_1}{\rightleftarrows}} M^{n+}(a'); \tag{4}$$

2) the electrochemical reaction

$$M^{n+}(a') + (n-m)\, e \underset{k_4}{\overset{k_3}{\rightleftarrows}} M^{m+}(a''); \tag{5}$$

3) the transport of the product materials away from the electrode

$$M^{m+}(a'') \underset{k_6}{\overset{k_5}{\rightleftarrows}} M^{m+}(a_0''). \tag{6}$$

Ions will be discharged to the metal at the electrode when m = 0. k_1, k_2, k_3, k_4, k_5, and k_6 are the rate constants for the various steps of the process and a'_0, a', a'', and a''_0 are, respectively, the activity of the reactant in the body of the melt, the activity of this same substance on the electrode surface, the activity of the product on the electrode surface, and the activity of this same substance beyond the electrode surface.

The rates of Steps (4), (5), and (6) can be calculated from the Law of Mass Action:

$$i' = k_1 a_0' \exp\left(-\frac{w_1}{RT}\right) - k_2 a' \exp\left(-\frac{w_2}{RT}\right) = \varkappa' a_0' - \varkappa' a'; \tag{7}$$

$$i = k_3 a' \exp\left(-\frac{w_3}{RT}\right) - k_4 a'' \exp\left(-\frac{w_4}{RT}\right) = k' a' \exp\left(-\frac{\alpha \varphi n F}{RT}\right) - k'' a'' \exp\left(\frac{\beta \varphi n F}{RT}\right); \tag{8}$$

$$i'' = k_5 a'' \exp\left(-\frac{w_5}{RT}\right) - k_6 a_0'' \exp\left(-\frac{w_6}{RT}\right) = \varkappa'' a'' \tag{9}$$

(for $a_0'' = 0$).

Activation energies are accounted for by the exp (-w/RT) terms, w_1, w_2, w_5, and w_6 being independent of the the potential

$$w_3 = w_0 + \alpha\varphi nF; \tag{10}$$

$$w_4 = w_0 - \beta\varphi nF, \tag{11}$$

with $k_1 = k_2$ for a diffusion process.

The rate $\underline{i}$ is equal to the rate i' when the process is stationary. On the other hand, i" is not always equal to $\underline{i}$, since Equation (9) shows that a" might then become infinite. The rate i" reaches a maximum:

$$i''_m = \varkappa'' a''_m. \tag{12}$$

when a" takes on its maximum value a''_m. Step (5) then becomes more rapid than Step (6). The product substance accumulates on the electrode surface. The activity of this substance below and above i''_m is given by

$$a'' = a''_m - \frac{i''_m - i''}{\varkappa''}, \tag{13}$$

while the activity a' is equal to

$$a' = \frac{i_d - i}{\varkappa'}, \tag{14}$$

with $i_d = \kappa' \alpha'_0$. The introduction of (13) and (14) into (8) gives

$$i = K' \frac{i_d - i}{\varkappa'} \exp\left(-\frac{\alpha\varphi nF}{RT}\right) - K''\left(a''_m - \frac{i''_m - i''}{\varkappa''}\right)\exp\left(\frac{\beta\varphi nF}{RT}\right), \tag{15}$$

$$i = \frac{\frac{i_d}{\varkappa'} - \frac{K''}{K'}\left(a''_m - \frac{i''_m - i''}{\varkappa''}\right)\exp\left(\frac{\varphi nF}{RT}\right)}{\frac{1}{K'}\exp\left(\frac{\alpha\varphi nF}{RT}\right) + \frac{1}{\varkappa'}}. \tag{16}$$

Equation (16) covers the various kinds of electrode polarization: electrochemical [Process (5)]; concentrational, type I [Process (4)] and concentrational, type II [Process (6)]. We will now consider three separate cases in which one, or more, of these processes can be neglected.

1. The discharge rate is high and i_d is less than i''_m;

$$\frac{1}{K'} \ll \frac{1}{\varkappa'}; \quad i_d \leqslant i''_m. \tag{17}$$

The first member in the denominator of the fraction of Equation (16) can be neglected. The quantity i" is equal to i. The result is

$$i = \frac{\frac{i_d}{\varkappa'} - \frac{K''}{K'}\frac{i}{\varkappa''}\exp\left(\frac{\varphi nF}{RT}\right)}{\frac{1}{\varkappa'}},$$

$$\varphi = \text{const} - \frac{RT}{nF}\ln\frac{i}{i_d - i},$$

i.e., Equation (1).

2. The discharge rate is high and the rate of Process (6) is at a maximum:

$$\frac{1}{K'} \ll \frac{1}{\varkappa'}; \quad i'' = i''_m. \tag{18}$$

The result is

$$i = \frac{\frac{i_d}{\varkappa'} - \frac{K''}{K'} a_m \exp\left(\frac{\varphi nF}{RT}\right)}{\frac{1}{\varkappa'}},$$

$$\varphi = \text{const} + \frac{RT}{nF} \ln (i_d - i),$$

i.e., Equation (2)

3. Ionic discharge is significant and the process whose rate is determined by the constant K" can be neglected, especially at high potentials:

$$K'' \ll K'; \quad |\varphi| \gg |\varphi_p|, \tag{19}$$

φ_p being the reversible electrode potential. The result is

$$i = \frac{\frac{i_d}{\varkappa'}}{\frac{1}{K'} \exp\left(\frac{\alpha \varphi nF}{RT}\right) + \frac{1}{\varkappa'}},$$

$$\varphi = \text{const} - \frac{RT}{\alpha nF} \ln \frac{i}{i_d - i},$$

i.e., Equation (3).

Thus, all of the experimentally observed relations can be derived from Equation (16) and the applicability of Equation (1), or (2), or (3) can be foretold.

The electrode reaction is described by Equation (1) when the metal deposits out on an electrode whose surface is being renewed, or when the electrode is chemically freed of the depositing metal, or when the electrochemical reduction passes from one step to another ($m \neq 0$). The surface of a nonrenewing electrode will become saturated with the depositing metal during the rapid development of a polarogram (nonstationary process). The activity of this metal (concentration) is proportional to the amount of electricity:

$$a'' = k \int_0^t i \, dt. \tag{20}$$

An approximate description of this process is given by Equation (1).

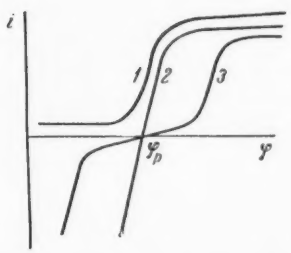

Fig.1. Polarographic curves

The electrode reaction is described by Equation (2) when the electrode surface is covered by a dense layer of the depositing metal.

The electrode reaction is described by Equation (3) when ionic discharge is retarded. The state of the separating metal is then of no significance because the rate of the reverse process of metallic ionization is low.

The various kinetic relations are differently reflected in the polarographic curves. Curve 1 of Figure 1 corresponds to Equation (1), Curve 2, to Equation (2), and Curve 3, to Equation (3). Curve 1 is characterized by the fact that the current flow is unidirectional, regardless of the potential, and Curve 3, by the fact that the current alters only slowly in the neighborhood of the equilibrium potential, the half-wave potential being displaced with respect to this equilibrium value.

The possibility of the application of one or the other of the kinetic equations can usually be decided upon from a study of polarograms in the coordinates: φ, log i ; φ, log $(i_d - i)$; φ, log $\frac{i}{i_d - i}$. The coefficient of the logarithmic term in Equations(1) - (3) can be obtained from these studies. The nature of the process is fixed more exactly from the cathodic and anodic branches of the polarization curve and from the position of this curve with respect to the equilibrium potential of the electrode in question.

LITERATURE CITED

[1] Yu. K. Delimarskii and I. D. Panchenko, Proc. Acad. Sci. USSR, 91, 115 (1953); Ukrain. Chem. J., 19, 47 (1953).

[2] I. D. Panchenko, Ukrain. Chem. J., 22, 153 (1956).

[3] E. Black and T. De Vries, Anal. Chem., 27, 906 (1955).

[4] H. Laitinen, C. Liu, and W. Ferguson , Anal. Chem., 30, 1266 (1958).

[5] Yu. K. Delimarskii and T. N. Kaptsova, J. Inorg. Chem., 3, 2751 (1958).

Received August 13, 1959.

AN INVESTIGATION OF THE ELECTROCHEMICAL PROPERTIES AND MOLECULAR FORM OF THE COPOLYMERS OF ETHYLENESULFONIC AND ACRYLIC ACIDS

Academician V. A. Kargin, S. Ya. Mirlina and A. D. Antipina

The M. V. Lomonosov State University, Moscow

The present investigation has involved a study of the electrochemical processes which occur in ethylenesulfonic and acrylic acid copolymers as the result of electrostatic interaction and the effect of these processes on the polymer chain. This study was carried out with aqueous solutions of the copolymers of ethylenesulfonic and acrylic acids and with polyethylenesulfonic acid. The viscosity and the electrical conductivity were investigated, potentiometric and conductimetric titrations were carried out, and studies were made with the electron microscope.

Sodium ethylenesulfonate and sodium acrylate were copolymerized in quartz ampules at room temperature for 36 hours, working under ultraviolet light in an atmosphere of nitrogen. The resulting polymeric salts were washed with an excess of 5% aqueous NaOH and purified by twofold reprecipitation from methanol. The copolymers with 10, 30, 40, or 50% acrylic acid do not dissolve in dimethylformamide which is a solvent for acrylic acid.

0.1% aqueous solutions of the copolymers which had been carefully purified by electrodialysis were titrated with 0.1 N NaOH, using a vacuum tube potentiometer and a glass electrode. The electrical conductivity was determined with a bridge circuit involving a ZG-10 audio-frequency oscillator and a 30-7 cathode oscillograph. These latter measurements were carried out in a polyethylene cell.

The microscopic studies were performed on a UÉM-100 universal electron microscope with an electron-optical magnification of 18-20,000.

EXPERIMENTAL RESULTS

It was noted that the decrease in viscosity of the copolymer with increasing concentration was most rapid in the solutions having the highest concentration of sulfo groups.

Coiling of the macromolecules occurs when the solution is concentrated or contains low-molecular salts but the strong electrostatic interaction of the molecular segments straightens these molecules into rigid cylinders on dilution. The viscosity of the copolymer solution can be expected to rise as the pH increases and, in turn, increases the degree of dissociation of the polyacrylic acid and the charge of the macromolecule. The relative viscosity, pH relation for the copolymers of ethylenesulfonic and acrylic acids shows a minimum at the neutralization point of the acrylic acid. A maximum is completely lacking on the viscosity curves for copolymers with low acrylic acid content.

The minimum on the viscosity curve is most pronounced in copolymers containing approximately equal numbers of ethylenesulfonic and carboxyl groups. The appearance of a minimum can be explained by the presence of ionized sulfo groups covalently bound to polymer chains in segments of high charge density, these groups attracting and holding counter ions to the polyion by coulombic interaction.

These counter ions will be firmly bound to the ionized groups to form ionic pairs which are electrically neutral and do not contribute to the transport of electricity. Neutralization of the charges of the sulfo-groups will produce dipoles and these will interact with the anions of the polyacrylic acid to produce more complex groupings in the form of ion triplets.

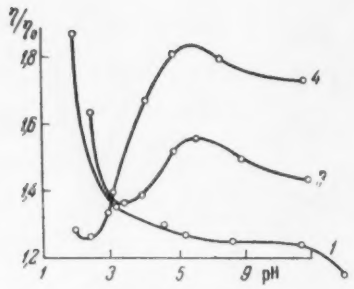

Fig.1. The relation between the relative viscosity and the pH in copolymers of ethylenesulfonic and acrylic acids: 1) with 10%, 2) with 30%, 3) with 40% acrylic acid.

The formation of ionic pairs should lead to a more dense structure and turning of the chain as the result of neutralization of the charges. The presence of ion triplets should give rise to extended fibril structures in addition to the dense coiled structures.

These suppositions have been confirmed by studies with the electron microscope. The copolymer at pH 3 shows an opened structure having the form of haphazardly interwoven fibrils (see Fig. 2a, on this page). The copolymer at pH 4, the neutralization point of the sulfo groups, shows a compact coiled structure arising from the presence of ion pairs (Fig. 2b). At pH 6, the neutralization point of the carboxyl groups, the opened structures are accompanied by dense coiled structures resulting from the increased electrostatic interaction due to the ion triplets.

The macroion chain is more flexible and twists more readily when the alkali is in excess (pH 11) and all of the charges are screened. Figure 2c actually shows a conglomeration of symmetric globules of varying density without mutual penetration.

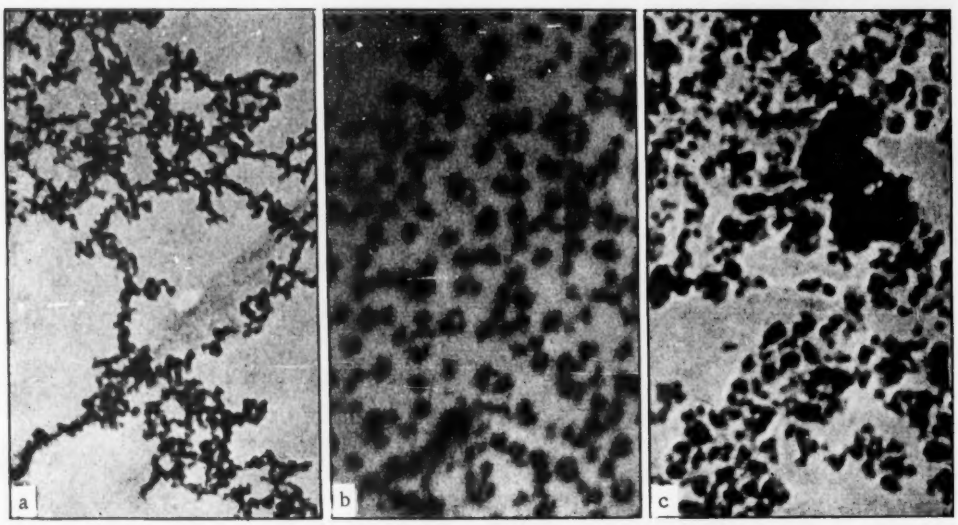

Fig. 2. Copolymers of ethylenesulfonic and acrylic acids containing 50% acrylic acid at: a) pH 3, b) the point of neutralization of the sulfogroups, pH 4, c) pH 11.

The transfer of the outer electrons and formation of ionic pairs or quasimolecules when the potential energy of ionic interaction in concentrated solutions of strong electrolytes is greater than the kinetic energy has been shown by V. K. Semenchenko [1].

The formation of ionic pairs and triplets has been confirmed by the experimental work of Semenchenko [2].

Bjerrum [3], and Fuoss and Krauss [4]. The electrostatic energy can be calculated from the potentiometric titration curve for the copolymer (Fig. 3) and increases linearly with pH, showing two breaks at points corresponding to the neutralization of the sulfoacid and the acrylic acid. This reflects an increase in the potential energy due to the ionic pairs and triplets.

The intramolecular electrostatic interaction for a given degree of neutralization has been characterized by the free-energy change, a quantity which can be evaluated from the equation of the potentiometric titration curve of copolymers of the ethylenesulfonic and acrylic acids:

$$\mathrm{pH} = pK_0 + \lg\frac{1-\alpha}{\alpha} + \frac{0{,}4343}{kT} = \frac{\partial F(v)}{\partial v}$$

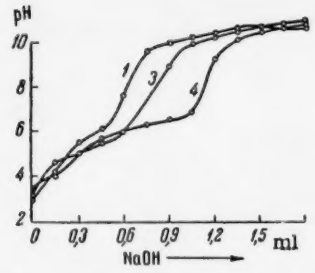

Fig. 3. Potentiometric titration curves for titration of the copolymers of ethylenesulfonic and acrylic acids with 0.1 N NaOH which resemble the curves for the titration of strong and weak acids: 1) 10%, 2) with 30%, 3) with 40% acrylic acid.

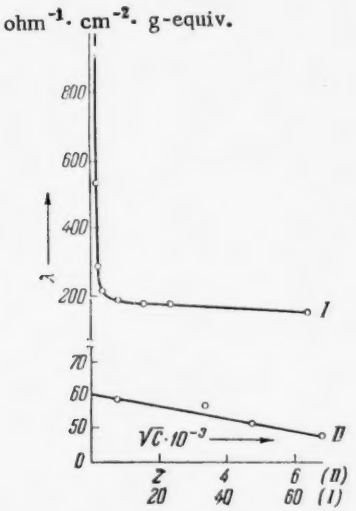

Fig. 4. The relation between the equivalent conductivity and $\sqrt{C}$: 1) for a copolymer with 50% acrylic acid; 2) for H_2SO_4.

The free energy and the electrostatic potential show minima at the neutralization point of the sulfo groups, this being due to the formation of ionic pairs and the turning of the macromolecule chain.

The potential rises sharply with progressive neutralization as a result of the increase in the charge and the untwisting of the dense rigid cylinders during the production of triplets involving the ion pairs $-SO_3'$-Na' and the polyions of the acrylic acid.

The effect of ionic association on the electrical conductivity was brought out by studing the concentration, conductivity relation for copolymers of ethylenesulfonic and acrylic acids, and by developing their conductimetric-titration curves (Fig. 4). It was established that the equivalent conductivity of the copolymers increases directly with $\sqrt{C}$, this being in good agreement with the general conductivity equation obtained from the theory of ionic pairs. Only at the higher dilutions is there a rapid rise in the equivalent conductivity, the situation then being similar to that for the weak electrolytes. The fact that the polymers show higher conductivity than H_2SO_4 is to be explained by the formation of conducting bridges between the associating groups.

From the results of this study it can be concluded that alteration in the form of the macromolecule chains by twisting and untwisting under strong electrostatic interaction is characteristic of solutions of the copolymers of strong and weak acids. The chain form alters in parallel with the free energy as the charge varies. The formation of the ionic pairs is itself responsible for the chain twisting in copolymers with high acrylic acid content and in solutions of pure polyethylenesulfonic acid where the ionic forces are insufficient for the production of more complex associations with untwisting of the chains.

LITERATURE CITED

[1] V. K. Semenchenko, Proc., Fifth Conference on Physical Chemistry, Leningrad, 1930, page 42.

[2] V. K. Semenchenko, Prog. Chem., 5, 687 (1938).

[3] Bjerrum, Zs. phys. Chem., 119, 145 (1926).

[4] Fuoss, Krauss, J. Am. Chem. Soc., 55, 1019 (1933).

Received July 15, 1959.

AN ELECTRONOGRAPHIC STUDY OF PASSIVE FILMS ON ZINC

A. I. Levin, M. E. Prostakov and G. D. Susloparov

The S. M. Kirov Ural Polytechnic Institute

(Presented by Academician A. N. Frumkin July 13, 1959)

The study of passivity involves either investigation of the electrode processes under which metals are rendered passive [1], or identification of the passive surface films [2].

Passive films 20-40 A in depth are formed on zinc under ordinary conditions but these cannot be detected microscopically [3]. The structures of such very thin surface films can be most effectively studied by an electronographic method based on the diffraction of electrons [4]. Results from electronographic studies of the structures of oxide films on iron, aluminum, copper, nickel, magnesium, and other metals are now available [5-7]. Most of these structural studies have been limited to films which were formed in air, even though many of these metals are employed technically in aqueous solutions of oxidizing agents. A comparison of the effects accompanying the interaction of metals and gaseous oxygen with those met in the formation of oxide films at a metal – electrolyte interface shows that different phenomena are in question here [8]. Thus A. V. Smirnov [9] has observed the formation of a very dense oxide film on zinc in air, the film specific gravity being 1.44 times greater than that of the metal in bulk. Anodic passivation of zinc in alkalis [10] at low current density is, on the other hand, possible only when there is separation of the rhombic modification of zinc hydroxide out of a saturated solution of zinc salts.

Some data on the structures of the oxide and hydroxide films which are formed on iron and aluminum in oxidizing solutions have already been obtained by the electronographic method [11-13]. The information on the existence and structure of the oxide films formed on zinc, a metal widely employed in protective coatings, in solutions of electrolytes is clearly contradictory. Thus, Finch and Quarrell [14] observed that these oxide films have a hexagonal structure with the lattice constants a = 2.63 A and c/a = 2.58.

P. D. Dankov, D. V. Ignatov, and I. A. Shishakov [15] have shown that the numerous reflection lines in the electronogram do not belong to either normal zinc oxide or to the hexagonal or rhombic modifications of zinc hydroxide. An electronographic study of zinc condensed on mica in vacuum has led these same authors to the conclusion that the diffraction pattern of zinc oxide is very weak. The rate of growth of the protective oxide film which forms on zinc in air is approximately 1 A per 100 hours at room temperature [16], but this is increased considerably by treating the surface of the protective oxide covering with oxidizing media, and, even more so, by anodic polarization. A protective film, 100-200 A in depth, can be formed in practice by anodic treatment of zinc in alkaline solution for 2-5 seconds.

The present investigation aimed at determining the structures of the surface films formed on zinc by liquid alkaline oxidizing media and by anodic treatment in solutions of pure alkalis. This study was carried out on a Russian ÉM-4 electron microscope with a "hot" cathode and a single lens. The accelerating potential was 35 kv. Photographs of the electron diffraction (the electronograms) were obtained by "reflecting" the electrons from the test surface. It is known that the image obtained by this method occupies only one half of the field, the other half being screened by the specimen [17]. The specimens of pure electrolytic zinc were 10× 15 mm and 1-1.5 mm thick. These specimens were cleaned in 10% HCl and then carefully washed in distilled water. The zinc was treated anodically in a 0.5% NaOH solution for 1, 2, or 5 seconds at current densities of 1, or 2, amp/dm^2 at room temperature, or 70°.

TABLE 1

Results of Measurements and Calculations on the Electronograms Obtained from the Electrochemical Passivation of Zinc Surfaces in a 0.5% Sodium Hydroxide Solution

Indices	Calc. interplanar spacing, A	Interplanar spacing from electronogram, A	Line characteristics	Indices	Calc. interplanar spacing, A	Interplanar spacing from electronogram, A	Line characteristics
100	2,85	2,84	Very strong	202	1,24	1,23	Very weak
002	2,60	—	—	104	1,82	—	—
101	2,49	2,47	Very strong	203	1,09	1,07	Medium
102	1,92	1,91	Medium	121	1,04	1,02	Medium
110	1,62	1,61	Strong	114	1,01	—	—
103	1,48	1,44	Weak	105	0,98	0,97	Weak
200	1,41	1,39	Medium	300	0,94	0,92	Very weak
112	1,38	1,37	Weak	123	0,91	0,89	Medium
201	1,36	1,35	Weak	302	0,88	0,87	Weak

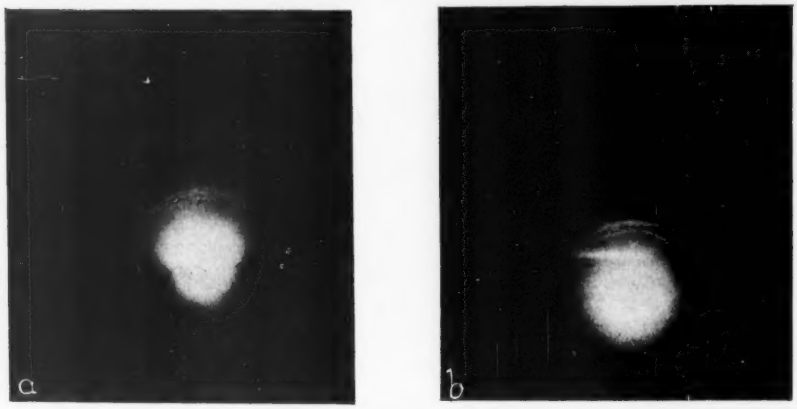

Fig. 1. Electronograms of hexagonal zinc oxide formed on the surface of a zinc specimen during anodic treatment in a 0.5% NaOH solution at a current density of 2 amp/dm^2; a) at 70°; b) at 20°.

The diffraction patterns of Figure 1a, b were obtained with different types of anodic treatment. These patterns became sharper when the time of treatment was lengthened and the temperature or current density was increased. Analysis of the electronograms shows (Table 1) a thin film of zinc oxide to have been formed on the zinc, this film having a hexagonal type of lattice with the parameters a = 3.248 and c = 5.203 A.

A study of mechanisms has led F. F. Faizulin and L. K. Yuldasheva [18] to the conclusion that the dissolution of zinc and the formation of a passive film proceed simultaneously at the anode, their data indicating an increase in the rate of growth of the oxide film with rising temperature, just as do our own. A rise in the temperature at fixed time of anodic treatment leads to a pronounced growth of the zinc oxide crystals on the specimen surface with an accompanying intensification in the electron diffraction. Thus it is possible to detect as many as 15 semicircles on the electronogram at 70° (Fig. 1a) but only 7 at 20° (Fig. 1b). Chemical passivation of zinc specimens was carried out in a solution which contained 20 g/liter of sodium chromate, 10 g/liter of

sodium hydroxide, 10 g /liter of tri-sodium phosphate, and 3 g/liter of the emulsifier OP-7. The specimens were first cleansed and washed and then immersed in this solution at 95-98° for 15-35 seconds.*

Electronograms of the surfaces of these specimens contained two diffuse semicircles of radii 2.1 and 1.19 (interplanar distances, d = 2.41 A and d = 1.37 A) which corresponded to the most intensive maxima in the complete diffraction pattern of the zinc oxide film.

Chromium could be detected spectrally on zinc, or zinc-plated iron, surfaces which had been rendered passive in a reduced solution, or in a chromate solution [19].

These electron diffraction lines indicate that finely crystalline zinc oxide is present on a zinc surface which has been treated in an alkaline chromate solution, despite the fact that this surface carries chromium atoms. Thus the case of zinc is one in which there is a fundamental difference between the oxidation of the metal by gaseous oxygen in the absence of moisture [9] and the passivation of the metal by dissolved oxidizing agents or by anodic polarization.

Electronographic investigations of the thin films which are formed on zinc by brief treatment in weak alkaline solutions point to the production of passive films of zinc oxide with hexagonal lattice type. The passivation of the electrode results from the fact that this modification of zinc oxide covers the metal with a dense, tightly adhering film. Thus the passivation of anodically dissolving zinc is quite dependent on the crystalline form of the developing film. Treatment of zinc in an alkaline chromate solution for 15-35 seconds at 90° produces a complex amorphous surface film which contains crystals of ZnO. Here, no final decision has been reached as to the mechanism of passivation. The marked retardation in the rate of film growth once a definite thickness has been reached indicates that the mechanism of transfer of ions and atoms departs more and more from the usual diffusion mechanism as the film thickness increases. In this case it is possible to make use of concepts which are to a certain degree analogous to those applying to the retarding action of adsorbed films of surface-active substances [20].

The strength of the field of the electric double layer diminishes as the film thickens so that the penetration of zinc ions through the film is impeded,and the rate of growth of the passive film is diminished [21].

LITERATURE CITED

[1] B. V. Érshler, Proc., Second Conference on the Corrosion of Metals, 2, 52 (1943); J. Phys. Chem., 14, 357 (1940); 18, 131 (1944); B. N. Kabanov, Proc. Acad. Sci. USSR, 31, 338, 582 (1941); L. Yu. Kurtts, The Problem of the Anodic Passivity of Metals [in Russian], Acad. Sci. USSR, Press, 1936.

[2] A. L. Kunin, Surface Phenomena in Metals (in Russian), Moscow, 1955.

[3] O. Kubashevskii and B. Hopkins, The Oxidation of Metals and Alloys (in Russian), Foreign Lit. Press, 1945.

[4] Z. G. Pinsker, The Diffraction of Electrons (in Russian), Moscow-Leningrad, 1949.

[5] G. Thomson, Proc. Roy. Soc., A, 128, 649 (1930).

[6] P. D. Dankov, The Catalytic Activity and Structure of Thin Metal Films (in Russian), Dissertation, Moscow, 1935.

[7] V. E. Loshkarev, The Diffraction of Electrons (in Russian), 1933.

[8] A. N. Frumkin, V. S. Bagotskii, et al, The Kinetics of Electrode Processes (in Russian), Moscow, 1952.

[9] A. V. Smirnov, Hot Zinc Plating (in Russian), Moscow, 1953.

[10] Z. A. Iofa, S. Ya. Mirlina and M. B. Moiseeva, J. Appl. Chem., 22, 983 (1949) [USSR].

[11] J. Jitake, S. Miyake, and T. Jimori, Nature, 139, 408 (1927).

*Careful twofold washing assured that the specimens would be completely freed of the passivator. The wash waters were analyzed for chromium ions.

[12] P. D. Dankov and I. A. Shishakov, Proc. Acad. Sci. USSR, 27, 554 (1939).

[13] P. D. Dankov, A. A. Kochetkov and I. A. Shishakov, Bull. Acad. Sci. USSR, Div. Chem. Sci., 1942, No.5, 274.

[14] G. J. Finch and A. G. Quarrell, Proc. Roy. Soc., A, 141, 398 (1923).

[15] P. D. Dankov, D. V. Ignatov and I. A. Shishakov, The Electronographic Investigation of Oxide and Hydroxide Films on Metals (in Russian), Acad. Sci. USSR, Press 1953.

[16] G. V. Akimov, The Theory and Methods of Investigation of the Corrosion of Metals (in Russian),Acad. Sci. USSR, Press, 1945.

[17] B. K. Vainshtein, Structural Electronography [in Russian],Avtoreferat ,Moscow, 1955.

[18] F. F. Faizullin and L. K. Yuldasheva, Records of the State University of Kazan, 116, vol. 5 (1956).

[19] F. F. Azhogin, Chromic Passivation of Zinc (in Russian), Dissertation, Moscow, 1949.

[20] A. N. Frumkin, Proc., Conference on the Effect of Surface-Active Substances, Vilna, 1957.

[21] N. Mott, Trans. Farad. Soc., 39, 472 (1940); 43, 429 (1947); N. Cabrera and N. Mott, Rep. Progr. Phys., 12, 163 (1949).

Received July 7, 1959.

THE EQUATION OF THE PHASE TRANSITION CURVE

G. A. Martynov

The Institute of Physical Chemistry of the Academy of Sciences of the USSR

(Presented by Academian G. V. Kurdyumov June 30, 1959)

The equation for the fusion curve has not yet been derived [1] although the differential Clausius-Clapeyron Equation relating pressure and melting point has been known for more than one hundred years, and several impirical expressions for the curve are available (see [2], for example).

The Clausius-Clapeyron Equation

$$T\Delta v\, dP = q\, dT \tag{1}$$

is obtained by differentiating the equality

$$\mu_1(T, P) = \mu_2(T, P), \tag{2}$$

in which μ_i is the chemical potential of the i-th phase (see [3], for example).

The quantities q (the heat change accompanying phase transition) and Δv (the change of molar volume in melting) of Equation (1) might seem to be arbitrary functions of the pressure P and the temperature T. This is not actually the case. The chemical potential is given by $\mu = u + Pv - Ts$, u, v, and s, being, respectively, the molar energy, volume, and entropy of the substance in question, $q = T(s_2 - s_1)$, so that Equation (2) can be rewritten as

$$q = \Delta u + P\Delta v, \tag{3}$$

with $\Delta u = u_2 - u_1$, $\Delta v = v_2 - v_1$.

If (3) is differentiated on the assumption that Δu and Δv are functions of T and P, and account is taken of the fact that [3]

$$\left(\frac{\partial u}{\partial T}\right)_P = c_p - P\left(\frac{\partial v}{\partial T}\right)_P; \quad \left(\frac{\partial u}{\partial P}\right)_T = -T\left(\frac{\partial v}{\partial T}\right)_P - P\left(\frac{\partial v}{\partial P}\right)_T, \tag{4}$$

(c_p is the heat capacity at constant pressure) the result will be the well-known expression

$$dq = \Delta c_p\, dT + \left\{\Delta v - T\left(\frac{\partial \Delta v}{\partial T}\right)_P\right\} dP. \tag{5}$$

This equation shows that $(\partial q / \partial P)_T$ is determined as a function of T and P once the relation $\Delta v = f(T, P)$ is given. Equation (5) represents a complete differential so that

$$\frac{\partial \Delta c_p}{\partial P} = -T\left(\frac{\partial^2 \Delta v}{\partial T^2}\right)_P \tag{6}$$

and thus $\left(\frac{\partial q}{\partial T}\right)_p = \Delta C_p = \varphi(T, P)$ relation is fixed to within an arbitrary function of the temperature by $\Delta v = f(T, P)$.

Equation (5) is obtained, just as the Clausius-Clapeyron Equation, by differentiating the condition for phase equilibrium, (2). Thus (1) can be integrated only if q and Δv satisfy (5). No sort of mathematical treatment will simultaneously reduce (1) and (5) to their parent, Equation (2), if this condition is not fulfilled.

It is known that a highly accurate integral relation between the temperature and the vapor pressure can be developed from the Clausius-Clapeyron Equation for many substances. This is due to the fact that the vapor phase participating in this equilibrium can be described by the Ideal Gas Law $Pv = RT$, over a wide temperature interval. The density of the vapor is much less than that of the condensed phase, so that $\Delta v \simeq RT/P$. A substitution of this last result into (5) shows that $(dq/dP)_t = 0$, and thus $q = q(T)$, i.e., the functions q and Δv are independent of one another in this case and Equation (1) can be integrated. This is clearly not true for fusion since then $(dq/dP)_t \neq 0$.

Experience proves that the Δv of fusion is a complex function of T and P, and the integration of (1) is difficult for this reason. Because of this we will develop $\Delta v = f(T,P)$ in a series and neglect all but the first members

$$\Delta v = \Delta v_0 + \alpha (T - T_0) + \beta (P - P_0), \tag{7}$$

here, $\alpha = v_2\alpha_2 - v_1\alpha_1 = \text{const}$; $\beta = -(v_2\beta_2 - v_1\beta_1) = \text{const}$; $\alpha_i = (1/v_i)(\partial v_i/\partial T)_p$ is the coefficient of expansion; and $\beta_i = -\frac{1}{v_i}\frac{\partial v_i}{\partial P}_T$ is coefficient of compressibility of the i-th phase. We will also suppose that $\Delta C_p = \text{const}$. Integration of (5) then gives

$$q = q_0 + \Delta c_p (T - T_0) + (\Delta v_0 - \alpha T_0)(P - P_0) + {}^1/_2\beta (P - P_0)^2. \tag{8}$$

Introduction of (7) and (8) into (1) yields

$$T\frac{dP}{dT} = \frac{q_0 + \Delta c_p (T - T_0) + (\Delta v_0 - \alpha T_0)(P - P_0) + {}^1/_2\beta (P - P_0)^2}{\Delta v_0 + \alpha (T - T_0) + \beta (P - P_0)}. \tag{9}$$

The change of variables

$$x = \alpha T, \quad z = [\Delta v_0 + \alpha (T - T_0) + \beta (P - P_0)]^2, \tag{10}$$

will lead (9) to the form

$$\frac{dz}{dx} - \frac{z}{x} = \frac{a}{x} + b + x, \tag{11}$$

in which a and b are certain constants. This is an ordinary linear differential equation. Its solution is

$$P - P_0 = \frac{1}{\beta}\left\{-[\Delta v_0 + \alpha (T - T_0)] \pm \right.$$
$$\left. \pm \sqrt{[\Delta v_0 + \alpha (T - T_0)]^2 - \frac{2\beta}{T_0}(q_0 - \Delta c_p T_0)(T_0 - T) + 2\beta \Delta c_p T \ln \frac{T}{T_0}}\right\}. \tag{12}$$

Equation (12) fixes $P = P(T)$ since Δv_0, α, β, and Δc_p are supposed to be known. The sign to be chosen for the radical of (12) will depend on whether Δv is positive or negative.

We have checked these conclusions by carrying out calculations on the ice – water system through Equation (12). Results from this check are shown in Table 1. The experimental data of [5] on $\Delta v = f(T, P)$ were treated by the method of least squares so as to obtain values for the coefficients Δv_0, α, and β of Equation (7) for these calculations.

The Table contains both experimental data and results of calculations based on (7) and thus gives an idea of the accuracy of approximations obtained through the latter. The values $q_0 = 3.336 \cdot 10^9$ erg/g and $\Delta c_p = 2.070 \cdot 10^7$ erg/g·deg [5] were adopted in calculating P from Equation (12). The Table shows that the deviation between the experimentally determined pressure and the calulated P does not exceed 4% over the pressure interval from 1 to 2045 atmospheres.

TABLE 1

$T-T_0$, °C	0	−5	−10	−15	−20	−22
Δv_{exp}, cm³/g	−0,0900	−0,1016	−0,1122	−0,1218	−0,1313	−0,1352
Δv_{cal}, cm³/g	−0,0900	−0,1015	−0,1120	−0,1221	−0,1315	−0,1351
P_{exp}, atmos	1	590	1090	1540	1910	2045
P_{cal}, atmos	1	594	1088	1506	1840	1963

In concluding, the author counts it to be his pleasant duty to express his thanks for the valuable remarks made by Prof. B. V. Deryagin in reviewing the manuscript of this article.

LITERATURE CITED

[1] A. V. Voronel', J. Tech. Phys., 28, 2630 (1958) [USSR].

[2] U. F. Simon and A. Glatzel, Zs. anorg. Chem., 178, 309 (1929).

[3] L. Landau and E. Lifshits, Statistical Physics (in Russian), 1951.

[4] V. V. Stepanov, A Course in Differential Equations (in Russian), 1953.

[5] N. E. Dorsey, Properties of Ordinary Water-Substance in all its Phases, N. Y., 1940.

Received June 28, 1959.

THE ELECTRODE PROCESSES ON GERMANIUM IN SULFURIC ACID SOLUTIONS OF OXIDIZING AGENTS

E. N. Paleolog, A. Z. Fedotova and N. D. Tomashov

The Institute of Physical Chemistry of the Academy of Sciences of the USSR

(Presented by Academician A. N. Frumkin July 10, 1959).

A study of the electrochemical behavior of germanium in solutions of electrolytes is of interest in connection with the electrochemical treatment of surfaces for developing the mechanism of spontaneous dissolution of semiconductors in corrosion and improving the characteristics of semiconducting devices. It is now definitely established that holes are involved in the anodic dissolution of germanium [1, 2, 3]. The mechanism of the cathodic processes on germanium has not yet been settled, however, and various opinions concerning it have been expressed in the literature [1, 4-6]. In investigating the mechanism of spontaneous dissolution of semiconductors we we have studied the kinetics of the electrode processes on germanium of various conduction types in H_2SO_4 solutions (pH 1.0) containing H_2O_2 or Fe^{3+}.

The monocrystalline germanium which was used in these measurements had the following characteristics:

	Specific resistance, (R), ohm · cm	Volume lifetime, (τ), μsec
n-Type germanium	13.0	360
p-Type germanium	21.0	350

A lead – tin alloy was employed for making electrical contact with the specimens which were 4-5 mm thick. The germanium was imbedded into polystyrene, its surface being polished with corundum powder and washed with doubly distilled water. An alkaline H_2O_2 solution, or a SR-4* solution, was used for corrosion. Each specimen was tested prior to measurement so as to be certain that there was no rectifying contact. Each experiment was carried out in the dark in a thermostat at 25 ± 0.1°. Control experiments under strong illumination were performed on certain specimens using a OI-7 illuminator with a focusing lense.

Figures 1 and 2 show cathodic polarization curves for germanium with hole, or electron, conduction. These measurements were made in agitated solutions which were in contact with air. The potentials used in developing the polarization curves were determined one minute after altering the current density. Measurements were carried out rapidly in order to avoid changing the state of the electrode surface during polarization.

The results show that the n-type germanium cathode behaves in each solution as a metallic electrode with a low efficiency for the discharge of hydrogen ions and a high overvoltage (1200 -1300 mv at 10 ma/cm^2). Oxidizing agents in solution (H_2O_2 or Fe^{3+}) are reduced on this cathode, the value of the maximum diffusion current altering regularly as the concentration of the oxidizing agent is varied.

*Solution composition: 15 cm^3 CH_3COOH, 25 cm^3 conc. HNO_3, 15 cm^3 conc. HF, and 0.06 cm^3 Br_2.

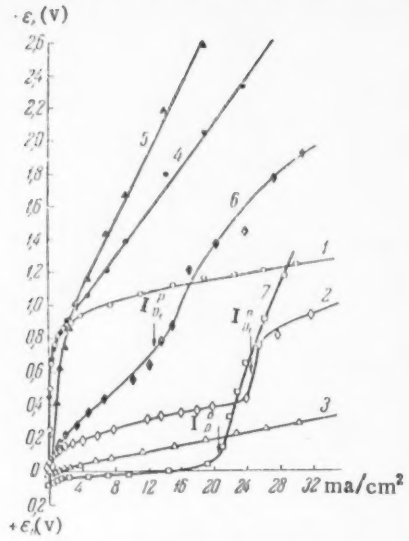

Fig. 1. Cathodic polarization of germanium in the presence of hydrogen peroxide. n-Type germanium: 1) H_2SO_4 (pH 1.0); 2) H_2SO_4 (pH 1.0) + 0.24 N H_2O_2; 3) 17NH_2O_2. p-Type germanium: 4) H_2SO_4 (pH 1.0); 5) 17 N H_2O_2; 6) H_2SO_4 (pH 1.0) + + 0.24 N H_2O_2; 7) 17 N H_2O_2 (under illumination).

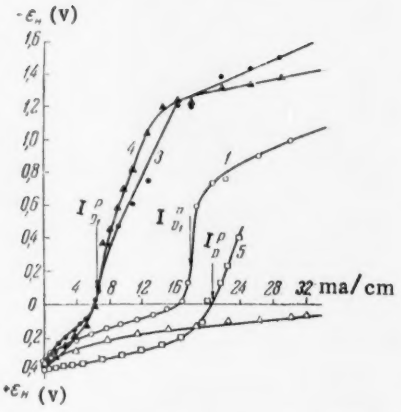

Fig. 2. Cathodic polarization curves for germanium in the presence of ferric chloride. n-Type germanium: 1) H_2SO_4 (pH 1.0) + 0.06 N $FeCl_3$; 2) H_2SO_4 (pH 1.0)+ + 0.2 N $FeCl_3$. p-Type germanium: 3) H_2SO_4 + 0.06 N $FeCl_3$; 4) H_2SO_4 (pH 1.0)+ + 0.2 N $FeCl_3$; 5) H_2SO_4 (pH 1.0) + 0.2 N $FeCl_3$ (under illumination).

An additional inhibition from the semiconduction of the cathode is observed with hole-conducting germanium (p-germanium), and this is true not only for the discharge of hydrogen ions but also for both reduction reactions: $Fe^{3+} + e \rightarrow Fe^{2+}$ and $H_2O_2 + 2H^+ + 2e \rightarrow 2H_2O$. This inhibition becomes appreciable at a current density of approximately 1.8 ma/cm² and then increases as the density rises.

The inhibition of the cathode reaction on p-germanium involves not only an increase in the slope of the corresponding segment of the polarization curve but also a considerable diminution in the value of the "maximum" diffusion current in the oxidizing solution ($I_D^p < I_D^n$). The "maximum" current for the reduction of iron on p-germanium in a H_2SO_4 + $FeCl_3$ solution is considerably less than that for reduction on germanium of the n-type and is independent of the amount of $FeCl_3$ in the investigated interval of concentrations. A diminution in the value of I_D for p-germanium is also observed in sulfuric acid solutions containing hydrogen peroxide.

Observation of the surface of the p-germanium electrode shows that the evolution of hydrogen begins at 1100-1300 mv in each solution except the 17 N H_2O_2. The discharge of hydrogen ions on p-germanium proceeds with a rather high and practically uniform inhibition in solutions of H_2SO_4 (pH 1.0) and H_2SO_4 (pH 1.0) + 0.24 N H_2O_2, and is facilitated by the Fe^{3+}.

Illumination leads to a marked acceleration in the reduction of Fe^{3+} and H_2O_2 on the p-germanium cathode, although even here there is a pronounced shift of the electrode potential in the negative direction at a current density of ~ 20 ma/cm², i.e., a "maximum" current appears here. With agitation, this current proves to be independent of the nature of the oxidant and is much lower than with n-germanium under similar conditions.

Anodic polarization curves for germanium with electron, or hole, conduction are shown in Figures 3 and 4. Here the rate of anodic dissolution of the p-germanium is practically independent of the nature and concentration of the substance added to the solution, the germanium remaining in the active state over the investigated range of current density. Holes participate in the anodic dissolution of n-germanium so that the rate of this process cannot exceed a certain limiting value ($I_{Sat.}$) which is fixed by the bulk hole concentration. The

introduction of hydrogen peroxide into solution brings about no alteration in the saturation current even though this current is markedly increased by the Fe^{3+}. Illumination of the electrode increases the anodic saturation current for n-germanium in H_2SO_4 (pH 1.0) by a factor of 17.

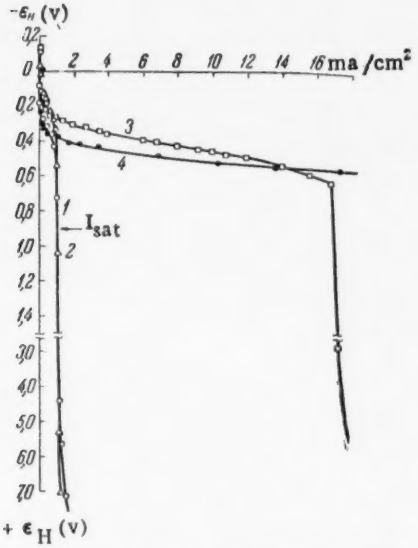

Fig. 3. Anodic polarization of germanium in the presence of hydrogen peroxide. n-Type germanium: 1) H_2SO_4 (pH 1.0); 2) H_2SO_4 (pH 1.0) + 0.24 N H_2O_2; 3) H_2SO_4 (pH 1.0) under illumination. p-Type germanium: 4) H_2SO_4 (pH 1.0).

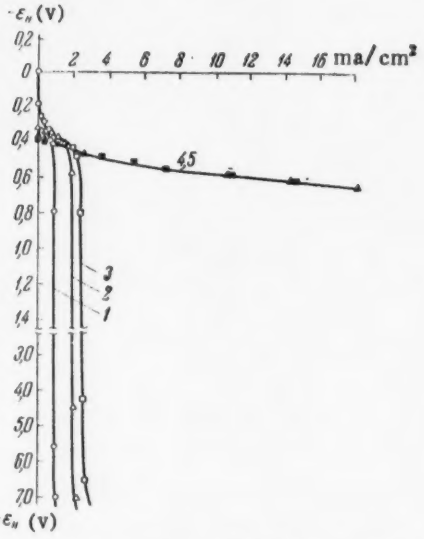

Fig. 4. Anodic polarization of germanium in the presence of ferric chloride. n-Type germanium: 1) H_2SO_4 (pH 1.0); 2) H_2SO_4 (pH 1.0) + 0.06 N $FeCl_3$; 3) H_2SO_4 (pH 1.0) + + 0.2 N $FeCl_3$. p-Type germanium: 4) H_2SO_4 (pH 1.0) + 0.06 N $FeCl_3$; 5) H_2SO_4 (pH 1.0) + 0.2 N $FeCl_3$.

An analysis of these results shows that the cathodic reactions on n-germanium are predominantly ones involving free electrons.

The marked inhibition of the cathodic process on p-germanium can be due to an insufficiency of free electrons when the conditions are such that these latter predominate in the reduction of Fe^{3+} and H_2O_2, or it can result from an additional ohmic potential drop in a hole-impoverished layer of p-germanium next to the surface. Valence electrons play the predominant role in the reduction reactions on the p-germanium in this last case.

The increase in the anodic saturation current density for n-germanium in the presence of Fe^{3+} can be due to a specific adsorption of these ions on the germanium surface with a resultant increase in the rate of recombination in the germanium layer adjoining the surface. The data of Gerisher and Beck[5]* show that this effect might also arise from a simultaneous reduction of the Fe^{3+} ions on the anode which would lead to an increase in the hole concentration.

These results indicate that the conduction type is of great significance in fixing the rates of electrode processes on germanium. Thus, there is a marked inhibition of the cathodic reduction of Fe^{3+} and H_2O_2 and the discharge of hydrogen ions in the case of p-germanium, while the anodic dissolution of n-germanium is impeded.

LITERATURE CITED

[1] W. Brattain and G. Garret, Bell Syst. Techn. J., 34, No.1 (1955).

[2] D. Turner, J. Electrochem. Soc., 103, No.4, 252 (1956).

*As in original.

[3] E. A. Efimov and I. G. Erusalimchik, J. Phys. Chem., 32, No.2 (1958) [USSR].

[4] H. Gerischer and F. Beck, Zs. phys. Chem., Neue Folge, 13, 389 (1957).

[5] E. A. Efimov and I. G. Erusalimchik, J. Phys. Chem., 32, 9 (1958) [USSR].

[6] F. Beck and H. Gerischer, Zs. Electrochem., 63, No.4 (1959).

Received July 10, 1959.

THE PROBLEM OF EVALUATING THE REACTIVITY OF EXPLOSIVES

A. I. Serbinov

The Institute of Chemical Physics of the Academy of Sciences of the USSR

(Presented by Academician N. N. Semenov May 25, 1959)

The reactivity of explosives is a factor of great importance for their combustion and detonation, and one which is significant in fixing the conditions under which these materials can be stored, the length of time which they can be held, and the conditions under which they can be safely handled.

The isothermal decomposition of an explosive follows a monomolecular law, and therefore:

$$k_1 = \frac{2,3}{\tau} \lg \frac{c_0}{c}. \tag{1}$$

The temperature dependence of the rate constant is given by the equation:

$$k_1 = Be^{-E/RT}, \tag{2}$$

in which E is the activation energy and B is a coefficient which is theoretically [1] of the order of the frequency of vibration of the valence bonds in the molecule, i.e., $10^{13} - 10^{14}$ sec^{-1}.

Experimental studies on the thermal decomposition of explosives in many cases have led, not to just one value of E, but to several, with several associated values of B, each many orders larger than the theoretical [2,12]. Exceptions are sometimes met where the B value is close to the theoretical [3]. E and B values for various explosives are to be found in the monograph of Andreev [4].

The value of the ignition lag, τ_i, in thermal detonation is also used in evaluating the reactivity of explosives and fixing the conditions under which these materials can be safely handled. The theory of thermal detonation which has been developed by Semenov [5] and Todes [6] shows the temperature dependence of τ_i to be given by the equation:

$$\tau_i = Ae^{E/RT}, \tag{3}$$

E being the activation energy and A, a coefficient which is inversely proportional to B. Investigations of the reactivity of explosives by the method of thermal detonation usually lead to a value for E, but not A. A can be readily evaluated theoretically, however. Semenov has shown [7] that the self-heating prior to detonation is low and the factor RT_0^2/E small, so that τ_i can be equated to the time τ of isothermal reaction at the initial temperature.

Thus it is possible to set up an approximation to the relation between τ_i, k_1, and T_0. From (1) and (2) there follows:

$$\tau_i = \frac{2,3 \lg c_0/c}{B} e^{E/RT}. \tag{4}$$

This last can be combined with (3) to obtain:

$$A = \frac{2,3 \lg c_0/c}{B}. \tag{5}$$

Thus A can be readily evaluated theoretically if the degree of breakdown of the explosive in the time τ_i is known. Apin [8], and Apin, Todes and Khariton [3] have shown that 5-10 % of the explosive will react in the time τ_i.

Equation (5) shows that a 10 % breakdown of the explosive corresponds to:

$$A \simeq \frac{10^{-1}}{B} \simeq 10^{-14} - 10^{-15} \text{ sec} \qquad (6)$$

An analysis of the temperature dependence of τ_i for various explosives indicates that the value of A is also frequently far from that predicted by the theory, being many orders higher in some cases and many orders less in others. The wide spread in the kinetic parameters of tetryl is shown by the values of E and the coefficients A and B which are given in Table 1.

It has seemed to us that this variation in the values of the coefficients must arise from the extensive extrapolation through 15- 18 orders, or more, which is always involved in evaluating quantities which represent nothing other than k_1 and τ_i at $T \to \infty$.

TABLE 1

The Energy of Activation, E, and the Frequency Factors for Isothermal Decomposition and Thermal Detonation of Tetryl

E, kcal/mole	lg B	lg A	Author
60,0 *	27,5		Farmer [10]
55,5 *	24,5		»
52,0 *	22,5		»
38,4	15,4		Robertson [11]
36,6	12,7		Andreev [4]
34,9	12,9		Cook and Abegg [12]
20,3	—	—7,6 **	Andreev [13]
14,4	—	—5,5 **	Henkin and McGill [9]
78,0	—	—36,5 **	Lukin and Roginskii [2]

*Recalculated by Roginskii [2].

**Recalculated by us from the data of the authors.

The range of the experimental studies must be widened if this extrapolation error is to be reduced and more trustworthy values obtained for the kinetic parameters. For this purpose, measurements were made on the ignition lag of several explosives for which this quantity varies by 3-5 orders, the time for 10 % isothermal decomposition of these substances at various temperatures being calculated from the data of other authors through Equation (1). All of this experimental material has been plotted in the coordinates log τ, $1/T$ in Figure 1. It is found that the experimental results covering an alteration of almost nine orders (from one second to several years) in the reaction time of any one material cluster around a single straight line, the corresponding frequency factor being approximately equal to the theoretical value for a monomolecular reaction. The extent of deviation from the mean E value in any one of the various series of experiments can be estimated from the two theoretical boundary lines which have been included in Figure 1 for each explosive; the E values for these lines differ from the average by 1-2 kcal/mole, the value of A having been obtained from the theoretical Equation (5). The B coefficient of this same equation was calculated from the vibrational frequency of the molecule of the explosive.

The valence vibrations of the characteristic groups of many of these explosives fall within the interval 1000-1700 cm^{-1} [15], or $3\text{-}5 \cdot 10^{13}$ sec^{-1}, and a common value of $4 \cdot 10^{13}$ sec^{-1} was therefore adopted for the materials which are under consideration here. We then have log B = 13.6 and Equation (6) gives log A = -14.6.

Figure 1 shows that the temperature dependence of τ_i and k_1 can be adequately represented by Equations (3) and (2), respectively, if use is made of the theoretical values of A and B. The activation energies of trinitrotriazidobenzene and liquid tetryl remain constant at 30.5 ± 0.5 and 35 ± 1 kcal/mole, respectively, over their range.

Each series of experiments which earlier gave a spread of E values and associated frequency factors (see Table 1) now falls between the theoretical lines corresponding to E values of 34 and 36 kcal/mole. A qualitative explanation can be given for each departure of an individual curve from the straight line corresponding to average E value. Thus the temperature coefficient of the reaction rate sometimes rises in the isothermal method because of an insignificant but progressive self-heating of the explosive charge, the alteration being the greater, the higher the initial temperature of the experiment, and this can lead to an increase in the calculated values of E and B (Lines 6 and 7 for tetryl). An apparent increased in E is observed in investigating the reactivity of explosives near the ignition boundary by the thermal detonation method, this being due to increased thermal loss at high values of τ_i with a gradual transfer to isothermal decomposition; there is also an apparent diminution in E at values of τ_i which are comparable with the time of heating of the explosive charge.

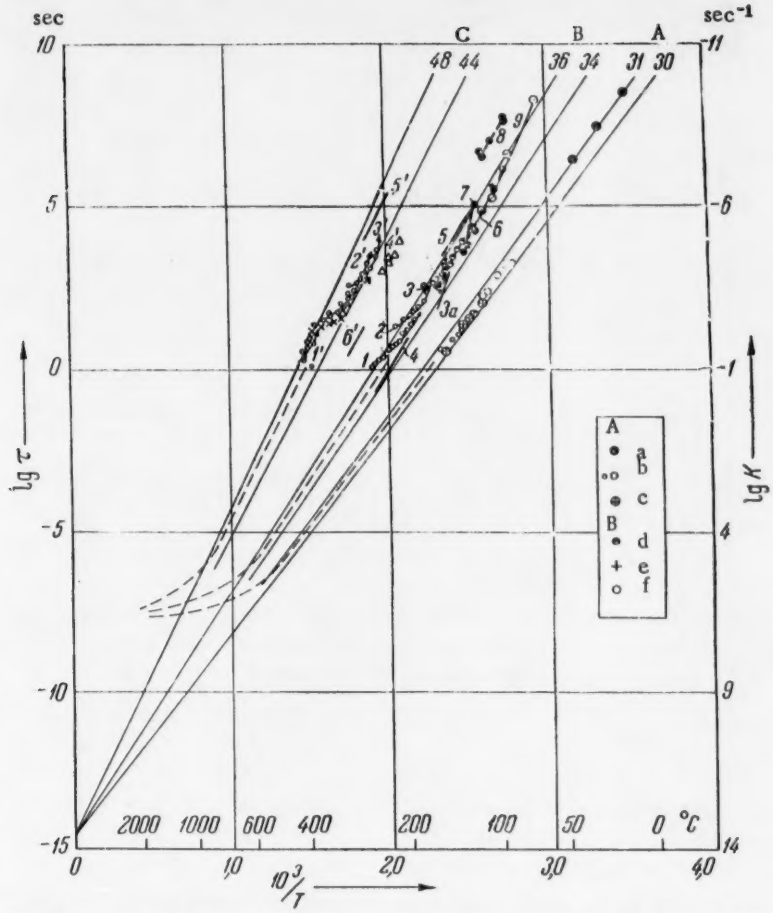

Fig. 1. The energy of activation for isothermal monomolecular decomposition and for thermal detonation of explosives, calculated from the theoretical values of the frequency factor. A) trinitrotriazidobenzene: a) Turek [19], b) Ioffe [20], c) Andreev [21]. B) tetryl: 1, 2, 3, author of this article; 3a, d) Lukin and Roginskii [14]; e) Khariton and Andreev [16]; 4) Robertson [11]; 5) Cook and Abegg [12]; f) Hinshelwood [17]; 6, 7, 8,) Farmer [10]; Solonina [18], Dubovitskii, Manelis, and Smirnov. C) trotyl: 1', 2', 3') author of this article; 4') Roginskii and Magid [22]; 5') Cook and Abegg [12]; 6') Robertson [23].

The data of Farmer [10] (Line 8) for crystalline tetryl at low percentage decomposition (0.2-1%) should be considered as the most trustworthy for this substance (Lines 8 and 9), the two lower points of Line 9 coming from data obtained by Solonina [18] at very high percentage breakdown (44%) where the autocatalysis is extensive. Thus the energy of activation for the decomposition of crystalline tetryl is larger than that of the liquid, or dissolved, tetryl by approximately one-half of the heat of fusion and is equal to 38 kcal/mole.

The data on the thermal detonation (Curves 1', 2', 3', 4') and isothermal decomposition (Lines 5' and 6') of trotyl show a considerable spread, the energy of activation for decomposition of this substance being estimated as 46 ± 2 kcal/mole. The data of Robertson (Line 6') has not been taken into account here in light of the criticism of Cook and Abegg [12].

Autocatalysis is frequently observed in laboratory investigations of the thermal breakdown of explosives at high percentage decomposition. It is clear, however, that the role of this factor in fixing the stability of explosives

has been overestimated since autocatalysis cannot occur at the very slight decomposition which is permitted in storing of these substances. Accepting 1% as a permissible value for the decomposition in an explosive during storage, the time of storage can be estimated through Equation (4)

$$\tau(1\%) = 10^{-15,6} e^{E/RT} \text{ sec} = 10^{-23,1} e^{E/RT} \text{ years} \quad (7)$$

T being the storage temperature in °K.

A trustworthy method for estimating the energy of activation of the thermal decomposition of the explosive is needed here.

Equation (2) and Figure 1 show that all of these materials decompose according to a monomolecular law so that the most trustworthy and direct determination of the energy of activation for any explosive is to be had through the equation:

$$E = 4,57\, T\, (\lg B - \lg k_1), \quad (8)$$

B is here a theoretical value obtained from the valence vibrations of the characteristic groups in the explosive molecule.

An adequate, but less accurate, determination of E can be had from the value of τ_i near the ignition limit (the so-called flash temperature) by using Equation (3):

$$E = 4,57\, T\, (\lg \tau_i - \lg A). \quad (9)$$

The lower accuracy of this equation is the result of the approximation involved in fixing a theoretical value of A through (5). Interest attaches to the question as to how far the temperature can be raised before these equations cease to reproduce the relation between the temperature and the ignition lag.

The law of monomolecular breakdown rests on the idea of molecular dissociation resulting from increased energy of valence vibrations, and the natural limit of applicability of these relations would thus be met at times of the order of the time of excitation and redistribution of the energy of the molecular valence bond, i.e., at 10^{-6} - 10^{-8} seconds. Thus there must be a departure from linearity in the kinetic region for the temperature dependence of the ignition lag beyond the limits of experimentation, this being indicated by the dotted lines in Figure 1.

I wish to thank Academician N. N. Semenov, K. I. Shchelkin, Corresponding Member, Acad. Sci. USSR, and Professor A. F. Belyaev for their interest in this work and for valuable suggestions.

LITERATURE CITED

[1] V. N. Kondrat'ev, The Kinetics of Gaseous Chemical Reactions (in Russian), Acad. Sci. USSR, Press, 1958, page 240.

[2] S. Z. Roginskii and L. M. Sapozhnikov, J. Phys. Chem., 2, 80 (1931) [USSR], S. Z. Roginskii, Zs.phys. Sowjet 1,640 (1932); S. Z. Roginskii, J. Phys. Chem., 3, 419 (1932) [USSR].

[3] A. Ya. Apin, O. M. Todes and Yu. B. Khariton, J. Phys. Chem., 8, 866 (1936) [USSR].

[4] K. K. Andreev, The Thermal Decomposition and Combustion of Explosives (in Russian), 1957, page 102.

[5] N. N. Semenov, Chain Reactions (in Russian), Leningrad, 1934.

[6] O. M. Todes, J. Phys. Chem., 13, 7, 868 (1939) [USSR]; O. M. Todes, Melent'ev, J. Phys. Chem., 13, 2, 1954 (1939) [USSR].

[7] N. N. Semenov, Bull. Acad. Sci. USSR, Div. Chem. Sci., No.5 (1953) [USSR].*

[8] A. Ya. Apin, Collected Papers on the Theory of Explosives (in Russian), Moscow, 1940, page 106.

[9] H. Henkin and R. McGill, Ind. and Eng. Chem., 44, No.6, 1391 (1952).

[10] R. C. Farmer, J. Chem. Soc., 117, 1432 (1920).

*Original Russian pagination. See C. B. translation.

[11] A. Robertson, Trans, Farad. Soc., 44, 677 (1948).

[12] M. A. Cook and T. Abegg, Ind. and Eng. Chem., 48, No.6, 1090 (1956).

[13] K. K. Andreev, Collected Papers on the Theory of Explosives (in Russian), Moscow, 1940, page 134.

[14] A. Lukin and S. Roginsky, Acta phisico-chimica URSS, 2, 385 (1935).

[15] M. V. Vol'kenshtein, M. A. El'yashevich and B. M. Stepanov, Molecular Vibrations (in Russian), 2, Moscow-Leningrad, 1949; Kohlrausch, Raman Spectra, Foreign Lit. Press, 1952 [Russian transl.].

[16] Yu. B. Khariton and K. K. Andreev, Collected Papers on Explosives, vol. 2, Moscow, 1935 [in Russian].

[17] C. N. Hinshelwood, J. Chem. Soc., No. 119/120, 721 (1921).

[18] A. A. Solonina, The Technology of Explosives (in Russian), 5, 71 (1925).

[19] O. Turek, Chimie et Industrie, 26, 781 (1931); S. Z. Roginskii and K. K. Andreev, J. chim. phis., 30, 487 (1933).

[20] A. D. Ioffe, Proc. Roy. Soc. A, 208, 188 (1951).

[21] K. K. Andreev, Collected Papers on the Theory of Explosives (in Russian), Moscow, 1940, page 134.

[22] S. Z. Roginskii and A. M. Magid, J. Phys. Chem., 2, 263 (1931).

[23] A. Robertson, Trans. Farad. Soc., 44, 977 (1948).

Received May 25, 1959.

A STUDY OF GRAFT POLYMERIZATION IN IRRADIATED TEFLON

Z. A. Sinitsyna, Yu. D. Tsvetkov, Kh. S. Bagdasar'yan
and V. V. Voevodskii, Corresponding Member, Acad. Sci., USSR

The Institute of Chemical Physics of the Academy of Sciences of the USSR
and The L. Ya. Karpov Institute of Physical Chemistry

New polymeric substances can be formed by irradiational graft polymerization, polymer molecules being grafted onto radicals in the framework of the basic polymer under the action of radiation. There are several variants of this kind of polymerization. It is obvious that the greatest practical and theoretical interest attaches to the case in which the polymer is irradiated in the absence of a monomer and graft polymerization proceeds as a subsequent dark reaction. We know of only one paper in which this type of graft polymerization has been studied for the case of polyethylene [1].

Earlier work with electron paramagnetic resonance (EPR) in the Institute of Chemical Physics has shown [2] that long-lived radicals are formed in the γ-ray irradiation of teflon in vacuum at low temperatures. The oxygen of the air converts these into peroxide radicals of the type $-CF_2-\underset{\displaystyle O-O\cdot}{\underset{|}{CF}}-CF_2-$, and these, in turn, can be held at room temperature for several months.

The present communication will present certain data on the graft polymerization of methylmethacrylate on films of this same material and will describe the results of an EPR study of these films.

Teflon films, 20-100 μ in thickness, were subjected to γ-irradiation in vacuum at room temperature. The dose strength was varied from 1 to 40 Mrad. The irradiated films were held in air at room temperature and then loaded into a dilatometer with a ground capillary. This dilatometer was filled with methylmethacrylate under vacuum. The dilatometer volume was 5 ml and the charge of teflon, 0.20 g in each case. Graft polymerization was carried out at 50°. The degree of polymerization was allowed to reach a definite value which was usually less than 15%, following which the homopolymer dissolved in the monomer was separated out with chloroform, the teflon film carefully treated with chloroform, and the homopolymer precipitated with methyl alcohol. The homopolymer and the teflon film were then brought to constant weight. The mean length, P, of the polymer chain in the homopolymer, was determined from viscosity measurements by using the equation [3]:

$$P = 4{,}15\,(100\,[\eta])^{1.25}, \qquad (1)$$

in which $[\eta]$ is expressed in deciliters/g. Equation (1) is applicable to the nonfractionated polymers resulting from chain extension or disproportionation. Results from the graft polymerization in the irradiation of teflon are shown in Table 1. The curves of Figure 1 cover the polymerization of methylmethacrylate on the irradiated teflon. The following conclusion can be drawn from Table 1 and Figure 1. Graft polymerization is accompanied by a simultaneous homopolymerization which clearly results from chain elongation through the monomer molecules.

The over-all rate of polymerization (homo- plus graft) remains constant as the dose is varied from 1 to 7 Mrad. The kinetic curves at 40 Mrad are characterized by a high initial rate with a subsequent rapid diminution of the velocity. The total rate of polymerization increases with increasing dose and diminishes as the interval

between irradiation and polymerization is increased. Variation of the film depth, i.e., the film surface area at fixed teflon charge, is without effect on the total rate of polymerization. From this,it follows that the rate of polymerization is not determined by the diffusion of the monomer into the teflon film.

The molecular weight of the homopolymer remains constant despite the variation in the total rate of polymerization, its value being the maximum fixed by chain extension through the monomer molecules for ordinary polymerization at the temperature in question.

The teflon film remains insoluble in chloroform even after 240% of methylmethacrylate by weight has been grafted to it. X-ray studies of the teflon film after methylmethacrylate grafting show that the crystallinity has diminished throughout the film and not merely on the surface. There is no observable decrease in the x-ray scattering maxima from a mere superposition of a methylmethacrylate film of requisite thickness onto the teflon film. *

TABLE 1

The Polymerization of Methylmethacrylate on Irradiated Teflon (Monomer concentration, 9.08 mole/liter; Volume of dilatometer, 5 cm^3; Teflon charge, 0.20 g)

Exp. No.	Film thickness, μ	Radiation dose, Mrad	Holding time, days	Ratio of weight of graft polymer to wt. of teflon	Ratio of wt. of homopolymer to wt. of graft polymer	Initial rate of polymerization, $\frac{mole}{liter \cdot sec} \cdot 10^6$	P
1	20	40	2	1,63	1,52	74,00	—
2	100	40	2	2,42	0,15	61,00	—
3	100	7	6	—	—	29,00	—
4	100	7	6	1,18	1,46	29,00	24500
5	20	2	1,5	1,80	0,90	31,50	24750
6	100	2	1,5	1,00	2,20	27,60	26800
7	60	2	9	—	—	14,20	—
8	100	2	9	0,91	1,70	12,60	24600
9	60	1	4	0,30	4,70	22,80	24500
10	100	1	4	0,24	5,00	20,20	24480

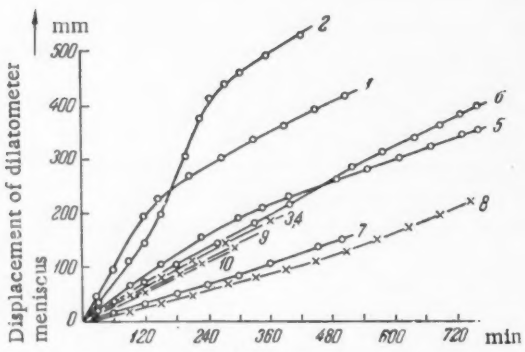

Fig.1. Curves for the polymerization of methylmethacrylate on irradiated teflon. The numbers on the curves designate the experiment numbers in Table 1.

Interesting results were obtained from an EPR study of graft polymerization on irradiated teflon films. These experiments were carried out in a cylindrical dilatometer, 0.35 cm in internal diameter and 0.7 ml in volume. The teflon films (0.135 g) were introduced into the lower portion of the dilatometer (1.5 cm) and the latter then filled under vacuum with methylmethacrylate in the usual manner. Polymerization was carried out in a thermostat at 70°. The dilatometer was periodically removed from the thermostat, quickly cooled to room temperature, and the EPR spectrum of the teflon film then measured directly in the dilatometer. Figure 2a shows the relation between I/I_0 and the time of polymerization, I and I_0 being, respectively, the intensity of the absorption line for the peroxide radical before polymerization and at the time t. Curve a follows the equation for a reaction of the first order with a constant of $2 \cdot 10^{-2} \cdot \cdot sec^{-1}$.

*The authors express their deep thanks to B. I. Zverev for carrying out these studies.

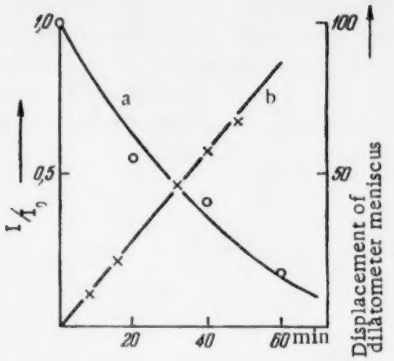

Fig. 2. The relation between I/I_0, the time of polymerization (a), and the variation of the total rate of polymerization (b).

Fig. 3. EPR spectra obtained during polymerization: a) lines of the peroxide radical; b) a portion of the spectrum of the polymethylmethacrylate radical.

The curve of Figure 2b shows the variation of the total rate of polymerization. This figure indicates that the total rate of polymerization is scarcely affected by a decrease in concentration of the peroxide radical of almost 80%. The spectrum of a second radical is gradually intensified as the intensity of the absorption lines of the peroxide radical diminish (Fig. 3). The exact analysis of this new spectrum is difficult because it is partially covered by the spectrum of the peroxide radical. The splitting of the observed components and the intensity ratios clearly correspond to the polymethylmethacrylate radical, whose spectrum is well known from the literature (see, for example, [4]).

Subsequent calculations have shown that it is not only the polymethylmethacrylate radicals which are grafted onto the initial polymer that have an extended life under the conditions of our experiments, but that the same is also true of the "free" polymethylmethacrylate radicals which are responsible for the formation of the homopolymer. The value of P for the homopolymer is independent of the total rate and equal to the maximum of 25,000, so that the rate of second-power chain rupture, $k_0 n^2$, must be much less than the rate of chain extension through the monomer molecules, $k_{max} nM$ (n is the concentration of the polymer radicals and M is the concentration of the monomer), i.e.,

$$\frac{k_{max} nM}{k_0 n^2} \gg 1. \qquad (2)$$

If it is supposed that homopolymerization proceeds throughout the entire volume of the dilatometer, it will then be possible to express the inequality of (2) as

$$\frac{k_{max}}{k_p} \frac{k_p^2}{k_0} \frac{M^2}{V} \geqslant 1,$$

k_p being the rate constant for chain growth and V, the rate of homopolymerization. A fraction of the order of unity is obtained on introducing numerical values of the constants $\frac{k_p}{k_{max}} = 25\,000$ and $\frac{k_p}{k_0^{1/2}} \approx 0.1$ and the rates of homopolymerization which are given in Table 1, a fact which is in contradiction to the inequality of (2). Thus it is clear that homopolymerization also proceeds only within the teflon film where the constant k_0 is quite low as a result of the gel effect.

It has been shown earlier [2] that reversible cleavage of the oxygen molecule with the formation of radicals of the type $\cdot R$.

$$-CF_2-\dot{C}F-CF_2-$$

occurs during vacuum heating of teflon containing peroxide radicals. Our experiments have proven that irradiated teflon which has been held in air and then heated in high vacuum for two hours at 190° will not induce the polymerization of methylmethacrylate. It is a curious fact that homopolymerization will proceed under these same conditions but at a diminished rate. It is possible that this is to be explained in terms of a polar effect arising from the presence of the fluorine atoms which would make it easier for a $\cdot R$. radical to tear a hydrogen atom from the monomer molecule than to combine at a double bond

$$R\cdot + CH_2 = \overset{CH_3}{\overset{|}{C}} - COCH_3 \rightarrow RH + CH_2 = \overset{\dot{C}H_2}{\overset{|}{C}} - COCH_3.$$

LITERATURE CITED

[1] D. Ballantine, A. Glines, G. Adler and D. Metz, J. polymer Sci., 34, 419 (1959).

[2] Yu. D. Tsvetkov, N. N. Bubnov, M. A. Makul'skii, Yu. S. Lazurkin and V. V. Voevodskii, Proc. Acad. Sci. USSR, 122, 1053 (1958).*

[3] N. Furman and R. Mesrobian, J. Am. Chem. Soc., 76, 3281 (1954).

[4] K. J. Abraham, H. W. Melville, D. W. Overnall and D. H. Whiffen, Trans. Farad. Soc., 54, 1133 (1958).

Received July 28, 1959.

*Original Russian pagination. See C. B. translation.

THE RELATION BETWEEN THE KINETIC CONSTANTS AND THE RATE OF FLAMELESS COMBUSTION OF SMOKELESS POWDER

A. F. Belyaev

The Institute of Chemical Physics of the Academy of Sciences of the USSR

(Presented by Academician B. N. Kondrat'ev July 9, 1959)

A number of studies [1-4] have shown that the rate of combustion of powders and explosives at atmospheric pressure and above is fixed by a reaction in the gaseous phase, where most of the evolution of heat takes place. The volatile explosives, including most of the commercial pulverizing explosives, form this gaseous phase by volatilization [1,2]. The nonvolatile smokeless powders form this phase by gasification [3], or dispersion [4], producing a smoke which burns and thereby sets free the major portion of the heat which is liberated in the reaction. The rate of reaction in the gas phase, or smoke, increases as the pressure rises and thus is greatest at the medium and high pressures, while the flow of heat out of the reaction zone of this gas accounts for the decomposition or volatilization of the condensed phase. Thus the reaction in the gas phase or smoke fixes the observed rate of "disappearance" of the condensed phase (its rate of volatilization, gasification, and dispersion) at elevated pressures.

It is now known from the work of P. F. Pokhil [4] that there are definite conditions under which combustion is propagated by the reaction in the condensed phase alone. The pressure can be reduced to such a value that a volatile explosive will cease to burn. Flameless combustion will take place in smokeless powders and other substances if this pressure reduction is carried far enough.

Powder at 2 mm of Hg pressure and less will burn without any sort of flame, the powder seeming to "melt" at a rate which is much less than the rate of flamed combustion at atmospheric pressure. Pokhil has proven convincingly that this flameless combustion results from a reaction in the condensed phase which leads to dispersion.

At one time the present author [2] applied the gaseous heat-transfer theory of Ya. B. Zel'dovich and D. A. Frank-Kamenetskii [5] to the combustion of evaporating nitroglycol, in which the reaction is known to take place in the gas phase. It was shown that this theory generally gives the correct order of magnitude for the rate of flame propagation in nitroglycol, as had also been noted by N. N. Semenov [6].

The weak point in this work was the assumption that the basic reaction was monomolecular and nevertheless dependent on the number of collisions [2]. This basic reaction should really be considered as bimolecular, as the author has done in [7]. The present note will consider the possibility of applying the Zel'dovich Theory to the case of flameless combustion where the only reaction is in the condensed phase. Zel'dovich [3] has given an expression, based on the general theory, for the rate of propagation of a thermal wave arising from isothermal reaction in a condensed phase

$$u = \frac{1}{\rho c_p (T_s - T_0)} \sqrt{2\eta Q \rho B l^{-E/RT_s} \frac{RT_s^2}{E}} \frac{\text{cm}}{\text{sec}}. \qquad (1)$$

Here, u is the rate of combustion, i.e., the rate of propagation of the thermal wave; ρ is the density of the

material; c_p is the specific heat; T_s is the temperature on the "burning" surface, i.e., the maximum temperature of the condensed phase; T_0 is the initial temperature of this substance; η is its coefficient of thermal conductivity; B is the frequency factor in the expression for the velocity constant; E is the energy of activation, and R is the molar gas constant.

The task which Zel'dovich set himself in deriving Equation (1) was that of obtaining an expression for the rate of displacement of the surface of violent effervescence arising from a volatile explosive as a result of reaction in the condensed phase, and determining the conditions required for such effervescence. It is clear, however, that this equation can be applied directly to the flameless combustion of powder in vacuum, where reaction in the condensed phase leads to propagation of the process and dispersion.

The attempt will now be made to carry out such a calculation for pyroxylin powder, values being available for all the requisite constants of this substance. Values of ρ, c_p, and η have been known for some time. There is considerable difference among the B and E values which are given by various authors. These quantities occur in products of the form $Be^{-E/RT}$, and the variation of such product is much less than that of either B or E considered separately. Use will be made of the data of Andreev and Samsonov [8] on the vacuum decomposition of pyroxylin. Values of T_s and Q for the flameless combustion of pyroxylin powder have been obtained by Pokhil [4]. Leipunskii [9] determined T_s somewhat earlier by an indirect method. The various numerical values are: $\rho = 1.6$ g/cm^3; $c_p = 0.29$ cal/deg · g; $\eta = 5.5 \cdot 10^{-4}$ cal/cm · sec · deg; $Q = 80$ cal/g; $B = 10^{17}$ sec^{-1}; $E = 44600$ cal/mole; $T_s = 573$°K (~ 300°C); and $T_0 = 363$°K. (Pokhil was able to observe stable flameless combustion of pyroxylin powder in vacuum only when the temperature was 90°C, or higher). These values give $u = 3.4 \cdot 10^{-2}$ cm/sec when introduced into Equation (1). The experimental value of Pokhil for the rate of flameless combustion at 90°C was $8 \cdot 10^{-2}$ cm/sec when introduced into Equation (1). The experimental value of Pokhil for the rate of flameless combustion at 90°C was $8 \cdot 10^{-2}$ cm/sec. Such agreement can be considered as good, although the rate of flameless combustion calculated from the Zel'dovich Equation is about one-half of the experimental value.

The divergence here could be accounted for fully by the possible errors involved in the determination of B and E. It is clear, moreover, that Zel'dovich has based his equation on the simplest monomolecular law. The final result would certainly be affected if the kinetics are actually more complex. A better agreement between experiment and theory could therefore not be expected in principle. We will now return to the relation between the rate of combustion, the pressure, and the initial temperature. The conditions prevailing in practice are such that the rate of combustion increases with the pressure and it is on this fact that internal ballistics are based. Pokhil [4] has shown that the rate of flameless combustion of powder is independent of the pressure over the interval from 2 to 30 mm of Hg, a result which is consistent with the lack of pressure-dependent terms in Equation (1). It is only at a pressure of 70 mm of Hg that the rate of combustion begins to increase. A visible flame appears at still lower pressures, but weakly and at a considerable distance from the powder surface. This flame becomes more clear as the pressure is raised and approaches the surface. It is obvious that the decomposition of the condensed phase at 70 mm of Hg is accelerated by the thermal flow out of the flame zone. Raising pressure brings about a further increase in the rate of combustion because of acceleration of the gas phase or smoke reaction with a resultant increase in the thermal flow out of the flame zone.

Pokhil claims [4] that the rate of flameless combustion increases rapidly with a rise in the initial temperature, going from 0.08 cm/sec at 90° to 0.14 cm/sec at 140°C to increase by a factor of 1.75. This increase in the rate of combustion can be accounted for by the Zel'dovich Equation if T_s is assumed to increase by 10°, going to 583°K when the initial temperature is raised from 90 to 140°. This assumption is in complete qualitative and quantitative agreement with the conclusions of Leipunskii [9] as to the increase of T_s and its relation to T_0.

Thus the Zel'dovich Equation (1) gives a good description of the flameless combustion of smokeless powder. Through this equation it is possible to obtain a correct value for the rate of combustion, as well as certain fundamental relations between the rate, the pressure, and the initial temperature. The following point should be emphasized here. There is, of course, no sense to calculating the rate of combustion through Equation (1). This rate is a quantity which can be measured precisely. The inverse problem is of great significance, however. Once the rate of combustion has been measured, and its relation to the pressure and the initial temperature have been experimentally established, it is then possible to draw important conclusions as to the nature of this combustion from Equation (1), deciding whether the gas phase is involved in this reaction and obtaining exact values for parameters such as E and T_s, which are difficult to measure.

The present author at one time studied the flameless combustion of fulminating powder in vacuum and determined the combustion rate (0.4 cm/sec) [10]. Pokhil has measured T_s for the flameless combustion of this substance. The value of the rate of flameless combustion, u, of fulminating powder which is obtained from Equation (1) by using the data on the kinetic constants and setting $T_s = 320°$ proves to be only a fraction of the experimentally determined value. The agreement here is somewhat worse than in the case of pyroxylin powder but, on the other hand, the values which are available for the kinetic constants (E, B, as well as T_s) of fulminating powder are less trustworthy. It can be assumed in the final analysis that the rate of flameless combustion of fulminating powder is also completely determined by reaction in the condensed phase, just as has been postulated by Pokhil [4].

A similar analysis for potassium picrate (a substance for which the value of T_s is not known) shows that T_s must be greater than 500° if the rate of combustion in vacuum is to be fixed by a simple monomolecular reaction in the condensed phase. If direct measurements should give a lower value of T_s the indication would be that the kinetics are of a more complex type.

The usual working conditions are such that the basic reaction proceeds in the gas or smoke phase, and this is especially true of the conditions which prevail in powder rocket motors. Here, the decomposition of the condensed phase arises principally from thermal flow out of the zone of the flame, or, more exactly, out of the zone of gas or smoke phase reaction. The study of the decomposition of the condensed phase has great interest, nonetheless; the decomposition begins in the condensed phase, which functions as a "supply" of products for the basic zone, in which the combustion rate is determined. The above examples indicate that the Zel'dovich Theory is indispensable to a study of the decomposition in the condensed phase.

LITERATURE CITED

[1] A. F. Belyaev, J. Phys. Chem., 12, 93 (1938) [USSR].

[2] A. F. Belyaev, J. Phys. Chem., 14, 1009 (1940) [USSR].

[3] Ya. B. Zel'dovich, J. Exp. Theo. Phys., 12, 498 (1942) [USSR].

[4] P. F. Pokhil, The Physics of Explosives, Collection No.2, Acad. Sci. USSR, Press, 1953, page 181 [in Russian].

[5] Ya. B. Zel'dovich and D. A. Frank-Kamenetskii, J. Phys. Chem., 12, 100 (1938) [USSR].

[6] N. N. Semenov, Prog. Phys. Sci., 23, 251 (1940); 24, 434 (1940) [USSR].

[7] A. F. Belyaev, Doctoral Dissertation, Moscow, 1946 [in Russian].

[8] K. K. Andreev and B. S. Samsonov, Proc. Acad. Sci. USSR, 114, 815 (1957). *

[9] Z. I. Aristova and O. I. Leipunskii, J. Phys. Chem., 20, 1391 (1946) [USSR].

[10] A. F. Belyaev and A. E. Belyaeva, J. Phys. Chem., 20, 1381 (1946) [USSR].

Received June 27, 1959.

*Original Russian pagination. See C. B. translation.

THE MECHANISM OF HYDROGEN PEROXIDE FORMATION IN THE CORROSION OF METALS

T. M. Abramova, I. L. Gankina, and A. S. Fomenko
L. V. Pisarzhevskii Institute of Physical Chemistry of the Acad. Sci. Ukr. SSR
(Presented by Academician A. N. Frumkin, July 13, 1959)

The formation of hydrogen peroxide during the reaction of metals with oxygen and water was first observed by Schonbein [1] in the middle of the 19th century and was later confirmed by several workers [2-8].

There is, however, no agreement as to the mechanism for the formation of hydrogen peroxide under these conditions. Some workers [1, 2] have proposed that the oxygen from the air, as well as that from the water, participates in the formation of H_2O_2. Others [3, 6, 9] claim that only the oxygen absorbed from the air is involved in the formation of H_2O_2 during corrosion. In recent years several workers [10] have demonstrated that hydrogen peroxide is also formed in the cathodic reduction of oxygen, with the following equations representing the overall process:

$$\left.\begin{array}{ll} \text{Acid medium} & O_2 \xrightarrow{+2e+2H^+} H_2O_2 \xrightarrow{+2e+2H^+} 2H_2O \\ \text{Basic medium} & O_2 \xrightarrow{+2e+H_2O} HO_2^- + OH^- \xrightarrow{+2e+H_2O} 4OH^- \end{array}\right\} \quad (I)$$

Since the atmospheric corrosion of metals is accompanied by oxygen-induced depolarization, then, according to sequence (I), H_2O_2 should be formed as an intermediate in the corrosion process by the reduction of oxygen on the cathodic portions of the surface, and its isotopic composition should correspond to that of the oxygen gas.

To verify and possibly confirm this mechanism for the formation of hydrogen peroxide as an intermediate in the atmospheric corrosion of metals we used a radioactive tracer technique. Due to the fact that in the course of metal corrosion both the hydrogen peroxide introduced into the corrosive medium and that formed during the corrosion are rapidly decomposed we used an isotopic dilution technique to identify all the hydrogen peroxide formed as an intermediate. The labeling was done with heavy oxygen O^{18}. The latter was either introduced initially into the corrosive medium in the form of labeled hydrogen peroxide, $H_2O_2^{18}$, or by bubbling oxygen gas through the solution as the metal was being corroded. If the reaction sequence (I) applies to the corrosion process, then the isotopic composition of the H_2O_2 initially added to the corrosive medium should undergo a change in such a manner as to approach the composition of the gas phase. And in fact we discovered that such an isotopic composition change did accompany the corrosion of zinc, magnesium, tin, aluminum, and cadmium in an aqueous solution of hydrogen peroxide; in these experiments oxygen was bubbled through solutions in which shavings of the respective metals were submerged.

During the corrosion of all of the above-described metals a very rapid decomposition of the hydrogen peroxide in solution was observed. In the case of zinc and cadmium from 10 to 20% of the initial peroxide was preserved for long periods of time (24 hours or more) in the form of water-insoluble peroxides mixed with other metal corrosion products. According to the literature data [11], the peroxides of Zn and Cd formed at the hydrogen peroxide concentrations used by us should have the general composition $MeO_2 \cdot n\,H_2O$, where n may vary from 0.4 to 2.

After completing the experiments, which lasted from 1 to 24 hours, depending on the corrosion rate of a

particular metal, the final concentration of the hydrogen peroxide and its isotopic composition in the corrosive medium were determined. In the case of zinc and cadmium, dilute (1:8) H_2SO_4 was added to the solution, since the acid dissolves the peroxides of these metals. The peroxide thus liberated went into solution, where its content was measured as the percent of that initially present and its isotopic composition determined. In experiments on magnesium, aluminum, and tin, hydrogen peroxide was determined directly in the corrosive medium after the latter was separated from the metal shavings and other corrosion products. The initial and final hydrogen peroxide concentration were determined by permanganate titration. The isotopic composition of hydrogen peroxide was determined mass-spectroscopically by using the oxygen liberated from the peroxide decomposition by potassium permanganate in acidic solution (the ratio of mass 34/32 was used).* As is well known, normally there is no oxygen exchange between hydrogen peroxide and water [12], and when the peroxide is decomposed by potassium permanganate all the oxygen comes from the peroxide [13]. The experimentally determined changes in the isotopic composition of hydrogen peroxide, which were produced by the corrosion of zinc, magnesium, aluminum, cadmium, and tin, are presented in Table 1. The experiments were carried out in complete darkness at room temperature.

TABLE 1

Change in the Isotopic Composition of Hydrogen Peroxide Caused by the Corrosion of Zinc, Magnesium, Cadmium, Aluminum, and Tin

Metal	Length of expt., hrs	H_2O_2 conc., %		Isot. compn., at.% (including natural compn.)			Change in the isot. compn. of H_2O_2, % of the initial
		Initial	Final	H_2O		O_2	
				Initial	Final		
Zn	3	1,49	0,01	1,20	1,07	0,20*	11
Zn	3	1,02	0,01	0,20*	0,27	1,01	35
Mg	2	3,01	1,03	1,14	0,93	0,20*	18
Mg	5	3,38	1,22	0,20	0,28	1,17	40
Cd	24	0,50	0,01	1,17	0,98	0,20*	16
Cd	24	0,65	0,01	0,20*	0,25	1,09	25
Al	24	0,54	0,03	1,18	0,83	0,20*	29
Al	24	0,54	0,03	1,18	0,88	0,20*	29
Sn**	4	0,41	0,01	1,01	1,05	0,20*	13
Sn**	4	0,41	0,02	0,20*	0,25	1,09	25

*Natural abundance.

**Experiments were carried out in the presence of NaCl (3% solution).

It is quite clear in Table 1 that an appreciable change in the isotopic composition of the initial peroxide concentration is observed after the corrosion of all of the examined metals. In experiments with $H_2O_2^{18} + O_2^{16}$ the O^{18} content in the peroxide decreases, while in those with $H_2O_2^{16} + O_2^{18}$ it increases. This change is fully compatible with the theory that the hydrogen peroxide is formed as an intermediate in the corrosion through the reduction of oxygen gas, for example, as shown in the reaction sequence (I).

The error in the mass-spectroscopic determination of the isotopic composition of oxygen could not have exceeded about 3%. But, as is shown in Table 1, the observed changes in the isotopic composition of hydrogen peroxide exceed the limit of probable error in the mass-spectroscopic measurements.

In the case of zinc and aluminum we also calculated the ratio between the amount of corroded metal and the amount of hydrogen peroxide formed. This was done by comparing the amount of metal converted into corrosion products (determined analytically) with the calculated amount of hydrogen peroxide formed on the cathodic portions of the surface by the reduction of oxygen. The calculations were based on assumption of the following reaction schemes for the corrosion of these metals:

*The authors wish to thank Engineer I. M. Protas for performing the mass-spectroscopic analyses.

$$2Zn + O_2 + 2H_2O = 2Zn(OH)_2 \quad \text{(II)}$$

$$4Al + 3O_2 + 6H_2O = 4Al(OH)_3 \quad \text{(III)}$$

Knowing the initial concentration and isotopic composition of $H_2O_2^{18}$, and having calculated (from the amount of metal corroded) the amount of $H_2O_2^{16}$ which should have formed during the corrosion, we computed the expected final isotopic composition of hydrogen peroxide. At the same time, we observed that all the oxygen gas consumed in the corrosion as shown in Reactions (II) and (III) was used to form the peroxide as shown in Reaction (I). As an example we will present the calculated final isotopic composition of hydrogen peroxide in one of the experiments with zinc: we used a 4.5 g zinc shaving and 9.9 cm^3 of $H_2O_2^{18}$ with an initial activity concentration of 2.5%. After O_2^{16} was bubbled through the solution for 4 hours, 0.081 g of zinc were corroded and 0.02 g of O_2^{16} were absorbed [as shown in Reaction (II)]. The initial O_2^{18} content in the hydrogen peroxide was 0.237 g, the final, 0.0047 g. The amount of O_2^{16} (0.02 g) absorbed in the corrosion reaction constituted 16% of the time average (during the reaction) of the oxygen present in the $H_2O_2^{18}$ which took part in the experiment. Since the initial O^{18} content in the peroxide was 1.22 at .%, its final content should in this case have been 1.02%, namely, 16% lower. The experimental value was 1.15 at .%, indicating an ~13% accuracy in the calculated value. In other cases the calculated isotopic compositions of the final hydrogen peroxide deviated from the experimental by 5-20%. This difference seems to be connected with the fact that some of the newly formed hydrogen peroxide is catalytically decomposed by direct contact with the metal surface before it has a chance to change the isotopic composition of the initial peroxide. Another possible reason for the observed discrepancies may be that the oxygen which is formed in the catalytic decomposition of hydrogen peroxide, and which has the same isotopic composition as the corrosive medium, also participates to some extent in the corrosion. The H_2O_2 freshly formed from this oxygen would not alter the isotopic composition of the total peroxide present in the corrosive medium.

The above-presented observed and calculated values for the final isotopic composition of hydrogen peroxide indicate that the formation of H_2O_2 can not be just a side reaction in the corrosion process but must constitute one of its main steps. Attempts to stabilize hydrogen peroxide in corrosion by means of addition oxyquinoline, sodium pyrophosphate, soduim silicate, etc., to the solution did not give the desired results.

Attempts to stabilize hydrogen peroxide in corrosion by adding oxyquinoline, sodium pyrophosphate, sodium silicate, etc., to the solution did not give the desired results.

The literature data, as well as our control experiments, indicate that the change in the isotopic composition observed during corrosion can not result from some side reaction involving oxygen exchange in the system: $H_2O_2 + O_2 + H_2O + Me(OH)_n$, in the presence of metal shavings. Hart and co-workers [14] found that in neutral or acidic media no oxygen exchange is observed between hydrogen peroxide and oxygen gas. That no exchange occurs between water and oxygen in the presence of oxides and hydroxides was shown by Mackenzie et al. [15]. Only slight exchange was detected between hydrogen peroxide and oxygen at pH = 11.75 under the effect of γ-radiation [14]; ultraviolet radiation had the same effect on the system: $ZnO + H_2O_2 + H_2O + O_2$ [16]. We found no oxygen exchange in the systems: $H_2O^{18} + H_2O^{16}$ and $H_2O^{16} + H_2O_2^{18}$, in the presence of Zn, Cd, Al, Mg, and Sn shavings under conditions corresponding to the experimental; oxygen gas had no effect on these systems either. Nor was any exchange observed in the systems: $Al(OH)_3 + H_2O_2$ and $ZnO_2 \cdot nH_2O + H_2O_2^{18}$. Consequently our experimental data on the change in the isotopic composition of hydrogen peroxide were not affected by any extraneous exchange of oxygen and are fully compatible with the proposed mechanism [Reaction (I)] for the formation of hydrogen peroxide as an intermediate in the corrosion of metals by water and oxygen.

LITERATURE CITED

[1] C. F. Schonbein, J. Prakt. Chem., 77, 138 (1859); W. Machu, Das Wasserstroffperoxyd und die Perferbindungen, Wien, 1951.

[2] W. R. Dunstan, H. A. D. Jowett, and K. Goulding, J. Chem. Soc., 87, 1548 (1905).

[3] M. Traube, Ber., 15, 2334 (1882).

[4] A. N. Bakh, J. Russ. Phys.-Chem. Soc. 29, 373 (1897).

[5] J. R. Churchill, Trans. Electrochem. Soc., 76, 341 (1939).

[6] J. Grunberg, Proc. Phys. Soc., 66, 399B, 153 (1953).

[7] I. L. Roikh, Proc. Acad. Sci. 108, 1102 (1956).*

[8] V. Seifert and K. Smrček, Hutnické listy,10, 595 (1955).

[9] A. N. Frumkin, Progr. Chem. 18, 9 (1949).

[10] A. N. Frumkin, V. S. Bagotskii, et al., The Kinetics of Electrode Processes, Moscow, 1952; A. N. Krasil'shchikov, Trans. Confer. on Electrochem., Izd.An SSSR, 1953, p. 71; V. S. Bagotskii, P. Ya. Yablokova, ibid, p. 57.

[11] S. Z. Makarov, L. V. Ladeinova, Bull. Acad. Sci. USSR, Div. Chem. Sci. 1957, No.1, 3; 1957, No.2, 139; I. S. Teletov, J. Russ, Phys.-Chem. Soc. 43, 131 (1911).

[12] C. A. Bunton, D. R. Llewellin, Research, 5, 142 (1952).

[13] J. Halperin, H. Taube, J. Am. Chem. Soc., 72, 3319 (1950).

[14] O. L. Forchheimer and H. Taube, J. Am. Chem. Soc., 74, 3705 (1952); 76, 2099 (1954).

[15] H. A. E. Mackenzie and A. M. Milner, J. S. Afric. Chem. Inst., 4, 79 (1951).

[16] M. Dole and D. P. Rudd et al., J. Chem. Phys., 20, 961 (1952).

Received July 13, 1959.

*Original Russian pagination. See C. B. translation.

THE TRANSPORT OF DISPERSED PARTICLES IN A GASEOUS STREAM DURING THE COMBUSTION OF POWDERS

N. N. Bakhman

Institute of Chemical Physics of the Academy of Sciences USSR

(Presented by Academician V. N. Kondrat'ev, July 9, 1959)

In several papers on the combustion of powders it was assumed that the partial dispersion of the original powder followed by a combustion of the dispersed particles in a gaseous stream constitute the principal steps in this process. At the same time it was occasionally assumed that the particles and the gas have equal velocities. Since there is no obvious reason why this should be so, it is interesting to examine the movement of particles near the charge surface.

When the combustion front passes the particles, which are at rest in the laboratory system of coordinates, they suddenly become exposed to a stream of gas. As the gas carries away some particles it is itself retarded. For particles of moderate dimensions the acceleration produced by the gaseous stream initially greatly exceeds the acceleration due to gravity, and hence the latter may be disregarded (as will become evident later), making the problem much simpler.

We will limit our study to the region where the particles are not reacting yet, and the gas and the solid particles streams are still distinct. We will first write the conservation laws.

The conservation of mass:

$$\rho_s u_s = (1-\beta) m_0 = (1-\beta) \rho_{s_0} u_{s_0}; \tag{1}$$

$$\rho_g [u_g - (1-\beta) u_{s_0}] = m_0 \beta; \tag{1'}$$

where $100(1-\beta)$ is percent dispersion; the subscripts g, s, and s_0 refer to the gas, the dispersed particles, and the initial solid, respectively; ρ_s is the mass of particles per unit volume of the stream; in (1') it was assumed that a part of the stream space is filled with particles.

For the average density of matter in the stream we will get:

$$\rho_{av} = \frac{(1-\beta) m_0}{u_s} + \frac{\beta m_0}{u_g}. \tag{1''}$$

The conservation of momentum:

$$p + \beta m_0 u_g + (1-\beta) m_0 u_s = p_0 + m_0 u_{s_0}. \tag{2}$$

The conservation of energy:

$$\beta m_0 \left(w_g + \frac{u_g^2}{2}\right) + (1-\beta) m_0 \left(w_s + \frac{u_s^2}{2}\right) - \lambda \frac{dT}{dx} = m_0 \left(w_{s_0} + \frac{u_{s_0}^2}{2}\right) - \lambda \frac{dT}{dx}\bigg|_{x=0}; \tag{3}$$

where $w_g = w'_g + \frac{\gamma p}{(\gamma-1)\rho_g}$; $w_s = w'_s + c_s(T_s - T_{s_0})$; $w_{s_0} - \beta w'_g - (1-\beta)w'_s =$ Q, the heat of sublimation.

The unknowns in this system of equations are ρ_g, u_g, p, and u_s. As far as w_s is concerned, it should be determined from the heat-exchange conditions, using the relationship $w_g = f(p, \rho_g)$; however, in two limiting cases w_s is known right away: for very small particles it can be assumed that

$$w_s = w'_g + c_s(T_g - T_0),$$

for very large particles that:

$$w_s \simeq w_{s_0}.$$

To determine the velocity of a particle u_s, we will use the following equation of motion (the density of particles is assumed to be ρ_{s0}):

$$\frac{4}{3}\pi r^3 \rho_{s_0} \frac{du_s}{dt} = \pi r^2 \xi \rho_g (u_g - u_s)^2, \tag{4}$$

where ξ is a coefficient determined by the particle shape and other properties; its value is approximately one.

The initial conditions are:

$$u_s = u_{s_0} \qquad x = 0 \quad \text{when } t = 0. \tag{5}$$

We thus get a closed system which can be solved by the method of successive approximations.

In a special case, where the degree of disperison is small and the value of $\lambda \cdot dT/dx$ changes very little within the limits of the examined zone, we can assume that ρ_g and u_g are approximately constant. Equation (4) can then be integrated directly. In a system describing the front we will find that the particle coordinate:

$$x = u_g t - \frac{4}{3}\frac{r}{\xi}\frac{\rho_{s_0}}{\rho_g}\ln\left[1 + \frac{3}{4}\frac{\xi}{r}\frac{\rho_g}{\rho_{s_0}}(u_g - u_{s_0})t\right]; \tag{6}$$

and that the particle velocity:

$$u_s = u_g - \frac{1}{\frac{1}{u_g - u_{s_0}} + \frac{3}{4}\frac{\xi}{r}\frac{\rho_g}{\rho_{s_0}}t}. \tag{7}$$

The solution obtained above enables us to estimate the orders of magnitude of the functions we are interested in. As an example, we will use the combustion of sulfur-free black powder at p = 1 atm. Taking: $\rho_{s0} = 1.65$, $^3/_4\,\xi \sim 1$; $\rho_g = p\mu/RT \sim 1 \cdot 46/82 \cdot 600 \sim 10^{-3}$ g/cm^3; $u_{s0} = 1.8$ mm/sec; $u_g \sim \rho_{s0} u_{s0}/\rho_g \sim 300$ cm/sec, we will get t_k, the time required to accelerate the particle to a velocity $u_s = ku_g$, and x_k, the distance traveled by the particle during that same time; the calculated results are presented in Table 1.

TABLE 1

r in μ	$k = 0,5$	$k = 0,9$	$k = 0,5$	$k = 0,9$
	t_k in sec		x_k in cm	
1	$5,5 \cdot 10^{-4}$	$5 \cdot 10^{-3}$	0,051	1,12
10	$5,5 \cdot 10^{-3}$	$5 \cdot 10^{-2}$	0,51	11,2
100	$5,5 \cdot 10^{-2}$	0,5	5,1	112

Our results indicate that the model in which the particle and the gas velocities are assumed equal within the combustion zone (which is of the order of several millimeters at p = 1 atm) is only applicable to particles equal to or smaller than 1μ. Otherwise, with particles ten microns in size or larger, one can assume that the particles form a stationary (in the laboratory system) lattice, which burn as the stream of the gas passes through it.

When the pressure is increased t_k and x_k become smaller. From Eq. (7) it follows that $t_k \sim \rho_{s_0} r \frac{1}{\rho_g u_g}$. Since for powders

$\rho_g u_g \sim p^n$, then $t_k \sim \frac{1}{p^n}$. When t_k is not too small one finds from Eq. (6) that $x_k \sim t_k \sim \frac{1}{p^n}$. But the width l of the examined precombustion zone shrinks with increasing pressure in the same manner:

$$l \sim \frac{\lambda_g}{c_{pg} \rho_g u_g} \sim \frac{1}{p^n},$$

so that conclusions presented for p = 1 atm are also valid at other pressures.

The average particle acceleration $a_{av} \sim k u_g / t_k$ for particles with a 1μ radius is ~ 270 g (at k = 0.5). In contrast, for particles with a 100μ radius $a_{av} \simeq g$, which provides additional evidence that such particles may be considered stationary within the combustion zone.

Received June 27, 1959

RECTIFICATION AT THE ELECTROLYTE – N-TYPE SEMICONDUCTOR CONTACT

Yu. A. Vdovich, B. M. Grafov, and V. A. Myamlin

Institute of Electrochemistry of the Academy of Sciences USSR

(Presented by Academician A. N. Frumkin, July 6, 1959)

The present and a preceding paper [1] are both devoted to the investigation of the boundary separating two phases, a semiconductor and an electrolyte. The problem is set up in the same fashion as before [1], with the difference, however, that holes are taken into consideration and the assumption is made that in an extrinsic N-type semiconductor the donor levels are completely ionized while the acceptor levels are completely filled up. The impurity levels are also presumed to be uniformly distributed throughout the semiconductor.

The electrochemistry of the present contact differs considerably from the electrochemistry involved in the anodic solutions of N-type germanium [2]. In the latter case the reaction also involved holes and was accompanied by the liberation of electrons. There was a P→N transition at the germanium electrode contact. The rectification produced by such P → N transitions is similar to that in solid rectifiers. One would naturally assume, however, that other types of reactions, involving only the electrons (or only the holes), are also possible on semiconductors. This type of an electrochemical reaction was observed by Yu. V. Pleskov and B. N. Kabanov [3].

For our calculations we will select a case where the contact reactions are of the type:

$$A^+ + e \rightleftarrows A \quad \text{or} \quad A^- \rightleftarrows A + e.$$

We will show that if the layer adjacent to the contact is deficient in both electrons and holes, at equilibrium, then there will arise in such a system a unique form of rectification which is not connected with a P→N transition. The following system of equations describe the semiconductor:

$$dz/dt = zy + \lambda(1 - B), \tag{1}$$

$$dP/dt = -Py - \frac{1}{k}\lambda B, \tag{2}$$

$$dy/dt = z - P - 1 + \nu, \tag{3}$$

$$-d\lambda B/dt = A(zP - b). \tag{4}$$

The symbols used in Equations (1) - (4) are the same as those used in paper [2], except that we have introduced in this case a dimensionless concentration of acceptor levels ν, while the current carried by the holes is denoted by λB.

We have applied the usual conditions at infinity:

$$dz/dt|_{t\to+\infty} = /dP\ dt|_{t\to+\infty} = dy/dt_{t\to+\infty} = d\lambda B/dt|_{t\to+\infty} = 0. \tag{5}$$

The selected type of electrochemical reaction (same as in paper [1]) imposes the following boundary conditions at the contact:

$$\lambda (1 - B^k) = \lambda_0 \left[\frac{z_k}{z_k^0} e^{-\alpha \Delta\psi'} - e^{\beta \Delta\psi'} \right], \quad \lambda B^k = 0. \tag{6}$$

The subscripts k, ∞, and 0 designate the values of these functions at the contact, at infinity, and at equilibrium ($\lambda = 0$) respectively; $\Delta\varphi'$ is the deviation of the potential drop within the Helmholtz double layer from the corresponding value at equilibrium, and is equal to $t_0 (y_k - y_k^0)$ [1].

Just as in paper [1], the electrolyte is located to the left of the contact, which is at $t = 0$; the current is considered positive if it flows from left to right, while the potential drop caused by a positive current is considered negative; the potential drop in the diffused portion of the double layer and the ohmic drop in the electrolyte are disregarded.

Combining Eqs. (1) and (2), substituting $z - P$ from Eq. (3), and integrating with respect to t from $+\infty$ to t, we get:

$$^1/_2 y^2 - {}^1/_2 y_\infty^2 = z + P - z_\infty - P_\infty - (1 - \nu)\psi + I_1,$$

where

$$\psi = \int_{+\infty}^{t} (y - y_\infty)\, dt, \qquad I_1 = -\lambda \frac{k+1}{k} \int_{+\infty}^{t} (B_\infty - B)\, dt.$$

The expression for I_1 will always appear in this form whenever the relationship between the various functions at infinity, imposed by the boundary conditions (5), are considered. ψ is a negative function since the field y increases as one goes from infinity to the contact, or theoretically speaking, z decreases during such a movement. Treating y and B as known functions in Equation (2) we get:

$$P = P_\infty e^{-\psi} + I_2,$$

where

$$I_2 = \int_{+\infty}^{t} \left(-P y_\infty - \frac{\lambda B}{k} \right) e^{\psi} dt.$$

Since the examined currents are extremely small ($|\lambda| \ll 1$), it turns out that whenever $-\psi \geq 1$, one can express y and P by the following equations:

$$^1/_2 y^2 = P_\infty e^{-\psi} - (1 - \nu)\psi, \quad P = P_\infty e^{-\psi}. \tag{7}$$

One can readily get a rough estimate of the neglected integrals I_1 and I_2. Only an electron current flows through the contact. Away from the contact some of the current is also carried by the holes. It is evident that the transition from a pure electron current at the contact to a mixed one away from the contact occurs at distances roughly equal to the diffusion length t_D. Keeping all this in mind we get:

$$|I_1| \leqslant |\lambda| b t_D \ll 1 \leqslant {}^1/_2 y^2, \quad |I_2| \leqslant P_\infty e^{-\psi} |\lambda| t_D \ll P_\infty e^{-\psi}.$$

It is convenient to introduce a function ψ^*

$$P_\infty e^{\psi^*} = (1 - \nu)\psi^*.$$

Then

$$^1/_2 y^2 = -(1 - \nu)\psi \quad \text{for} \quad -\psi < \psi^*; \qquad ^1/_2 y^2 = P_\infty e^{-\psi} \quad \text{for} \quad -\psi > \psi^*. \tag{8}$$

Treating y and B as known values in Equation (1) we get:

$$z_k = z_\infty e^{\psi_k} + e^{\psi_k} \int_{-\psi\sim 1}^{\psi_k} e^{-\psi} \frac{zy_\infty + \lambda(1-B)}{y - y_\infty} d\psi + I_3,$$

where

$$I_3 = e^{\psi_k} \int_{+\infty}^{t(-\psi\sim 1)} e^{-\psi} (zy_\infty + \lambda(1-B))\, dt.$$

The term zy_∞ in the first integral of Equation (9) can be neglected in comparison with the λ (1-B) term, since the terms have comparable magnitudes only at infinity. As the contact is approached, the electron density z decreases. The exponential coefficient makes the integral highly dependent on the upper limit, while an electron deficiency in the region adjacent to the contact sharply reduces the value of integrals containing zy_∞ terms. The function B can also be dropped, since it changes from zero at the contact to $B_\infty \sim b$ at infinity, while $b \ll 1$. If $-\psi_k < \psi^*$, the trimmed integral containing λ is integrated by parts just once. This integration gives a nonintegral function and another integral which can, however, be neglected since the integrated component exceeds it by a factor of $2(-\psi_k)$, where $-\psi_k \gg 1$.

The value of the integrated component depends primarily on the upper limit. Hence a poor choice of the lower limit will not affect the results of integration. Considering the small value of the examined current λ we can also neglect the integral I_3; the latter is estimated in the same way as I_1 and I_2. We will be left with:

$$z_k = z_\infty e^{\psi_k} + \frac{-\lambda}{\sqrt{2(-1+\nu)\psi_k}}. \tag{10}$$

If $-\psi_k > \psi^*$, the trimmed integral containing λ is split into two parts: one between the limits $(-\psi\sim 1, -\psi^*)$, another between the limits $(-\psi^*, \psi_k)$. When $|\psi_k + \psi^*| \ll 1$ the second integral can be disregarded. The retained first integral is then treated in the same fashion, as was the one above which yielded Equation (10). We will then get:

$$z_k = z_\infty e^{\psi_k} + \frac{-\lambda e^{\psi_k + \psi^*}}{\sqrt{2(1-\nu)\psi^*}}. \tag{11}$$

An examination of Equation (10) indicates that a flow of negative current rapidly reduces the first term in z_k and the second term assumes a leading role. A state in which both terms contribute equally to z_k will be denoted by the subscript s. Let us assume that $-\psi_{ks} < \psi^*$. Then:

$$\frac{1}{2} z_{ks} = z_\infty e^{\psi_{ks}} = \frac{-\lambda_s}{\sqrt{2(1-\nu)(-\psi_{ks})}}.$$

Applying the boundary condition (6), we get:

$$-\lambda_s = \frac{\lambda_0 e^{\beta \Delta\phi_s'}}{1 + \frac{\lambda^0}{z_k^0} \frac{2e^{\alpha\Delta\psi_s'}}{\sqrt{2(-1+\nu)\psi_{ks}}}} = \frac{\lambda_0}{1 + \frac{\lambda_0}{z_k^0} \frac{2}{\sqrt{2(-1+\nu)\psi_{ks}}}},$$

since

$$\Delta\phi_s' = t_0 (y_k^s - y_k^0) \leqslant t_0 y_k^s = t_0 \sqrt{-2(1-\nu)\psi_{ks}} < t_0 \sqrt{2(1-\nu)\psi^*} \ll 1.$$

If also $z_k^0 \ll \lambda_0$, then

$$-\lambda_s = \frac{1}{2} z_k^0 \sqrt{2(1-\nu)(-\psi_{ks})} \ll \lambda_0.$$

Let us calculate the total potential drop ψ_t in various regions of the λ current. ψ_t is defined by the equation:

$$\psi_t = \Delta\psi_0 + \Delta\psi' - \psi_k - \lambda t_l,$$

where $\Delta\psi_0$ is the equilibrium potential difference in the Helmholz layer, and $-\lambda t_l$ the ohmic potential drop. For currents $\lambda > -\lambda_0$, by applying the boundary condition (6) in the form $\lambda/\lambda_0 = z_k/z_k^0 - 1$, and using Equations (10) and (11), we get :

$$\psi_t = \Delta\psi_0 - \ln\left[\frac{z_k^0}{z_\infty}\left(1+\frac{\lambda}{\lambda_0}\right)\right] - \lambda t_l, \qquad \lambda > \lambda_s; \tag{12}$$

$$\psi_t = \Delta\psi_0 + \frac{\lambda^2}{2(1-\nu) z_k^{0\,2}\left(1+\frac{\lambda}{\lambda_0}\right)^2}, \qquad \lambda^* < \lambda < \lambda_s; \tag{13}$$

$$\psi_t = \Delta\psi_0 + \psi^* - \ln\left[-\frac{z_k^0}{\lambda}\left(1+\frac{\lambda}{\lambda_0}\right)\sqrt{2(1-\nu)\psi^*}\right], \qquad -\lambda_0 < \lambda < \lambda^*. \tag{14}$$

For currents $\lambda < -\lambda_0$, by applying the boundary condition (6) in the form $-\lambda/\lambda_0 = e^{\beta\Delta\varphi'}$, and the second of the two Equations (8), we get

$$\psi_t = \Delta\psi_0 + \frac{1}{\beta}\ln\left(-\frac{\lambda}{\lambda_0}\right) - \ln P_\infty + \ln\left[\frac{1}{2\beta^2 l_0^2}\ln^2\left(-\frac{\lambda}{\lambda_0}\right)\right] - \lambda t_l. \tag{15}$$

An approximate form of the volt-ampere characteristic given by Equations (12) - (15) is shown in Fig. 1.

The above-presented calculations were based on the assumptions that $-\psi_{ks} < \psi^*$ and $z_k^0 \ll \lambda_0$. If, however, the condition $-\psi_{ks} < \psi^*$ holds at the contact but $z_k^0 \gg \lambda_0$, then it can be demonstrated that the inflection of the volt-ampere characteristic will be displaced to the left, to a current $\lambda = -\lambda_0$. Its height will still remain equal to ψ^*. The average slope of the inflection will now be approximately $1/t_0\lambda_0$, whereas in the first case it was about $1/z_k^0$.

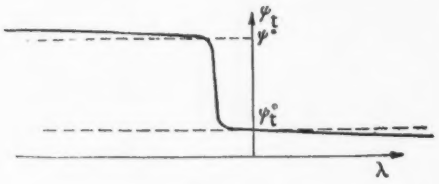

Fig. 1.

The case where $-\psi_{ks} > \psi^*$ is not of any interest. It gives a smooth, volt-ampere characteristic without an inflection. In this case, the rectification is quenched by the excessive space charge of the holes.

Hence, our calculations have shown that the examined contact possesses several valuable properties.

When ψ^* is sufficiently large and the contact is initially electron deficient, the volt-ampere characteristic curve exhibits a typical, almost vertical inflection and a very small blocking current.

The existence of a unique break-down voltage ψ^*, which is of the same magnitude as the forbidden band width constitutes a considerable drawback of this contact. Consequently, the examined case is most interesting for semiconductors with broad forbidden bands. The contact exhibits no rectification when $\psi_t > \psi^*$ due to the great space charge of the holes.

The results obtained in this work can, of course, be extended to an electrolyte-P-type semiconductor contact. In such cases our calculations are valid provided only the holes participate in the electrochemical reaction.

The authors wish to thank corresponding member of the Acad. Sci. USSR V. G. Levich for a valuable discussion.

LITERATURE CITED

[1] Yu. A. Vdovin, V. G. Levich, and V. A. Myamlin, Proc. Acad. Sci. 124, 350 (1959).*

[2] Yu. A. Vdovin, V. G. Levich, and V. A. Myamlin, Proc. Acad. Sci. 126 (1959).*

[3] Yu. V. Plaskov and B. N. Kabanov, Proc. Acad. Sci. 123, 884 (1958).*

Received July 6, 1959.

*Original Russian pagination. See C. B. translation.

THE FORMATION OF POROUS STRUCTURE IN SILICA GEL IN THE PRESENCE OF VOLATILE COMPOUNDS

Z. Z. Vysotskii and M. V. Polyakov

L. V. Pisarzhevskii Institute of Physical Chemistry of the Academy of Sciences Ukr. SSR

(Presented by Academician A. N. Frumkin, July 13, 1959).

A successful solution of several theoretical and practical problems associated with adsorption depends largely on the proper choice of adsorbers with a porous structure most suitable for studying the given problem. As has become apparent in recent years, in several problems, particularly those connected with the specific adsorption, the chemical nature and structure of the adsorbing surface are also very important. Hence there is certainly a great need for the development and improvement of different methods of regulating the structural adsorption properties of adsorbers. Earlier, one of us [1-3] developed a method for the formation of pores and surface relief in silica gels by the dehydration of silicic acid hydrogels in the presence of volatile compounds with various structures. The results obtained in those cases indicated a definite relationship between the molecular structure of the volatile compounds and the final structure of the dry silica gel; consequently we proposed a mechanism to explain the specific porous structure and the form of silica gel surface formed. Besides, it was shown [3] that not only surface-active agents [4] substantially affected the porosity of silica gel, but any compounds the vapors of which could be absorbed by silica gel, particularly benzene, toluene, and xylene.

In the period between 1949 and 1958 many foreign workers, in attempting to prepare selective adsorbers, obtained silica gels which selectively adsorbed those compounds in whose presence the original silicic acid hydrogels were dehydrated: dyes of the methylorange series [5-9], one of two optical isomers [10,11], and organic bases of the pyridine series [12]. After a study of the adsorption properties of these selective adsorbers, a mechanism was proposed [5, 6, 8, 13] for the structure formation in these gels which was in no way different from that proposed earlier by one of us [1-3, 14].

The increased interest in this method of preparing selective adsorbers as well as recent attempts to revive the theories concerning the dominant role of the surface tension of the intermicellar liquid in the formation of the porous structure in silica gel [15] induced us to check the results obtained earlier by one of us with regard to the feasibility of structure formation in silica gel prepared in the presence of surface-active volatile compounds. The results of this investigation are presented below.

The silicic acid hydrogel was prepared in the usual manner: a sodium silicate solution was added to a solution of sulfuric acid; after syneresis of the cooled sol the hydrogel was broken into small pieces (1-1.5 cm along the edge) and washed with weakly acidic (H_2SO_4, 1:5000) conductivity water to remove soluble salts. The washed hydrogel was separated into individual pieces, each of which was laid on a Petrie dish and placed into a separate dessicator containing concentrated sulfuric acid; into each dessicator we then placed a beaker with the appropriate volatile liquid: benzene, toluene, or o-xylene. The control hydrogel sample was divided into two parts, one of which was dehydrated in a similar dessicator containing the acid but not the hydrocarbon, while the other was exposed to open air in the laboratory. Dehydration was carried out for three months at room temperature. The structural adsorption properties of the silica gels thus prepared were investigated by determining the adsorption isotherms of benzene vapor at 20° in a vacuum apparatus on a McBain balance. The resulting isotherms are presented in Fig. 1 and 2.

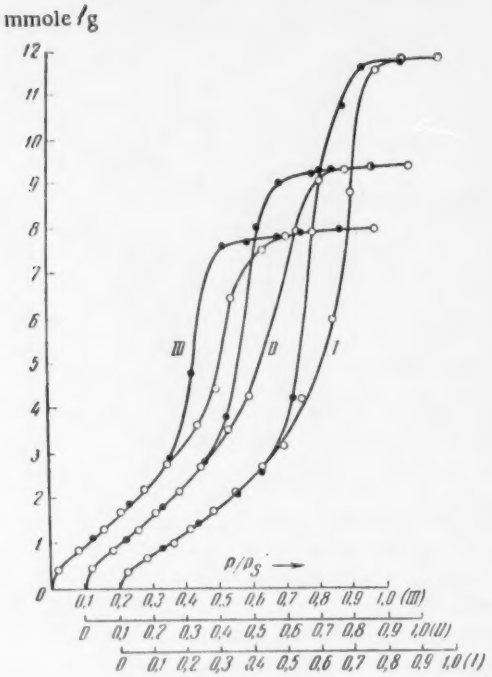

Fig. 1. The 20° adsorption isotherms for benzene vapor on silica gels, formed in an atmosphere of: I) benzene; II) toluene; III) xylene. The solid dots denote desorption.

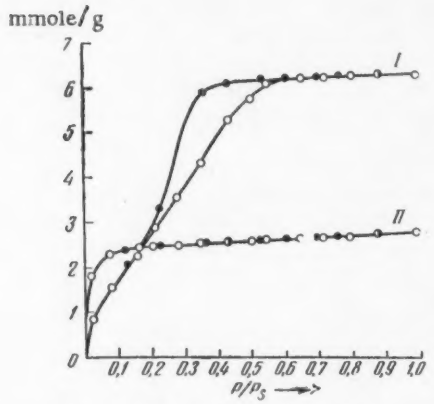

Fig. 2. The 20° isotherms for the adsorption of benzene vapor on control silica gels dried over sulfuric acid (I), and in air (II).

Figure 1 shows that the adsorption isotherms of benzene on a silica gel formed in the presence of benzene vapor begin rising much further to the right than in the case of samples dehydrated in the presence of toluene; the adsorption and desorption isotherms of gels treated with xylene are displaced even further to the left. When $P/P_s = 1$ the benzene-treated silica gel adsorbs 11.8, the toluene-gel 9.4, and the xylene-gel 8.0 millimoles, respectively of benzene per gram; the respective median pore radii (calculated from the isotherms) are: 40, 30, and 25A. As may be seen from the initial isotherm segments, the specific surfaces of these adsorbers are also different. Thus we have fully confirmed our previous results which showed that the structural adsorption properties of silica gels change smoothly when the gels are prepared in the presence of: benzene, toluene, and o-xylene, respectively.

By comparing the three isotherms in Fig. 1 with the curves in Fig. 2 we can see that the porous structure of gels formed in the presence of benzene, toluene, and xylene differs considerably from the structure of the control gels; the control sample dehydrated in air is highly microporous while that dehydrated in the dessicator over sulfuric acid can only adsorb 6.3 millimoles of benzene and has an ~ 16A median pore radius. Therefore all the gels formed had much larger pores than did the control samples.

Before attempting to explain our results one must keep in mind the fact that, as was shown by specially designed experiments, the initial intermicellar liquid is almost entirely replaced by the respective hydrocarbon towards the end of the formation period, while in the case of the control gel dehydrated over sulfuric acid the pores become empty (when the gel was subsequently dehydrated in a dessicator for 2½ hours at 150° it only lost ~ 2% of its weight). At the same time the pores of the control gel dried in air remained almost full of water at the end of dehydration (~28% of water lost on drying in a dessicator).

Comparing the dipole moments of benzene, toluene, and o-xylene (0, 0.39, and 0.62 Debyes respectively), the saturated vapor pressures at 20° (74.1, 22.5, and 10.1 mm), the parachors (207.1, 246.1, and 285.1), and other properties, with the regular changes in the maximum adsorption volumes, pore radii, and the distribution of the initial isotherm segments of the investigated silica gels, we can see that the properties of fully formed gels (those pertaining to both the porous structure inside and to the surface structure) are related in a certain manner to the structures and properties of the molecules involved in the formation of the gel. Let us note that in this work, as well as in a previous paper by one of us [1], the ratios between the maximum adsorption volumes (on the average 0.82) are close close to the ratios between the molecular weights of the compounds present during the formation (0.86).

At the same time, the idea that the surface tension of the intermicellar liquid constitutes the controlling factor in the formation of the porous structure in silica gel [15] turns out to be clearly in conflict with the facts. The experimental results indicate that the surface tensions of benzene, toluene and xylene, which are almost identical at 20° (28.8, 28.5, and 30.0 dynes/cm, respectively) are not related in any way to the regular variations in the gel structure when one proceeds from benzene to xylene. Previously some results have also been obtained [16-18] which indirectly disproved the above-criticized ideas; the results obtained in the present work may, in our opinion, be used directly to disprove the erroneous emphasis on the surface tension. We believe that the chemical nature of the micelles in a silicic acid gel and its chemical-crystal structure constitute the fundamental factors determining the type of structure eventually assumed by the silica gel. The nature of the intermicellar liquid is important in so far as the liquid interacts with the labile portions of the gel skeleton when the latter is compressed during dehydration, and produces a specific arrangement of the surface groups (for example, hydroxyls) on the silica-gel skeleton; meanwhile, the liquid present in the gel pores, which molds the gel skeleton surface, as one could say "in its own image," undoubtedly exists in a state different from the usual three-dimensional liquid.

Thus, in our opinion, the type of porous structure assumed by the dry silica gel is rigidly controlled and actually predetermined by the chemical nature and physical structures of the micellar surfaces in gels, since the capillary forces which contract the gel skeleton during dehydration depend (under similar conditions) on the degree of gel-surface wetting by the intermicellar liquid.

The precise details of the mechanism leading to a specific type of an adsorption site on the silica gel surface are not clear as yet. We may only propose several more or less probable hypotheses with regard to this matter: 1) the molecules of the volatile compound present during dehydration are adsorbed on the micellar surface, interact with the surface hydroxyl groups orienting them according to their own structure and creating local changes in the geometric distribution of the OH-groups ("imprints", see [3]) on a chemically homogeneous adsorber surface; 2) the volatile hydrocarbons produce local variations in the number of hydroxyls covering the surface (degree of hydration of silica); 3) the hydrocarbon alters not only the surface relief, but also the relative distribution of atoms in layers lying deeper inside the adsorber; 4) individual sections of the silica gel surface retain tightly adsorbed volatile compound molecules, which cannot be removed by pumping or washing and have pronounced effects on the adsorption properties of silica gel; 5) when the orthosilicic acid is condensed in the presence of volatile organic compounds one cannot exclude the possibility that chemical surface compounds are formed between the hydrocarbons and the siliceous residue of the silica gel, even at room temperature [19].

LITERATURE CITED

[1] M. V. Polyakov, J. Phys. Chem. 2, 799 (1931).

[2] M. V. Polyakov, P. M. Stadnik, et al., J. Phys. Chem. 4, 454 (1933).

[3] M. V. Polyakov, L. P. Kuleshina, I. E. Neimark, J. Phys. Chem. 10, 100 (1937).

[4] V. S. Veselovskii, I. A. Selyaev, J. Phys. Chem. 6, 1171 (1935).

[5] F. H. Dickey, Proc. Nat. Acad. Sci., 35, 227 (1949).

[6] F. H. Dickey, J. Phys. Chem., 59, 1039 (1955).

[7] S. A. Bernhard, J. Am. Chem. Soc., 74, 4946 (1952).

[8] R. Curti, U. Colombo, and F. Clerici, Gazz. chim. ital., 82, 491 (1952).

[9] R. Curti, and U. Colombo, Chimica Industria, 33, 103 (1951).

[10] R. Curti and U. Colombo, J. Am. Chem. Soc., 74, 3961 (1952).

[11] A. H. Beckett and P. Anderson, Nature, 179, No.4569, 1075 (1957).

[12] A. Waksmundzki, Roczniki Chemii, 32, 323 (1958).

[13] R. G. Haldeman and P. H. Emmett, J. Phys. Chem., 59, 1039 (1955).

[14] Z. Z. Vysotskii, and M. V. Polyakov, J. Phys. Chem. 30, 1901 (1956).

[15] I. E. Neimark, Progr. Chem. 25, 748 (1956).

[16] Z. Z. Vysotskii and V. V. Shalya, J. Appl. Chem. 32, 35 (1959).*

[17] Z. Z. Vysotskii and V. V. Shalya, Colloid J. 20, 29 (1959).*

[18] Z. Z. Vysotskii, and V. V. Shalya, Trans. All-Union. Sci. Tech. Confer. on Adsorp., Leningrad, 1957.

[19] R. E. Benson and J. E. Castle, J. Phys. Chem., 62, 840 (1958).

Received July 1, 1959.

*Original Russian pagination. See C. B. translation.

A KINETIC, AN ADSORPTION, AND AN X-RAY CRYSTALLOGRAPHIC STUDY OF THE DECOMPOSITION OF MAGNESIUM CARBONATE

V. A. Gordeeva, G. M. Zhabrova, and M. Ya. Kushnerev

Institute of Physical Chemistry of the Academy of Sciences USSR

(Presented by Academician V. I. Spitsyn, July 13, 1959)

As a rule, the kinetics of solid state reactions cannot by themselves provide enough data to elucidate the rules governing topochemical processes and permit an understanding of the reaction mechanism. Hence it was interesting to follow one such process by using several methods: kinetic, adsorption, and x-ray crystallographic.

As an example of a topochemical reaction we picked the decomposition of magnesium carbonate, the preparation of which was described before [1]. X-ray diffraction studies showed that the initial samples of $MgCO_3$ contained less than 5% of $MgCO_3 \cdot 3H_2O$.

The decomposition kinetics of magnesium carbonate and the adsorption measurements were carried out in a vacuum apparatus using a McBain quartz-spring balance. We found that interruptions had no effect on the rate of the topochemical reaction, and were therefore able to follow the changes in the specific surface in the course of the reaction.

A BSV-4 tube with a copper anode constituted the x-ray source. β-radiation was not filtered out. We placed 3.5 ml of $MgCO_3$ (3 to 5 ml) into a thin capillary made of molybdenum glass. The capillary was connected to the vacuum apparatus and inserted into a cylindrical electric furnace which contained two symmetrically located openings, for the passage of incident and diffracted radiation.

A horizontal cell was placed at a distance which permitted a simultaneous recording of the 1st and 2nd characteristic reflections from the initial and final solid phases. Such a cell permitted a 0.02A resolution.

The x-ray diffraction of each sample was recorded at temperatures at which definite degrees of decomposition were obtained. We subsequently compared the reflection intensities from the initial and final phases with the corresponding intensities from an artificial $MgCO_3$ + MgO mixture, prepared from a carbonate ignited at 400°. We followed the changes in the reflection intensities of $MgCO_3$ (112) and intensities from the double reflection of $MgCO_3$ (120) + MgO(002).

As can be seen in Fig. 1, not all the kinetic curves exhibit an induction period. Over one of the kinetic curves we superimposed the points obtained in a certain x-ray diffraction experiment in which the percent decomposition was also followed. The points fit the curve quite well, indicating that x-rays have no noticeable effect on the reaction rate. The experimental curves of percent decomposition vs. time were worked out by means of two kinetic equations:

$$1 - (1 - \alpha)^{1/3} = K_1 t; \quad (1)$$

$$-\ln(1 - \alpha) = K_2 t, \quad (2)$$

where α is the fraction decomposed, t the time, and K the rate constant. As was shown by S. Z. Roginskii and O. M. Todes [2,3], the two equations represent two distinct reaction mechanisms. Equation (1) represents an instantaneous formation of a great number of nuclei over the entire grain surface and the propagation of the

new phase front towards the inside. Eq. (2) represents the reverse limiting case, where a single nucleus grows throughout the entire grain. As we have shown somewhere else *, Equations (1) and (2) are indistinguishable in the decomposition range from 0.2 to 0.7 (20 to 70%).

TABLE 1

Temp., °C	Amt. of carbonate decomp., %	Interplanar distance of the double reflection from $MgCO_3$(120) + MgO(002), d in A	Temp., °C	Amt. of carbonate decomp., %	Interplanar distance of the double reflection from $MgCO_3$(120 + MgO(002), d in A.
375	0	2,19	425	0	2,19
	16,5	2,19		53	2,17
	34,0	2,19		64,5	2,15
	53,0	2,18		71,0	2,13
	60,5	2,18		77,5	2,13
	70,0	2,17		81,0	2,11
	74,5	2,17			
	78,0	2,16			
	80,5	2,15			
	82,0	2,14			

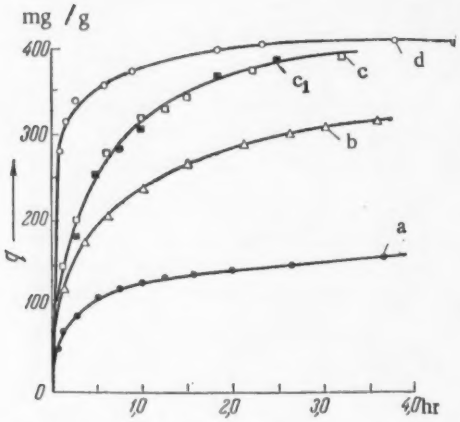

Fig.1. Kinetic curves for the decomposition of magnesium carbonate (q is the amount of carbon dioxide evolved, in mg per gram of $MgCO_3$): a) at 320°; b) at 350°; c) at 375° (c_1, points obtained in the x-ray diffraction experiment); d) at 425°.

Equation (1) gave an activation energy of 26 kcal/mole, while Equation (2) gave 27 kcal/mole. Hence, since the kinetic equations are indistinguishable it is impossible to determine the rate-determining step in the given topochemical reaction. Therefore, to solve this problem it was necessary to study the reaction by other means. In Fig. 2 we have plotted a characteristic curve for the increase in the specific surface during the decomposition of magnesium carbonate. In order to determine whether the observed specific-surface increase was solely due to the greater specific surface of the newly formed MgO phase, or was also caused by some cracking of the initial carbonate surface, we calculated the total surface $S_{tot} = \alpha' S' + \alpha'' S''$ (assuming that the specific surfaces of the initial solid phase and the newly formed one are additive); α' is the mole fraction of MgO; S' the specific surface of MgO when the carbonate is completely decomposed (330 m^2/g); α'' the mole fraction of undecomposed $MgCO_3$; and S'' its specific surface (37 m^2/g).

Calculations show that the deviations from the assumed additive character are small (from 10 to 30%). The molar specific surface of magnesium oxide remains a linear function of its concentration during the decomposition of magnesium carbonate (Fig. 2), which seems to indicate that magnesium oxide does not undergo any noticeable thermal sintering. A similar function for the molar specific surface was established by Danesh [4] in the case of magnesium oxide formed from magnesium oxalate.

Table 1 shows that up to a 35-40% decomposition of $MgCO_3$ the interplanar distance d remains constant. This indicates that in the given decomposition range the reflections from MgO are not superimposed on those from $MgCO_3$. But after 35-40% decomposition, reflections from MgO are imposed on those from $MgCO_3$.

*A supplementary handbook on catalysis, in print.

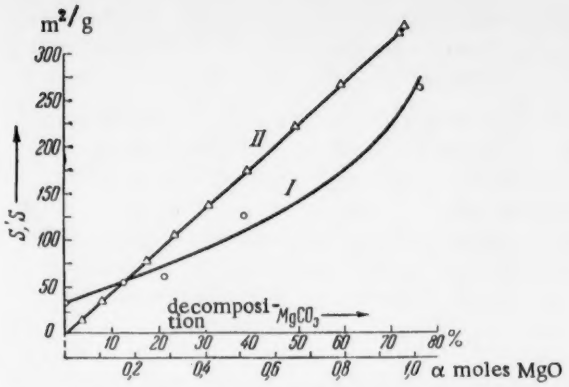

Fig.2. Change in the total specific surface (I) and in the specific surface of MgO (II) during the decomposition of magnesium carbonate as a function of MgO mole fraction.

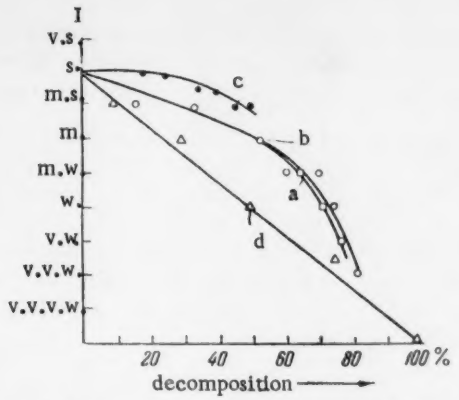

Fig. 3. Changes in the reflection intensity from $MgCO_3$(112) during the decomposition of $MgCO_3$; a) at 425°; b) at 375°; c) at 320°; d) artificial mixture.

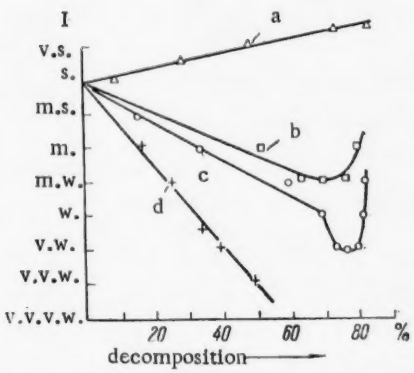

Fig. 4. The total change in the reflection intensity from $MgCO_3$ (120) and MgO (002) during the decomposition of $MgCO_3$: a) artificial mixture; b) at 425°; c) at 375°; d) at 320°.

At 425° d changes in a similar manner with increasing percent decomposition. This may possibly be explained by assuming that the MgO initially formed is amorphous, then crystallizes until it attains dimensions resolvable by x-ray techniques, >30 A. The higher the temperature the faster should the crystallization proceed.

In Fig. 3, we have plotted the reflection intensities from $MgCO_3$ (112) and from an artificial mixture of $MgCO_3$ + MgO, where the carbonate surface does not seem to become coated with magnesium oxide and consequently the reflection intensity from $MgCO_3$ changes linearly. The increased reflection intensity from $MgCO_3$ (112), relative to that from the artificial mixture, which was composed of fully crystalline components, may be explained by assuming that the incoherent radiation scattering is not proportional to the amount of magnesium oxide and carbonate present. Considering that the incoherent scattering does not affect to any appreciable extent the fraction of coherent scattering from each crystalline component, we have to conclude that the component being formed (MgO) is hardly involved at all in the coherent scattering at low percent decompositions; such a behavior is typical for solids which are amorphous to x-rays. At high percent decompositions (60-70% at 375-425°) the amount of new component producing coherent scattering increases while the carbonate intensity curve declines sharply.

From the preceding discussion one may conclude that the MgO formed at low percent decompositions is in part amorphous to the x-ray and in part crystalline. The lower the decomposition temperature the greater the amorphous phase fraction. While studying the dehydration of magnesium sulfate S. Z. Roginskii, A. B. Shekhter, et al. [5] also observed the formation of amorphous or microcrystalline products.

Figure 4 shows that the double line intensity in the artificial mixture increases with increasing MgO content. It seems that magnesium oxide can produce more coherent scattering than can the carbonate. When mixtures of the two components are formed during the topochemical decomposition of magnesium carbonate one observes a decline in the double line intensity.

These results lead to the same conclusions as before, that at small degrees of decomposition there is formed some MgO amorphous to x-ray. It should be noted that on the strength of the data given in Table 1 and Fig. 3 one

could postulate that the MgO exhibits pseudomorphism, which was proposed by certain workers [6]. However, such a case would be in conflict with the nature of the curves plotted in Fig. 4, since in the case of pseudomorphism the curves would have some segments parallel to the abscissa; nothing of the sort is observed even at low temperatures.

With the help of the x-ray crystallographic analysis let us try to select one of the two previously discussed topochemical reaction mechanisms. According to Equation (1) numerous MgO nuclei (amorphous to x-rays) are formed on the magnesium carbonate surface; these slowly and simultaneously begin to grow inwards and crystallize to a size > 30A. In such a case the double line intensity (Fig. 4) should initially decline, since the coherent scattering from the carbonate diminishes while the coherent scattering from magnesium oxide is insignificant due to the large amorphous component. Towards the end of the reaction the double line intensity should sharply increase due to the increased fraction of coherent scattering from MgO. And such is precisely the case in Fig. 4. According to Equation (2) a small number of inward-growing nuclei are formed on the crystal surface. In such a case the composition of the crystal surface would be similar to that in the artificial MgO + $MgCO_3$ mixture. This would produce a convergence between the double line intensity (MgO, $MgCO_3$ and the corresponding intensity in the artificial mixture. However, nothing of the sort was observed in our experiment. Let us note that all the relationships shown in Fig. 4 are only valid up to~ 70% decomposition, after which the curves for the MgO + + $MgCO_3$ double line intensity exhibit a sharp bend; the latter seems to be connected with crystallization. As a rule, either one of the two rate laws for the topochemical reaction is found to be valid up to 70-75% decomposition. Thus the data obtained for the decomposition of magnesium carbonate (in vacuo) suggest that the mechanism described by Equation (1) is more probable than that described by Equation (2).

LITERATURE CITED

[1] G. M. Zhabrova, M. D. Sinitsyna, and S. Z. Roginskii, Proc. Acad. Sci. 124, No.2, 354 (1954).

[2] S. Z. Roginskii and O. M. Todes, Bull. Acad. Sci. USSR, Div. Chem. Sci. 1940, No.4, 475.

[3] O. M. Todes, J. Phys. Chem. 14, 1224 (1940).

[4] V. Danesh, Proc. of the Confer. on the Phys. and Phys-Chem. of Catalysis, Moscow, 1958.

[5] S. Z. Roginskii, A. B. Shekhter, et al. Proc. Acad. Sci. 68, No.5, 879 (1949).

[6] R. J. Razouk and R. Sh. Mikhail, J. Phys. Chem., 61, No.7, 886 (1957).

Received July 3, 1959.

Card + Photo

SOLID SOLUTIONS IN THE AlSb – InSb SYSTEM

N. A. Goryunova and B. V. Baranov

Physicotechnical Institute of the Academy of Sciences, USSR

(Presented by Academician A. N. Frumkin, July 13, 1959)

The forbidden band width and mobility of charge carriers are the two fundamental parameters which determine the possible applicability of a product in the field of electronics. The laws governing the variations of these parameters with the composition in solid substitution compounds are not known. Experimental results which should provide a basis for a comprehensive solution of this problem have only very recently begun to accumulate. However, even the most elementary ideas lead us to believe that the AlSb – InSb system should prove to be the most interesting (with reference to the above-discussed problem) if it forms solid substitution solutions.

Considering the exceedingly high mobility of charge carriers in indium antimonide (according to the most-recent data [1], $8 \cdot 10^5 - 10^6$ $cm^2/V \cdot sec$ at 77° K) combined with a large forbidden band width (1.6ev) in aluminum antimonide, we would hope to obtain highly useful products from solid solutions formed in the fused salts, even if the properties should change unfavorably.

However, the existence of solid solutions in the AlSb – InSb system has not been, until now, conclusively proven. Similar systems studied so far, such as: AlSb–GaSb and InSb–GaSb, are composed of binary compounds which differ much less in their melting points than do aluminum and indium antimonides. A great difference between the melting points seems to create additional difficulties with respect to the homogenization of solid solutions. To this we may attribute the fact that all the attempts to prepare homogeneous solid solutions in the AlSb–InSb system have so far failed. Even after heating of the alloys for 2500 hours (a technique developed by Woolley and Smith [2]), we were unable to establish the solubility of the components over a wide concentration range (see Fig.1). We also found that zone refinement is not suitable for the AlSb–InSb alloys.

A careful examination of all the previous work, and some of our initial experiments, suggested that a special homogenization technique may be required to produce solid solutions in this system. Below we have presented, in brief, the results of our work along these lines.

The impurities in the starting materials (Al, Sb, In) did not exceed 0.005%. The preparations were carried out in covered graphite crucibles, which were sealed in quartz tubes filled with spectroscopically pure argon.

To achieve a more effective mixing, the samples were agitated for an hour at the maximum temperature (1100°). They were then tempered by submerging the glowing tubes in brine. Crystallization occurred at the instant the tubes burst; the resulting samples consisted of plates and highly porous fragments. A microstructural investigation revealed the existence of finely dispersed dark and light crystals, which were mixed with each other and exhibited a wide distribution of microhardness with values confined to the vicinity of each of the respective binary components. The x-ray crystallographic study of all the alloys yielded Debye plots containing two-line systems.

The samples were next heated above the melting point of aluminum antimonide. Depending on the composition, the temperature used with various samples ranged from 540 to 600°C. Distillation of antimony prevented any annealing above 600°C. We also tried annealing in sealed-off tubes filled with spectroscopically pure argon for 120 to 500 hours. We worked on the assumption that at higher temperatures the diffusion rate should be greatly

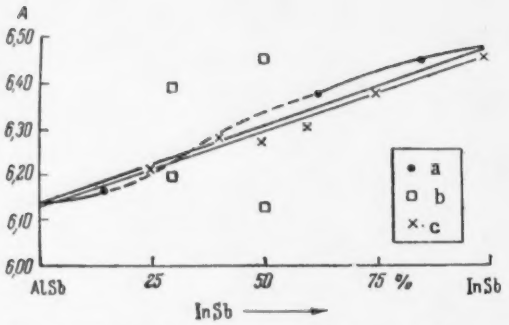

Fig. 1. Change in the lattice identity period in the AlSb–InSb system [2]: a) single-phase region; b) two-phase region; c) experimental results.

accelerated, preventing the elimination of indium antimonide (or a low concentration solid solution derived from it) caused by a close contact with finely dispersed phases of different compositions.

The investigation of our alloys yielded the following results.

A microstructural investigation revealed that the dark crystals disappeared and that the microhardness distribution in each alloy became small in comparison with that in the unhomogenized samples. The absolute microhardness was intermediate between the respective values in the starting binary compounds.

The Debye plots of each alloy gave only one system of practically undiffused lines. The calculated identity periods obeyed Vegard's law (see Fig. 1). A thermal analysis, which is more sensitive to the presence of another phase than is x-ray diffraction, revealed weak effects at about 500° besides the strong effects typical of solid solutions.

Our experiments revealed that the weak effects were caused by the presence of a small amount of the indium antimonide + antimony eutectic mixture in the alloys. The formation of excess antimony is unavoidable when such alloys are prepared in graphite crucibles, due to the formation of aluminum carbide. Formation of the eutectic can be avoided by using crucibles made of aluminum oxide. The materials used in our experiments were so pure that the resulting aluminum antimonide, as well as the unhomogenized alloys with indium antimonide, required 500 hours in air for a complete oxidation. It is worth noting that the homogeneous solid solutions of the same purity, particularly in the concentration range from 50-100% InSb, not only failed to disintegrate in air but even withstood the action of water for 2000 hours.

Thus by first tempering, then annealing our alloys at temperatures high above the melting point of the low-melting component we were able to get irrefutable proof for the existence of solid solutions over a wide concentration range in the AlSb–InSb system.

The next problem involves a detailed study of the composition diagram for this system and a preparation of even purer homogeneous and solid alloys for a detailed investigation of the electrical properties.

LITERATURE CITED

[1] K. I. Vinogradova, V. V. Galavanov, et al., Solid State Physics, 1, No.3, 403 (1959).

[2] J. C. Woolley, and B. A. Smith, Proc. Phys. Soc., 72, No.464, 214 (1958).

Received June 22, 1959.

THE ELECTROPLATING OF COPPER AND CADMIUM ON SOLID ELECTRODES USING HIGH CURRENT DENSITIES

G. A. Emel'yanenko and E. Ya. Baibarova

Dnepropetrovsk State University, (named after the 300th Anniversary of the Unification of Ukraine with Russia)

(Presented by Academician A. N. Frumkin, July 13, 1959)

By studying the voltage vs time functions Roiter and co-workers were the first to demonstrate experimentally the applicability of the delayed ionic-discharge theory [1] to the electroplating of metals on solid cathodes at very low current densities [2].

Under these conditions, however, the effects of cathodic passivity hinder a study of the reaction kinetics. According to P. V. Hillson [3], at low current densities only activated areas, constituting about 3-10% of the total, participate in the reaction. At high current densities the discharge of metallic ions ought to proceed over the entire solid electrode surface.

Applying the delayed discharge and nonstationary diffusion equations P. Delahay [4] and other workers proposed a criterion for high current-density electrode processes which makes it possible to distinguish the electrochemical and concentration polarizations, and developed a method for the determination of the kinetic reaction parameters (discharge rate constants and transport number α). They used for this purpose the function: $\log\left[1-\left(\frac{t}{\tau}\right)^{1/2}\right]=f(\varphi)$, where τ is the migration time, t the length of electrolysis, and φ the electrode potential.

Recently the above-discussed method has been extended to the study of electroplating of several metals on solid electrodes [5]. The main drawback of this method, as the workers who developed it admitted themselves, resides in the well-known uncertainty of the τ value obtained from $\varphi - t$ curves, which in turn reduces the accuracy with which the degree of irreversibility and the kinetic reaction parameters can be determined.

A method involving the determination of $it^{1/2}$ as a function of i at a constant φ (where i is the current density) would be of great value as a means of differentiating between the electrochemical and concentration polarizations. Such a method was introduced by L. E. Gierst [6], who actually started with a somewhat formal analysis of the various assumptions made in describing the electrode potential as a function of the discharge rate constant. Despite its obvious advantages the method has not so far been developed or systematically applied to the study of the electroplating of metals on solid electrodes at high current densities. Moreover, the inadequate knowledge of these processes hinders any improvement of the available, and development of new, technological methods for the electrolytic preparation of compact and powdered metals.

In the present work we aimed at finding out whether the fundamental kinetic equations for the delayed discharge and nonstationary diffusion are applicable to the electroplating of copper and cadmium on like solid electrodes at high impressed current densities. To the sulfates of these metals we added an excess of supporting electrolyte and studied the solutions at 18-20°C.

When the concentration polarization arises as a result of a retarded diffusion of metal ions to the cathode surface,

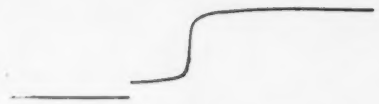

Fig. 1. The oscillogram of $\Delta\varphi$ vs t for 0.05M $CdSO_4$ + 0.5 M Na_2SO_4 at i = = 8ma/cm^2 (1 mm on the time axis is equivalent to 1 sec, and on the polarization axis to 80 mv).

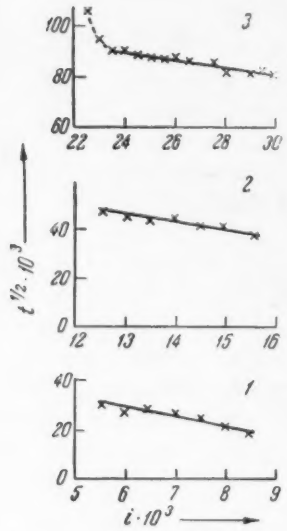

Fig. 2. A plot of $it^{1/2}$ against i. 1) 0.05 M $CdSO_4$ + 0.5M Na_2SO_4 (0.25 v); 2) 0.1M $CuSO_4$ +0.5M H_2SO_4 (0.40 v); 3) 0.2M $CuSO_4$+ + 0.5M H_2SO_4 (0.40v).

$$it^{1/2} = {}^1/_2 zF\pi^{1/2} D^{1/2} c_0 \left[1 - e^{-zF\Delta\varphi/RT}\right] *,$$

where c_0 is the concentration of metal ions far from the electrode, D the diffusion coefficient of the metal ions, and $\Delta\varphi$ the electrode polarization.

When $\Delta\varphi \geq 0.1$ the exponential term may be neglected, and we get

$$it^{1/2} = {}^1/_2 zF\pi^{1/2} D^{1/2} c_0. \qquad (1)$$

In such a case $it^{1/2}$ is independent of i and $\Delta\varphi$.

TABLE 1

The Values of $it^{1/2} \cdot 10^3$ (amp · cm^{-2}·sec$^{1/2}$) at Various Cathode Polarizations

$i \cdot 10^3$, amp·cm^{-2}	$\Delta\varphi$, v				
	0,25	0,30	0,35	0,40	0,45
	0,05*M* $CdSO_4$+0,5*M* Na_2SO_4				
8,0	22	23	25	—	25
8,5	18	21	23	23	23
$i \cdot 10^3$, amp·cm^{-2}	$\Delta\varphi$, v				
	0,40	0,50	0,60	0,70	
	0,2*M* $CuSO_4$ + 0,5*M* H_2SO_4				
29,5	83	89	93	93	
30,0	82	88	95	95	

When concentration changes on the electrode give rise to electrochemical polarization,

$$it^{1/2} = {}^1/_2 zF\pi^{1/2} D^{1/2} c_0 \left[1 - \frac{i}{k_1 c_0} e^{-\alpha zF(\Delta\varphi - \varphi_p)/RT}\right] **$$

where φ_p is the equilibrium electrode potential, $k_1 = ke^{W_0/RT}$ (k is the discharge rate constant, W_0 activation energy at $\varphi = 0$). In deriving this equation we assumed that the currents produced by the double layer charges and by the ionization of metals are negligible and also that the discharge of ions follows first-order kinetics. In such a case $it^{1/2}$ is inversely proportional to i at constant $\Delta\varphi$ and directly proportional to $\Delta\varphi$ at constant i.

In cases where k_1 and $\Delta\varphi$ are large the exponential term in Equation (2) becomes very small and Equation (2) changes into Eq. (1), where diffusion controls the reaction.

Our experimental data on copper and cadmium are in good agreement with these functions.

In Fig. 1 we reproduced the oscillogram of $\Delta\varphi$ vs t*** as an example; in Fig. 2 we plotted $it^{1/2}$ against i, and in Table 1 we listed the values of $it^{1/2}$ at various cathode polarizations in some of our electrolytes.

*This function can be derived from the well-known equation for the concentration polarization and the Sand-Levich equation for nonstationary diffusion [7].

**Equation (2) is a simultaneous solution of the delayed discharge and diffusion equations.

***The oscillograms were recorded on a MPO-2 oscillograph.

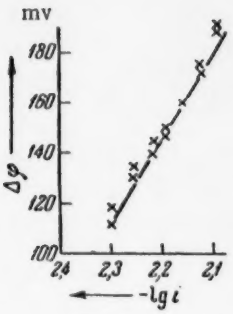

Fig. 3.

We found that in accordance with Equation (2) $\underline{it}^{1/2}$ is indeed a linear function of i* and increases with $\Delta\varphi$. The latter function approaches a fixed limit, given by Equation (1), which was also confirmed by calculating the ionic diffusion coefficients of copper and cadmium using the limiting values of $\underline{it}^{1/2}$. Thus, for example, for 0.05M Cd^{++} at $\Delta\varphi = 0.45$ v, $\underline{it}^{1/2} \simeq 0.024$ amp · cm^{-2} · sec^{-} and $D \sim 0.78 \cdot 10^{-5}$ cm^2/sec; the latter is in agreement with the values of D calculated by other methods. With copper, higher cathode polarizations are required than with cadmium in order to attain the limiting value of $\underline{it}^{1/2}$, which fact is attributed to a greater degree of reaction irreversibility.

Our results indicate that it is possible to use the oscillographs of $\Delta\varphi$ vs $\underline{t}$ on solid electrodes for the determination of diffusion coefficients.

When $\underline{t}$ is small enough so that $\underline{it}^{1/2}$ may be neglected in comparison with $\frac{1}{2} z F \pi^{1/2} D^{1/2} c_0$ Equation (2) is transformed into the equation:

$$\Delta\varphi = \text{const} + \frac{2{,}303RT}{\alpha z F} \lg i,$$

which may be used to calculate the transport number α.

In Fig. 3 we have plotted $\Delta\varphi$ against $\log \underline{i}$ in 0.05M $CdSO_4$ + 0.5M Na_2SO_4 (for $\simeq 0.02$ sec). The value of α calculated from the slope is 0.09. This value is close to $\alpha = 0.08$, which was determined by the Faraday rectification method for the discharge of Cd and Hg in the presence of K_2SO_4 [8].

Therefore we can conclude on the basis of our experiments that the electroplating of copper and cadmium from the investigated solutions at high current densities proceeds under conditions where, besides concentration effects, there also occur some electrochemical changes on the solid electrodes. The kinetic equations for delayed discharge and concentration polarization are applicable to these processes. When the solution in the vicinity of the cathode becomes deficient in the discharging metal ions, making the potential more negative (Fig.1), the process rapidly becomes diffusion controlled instead of being controlled by the electrochemical reaction. At the same time our observations have shown that the electroplated metal changes from a compact to a loose deposit on the electrode surface.

LITERATURE CITED

[1] A. N. Frumkin, V. S. Bagotskii, Z. A. Iofa, and B. N. Kabanov, The Kinetics of Electrode Reactions, Moscow (1952) [In Russian].

[2] V. A. Roiter, V. A. Yuza, and E. S. Poluyan, J. Chem. Phys. 13, 605, 805 (1939).

[3] P. Y. Hillson, Trans. Farad Soc., 50, 385 (1954).

[4] P. Delahay and T. Berzins, J. Am. Chem. Soc., 75, No.10, 2486 (1953); P. Delahay and C. C. Mattax, J. Am. Chem. Soc., 76, No.3, 874 (1954).

[5] T. Pavlopoulos, and J. D. H. Strickland, J. Electrochem. Soc., 104, No.9, 568 (1957).

[6] L. E. Gierst, Zs. Elektrochem., 59, 784 (1955)

[7] V. G. Levich, Physicochemical Hydrodynamics, Izd AN SSSR (1952) [In Russian].

[8] G. C. Barker, R. L. Faircloth, and A. W. Gardner, Nature, 181, No.4604, 247 (1957).

Received May 19, 1959.

*If convection is involved the function of $\underline{it}^{1/2}$ vs. $\underline{i}$ will loose its linear character, or in other words, if $\underline{i}$ is such that the time required to attain a definite electrode polarization is large. This can be shown by the dotted section of line 3 in Fig. 2.

TRANSITION TEMPERATURES IN SYNTHETIC POLYMERS WITH RIGID CHAINS

P. V. Kozlov, A. Endrykhovskaya, and Academician V. A. Kargin

M. V. Lomonosov Moscow State University

It is a well-known fact that the flexibility of polymers depends on the chemical structure of the molecular chains constituting the polymer and on the degree of interaction between chain segments.

The properties of polymers with flexible chains, particularly their transition temperatures, have been investigated in great detail [1-3]. One of us also studied the transitions in nitrocellulose, which has very rigid chains. The polymer was plasticized and the transitions were studied as a function of its molecular weight [4]. It seemed also worth-while to study the transition points of synthetic rigid-chain polymers; such an investigation would be of a great practical value since it involves the methods and conditions used in industrial processing.

As an example we picked polyurea, which has a particularly rigid molecular structure. Polyurea was prepared by condensation polymerization at a boundary between two liquid phases. This technique has been successfully applied to the synthesis of several high molecular weight condensation polymers [5,6]. The method essentially involves a slow diffusion-controlled condensation polymerization between the reactive bifunctional monomers, dissolved in two immiscible liquids, in contact with each other. We thus prepared our polyurea resin by dissolving phosgene in benzene and hexamethyl diamine in water. A 7% sodium oleate was used as emulsifier.

By carrying out the synthesis of polyurea several times we were able to find the optimum conditions for the preparation of high molecular weight products. These conditions are: the reaction, which is instantaneous at room temperature, will result in the formation of a high molecular weight polymer only if a 15% solution of hexamethylene diamine is saturated with sodium carbonate and sodium chloride. After the polymer precipitates it is filtered out, washed thoroughly with water, and dried. The white powdered, polyurea was completely insoluble in most of the common organic solvents, with the exception of cresol and formic acid. The polyurea swells in dimethyl formamide, furfuryl alcohol, and pyridine. To isolate the fraction with the highest molecular weight we dissolved the polyurea in cresol and fractionally precipitated the compound from a 0.2% solution with diethyl ether. X-ray and electron diffraction data indicated that the polyurea thus prepared was amorphous and had a highly ordered molecular structure (Fig. 1). The thermomechanical studies, carried out on a variable-weight dynamometric balance [1], gave a linear relationship between deformation and temperature (Fig. 2, 1), indicating that up to the decomposition temperature the polyurea remained a glass. At temperatures around 230-300°C the sample undergoes a gradual chemical decomposition, evidently due to oxidation.

As is well known, transition points can be substantially lowered by plasticizing rigid-chain polymers, and we therefore used this technique on polyurea. We used two plasticizing processes: by the use of other polymers with flexible chains and the use of low molecular weight solvents. For the first process we used a 1:1 copolymer between caprolactam and adipic acid; m-cresol was used as the low molecular weight liquid in the second process. The thermomechanical properties of the initial polymers and of their mixtures are shown in Fig. 2. The results indicate that actually only the transition point into the viscous state can be decreased below the chemical decomposition temperature when the polyurea to the copolymer ratio is 1:1.6 (Fig. 2, 3).

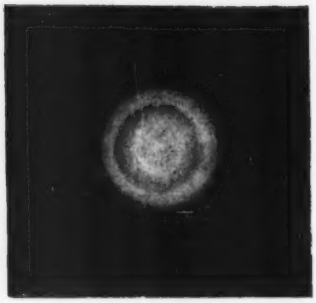

Fig. 1. An electron diffraction pattern of polyurea.

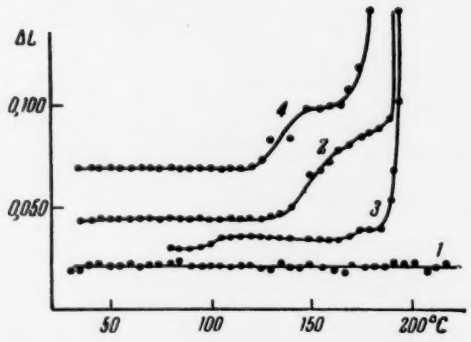

Fig. 2. Thermomechanical curves. 1) Polyurea; 2) copolymer (1:1); 3) a 1:1.6 mixture of the polyurea and the copolymer; 4) a similar 1:4 mixture.

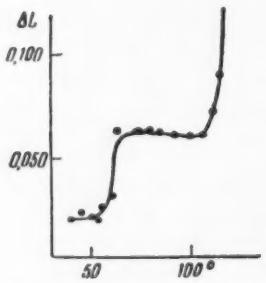

Fig. 3. The thermomechanical curve of polyurea plasticized with cresol.

By increasing the amount of the copolymer to 75% (by weight) we were able to detect both transition points: the flow point T_f and the vitrification point T_v (Fig.2,4). Of course, when such large amounts of copolymer are mixed with the polyurea the copolymer will essentially be responsible for the observed thermomechanical properties of the mixture. However, the plasticizing effects of the copolymer can be shown by comparing the thermomechanical curves of the individual mixture components. If there were no plasticizing action the mixture as a whole would not have exhibited a T_f. From these results one can, in addition, conclude that it is evidently possible to render flexible polymers more rigid by mixing them with fixed amounts of rigid-chain polymers (provided the two are mutually miscible).

In trying to plasticize polyurea with low molecular weight compounds we encountered great difficulties. The problems were connected with the fact that the solubility of this polymer is very limited, even in cresol, and the solubility increases with rise in temperature. We therefore had to use a rather unusual method of plasticizing, which permitted only a qualitative study of its effects. A polyurea tablet was placed in an aluminum cup filled with cresol, kept in this state for 4 hours, and studied on a dynamometric balance under these same conditions. The results of these tests, shown in Fig. 3, demonstrate unequivocally the plasticizing action of cresol on polymers. The experimental results indicate that the transition points of rigid-chain synthetic polymers which have no chemically bonded three-dimensional branches and whose transition points normally lie above the chemical decomposition temperature can be decreased by various plasticizing techniques, and consequently the polymers can be processed into various plastic products.

LITERATURE CITED

[1] V. A. Kargin and T. I. Sogolova, J. Phys. Chem. 23, 530 (1949).

[2] V. A. Kargin and Yu. M. Malinskii, Proc. Acad. Sci. 72, 725 (1950).

[3] V. A. Kargin and Yu. M. Malinskii, Proc. Acad. Sci. 72, 915 (1950).

[4] P. V. Kozlov and E. F. Russkova, Proc. Acad. Sci. 99, 105 (1954).

[5] V. A. Kargin and S. E. Bresler, Acad. Sci. USSR News, 2, 78 (1958).

[6] G. Mark, Chem. Sci. and Industry, 4, 96 (1959).

Received September 1, 1959.

A MECHANISM FOR THE REDUCED HYDRATION RATE OF CALCIUM OXIDE TREATED WITH SURFACE-ACTIVE PLASTICIZERS

S. I. Kontorovich, E. E. Segalova, and Academician P. A. Rebinder

Institute of Physical Chemistry of the Academy of Sciences USSR.
Chair of Colloidal Chemistry at the M. V. Lomonosov Moscow State University

Surface-active agents of the calcium lignosulfanate type (sulfite cellulose brine products, s.c.b.) are used extensively to reduce the hydration rate of calcium oxide during setting [1], thus allowing wet grinding of unslaked lime used for cementing, and also the installation and reinforcement of materials and products derived from lime, without decreasing its ultimate strength. It has heretofore been assumed [2] that the initial hydration step slows down or even ceases entirely when the layers of a compounds adsorbed on the cement grain surface reduce the reaction rate with water by forming high diffusion barriers in intermediate layers.

The experiments described in the present paper showed that the formation of adsorption films on the initial calcium oxide surface constitutes neither the sole nor even the main reason for the rate-reducing effects of the surface-active agents.

The suspensions of portland clinker [3] and tricalcium aluminate [4] previously studied in our laboratory have demonstrated that the compound added to the liquid phase of the suspension is adsorbed on the nuclei of the new structure formed during the hydration of the cement. The formation of an adsorption layer greatly reduces the growth of new nuclei by stabilizing their colloidal dimensions.

The formation of stabilized nuclei will continue until practically the entire surface-active agent is removed from the liquid suspension phase. Only then will there arise nuclei capable of growing and fusing, i.e., of forming a crystal structure. When calcium oxide is hydrated in the presence of some s.c.b., tiny crystalline nuclei of $Ca(OH)_2$, are also formed and are stabilized by the added agent [5,6].

TABLE 1

The $Ca(OH)_2$ Content (g/liter) in the Filtrate Obtained from a 4% Suspension of CaO to which Various Amounts of s.c.b. Were Added.

Filter pore diameter, μ	Time between preparation and filtration of the suspension, min	s.c.b. content in the initial suspensions, g/100 ml of solution				
		0,24	0,36	0,96	1,92	4,0
1—2,5	1—1,5	2,20	2,97	4,34	4,74	5,60
20—25	1—1,5	3,87	4,50	5,00	6,30	6,90
20—25	10	4,02	4,50	6,10	6,9	7,50

In Table 1 we have presented the analytically determined $Ca(OH)_2$ concentrations in filtrates prepared from CaO suspensions and containing various amounts of s.c.b. but having practically identical specific conductances ($k = 18.5\text{-}19.0 \cdot 10^{-3}$ $ohm^{-1} \cdot cm^{-1}$.

It should be noted that the electrical conductance of such filtrates depends almost entirely on the concentration of $Ca(OH)_2$ in solution, since the contribution from the unadsorbed s.c.b. remaining in solution is very small [5].

Table 1 shows that for equal specific conductances (which indicate similar liquid phase compositions) the amount of $Ca(OH)_2$, as determined by titration, increases when more s.c.b. is added, when coarser filter is used, and also when the filtration is delayed. These results could only be explained by assuming that stabilized colloidal $Ca(OH)_2$ particles pass into the filtrate.

The very slow decrease in supersaturation of the filtrates, followed by the decline in the specific conductance (a 3-5% decline in 24 hours), indicates that these filtrates were not supersaturated with $Ca(OH)_2$ extensively enough to form new nuclei, while those already present recrystallized very slowly due to the fact that their surface was blocked with adsorbed layers of the s.c.b.

We can assume that the reduced hydration rate of CaO in the presence of s.c.b. is essentially due to a reduced solution rate of CaO in the highly supersaturated solution; the supersaturation level is maintained by the enhanced solubility of colloidal $Ca(OH)_2$ nuclei, stabilized with the surface-active agent according to Thompson's rule.

Actually, since the solution rate is proportional to the difference between the concentration of a hypothetical calcium oxide solution (maximum supersaturation) and the actual concentration at a given instant, then it is quite obvious that CaO will dissolve much slower in a solution where the high concentration is constantly being maintained with the help of stabilized colloidal $Ca(OH)_2$ particles, than in a simple saturated solution of $Ca(OH)_2$, and consequently the rate of the entire hydration process will be reduced.

To prove that the above-made assumptions were correct it was necessary to investigate the hydration rate of calcium oxide in solutions highly supersaturated with $Ca(OH)_2$, or in other words, in a filtrate containing stabilized $Ca(OH)_2$ nuclei. The final concentration of the unbound surface-active agent should be small enough in such a filtrate that its effects on the hydration rate may be neglected.

The final concentration of s.c.b. in the filtrates was determined with a photoelectric microcolorimeter [7]. The calibration curve was constructed using standard s.c.b. solutions acidified with concentrated HCl; in these the calcium ion concentration was made approximately the same as that in the experimental solutions where the final s.c.b. concentration was determined, since the solution color depends on the calcium ion concentration. The final s.c.b. concentration thus determined in an acidic solution included not only the free s.c.b. in the liquid phase, but also the amount adsorbed on the colloidal particles which had passed through the filter, and was therefore somewhat too high.

The hydration rate of calcium oxide was followed by carrying out the experiments in Dewar flasks and recording the temperature increase produced when a 25% CaO + 75% $CaCO_3$ mixture (the latter was used as an inert filler) were slaked with s.c.b. solutions of various concentrations (0, 0.05, and 0.75g/100 ml of solution) and with colloidal solutions prepared by agitating 1.5 g of CaO in 50 ml of a 0.75% s.c.b. solution for 10 min. The liquid phase of the resulting suspension was separated from solid residue in two ways: it was either filtered through a 2μ pore diameter filter (solution A) or decanted after the larger particles had settled down (solution B). Solutions A and B had identical specific conductances, equal to $18.00 \cdot 10^{-3}$, which corresponds to a solution supersaturated with $Ca(OH)_2$ (for a saturated $Ca(OH)_2$ solution $k = 7.8 \cdot 10^{-3}$) but unsaturated with CaO (for a metastable saturated CaO solution $k = 22.00 \cdot 10^{-3}$). The total $Ca(OH)_2$ and s.c.b. content in solution A was 0.47 and 0.05g/100 ml of solution, respectively, and in solution B 2.8 and 0.75g/100 ml, respectively.

Curves 1 and 2 in Fig. 1 show that the addition of 0.05 g of s.c.b. per 100 ml of solution has very little effect on the rate of CaO hydration. When the mixture is, however, slaked with solution A, which has the same s.c.b. concentration but is highly supersaturated with $Ca(OH)_2$, the hydration rate is reduced (See curve 2, Fig.1). Since the net effects of s.c.b. can be neglected, the reduced hydration rate can only be attributed to the adverse effects of supersaturation on the solution rate of CaO.

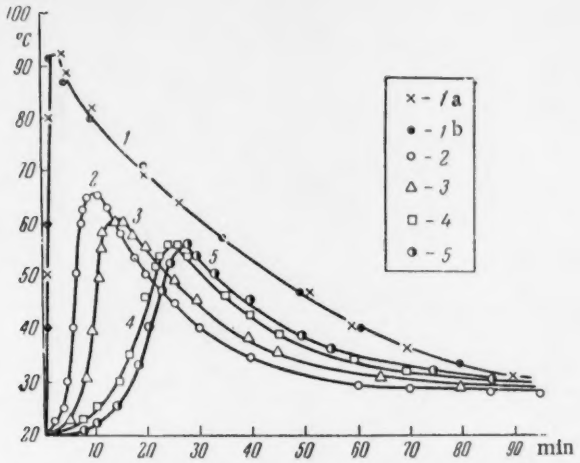

Fig. 1. Temperature changes observed when a 25% CaO + + 75% $CaCO_3$ mixture is slaked with various solutions (V/T = 0.4). 1a) Distilled water; 1b) 0.05% s.c.b. solution; 2) solution A; 3) solution C; 4) solution B; 5) 0.75% s.c.b. solution.

When we add to the mixture solution B having the same specific conductance as solution A but containing many more colloidal particles, the hydration rate decreases much more (Curve 4, Fig. 1) than in the case where solution A was used, and it becomes practically identical with the rate observed when the mixture is slaked with a 0.75% s.c.b. solution (Curve 5, Fig.1). Therefore, the higher the concentration of the colloidal particles (for any fixed initial degree of supersaturation) the longer will the supersaturation be maintained, thus effectively reducing the rate of CaO solution and consequently the rate of the entire hydration process.

If solution B is left standing for 24 hours, the supersaturation level declines as a result of recrystallization and the specific conductance decreases from 18.00 to 14.00 · 10^{-3} although the total $Ca(OH)_2$ and s.c.b. content remains constant. The less-pronounced hydration rate reduction observed when the mixture is slaked with a solution thus aged (solution C, Curve 3 in Fig. 1) underscores the great importance of the absolute magnitude of supersaturation in determining the hydration rate of calcium oxide.

Therefore, we have to assume that the basic cause underlying the retarding action of surface-active plasticizers, such as s.c.b., on the hydration rate of CaO involves the decreased solution rate of calcium oxide in the excessively supersaturated solution; the latter is supported by the stabilized colloidal $Ca(OH)_2$ particles, the growth of which is sharply reduced by the surface-active agent.

LITERATURE CITED

[1] G. I. Logginov, P. A. Rebinder and V. P. Sukhova, Proc. Acad. Sci. 99, No.4 (1954).

[2] Yu. M. Butt and T. M. Berkovich, Cements Containing Surface-Active Agents, Moscow (1953); S. V. Shestoperov, T. Yu. Lyubimova and F. M. Ivanov, Proc. Acad. Sci. 70, No.6 (1956).*

[3] O. I. Luk'yanova, E. E. Segalova, and P. A. Rebinder, Proc. Acad. Sci. 117, No.6 (1957).*

[4] E. E. Segalova, E. S. Solov'eva, and P. A. Rebinder, Proc. Acad. Sci. 113, No.1 (1957).*

[5] E. E. Segalova, S. I. Kontorovich and P. A. Rebinder, Proc. Acad. Sci. 123, No.3 (1958).*

[6] A. M. Smirnova and V. P. Sukhova, Theses presented at the 4th All-Union Conference on Colloidal Chemistry p. 144 (1958) [In Russian].

[7] O. I. Luk'yanova, E. E. Segalova, and P. A. Rebinder, Colloid J. 19, No.1 (1957).

*Original Russian pagination. See C. B. translation.

Received July 31, 1959.

MULTIPLE PHASE INVERSION IN EMULSIONS

L. Ya. Kremnev and L. A. Borodina

The State All-Union Highway Scientific-Research Institute

(Presented by Academician P. A. Rebinder July 9, 1959)

The conversion of a concentrated direct O/W emulsion into an inverted W/O emulsion is usually brought about by altering the properties of the emulsifier, e.g., by replacing a hydrophilic alkali soap with an oleophilic alkaline earth soap, or by using a neutral electrolyte to salt a soap out of an aqueous solution. Most of the experimental work in this field has been carried out on pairs of immiscible liquids of low Newtonian viscosity [1]. Here, breaking results when phase inversion is attempted in maximum concentration emulsions where the bulk concentration is considerably in excess of 74%, the value corresponding to maximum density of packing of identical spheres.

Thixotropic structured liquids behave differently. Asphalts and tars belong to this class of substances, these materials having high effective structural viscosities which diminish sharply as the temperature rises and breakdown of the spatial structures from the kinetic energy of thermal motion becomes extensive. It has been shown earlier that asphalts and tars in the structured liquid state * can form both direct and inverted emulsions (including maximum emulsions of the O/W type), depending on the conditions of emulsification, with full retention of the typical hydrophilic properties of the emulsifier.

This fact makes it possible to carry out multiple phase inversion in these emulsions. A W/O-type emulsion is always formed in the first stage of mixing a structured liquid asphalt with an aqueous solution of a hydrophilic emulsifier. The droplets of the aqueous phase can be stabilized here by the mechanically stable asphalt structure and by oleophilic surface-active substances which may be present in the system.

It is characteristic that such an inverted emulsion is like the asphalt itself in being a viscous structured system, i.e., a spatial network filled with water droplets. The asphalt with its liquid filling is a classic instance of a gel and possesses all of the characteristic properties of the latter, including the ability to undergo syneresis. The maximum concentration of the inverted emulsion depends on the amount of the emulsifier in the aqueous phase, but it is usually well below the limit corresponding to maximum packing density of identical spheres.

Furthermore, an emulsion of the W/O type is formed on mixing with an excess of the aqueous solution of the emulsifier, the concentration of the direct emulsion readily passing to the limiting value with further dispersing of new portions of the asphalt.

The resulting limiting O/W-type emulsion once more goes over into a W/O emulsion when it is agitated with a small excess of the unemulsified asphalt. This completes one phase-inversion cycle which can be repeated n times to give the multiple inversion represented by $(B/W \leftarrow M/B)_n$.

Figure 1 presents results on emulsification and phase inversion which have been obtained with B-5 asphalt and aqueous solutions of various hydrophilic anionic and cationic active emulsifiers at 20°, the asphalt being in the structured liquid state.

---

* All brands of asphalt will pass from the solid form into the structured liquid state at temperatures in excess of 40° [2], and the less viscous types, such as B-5, are structured liquids even at ordinary temperatures.

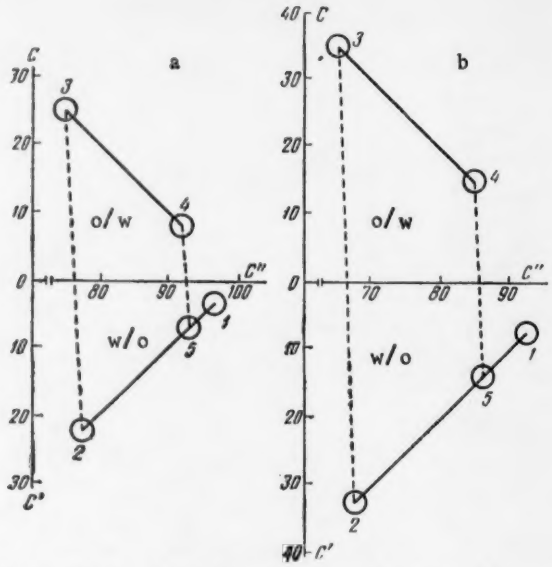

Fig. 1. Cycle of multiple phase inversion in emulsions: a) in inverter A; b) in sulfo-alcholic liquor.

There was no particular difficulty in carrying out repeated inversions of 5-6 cycles, and this number could be increased at will since it was limited by the volume of the vessel alone. Elevated temperatures were used in emulsification and phase inversion of the viscous asphalt in order to insure that the latter be in the structured liquid state. Similar results were obtained with tars.

Different mechanisms are involved in the phase inversion of direct and inverted emulsions. The asphalt drops of the limiting direct emulsion are deformed into pentagonal dodecahedra which are separated by extremely thin films of the aqueous solution and thereby kept from coagulating. On the basis of the complete differential curves showing the distribution of droplets over dimensions, we have concluded that the minimum critical depth of the protective films in the limiting asphalt emulsions is of the order of 10^{-6} cm. The continuous spatial structure of extremely thin protective aqueous films has low stability [3] and can be readily broken mechanically by mixing the limiting emulsion with a small excess of the unemulsified asphalt. The action of the molecular forces of surface tension causes the separate water films to take on the form of microscopic spherical droplets when the network breaks. These droplets are then incorporated in the voids of the continuous spatial network which once more develops from coalescence of the unprotected asphalt drops. Thus an inverted emulsion is formed from the direct emulsion. The theory of Academician P. A. Rebinder [4] indicates that the stability of the inverted emulsion is fixed by the universal structural-mechanical barrier, especially with hydrophilic emulsifiers of high concentration. The concentration of the inverted emulsion which is produced in the phase inversion can be increased somewhat by mixing with additional portions of the aqueous solution of the emulsifier.

Such a W/O emulsion is a gel-like system of asphalt filled with water droplets and it can be dispersed under favorable conditions in an excess of aqueous solution of the emulsifier with inversion and production of a stable direct emulsion.

LITERATURE CITED

[1] V. Clayton, Emulsions, translated from the English under the Editorship of Academician P. A. Rebinder, Foreign Lit. Press, 1950.

[2] N. V. Mikhailov and S. Ya. Shalyt, Colloid J., 18, 609 (1956).*

*Original Russian pagination. See C. B. translation.

[3] L. Ya. Kremnev and S. A. Soskin, Colloid J., 11, 24 (1949).

[4] P. A. Rebinder, Colloid J., 20, 527 (1958).*

Received June 11, 1959.

*Original Russian pagination. See C. B. Translation.

A THERMODYNAMIC STUDY OF THE KBr–RbBr–H_2O SYSTEM AT 25°

L. L. Makarov and G. S. Popov

The A. A. Zhdanov State University, Leningrad

(Presented by Academician A. N. Terenin June 22, 1959)

The free energy of formation of KBr–RbBr–H_2O solid solutions was evaluated in the present work by developing the 25° solubility isotherm in the KBr–RbBr–H_2O system and measuring the pressure of water vapor above ternary solutions. The apparatus and the analytical procedure which were employed here were similar to those described in [1]. The activity coefficients for the components in the various phases were calculated through the following equations:

The Storonkin-Shul'ts Equation [2, 3]

$$\lg f_i^{(\$)} x_i^{(\$)} = \int \varphi(x)\, x_n^{(\$)} d \lg a_{H_2O}, \tag{1}$$

in which $\varphi(x) = \frac{x_{H_2O}^{(1)}}{x_i^{(\$)} x_n^{(1)} - x_n^{(\$)} x_i}$, f is the activity coefficient, x is the mole fraction, and the integral is evaluated for alteration of composition along the solubility isotherm.

The McKay-Perring Equation [4]

$$0{,}036 \lg \frac{m\gamma_i}{M_i \Gamma_i} = \int_0^{\lg a_{H_2O}} \left\{ x_n' \left[\frac{\partial \left(\frac{1}{m} \right)}{\partial x_n'} \right]_{a_{H_2O}} - \frac{1}{m} + \frac{1}{M_i} \right\} d \lg d_{H_2O}, \tag{2}$$

in which m is the total molar concentration of electrolytes ($m = m_i + m_n$), γ_i is the activity coefficient of the i-th component of a ternary solution in which the water activity is fixed at a_{H_2O}, and M_i and Γ_i are, respectively, the molarity and the activity coefficient of this component in a pure aqueous solution in which the water activity is also a_{H_2O}. The integral is evaluated for alteration of composition along a section $x_n' = m_n/m = \text{const}$.

The results of [5] are in good agreement with those of the present work (Table 1) and they have therefore been used in the calculations.

The isothermal vapor pressure, p_{H_2O}, curve for the saturated KBr–RbBr solutions is smooth and has a minimum at the congruent point (D = 1) where the solubility m is a maximum, just as required by theory [2].

An isothermal - isotonic study of the ternary solutions (T, a_{H_2O} = const, x_n' variable) leads to a linear relation, exact to within 0.2%, between $1/m$ and x_n':

$$\frac{1}{m} = \frac{1}{M_i} + \alpha x_n', \tag{3}$$

α being the slope.

TABLE 1

$x^{(s)}_{RbBr}$	Liquid phase composition			$D_{Rb,\ KBr}$*	p_{H_2O}
	m_{RbBr}	m_{KBr}	m		
$\sim 10^{-6}$	$\sim 10^{-5}$	5,748	5,748	0,404	19,178
0,059	0,842	5,268	6,110	0,391	18,987
0,214	2,233	4,427	6,660	0,540	18,673
0,319	2,936	3,972	6,908	0,633	18,523
0,326	3,054	3,903	6,957	0,674	18,505
0,400	3,331	3,689	7,020	0,738	18,455
0,425	3,528	3,576	7,104	0,750	18,436
0,433	3,681	3,354	7,035	0,697	18,420
0,512	3,882	3,260	7,142	0,882	18,417
0,529	3,838	3,348	7,186	0,979	18,417
0,533	4,061	3,120	7,181	0,878	18,417
0,646	4,360	2,702	7,062	1,133	18,431
0,757	4,912	2,116	7,028	1,341	18,483
1,00	6,737	$\sim 10^{-3}$	6,737	—	18,884

*Coefficient of crystallization. $D = \dfrac{x^{(s)}_{RbBr}\, m^{(l)}_{KBr}}{x^{(s)}_{KBr}\, m^{(l)}_{RbBr}}$.

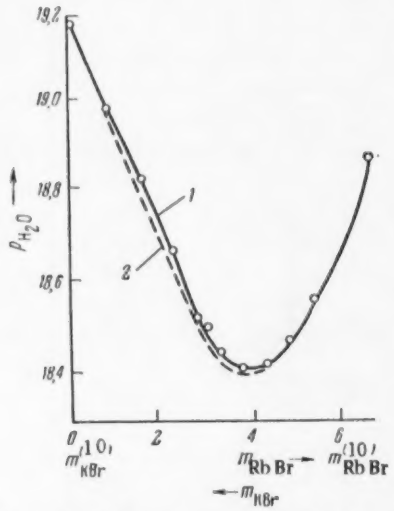

Fig. 1. Isothermal curve showing the vapor pressure of water above solutions saturated with respect to mixtures of KBr and RbBr at 25°: 1) results from direct isotonic measurements; 2) values of p_{H_2O} obtained from Equation (3).

The broken curve of Figure 1 covers values of p_{H_2O} which were obtained from Equation (3) by extrapolation over narrow intervals. The agreement between the two curves is good. These curves were used in evaluating p_{H_2O} for solutions in which the solid phase composition was known and led to the results given in Table 1.

Equation (1) was not used for concentrations lying in the interval $0.42 < x^{(s)}_{RbBr} < 0.65$ since the integral function $\varphi(x)\, x^{(s)}$ is very sensitive to experimental errors within this range ($\varphi(x) \to \pm\infty$ when $D \to 1$).

Condition (3) reduces the McKay-Perring Equation to

$$\left[\frac{m\gamma_i}{M_i\Gamma_i}\right]_{a_{H_2O}} = 1. \qquad (4)$$

The activity coefficients are given in Table 2. There is good agreement between the results which were obtained by the various methods. This fact is illustrated by Figure 2 which shows the relation between $f^{(s)}_{RbBr}$ and the composition of the solid solution. A maximum appears on the $f^{(s)}_{RbBr}$ curve at a low value of $x^{(s)}_{RbBr}$, just as in the case of KCl–RbCl solutions [6]. It is scarcely likely that this can be the result of experimental error, for the error in the determination of $f^{(s)}_{RbBr}$ at any one concentration is less than 2% and has only slight effect on the calculated results. The form of the $f^{(s)}_{RbBr}$ curve in the neighborhood of $x^{(s)}_{RbBr} = 1$ is such as to indicate the existence of a similar maximum on the $f^{(s)}_{KBr}$ curve. Nevertheless, the mean of values obtained from Equations (1) and (4)* was used in calculating $f^{(s)}_{KBr}$ from the Gibbs-Duhem Equation. Small variations in $f^{(s)}_{i}$ have very little effect on the value of ΔZ.

*$f^{(s)}_{KBr}$ cannot be determined directly from Equation (4) because of the large error which is involved in extrapolating M_{KBr} and Γ_{KBr}.

TABLE 2

Activity Coefficients for RbBr and KBr at 25°

$x^{(s)}_{RbBr}$	m_{RbBr}	m_{KBr}	Activity coefficients				
			γ_1, from Equa. (4), M.-P.	γ_1, from Equa. (1), S.-S.	f_1, from M.-P.	f^*_{RbBr}, from Equas. (1)(4)	f_{KBr}
$\sim 10^{-6}$	$\sim 10^{-5}$	5,748	0,564	—	2,18	2,18	1,00
0,068	1,030	5,162	0,557	0,496	2,41	1,95	1,00
0,206	2,210	4,430	0,549	0,523	1,78	1,66	1,03
0,336	3,080	3,850	0,542	0,527	1,54	1,48	1,08
0,422	3,526	3,535	0,537	0,530	1,40	1,38	1,12
0,512	3,860	3,260	0,535	(0,535)*	1,27	1,27	1,20
0,533	4,010	3,120	0,534	(0,534)*	1,26	1,26	1,22
0,655	4,490	2,625	0,534	(0,534)*	1,15	1,15	1,40
0,716	4,735	2,370	0,533	0,534	1,10	1,11	1,52
0,779	5,047	2,030	0,532	0,534	1,07	1,08	1,65
0,814	5,285	1,765	0,531	0,534	1,05	1,06	1,78
0,861	5,475	1,545	0,529	0,534	1,03	1,04	2,01
0,884	5,620	1,380	0,527	0,532	1,02	1,04	2,01
0,899	5,505	1,510	0,524	0,540	0,974	1,03	2,17
1,00	6,74	$\sim 10^{-3}$	0,514	0,514	1,00	1,00	—

*Values obtained from Equation (4).

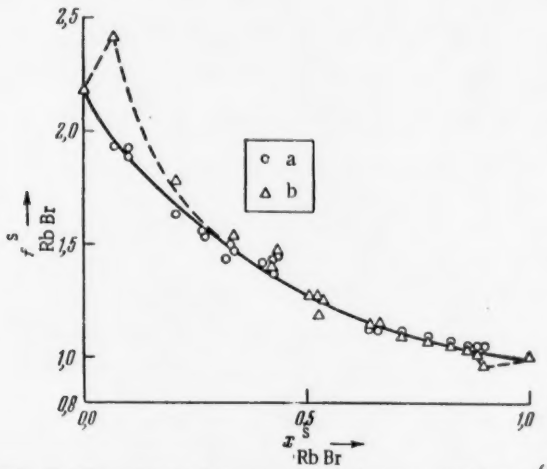

Fig. 2. The relation between the activity coefficient, $f^{(s)}_{RbBr}$, and the composition of the solid solution: a) results obtained from Equation (1); b) results obtained from Equation (4).

Table 3 gives values of the unavailable energy, $T\Delta S$, and the change in free energy, ΔZ, and enthalpy, ΔH, the principal thermodynamic functions, for formation of KBr–RbBr solid solutions from the pure salts at 25°. Experimental values of ΔH are not available; the table contains values from Durham and Hawkins [7] and other values which we have calculated from the fourth-approximation equation of the Wasastjerna statistical theory [8] which is generally capable of reproducing the experimental results to within the limits of error [9,10]. Only values based on [8] were used in the calculation of $T\Delta S$ and the results obtained are no more than provisional.

TABLE 3

x_{RbBr}	$-\Delta Z$	ΔH		$T\Delta S$	$T\Delta S$ from [11]	$T\Delta S$ from the Stirling equation
		from [7]	from [8]			
0,1	150	36	81	234	190	194
0,2	222	—	135	357	288	295
0,3	260	84	166	428	345	361
0,4	280	—	180	462	374	400
0,5	283	100	182	466	384	412
0,6	270	—	176	448	376	400
0,7	242	82	159	403	347	361
0,8	202	—	126	326	289	295
0,9	132	36	176	207	191	194

The Stirling Equation and the Wasastjerna-Hovi Theory [11] were used in obtaining values of $T\Delta S$ from ΔH and ΔZ. The error in ΔS is clearly less than 5 % and it can therefore be concluded that KBr—RbBr solid solutions are not regular, despite suppositions to the contrary in [7]. The relation between the ΔS values from the various theories is entirely analogous to that which numerous investigators have observed earlier in KCl—NaCl [12], KCl—KBr [13], etc., solid solutions, and obviously results from the presence of a certain number of Schottky defects.

LITERATURE CITED

[1] A. P. Ratner and L. L. Makarov, J. Phys. Chem., 32, 1809 (1958) [USSR].

[2] A. V. Storonkin and M. M. Shul'ts, Herald, Leningrad State University, 11, 153 (1954).

[3] A. V. Storonkin, M. M. Shul'ts, and T. P. Makarova, J. Phys. Chem., 32, 10 (1958) [USSR].

[4] H. A. C. McKay, and J. K. Perring, Trans. Farad. Soc., 49, 362, 163 (1953).

[5] G. S. Durham , E. J. Rock and J. S. Frayn, J. Am. Chem. Soc., 75, 23, 5792 (1953).

[6] A. P. Ratner and L. L. Makarov, J. Inorg. Chem., 3, 46 (1958) [USSR].

[7] G. S. Durham and J. Hawkins, J. Chem. Phys., 19, 2 (1951).

[8] J. Wasastjerna, Soc. Sci. Fenn. Comm. Phys. Math., 15, 3 (1951).

[9] V. Hovi, ibid., 15, 3 (1951).

[10] B. W. Lister and N. F. Meyers, J. Phys. Chem., 62, 2, 145 (1958).

[11] V. Hovi, Soc. Sci. Fenn. Comm. Phys. Math, 15, 15 (1950).

[12] W. T. Barret and W. E. Wallace, J. Am. Chem. Soc., 76, 2, 370 (1954).

[13] W. H. McCoy, W. E. Wallace, J. Am. Chem. Soc., 78, 23, 5995 (1956).

Received June 16, 1959.

A COMPARATIVE STUDY OF INDUCED CONDUCTIVITY AND FREE RADICALS IN THE RADIOLYSIS OF SOLID PARAFFIN

V. L. Tal'roze and E. L. Frankevich

The Institute of Chemical Physics of the Academy of Sciences of the USSR

(Presented by Academician V. N. Kondrat'ev July 10, 1959)

The mechanism of the free-radical formation is one of the principal problems of radiation chemistry and one which has assumed added significance in connection with the production of "frozen" radicals through irradiation. It has become the custom to refer in the literature to radicals of "ionizational" or "nonionizational" origin. The first of these terms is generally used to designate radicals arising from recombination of the charged particles which are produced by the radiation. In addition to recombination, these ion-molecule reactions can also play a vital role in the formation of free radicals. The significance of these reactions has found expression in the Lind hypothesis [1] and has been fully confirmed by the present authors [2, 3], by Stevenson and his co-workers [4], and by Field, Franklin, and Lampe [5]. This work has demonstrated the exceptional chemical activity of ions in the gaseous phase.

There is no doubt that gas-phase radicals of "ionizational" origin are accompanied by other radicals arising from the direct dissociation induced by electron impact. The most recent evidence on this point has been obtained by Firestone [6]. Differences in regard to energy-transfer processes, the presence of "cell" effects, and the thermodynamics of charged particles all undoubtedly lead to vital distinctions in the genesis of free radicals and ions in condensed and in gaseous phases. Less energy is required for ionization in a condensed phase than in a gaseous phase. It can be supposed that a first approximation to the ionization potential of a molecule in a condensed phase would be given by [7]: $I_c = I - 2E$, I being the ionization potential in the gaseous phase, and E, the polarization energy. Measurements on the temperature dependence of the electrical conductivity of solid hydrocarbons give an activation energy of ~0.5 - 1.1 ev [8,9]. This would correspond to an ionization energy of 1-2.2 ev, if it is assumed that the temperature variation is determined by the ionization step, and that the recombination of the current carriers follows a second-power law. The ionization potential of such a substance in the gaseous phase is, on the other hand, 6-10 ev. Thus the observed diminution in the ionization energy is quite large in every case, even though it cannot always be described by the equation $I_c = I - 2E$; it should be noted further that the polarization energy can scarcely be evaluated with accuracy since it is quite sensitive to a number of factors which are known only imperfectly for substances of this kind.

As far as we know, attention has not yet been turned to the fact that the diminution of the ionization potential in a condensed phase can entail a sharp reduction in the probability of free radical formation through recombination of ion pairs, a process which is very significant to gas phase* radiolysis. Thus an ion pair whose energy of formation was, for example, 2 ev would not liberate enough energy in recombining to break most bonds. Analysis also shows passage from the gaseous to the condensed phase to be accompanied by a decrease in the heat of reaction for ion-molecule processes, many of these reactions being exothermic in the gaseous phase and endothermic in condensed phase.

Thus it might be supposed that the basic elementary reaction involved in free-radical formation by radiolysis of a condensed phase would be the direct rupture of a bond with the production of two neutral particles, or one neutral particle and one charged particle. It is to be noted, on the other hand, that the cell effect frequently leads to preferential break off of the H atom from compounds which contain this element.

*We have assumed at the outset of this study that the free radicals which are formed in the radiolysis of a condensed phase are largely of ionizational origin [12].

The authors have attempted to find an experimental approach to the problem of ion-radical "interaction" in the radiolysis of a condensed phase. The EPR method was used here for a combined study of the conductivity induced in solid paraffin by a beam of high-speed electrons, and the generation and breakdown of free radicals.

The melting point of the paraffin was 52-55°C, and corresponded to approximate maximum content of the C_{28} alkanes. It is clear that this paraffin did not contain easily ionizable substances, since the temperature dependence of its "dark" conductivity was somewhat more marked than was the case with the very pure paraffin studied by Ril' [8].

The electrical conductivity was measured by fusing aluminum foil electrodes, 30μ in thickness, into a paraffin cylinder which was 3 mm long and 10 mm in diameter. The area of that portion of the electrodes which was sealed in the paraffin was 5×3 mm^2, and the electrodes were separated from one another by 1 mm. The test specimen was set into a cylindrical container through which nitrogen (from evaporation of the liquid out of a Dewar flask) was passed. The nitrogen reached this container by passing through a brass tube whose temperature was fixed by a spiral winding. The temperature of the specimen could be varied from -120 to + 50°C. The temperature was measured by a thin thermocouple which was inserted in the space between the electrodes.

A potential difference, V, of 1000 volts was applied to the electrodes of the specimen, and the current flow then measured on an ÉPP-09 recording potentiometer after being fed through an EMU-2 electrometric amplifier. This arrangement was used in measuring both the "dark" conductivity and the conductivity of specimens which had undergone preliminary irradiation. Irradiation with 1.6 Mev electrons at the temperature of liquid nitrogen and in an atmosphere of nitrogen was carried out on the cascade generator of the Institute of Chemical Physics of the Academy of Sciences of the USSR. Decelerated electrons which had fallen on a lead target were used in direct measurement of the conductivity under irradiation.

The specimens were inserted in the EPR apparatus of the Institute of Chemical Physics of the Academy of Sciences of the USSR [10] after preliminary irradiation with high-speed electrons and making of simultaneous measurements of the conductivity and the electron paramagnetic resonance spectra, with the resonator set directly at the point where the electron beam left the accelerator. Each specimen had the form of a cylinder, 4 mm in diameter, into which copper electrodes, 3 mm wide and separated by 1.5 mm, and a fine thermocouple, were sealed. The specimen was placed inside the resonator. The temperature of the specimen could be varied from +150 to -100°C by blowing a stream of heated or cooled nitrogen over it.

The conductivity of the paraffin was increased by irradiation with x-rays, just as was anticipated.

The conductivity fell under the action of the electron beam at temperatures in the interval 77-250°K, the time of fall being less than the time constant of the electrometric circuit (0.5 sec). This same rapid decrease in the conductivity was also observed at higher temperatures when the beam was first turned on, but this was followed by a more gradual diminution. The higher the temperature of the specimen, the smaller the proportionate decrease in the induced conductivity during the time of this "rapid" diminution (Fig. 1).

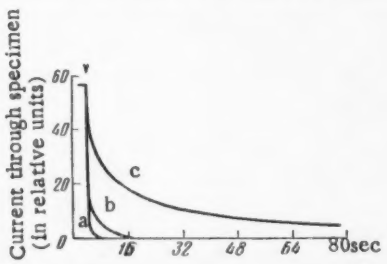

Fig. 1. The decrease in the conductivity of paraffin when the beam was quickly turned on (the arrow indicates the instant at which the electron beam was turned on): a) decrease at 113°K; b) at 213°K, c) at 300°K.

Experiments were carried out in which the paraffin was first given a preliminary irradiation with high-speed electrons at 77°K and its conductivity then measured as it warmed up. A "flare-up" effect was observed under these conditions, the conductivity becoming pronounced many degrees below the point at which ordinary "dark" conductivity would appear on heating an unirradiated specimen, and then falling to the dark value with further heating (Fig. 3, b). This flare-up in the conductivity was not observed when the specimen was subjected to a second cooling and heating. The gradual fall in the value of σ after breaking off irradiation which we have observed in paraffin has also been noted in polyethylene by Fowler [11].

It would seem that our experiments in which the conductivity and the EPR spectra characterizing the free radical content of the specimen were simultaneously recorded would be vital to an understanding of the flare-up effect in the conductivity.

The results show the temperature-time region (the tempeature and the time alter simultaneously) associated with the conductivity flare up to be exactly that in which there is a diminution in the intensity of the EPR spectra. An arbitrarily selected EPR spectrum from these experiments is shown in Fig . 2. The line intensities in this spectrum correspond to an alkyl radical of the type a ~~$\overset{H}{\underset{H}{C}}-\overset{|}{\underset{H}{C}}-\overset{H}{\underset{H}{C}}$~~.

Fig.2. EPR spectrum for irradiated paraffin, recorded at 180° K.

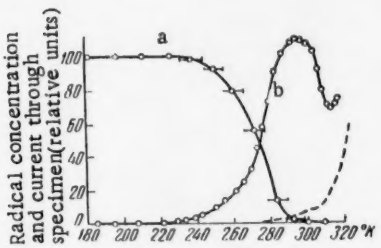

Fig. 3. The alteration in the radical concentration and conductivity of irradiated paraffin during heating. Heating rate; 22°/min. a) Radical concentration, in arbitrary units; b) relative alteration of the current through the specimen with a potential of 1000 volts on the electrodes. The broken curve shows the alteration of the dark conductivity of the specimen.

The curves of Fig.3 show the temperature variation of the conductivity and free radical content of the irradiated specimen. There is a large error in the value of the temperature, but this is due to the temperature gradients which arise invariably when a specimen is rapidly heated, and is not the result of inaccuracies in the measurements. The authors advance the following explanations for the effect in question: 1. The flare-up in the conductivity arises from thermal ionization of radicals while the decrease in the conductivity is due to loss of these ions. 2. The flare-up in the conductivity is due to local evolution energy during recombination of radicals. This energy (~ 3 -4 ev) is more than adequate for formation of ions if the ionization energy is actually as low as the data on the thermoelectrical conductivity of the paraffin (1.1-1.5 ev) would indicate. Both the flare-up in the conductivity and the loss of radicals are due to the acceleration of the diffusional movement of each type of particle in the lattice as the temperature rises.

The experiments which have been carried out clearly do not justify a choice between these mechanisms. It is obvious, however, that an attempted solution of this problem must take account of experiments on the diminution of conductivity after cutting off the radiation. Thus Curve c of Figure 1 has been obtained at 300° K where the life of the radicals in the paraffin is measured in seconds, or fractions of a second. There are practically no radicals present during the many seconds which are covered by the portion of the curve on which the conductivity is falling, and here it is a matter of a comparatively slow recombination of the ions.

It is interesting to note that there is approximately the same rate of diminution in the conductivity at the same temperature beyond the maximum "flare-up" (Fig.3). Is it possible that this is a definite indication that charge migration is a slow process in which barriers must be surmounted? Such may indeed be the case, though not necessarily so, since it can be a simple matter of a very low ion concentration. Thus the "life-time" of the ions, τ, will be of the order of 10 sec if recombination is assumed to be a second-order process in which the velocity constant, k, is equal to 10^{-10} cm^3/sec and the ion concentration is $\sim 1k/\tau = 10^9$ ion/cm^3. Such a concentration would lead to a conductivity of $\sim 10^{-13}$ $ohm^{-1} \cdot cm^{-1}$ if the charge mobility is assumed to be $\sim 10^{-3}$ $cm^2/v \cdot sec$, a reasonable figure if the effective transfer mass is that of a hydrated ion or proton.

Acceptance of either of the first two proposed mechanisms would lead to the basic conclusion that the production of free radicals can lead to formation of ions in solid or liquid substances which are undergoing radiolysis, or have undergone radiolysis. The sharp decrease of the ionization energy in a condensed phase, as compared with the gaseous phase, can thus lead to an interesting "inversion" of the relation between formation of ions and radicals: a) free radicals are

produced in large measure by ion reactions when radiolysis takes place in the gaseous phase; b) ions are products of free radical reactions when radiolysis occurs in a condensed phase.

It would seem that these conclusions might be of significance, not only for radiation chemistry, but possibly for the general chemistry of numerous reactions which proceed through radicals and ions.

We wish to express our indebtedness to Academician V. N. Kondrat'ev for valuable discussions, to G. I. Krivonosov and V. N. Shamshev for their aid in obtaining the EPR spectra, and to the members of the High-Voltage Group for carrying out the irradiations.

LITERATURE CITED

[1] S. C. Lind, and D. C. Bardwell, J. Am. Chem. Soc., 48, 2335 (1926).

[2] V. L. Tal'roze and A. K. Lyubimova, Proc. Acad. Sci. USSR, 86, No.5, 909 (1952).

[3] V. L. Tal'roze and E. L. Frankevich, Proc. First All-Union Conference on Radiation Chemistry,1957, Moscow, 1958.

[4] D. P. Stevenson and D. O. Schissler, J. Chem. Phys., 23, 1353 (1955).

[5] F. H. Field, J. L. Franklin,and F. W. Lampe, J. Am. Chem. Soc., 78, 5697 (1956).

[6] R. F. Firestone, J. Am. Chem. Soc., 79, 5593 (1957).

[7] L. E. Lyons, J. Chem. Soc., 1957, No.12, 5001.

[8] N. V. Ril', J. Phys. Chem., 29, 959 (1955).

[9] D. C. Northrop and O. Simpson, Proc. Roy. Soc., 234, 124 (1956).

[10] Yu. N. Molin, A. T. Koritskii, et al, Proc. Acad. Sci. USSR, 123, No.5, 882 (1958); A. G. Semenov and N. N. Bubnov, Inst. and Exp. Tech. No.1 (1959)[USSR].

[11] J. F. Fowler, Proc. Roy. Soc., 236, 464 (1956).

[12] V. L. Tal'roze, Bull. Acad. Sci. USSR, Div. Chem. Sci., 1959, No.2, 369*.

Received July 1, 1959.

*Original Russian pagination. See C. B. translation.

THE ISOTHERM FOR THE ADSORPTION OF THE TETRABUTYL-AMMONIA CATION ON MERCURY

Academician A. N. Frumkin and B. B. Damaskin

Measurement of the differential capacity is one of the principal methods of studying the adsorption of a surface active organic substance at an electrode/solution interface [1-4]. The extent of coverage of a surface by an adsorbed material, θ, has been evaluated in a number of papers [5-7] through the equation

$$C = C_0(1 - \theta) + C'\theta, \tag{1}$$

in which C_0 and C' designate, respectively, the differential capacity at $\theta = 0$, and at $\theta = 1$. Parsons [8] has expressed doubt as to the applicability of Equation (1) for determining θ, since the capacity C is not, in general, a linear function of θ. Frumkin has claimed [9] that the adsorption is linearly related to the surface charge through

$$\varepsilon = \varepsilon_0(1 - \theta) + \varepsilon'\theta, \tag{2}$$

where ϵ_0 and ϵ' designate, respectively, the surface charge at $\theta = 0$, and at $\theta = 1$. Equation (3.7) of [8] shows that the assumption of constancy of ϵ_0 and ϵ' is not strictly valid, though the errors resulting from it are not large. Equation (2) leads to

$$C = C_0(1 - \theta) + C'\theta + (\varepsilon' - \varepsilon_0)\frac{d\theta}{d\varphi}, \tag{3}$$

in which φ is the electrode potential. The last member of this equation is the pseudocapacity, a quantity which is related to the adsorption - desorption process. Neglect of this member is the principal cause of the breakdown of Equation (1). This equation should be approximately valid in the region of maximum adsorption where $d\theta/d\varphi \approx 0$. It can be applied at potentials under which an organic material is desorbed from the electrode surface if use is made of the capacity values which have been determined at infinitely high current frequency [2], where the member containing $d\theta/d\varphi$ reduces to zero.

Data on the differential capacity have been used in the present work to study the relation between the concentration, c, and the degree of surface coverage by tetrabutylammonia (TBA) cations through Equation (1). The pseudocapacity proves to be insignificant at the low $[(C_4H_9)_4N]I$ concentrations and relatively high current frequencies (ν = 10,000 kc) which were employed here [2] so that this factor introduced only slight distortion into θ vs c curves when extrapolating the capacity to $1/\sqrt{\nu} \to 0$ and it cannot therefore have affected the conclusions.

Frumkin has indicated [9] that S-shaped θ vs c curves are to be expected in the adsorption of organic materials of sufficiently high molecular weight, these curves being represented by the equation

$$Bc = \frac{\theta}{1 - \theta} e^{-2a\theta}, \tag{4}$$

in which B and a are constant when φ = constant. The value of a is fixed by the van der Waals' attraction between the adsorbed particles. We have shown earlier [10] that supporting anions are dragged into the electrical double layer during adsorption of TBA cations from 1 N solutions of KCl, KBr, and KI, thus increasing the attraction between the adsorbed organic cations and diminishing the repulsion between the free cation charges.

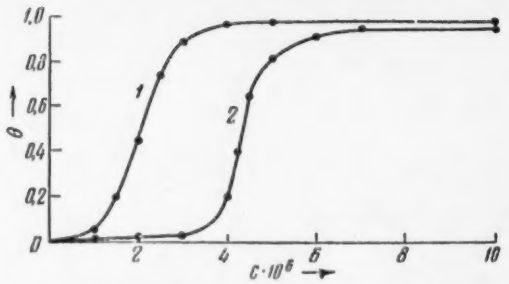

Fig. 1. Isotherms for adsorption of TBA cations out of a 1 N KI solution: 1) φ = -1.1 v; 2) φ = — 1.2 v (SCE); t = 2.5 min; 25°.

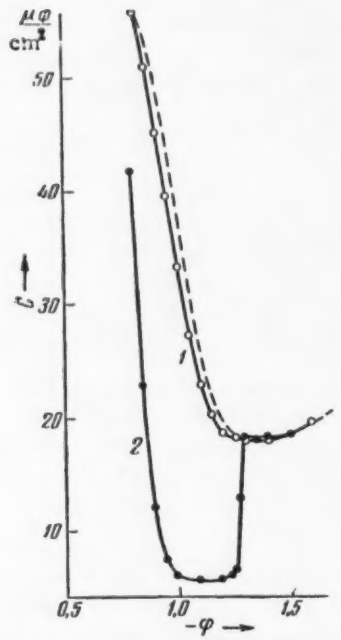

Fig. 2. Curves showing the differential capacity in a 1 N KI + 10^{-5} N $[(C_4H_9)_4N]I$ solution: 1) t = 4 sec; 2) t = 2.5 min; the dashed curve is for 1 N KI. 10 000 kc; 25°.

Figure 1 shows isotherms for the adsorption of TBA cations out of a 1 N KI solution which were obtained from the capacity of a hanging mercury droplet electrode. These capacitances were measured 2.5 minutes after forming a clean mercury surface, using the impedance bridge circuit which has been described earlier in [11]. It is to be noted that this time is inadequate for establishing full adsorptional equilibrium at these low $[(C_4H_9)_4N]I$ concentrations and these isotherms are, therefore, not entirely reversible.* Figure 1 shows the adsorption isotherms to have the S-form even in the region of maximum adsorption (φ = -1.1; -1.2 v against SCE), this characteristic becoming still more pronounced as the potential is increased in the negative direction. These observations are in accord with theory [9], for the latter indicates that the variation of the surface area per adsorbed molecule with potential is such that the attractive constant a of Equation (4) must be increased, and the S-form of the isotherm become more pronounced, as the surface potential is made more negative.

Figure 2 gives capacity curves which have been developed for a hanging droplet electrode (t = 2.5 min), and a dropping electrode (t = 4 sec)**, in a 1 N KI + + 10^{-5} N $[(C_4H_9)_4N]I$ solution. These curves indicate that the number of TBA ions adsorbed here depends markedly on the time, t, which elapses after forming the clean mercury surface. It is for this reason that the θ vs c curves obtained from the data on the capacity of the dropping electrode in the potential region of maximum adsorption differ from similar curves obtained for the hanging mercury drop. Thus the θ, c relation for the dropping electrode at φ = = -1.0; -1.3 v (SCE) can be represented in a first approximation by two straight lines, one issuing at an angle from the origin of coordinates and the other corresponding to θ = 1 (Fig.3). The θ, c relation which we have developed from the Ilkovic Equation ***

$$\theta = \frac{\Gamma}{\Gamma_m} = 0{,}627\frac{D^{1/2}m^{2/3}t^{1/6}c}{S\Gamma_m} = 1{,}545\cdot 10^4 c, \qquad (5)$$

* Longer time intervals were not employed because they led to an obscure capacity–time relation, the capacity passing through a minimum without reaching a limiting value even after agitation for an hour. This effect is possibly due to some sort of gradual change in the TBA, and calls for further study.

** The capacity of the dropping electrode was measured by a procedure which was only slightly different from that described by Grahame [12].

*** m = 1.68 mg/sec, S = 0.03 cm², and t = 4 sec, under the experimental conditions. The diffusion coefficient, D, was obtained from the Nernst Equation and the mobility of the TBA cation, while the maximum adsorption, Γ_m, was evaluated from the cation dimensions. This led to $D = 5.18 \cdot 10^{-6}$ cm² /sec and $\Gamma_m = 2.17 \cdot 10^{-10}$ moles/cm².

gave a good representation of the curve obtained experimentally at φ = -1.0 v (Fig. 3). This result indicates that the adsorption of TBA cations on the dropping electrode is almost completely determined at these potentials by the number of ions which are able to diffuse to the mercury surface. Our data are in agreement with the conclusions of Delahay and Trachtenberg [5], but stand in contradiction to the results of Laitinen and Mosier [7].

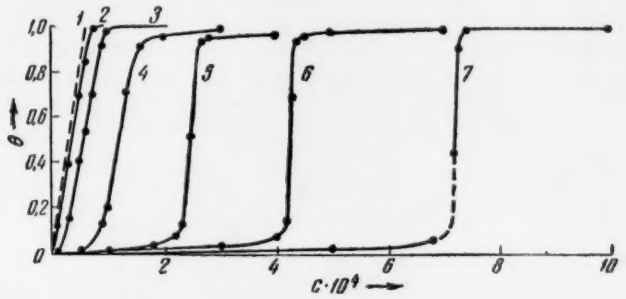

Fig. 3. Isotherms for the adsorption of TBA cations from 1 N KI: 2) φ = - 1.0 v; 3) φ =-1.3 v; 4) φ =-1.4 v; 5) φ=-1.47 v; 6) φ = =-1.50 v; 7) φ=-1.53 v (SCE). t =4 sec; 25°. Line 1 was developed from the Ilkovic Equation.

The adsorption of large organic cations on a mercury surface diminishes at more negative potentials, just as does the adsorption of neutral molecules, despite the electrostatic attraction [13]. It is then necessary to increase the $[(C_4H_9)_4N]$ I concentration in order to obtain a given degree of coverage. The diffusional current of TBA cations to the mercury surface is increased thereby and the adsorption isotherm becomes more nearly reversible. At c = $4 \cdot 10^{-4}$ N, the number of TBA ions which are transported to the surface of the mercury drop by a 4 second diffusional current is sufficient for the formation of approximately six monolayers. Figure 3 shows that the θ, c curve takes on the characteristic S-form under these conditions. The interaction between the adsorbed ions finally becomes so large at still more negative potentials that the value of θ alters abruptly with increase in c. This confirms the hypothesis which was advanced earlier to the effect that there is a definite potential at which abrupt breakdown occurs in the adsorption layer formed by the interaction of TBA cations which experience an additional bonding through iodide ions [10].

The applicability of the Frumkin Theory [9] to the adsorption of surface active cations was checked by establishing the relation between the electrode potential and the TBA adsorption. The addition of small amounts of $[(C_4H_9)_4N]$ I to 1 N KI leads to only a minute displacement in the null-charge potential (NCP) so that the theory of [9] with θ = 0.5 gives

$$\ln \frac{c}{c_n} = \frac{1}{RT\Gamma_m} \frac{C_0 - C'}{2} \varphi_a^2, \qquad (6)$$

φ_a being the electrode potential measured with respect to the NCP, and c_n, the TBA concentration corresponding to θ = 0.5 at the NCP (φ=-0.83 v against SCE). We can set $C_0 - C' = 14\ \mu\varphi/cm^2$ and $\Gamma_m = 2.17 \cdot 10^{-10}$ moles/cm^2 to obtain

$$\lg \frac{c}{c_n} = 5{,}67\varphi_a^2 = 5{,}67\,(\varphi + 0{,}83)^2. \qquad (6a)$$

Data which had been obtained at φ = -1.53 v was set into Equation (6a) to give $c_n = 1.195 \cdot 10^{-6}$ N. We present below experimentally observed values of c $\cdot 10^4$ at θ = 0.5 and values which have been calculated through Equation (6a).

φ, v (SCE)	−1,53	−1,50	−1,47	−1,40	−1,30
Calculated	(7,20)	4,15	2,50	0,835	0,214
Experimental	7,2	4,3	2,5	1,20	0,58

It is clear that there is good agreement between theory and experiment at - 1.50 and - 1.47 v, a fact indicating that the theory of [9] is applicable to surface-active TBA cations as well as to neutral organic molecules. The calculated values of $\underline{c}$ are markedly lower than the experimental at less-negative potentials since the adsorption of the TBA cations is then determined partially by diffusion and the $\theta, \underline{c}$ relation does not correspond to a reversible isotherm.

LITERATURE CITED

[1] A. Ksenofontov, M. Proskurnin, and A. Gorodetskaya, J. Phys. Chem., 12, 408 (1938) [USSR].

[2] V. I. Melik-Gaikazyan, J. Phys. Chem., 26, 560, 1184 (1952) [USSR].

[3] I. R. Miller and D. C. Grahame, J. Am. Chem. Soc., 78, 3577 (1956); 79, 3006 (1957).

[4] W. Lorenz and F. Möckel, Zs. Elektrochem., 60, 507 (1956); 62, 192 (1958).

[5] P. Delahay and P. Trachtenberg, J. Am. Chem. Soc., 79, 2355 (1957).

[6] R. S. Hansen, R. E. Minturn, and D. A. Hickson, J. Phys. Chem., 60, 1185 (1956); 61, 953 (1957).

[7] H. A. Laitinen, and B. Mosier, J. Am. Chem. Soc., 80, 2363 (1958).

[8] R. Parsons, Trans. Farad. Soc., 55, 999 (1959).

[9] A. N. Frumkin, Proc. L. Ya. Karpov Institute, vol. 5, 3 (1926); vol. 4, 56 (1925); Zs. Physik, 35, 792 (1926).

[10] A. N. Frumkin, B. B. Damaskin, and N. B. Nikolaeva-Fedorovich, Proc. Acad. Sci. USSR, 115, 751 (1957). *

[11] B.B. Damaskin, J. Phys. Chem., 32, 2199 (1958) [USSR].

[12] D. C. Grahame, J. Phys. Chem., 61, 701 (1957).

[13] E. P. Andreeva, J. Phys. Chem., 29, 699 (1955) [USSR].

Received September 10, 1959.

*Original Russian pagination. See C. B. translation.

THE $I^{1/2}$ RULES FOR THE ACTION OF RADIATION ON SOLUTIONS

B. V. Érshler

(Presented by Academician A. N. Frumkin August 14, 1959)

The representation of an irradiated solution as a uniform volume distribution of radicals and molecular products is one which has been generally accepted in the radiation chemistry of dilute solutions. We will consider the special rules which must pertain to cases in which this representation is applicable.

Let the irradiated solution contain various types of particles, m_1, m_2,..., m_k, some of these particles being radicals and some, molecular products. We will suppose that the reactions involving these particles are bimolecular. The following equation can then be set up for the particles m_i

$$\sum_i^{\rightarrow} k_n (c_{n_1})(c_{n_2}) + \sum_i^{\leftarrow} k_l (c_{l_1})(c_{l_2}) + I\, C^0_{m_i} = I\, G_{m_i}. \tag{1}$$

$G^0_{m_i}$ being the "initial" yield of m_i, i.e., the number of these particles obtained directly from the water by absorption of 100 ev of radiant energy, and G_{m_i}, the total yield of the m_i, i.e., the number of these particles obtained from the direct action of the radiation on the water, and from secondary bimolecular reactions during the time required for absorption of 100 ev of radiant energy. The sign $\sum_i^{\rightarrow}$ designates the sum of the rates of those bimolecular reactions 1, 2, 3,..... which produce the particles m_i, k_n being the rate constant for the n-th such reaction and c_{n_1} and c_{n_2}, the concentrations of the particles participating in it. The sign $\sum_i^{\leftarrow}$ designates a similar sum for the l reactions in which particles m_i are consumed, the index l giving the number of such a process. I represents the radiant energy absorbed by the solution in one second. The quantity I is expressed in the absorption units 100 N ev / liter · sec, N being Avogadro's Number, and concentrations are expressed in moles per liter.

The radical concentrations are low and one should therefore set $G_{m_i} = 0$ in each of those equations of (1) which refers to a radical. In addition, one should set $G^0_{m_i} = 0$ in each of these equations which applies to a radical that does not come from the water directly, e.g., HO_2. It is clearly necessary to also set $G^0_{m_i} = 0$ in the equations for those molecular products which do not come from the water directly. The result is a system of k equations which fully characterize the behavior of the irradiated solution. It is difficult to find a solution for a system of this type in which there are many variables of powers higher than the first, but it will be shown below that it is possible to adduce certain important properties of such system without the necessity of solving it.

1. Stationary State. Here each of the k types of particles must satisfy a condition of the form

$$G_{m_i} = 0. \tag{2}$$

The equations of (2) can be introduced into (1) to obtain a system of k equations in the k unknown concentrations. A study of this system will show that the stationary concentration of each type of particle must be directly proportional* to $I^{\frac{1}{2}}$.

*The unknown particle concentrations actually enter this system in the form of products of two variables and all of the free members contain a multiple of I to the first power.

Thus the k equations of (1) assure that the $G_{m_i}[I^{1/2}]$ curve for each of the k types of particles will be a straight line under stationary conditions.

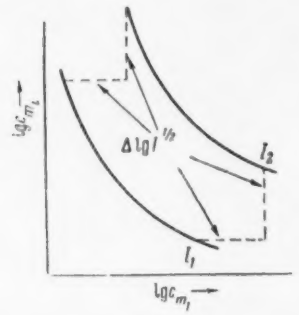

Fig. 1. The $I^{1/2}$ rule for stationary conditions.

It may be that one of these k equations can be obtained from the others (a decision on this point can be reached without the necessity of solving the system), in which case the system will have one degree of freedom and the concentration of one type of particle, m_1, for example can be arbitrarily altered under stationary conditions. In this case we construct curves showing the log c_{m_i} vs log c_{m_1} relations for the remaining k-1 particles at a certain value of the radiation intensity I_1. The equations of (1) show that passage to a new intensity I_2 will displace each of these curves parallel to itself along both the log c_{m_i} and the log c_{m_1} axes by a distance equal to the increase in the quantity log $I^{\frac{1}{2}}$, the curve form remaining unaltered. Figure 1 shows the displacement in an arbitrary log c_{m_i} curve resulting from alteration in the intensity I.

It may be that p of these equations can be obtained from the remaining ones, in which case it will be possible to alter arbitrarily the concentrations of p-type particles, m_1, m_2,..... m_p, say. We construct curves showing the relation between log c_{m_i} and log c_{m_1} and log c_{m_1} for given intensity I_1 and arbitrarily selected values of the concentration of the p - 1 "free" particles, $(c_{m_2})_1$, $(c_{m_3})_1$,....,$(c_{m_p})_1$, say.

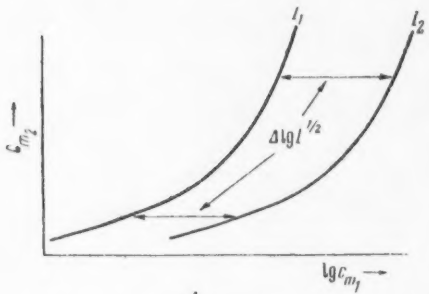

Fig. 2. The $I^{1/2}$ rule for a radiational process.

The k-p equations now characterizing the system show that passage to intensity I_2 will displace all of these curves in the same manner as the curve of Figure 1 was displaced, if the concentrations of the p-1 types of "free" particles are altered to new values, $(c_{m_1})_2$, which satisfy the relations

$$\frac{(c_{m_2})_1}{(c_{m_2})_2} = \frac{(c_{m_3})_1}{(c_{m_3})_2} = \ldots = \frac{(c_{m_p})_1}{(c_{m_p})_2} = \frac{I_1^{1/2}}{I_2^{1/2}}. \qquad (3)$$

2. Reaction. We will consider a case in which $G_{m_1} \neq 0$ and $G_{m_2} \neq 0$, while the remaining types of particles, 3, 4,...,k, satisfy the conditions of (2).

The particles of type m_2 will be supposed to arise from particles of type m_1, and G_{m_1} will therefore be related linearly to G_{m_2}.

Substitution of the linear expression for G_{m_1} in terms of G_{m_2} in the k equations of (1) will lead to k equations in k + 1 unknowns, namely, the k concentrations and G_{m_2}. A curve showing the relation between G_{m_2} and log c_{m_1} at the intensity I_1 is constructed by arbitrarily altering the concentration of m_1. Our system of equations shows that passage to intensity I_2 will displace this curve parallel to itself along the log c_{m_1} axis by an amount equal to the increase in log $I^{1/2}$, without altering its form. Figure 2 represents this type of displacement in an arbitrary G_{m_2} curve. Such a rule as is illustrated by Figure 2 has recently been shown to apply to the decomposition of hydrogen peroxide [1].

This analysis remains valid for a system with any number of degrees of freedom and with any relationship between the particle yields.

The two general laws of radiolysis which have been deduced for 1) stationary conditions, and 2) radiational processes will apply to all types of irradiation, if this model of the irradiated solution is correct. This conclusion is independent of the reaction mechanism and the exact nature of the reactions which are included in the equations of (1). Thus, it is possible to draw the following conclusions.

1. The degree of conformation to the $I^{1/2}$-rules can serve as a criterion for judging the applicability of this model to various types of irradiation and to various systems. The greater the proportion of the radicals which react in the track zone without entering the bulk of the solution, the less will the yield and stationary concentration of the molecular products depend on the intensity of irradiation, and the poorer the conformation to the two $I^{1/2}$-rules. The limiting case is that in which the stationary concentrations and yields are completely independent of the magnitude of I.

2. The proportion of the radicals which are not able to pass out of the track zone can obviously be evaluated from the extent of departure from the $I^{1/2}$ rules.

3. Departures from the $I^{1/2}$ rules can also occur because of direct action of the radiation on the dissolved substances or because of solution reactions which are not bimolecular. Such departures can be used for disclosing effects of this type in cases in which the model is clearly applicable.

LITERATURE CITED

[1] B. V. Érshler, M. A. Nezhevenko, and G. G. Myasishcheva, Proc. Acad. Sci. USSR, 126, No.1 (1959).*

Received July 23, 1959.

*Original Russian pagination. See C. B. translation.

A MASS-SPECTROMETRIC DETERMINATION OF THE HEAT OF SUBLIMATION OF BORON

P. A. Akishin, O. T. Nikitin, and L. N. Gorokhov

The M. V. Lomonosov State University, Moscow

(Presented by Academician V. N. Kondrat'ev July 16, 1959)

A knowledge of the heat of sublimation (ΔH_0^0) of elementary boron is indispensable to many of the important calculations of thermodynamics and thermochemistry. Nevertheless, there has been a considerable spread in the values of the heat of sublimation of boron which have appeared up until very recently in the handbooks [1-3]; these have been based on provisional data and have ranged from 75 to 115 kcal/g.at.

A value of 140.9 ± 2 kcal/g at. for the heat of sublimation of boron was reported in 1955 by Skinner and Smith [4] in a paper citing unpublished data of Searsy and Mayers. In 1957, the latter authors published [5] the results of a study involving the vaporization of crystalline boron from graphite, tantalum, and zirconium diboride effusion chambers. It was considered [5] that the most trustworthy results were those obtained in vaporizing the boron from the zirconium diboride chamber since this material neither interacts with boron nor forms solid solutions with it; these data led to the value $H_{298}^0 = 139 \pm 4$ kcal/g. at.* The work of [5] is not free of defects. Thus, the tantalum diaphragm of the zirconium diboride effusion chamber may have acted as a "trap" for boron atoms. Equilibrium will be established between the solid and vapor phases in an effusion chamber if the vapor molecules, or atoms, undergo multiple reflection on the chamber walls. The Knudsen Effusion Method is equivalent to the Langmuir Method of open surface vaporization when each such collision involves absorption of the vapor molecules, or atoms, through chemical reaction, solid solution formation, etc. with the walls of the chamber; the vapor pressure of the boron will then be considerably reduced if its coefficient of vaporization α, is less than 1.

The coefficient of vaporization of boron was not determined by the authors of [5]. The data of [5] on the heat of sublimation of boron are the most trustworthy that are to be found in the literature, but they stand in need of confirmation, and possibly refinement, through repetition of the measurements. The present study has involved a determination of the heat of sublimation of boron by combining effusion-chamber vaporization with a mass-spectrometric measurement of the composition and absolute pressure of the vapor.

The working specimen of boron was 99.1% pure** and was shown by x-ray analysis to be an amorphous phase with crystalline traces; it was carried almost completely into the crystalline state by heating in vacuum at 2000-2100°K for ½ hour (similar data are to be found in [6]). The molybdenum and tantalum effusion chambers which were constructed for the vaporization of the boron had their inner surfaces completely covered ("lined") with well-pressed crystalline boron to give a "boron" chamber 2 mm in diameter, 5 mm in height, with 0.5 mm walls.

The effusion chamber was inserted into the vaporization block (Fig.1) of the ion source of a MS-3 mass-spectrometer. The chamber was heated by electron bombardment and its temperature measured pyrometrically by observing through a special window the luminosity of a blind canal, 0.3 mm in diameter and 2 mm in length, which had been drilled into the under side of the chamber to give a good reproduction of black-body radiation [7].

*Recalculation to 0°K gives $\Delta H_0^0 = 137.8$ kcal/g. at.

**We would like to express our indebtedness to A. F. Zhigach for furnishing this material.

The OPPIR-09 pyrometer was equipped with an objective for the pyrometry of small specimens and was calibrated against a standard OP-48 pyrometer over the 1400-2000°K temperature interval; the maximum error in the determination of the temperature was ± 10°. Ion currents to 10^{-7} ampere were measured on the ion-electron transducer described in [8,9]. A special screen was used to prevent access of vapors to the ionization region during measurement of the background intensity in the apparatus. A more detailed description of this apparatus for determining the vapor composition and heat of sublimation of difficulty volatile substances will be given in an article which is to appear in "Apparatus and Experimental Techniques".

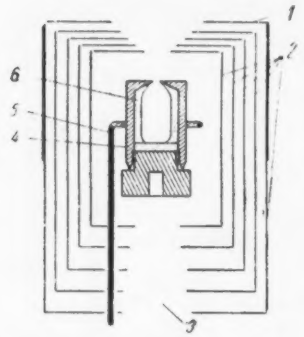

Fig. 1. Sketch of vaporization block: 1) cover of vaporization block; 2) welded tantalum screens; 3) pyrometer openings in the bottoms of the screens; 4) effusion chamber; 5) cathode; 6) "lined" walls of compressed boron.

The mass-spectrum of the vaporous boron showed only the $(B^{10})^+$ and $(B^{11})^+$ ions; B_2^+ ions could not be detected and the content of these ions at 2100°K was less than 1%.

The method proposed by Inghram and his co-workers [10,11] was used in determining the absolute pressure of the vapors.

A preliminary vaporization of silver was carried out with the chamber intended for use with boron. The equilibrium vapor pressure of silver was calculated from the data of [12].

The sensitivity of the apparatus with respect to boron, s_B, is expressed by the equation:

$$s_B = \frac{I_{B^+} T k_B}{p_B} = s_{Ag} \frac{\gamma_B}{\gamma_{Ag}} \frac{\sigma_B}{\sigma_{Ag}}, \qquad (1)$$

in which $s_{Ag} = \frac{I_{Ag^+} T k_{Ag}}{p_{Ag}}$ is the sensitivity with respect to silver; I_{B^+} and I_{Ag^+} are the intensities of the B^+ and Ag^+ ion currents, respectively; p_{Ag} and p_B are the equilibrium vapor pressures of silver and boron, respectively; k_{Ag} is a correction for the isotopic composition of the silver; σ_B/σ_{Ag} is the ratio of the effective ionization cross-sections of boron and silver (a quantity which is equal to 0.14, according to [13]); γ_B/γ_{Ag} is a coefficient allowing for the relative effectiveness of boron and silver ions in dislodging electrons from a target (a quantity which was set equal to 2 on the basis of the data of [9]); and k_B is a correction for the isotopic composition of the boron. The absolute value of the pressure of saturated vapors of boron could be readily determined from Equation (1), once s_B and I_{B^+} were known.

The heat of sublimation, ΔH_0^0, of the boron was calculated from the equation:

$$\Delta H_0^0 = (\Delta \Phi^* - R \ln p_B) T, \qquad (2)$$

in which $\Delta \Phi^* = \Phi_V^* - \Phi_S^*$ is the change in the reduced thermodynamic potential; R is the molar gas constant; p_B is the pressure of boron vapors; and T is the absolute temperature.

Results from one experiment on the measurement of the heat of sublimation of boron are presented in extended form in Table 1, and the results from 7 experiments are given in Table 2, together with the mean deviation from the arithmetic mean of ΔH_0^0. The mean of 24 measurements on the free vaporization of boron at various temperatures gave the result ΔH_0^0 = 137.9 ± 0.8 kcal/g. at.

Study was made of the relation between the value of ΔH_0^0 and the chamber parameter S/aK, and the coefficient of vaporization, α, was calculated from the equation

$$\alpha = \frac{p_L S - p_K a K}{p_K S}, \qquad (3)$$

taken from [14]; here p_L is the vapor pressure measured by the Langmuir Method of free evaporation; p_K is the vapor pressure measured by the Knudsen Method; S is the area of the vaporization surface; a is the area of the effusional orifice and K is the Clausing coefficient. Equation (3) shows the vaporization coefficient, α, of boron to be equal to 0.2-0.3 over the 1600-2000°K interval.

TABLE 1

The Vaporization of Boron from a Boron-Lined Molybdenum Effusion Chamber

T, °K	I_{B^+}	p atm	Φ_g^* [1]	Φ_s^* [1]	ΔH_0^0, kcal/g·at.
2096	7,36	$1,18 \cdot 10^{-6}$	41,3550	6,131	130,7
2117	8,56	$1,39 \cdot 10^{-6}$	41,4041	6,181	131,3
2024	5,20	$8,07 \cdot 10^{-7}$	41,1800	5,959	127,7
2127	7,44	$1,21 \cdot 10^{-6}$	41,4273	6,204	132,5
2158	18,56	$3,07 \cdot 10^{-6}$	41,4992	6,277	130,4
2196	34,80	$5,86 \cdot 10^{-6}$	41,5873	6,366	129,9
2106	12,80	$2,07 \cdot 10^{-6}$	41,3687	6,155	128,9
2090	4,32	$6,92 \cdot 10^{-7}$	41,3404	6,117	132,5
2137	7,44	$1,22 \cdot 10^{-6}$	41,4505	6,228	133,1
2190	10,96	$1,84 \cdot 10^{-6}$	41,5734	6,352	134,6
2231	22,80	$4,92 \cdot 10^{-6}$	41,6652	6,445	132,8
2190	12,64	$2,12 \cdot 10^{-6}$	41,5734	6,352	134,0
2148	22,40	$3,69 \cdot 10^{-6}$	41,4760	6,253	129,0
				Mean	131,3±1,7

*The authors wish to express their thanks to L. V. Gurvich who was kind enough to furnish the values of Φ_V^* and Φ_S^*.

TABLE 2

Combined Table of ΔH_0^0 Values for Boron

Experiment	Number of measurements	Chamber parameter, S/aK	Mean value of ΔH_0^0, kcal/g · at	Experiment	Number of measurements	Chamber parameter, S/aK	Mean value of ΔH_0^0, kcal/g · at
1	11	$7 \cdot 10^2$	131,0±1	5	11	$7 \cdot 10^2$	134,0±1
2	10	$7 \cdot 10^2$	130,1±0,6	6	13	$3 \cdot 10^3$	131,3±1,7
3	8	$7 \cdot 10^2$	131,2±0,5	7	12	$7 \cdot 10^2$	131,6±0,6
4	10	$7 \cdot 10^2$	132,0±0,5			Mean . . .	131,6±0,9

The 7 experiments of Table 2 give a mean ΔH_0^0 value of 131.6± 5 kcal/g. at. being estimated on the basis of: a maximum absolute error of $\Delta T = 10°$ in the temperature measurement; a maximum relative error $\Delta s/s = 0.1$ in the sensitivity; a maximum relative error of $\Delta\sigma/\sigma = 0.3$ in the ionization cross-section; and a maximum relative error of $\Delta\gamma/\gamma = 0.5$ in the coefficient of ionic-electronic emission.

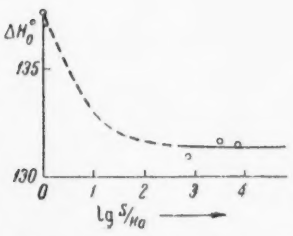

Fig.2. The relation between ΔH_0^0 and the chamber parameter S/Ka.

Thus this work has given a value of 131.6 ± 5 kcal/g. at. for the heat of sublimation, ΔH_0^0, of boron, a result which is somewhat lower than that of [5].

This difference in the values of the heats of sublimation can be accounted for by supposing that Searsy and Mayers did not succeed in establishing the equilibrium pressure of boron vapor in [5] and were thereby led to a result which was too high.

LITERATURE CITED

[1] E. R. Bichowsky and F. D. Rossini, The Thermochemistry of Chemical Substances (N. Y., 1936).

[2] L. Brewer, L. A. Bromley, et al., The Chemistry and Metallurgy of Miscellaneous Materials, Thermodynamics (N.Y.–Toronto – London, 1950).

[3] F. D. Rossini, D. D. Wagman et al., Selected Values of Chemical Thermodynamic Properties, USNBS Circ. 500 (Washington, 1952).

[4] V. A. Skinner and W. B. Smith, Trans. Farad. Soc., 51, 19 (1955).

[5] A. W. Searsy and C. E. Mayers, J. Phys. Chem., 61, 954 (1957).

[6] H. L. Johnston, H. N. Hersh and E. C. Kerr, J. Am. Chem. Soc., 73, 1112 (1951).

[7] I. C. De Vos, Physica, 20, 669 (1954).

[8] W. Schutze and F. Bernhard, Zs. Phys., 145, 44 (1956).

[9] K. M. Kuznetsov, Proc. Scientific-Research Institute of the Ministry of the Radio-Technical Industry of the USSR, vol.2, (38) (1957).

[10] W. A. Chupka and M. G. Inghram, J. Phys. Chem., 59, 100 (1955).

[11] R. F. Porter, W. A. Chupka, and M. G. Inghram, J. Chem. Phys., 23, 216 (1955).

[12] M. C. Low and C. E. Birchenall, J. of Metals, 3, 707 (1953).

[13] J. M. Otvos and D. P. Stevenson, J. Am. Chem. Soc., 78, 546 (1956).

[14] A. N. Nesmeyanov and N. É. Khandamirova, Prog. Chem., 28, 117 (1959).

Received July 15, 1959.

LIMITING CASES OF COMBUSTION IN MIXED SYSTEMS

N. N. Bakhman

The Institute of Chemical Physics of the Academy of Sciences of the USSR

(Presented by Academician V. N. Kondrat'ev July 9, 1959)

The rate of combustion of a mechanical mixture of a combustible solid and an oxidizing agent is known to depend on the dimensions of the reacting particles. It is of interest to determine the limiting forms assumed by this relation for cases in which the particle dimensions are either very large or very small.

The limiting case of a system of extremely large particles is clearly that in which a semispace filled with the combustible solid is bounded by a second semispace filled with the oxidizing agent. Experiments were carried out on solid inorganic oxidizing agents which had been compressed into bars or sheets in cylindrical or plane-parallel plexiglass forms. The thickness of the plexiglass was greater than the depth of the layer which would undergo combustion in the course of the experiment. The charge was ignited by a nichrome spiral at the upper edge of the plexiglass-oxidant interface. A fairly constant flame velocity was usually established after a brief period of initial acceleration. A conical recess was formed in the combustion and advanced with the flame. Photography was used in measuring the rate of flame propagation, $\underline{v}$, along the reagent interface as a function of the pressure, $\underline{p}$, of the inert gas (nitrogen), the characteristic dimension, $\underline{d}$, of the oxidant layer, and the relative density, δ, of the oxidant.

The flame velocity tended to a definite limit as the value of $\underline{d}$ was increased (Fig. 1). Experiments were also carried out in a steel cell in which only the forward wall was made of plexiglass. Such a cell could serve as a model of a system of infinitely large particles when the oxidant layer was not too thin. The value of $\underline{v}$ increased at first as the layer of oxidant in the steel cell was made deeper (this was due to diminished heat loss in the steel) and then began to alter slowly, tending to that value $v_{lim} \neq 0$ which is associated with $d \to \infty$. The fact that $\underline{v}$ was independent of $\underline{d}$ when the value of the latter was sufficiently large indicated that the rate was determined essentially by conditions prevailing near the apex of the combustion recess.

The rate of flame propagation along the plexiglass-oxidant interface was dependent on the chemical nature of the oxidant. This appeared, first of all, in the fact that not all of those oxidants which were thermodynamically capable of supporting combustion would actually support combustion in this system. The v, p relations for the test oxidants (Fig.2) were also quite different. For $KClO_4$, $\underline{v}$ depended linearly on $\underline{p}$ [v(mm/sec) = 0.8 + 0.1 p (atmos)]; the dependence was somewhat stronger than linear for $KClO_3$, it was practically independent of $\underline{p}$ in $KMnO_4$ over the interval from 5 to 100 atmos, with $\underline{v}$ very low in absolute value and it finally showed a maximum with BaO_2, a substance which did not support combustion at all when the value of $\underline{p}$ was sufficiently high. This behavior of BaO_2 was in all probability related to the reversibility of the reaction $BaO_2 \rightarrow BaO + 0.5\ O_2$, which results in retarded consumption of the BaO compound at elevated pressure.

The value of $\underline{v}$ also depended on the relative density of the oxidant. It is true that $\underline{v}$ was independent of δ at low pressure in the case of $KClO_4$ over the interval from $\delta = 0.5$ to $\delta = 0.9$. But the value of $\underline{v}$ for $KClO_4$ at high $\underline{p}$ (that is to say, at sufficiently high $\underline{v}$) increased rapidly as δ diminished, the product $v\delta = f(\delta)$ passing through a maximum.

This difference was explained by the fact that the combustion products penetrated into the depth of the oxidant and began to play an important role in the convectional heat transfer at the high burning rates. A

diminution in δ favored this penetration but made the heat losses at the walls more significant.

Only those systems in which the interface between the reagents was continuous showed a characteristic limiting velocity, $v_{lim} \neq 0$. On the other hand, combustion was extinguished in ordinary systems with haphazardly distributed particles and discontinuous reagent interfaces when the particle dimensions exceeded a certain critical value and the connecting links between particles of a given type become too large.

The combustion rate increased as the particle dimensions were diminished, but the effect was not pronounced when both of the reagents were volatile. Curve V of Fig.2 shows the variation of the normal rate of combustion, u_n, of a stoichiometric mixture of $KClO_4$ and plexiglass in which most of the particles were less than 10μ in dimensions. The value of u_n increased with p, but more weakly than v, [u_n (mm/sec) = 1.4 $p_{(atmos)}^{0.64}$] and was only several fold greater than the value of v on Curve I (~3.3-fold at p = 10 atmos and ~2.7-fold at p = 100 atmos) which had been constructed for d = 6 mm with v quite close to v_{lim}.

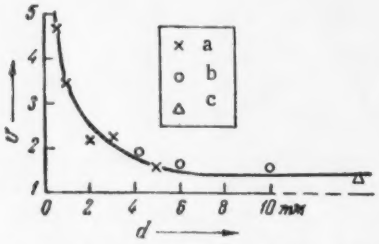

Fig.1. The relation between the flame velocity and the characteristic dimension of the oxidant layer ($KClO_4$; P_{N_2} = = 10 atmos): a) plane-parallel cell; b) cylindrical form; c) steel cell.

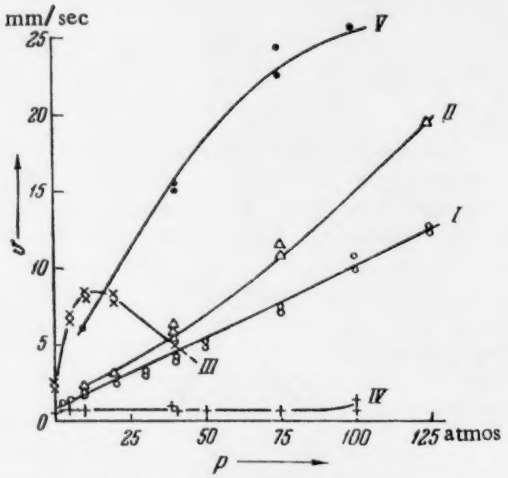

Fig.2. The relation between the flame velocity and the pressure (cylindrical form, d = 6 mm): I) $KClO_4$; II) $KClO_3$; III) BaO_2; IV) $KMnO_4$; V) stoichiometric mixture of $KClO_4$ and plexiglass.

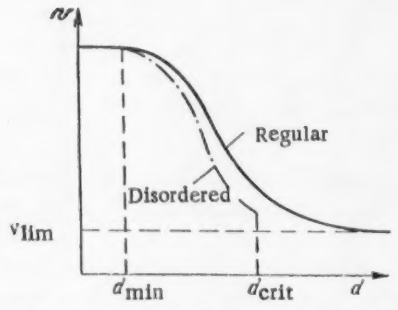

Fig. 3. Asymptotic form of the relation between the flame velocity and the particle dimensions.

The rate of combustion should increase with diminishing particle dimensions only as long as the depth of the mixing zone of the reatent vapors, $l_{mix} \sim u_{vap} \cdot d^2/D_{vap}$ (D_{vap} is the diffusion coefficient) exceeds the depth of the heating zone of the homogeneous vapor mixture, $l_{heat} \sim \lambda/c\rho u \sim 1/p^n$. Increasing p should reduce the minimum particle dimension below which the combustion rate is independent of d, since $l_{heat} \sim 1/p^n$, while l_{mix} is independent of p in a first approximation.

Thus the curve showing the relation between the rate of combustion and the particle dimensions in a system having a continuous interface between the combustible solid and the oxidant must be S-shaped, whereas the curve for the usual disordered mixture should show a plateau at low particle dimensions and break at higher dimensions.

Received June 27, 1959.

A STUDY OF THE ELECTRON PARAMAGNETIC RESONANCE SPECTRA OF THE NEGATIVE IONS OF CERTAIN AROMATIC AND HETEROCYCLIC COMPOUNDS

V. V. Voevodskii, Corresponding Member, Acad. Sci. USSR,
S. P. Solodovnikov, and V. M. Chibrikin

The Institute of Chemical Physics of the Academy of Sciences of the USSR

The e.p.r. spectra of the anions of a number of aromatic polycyclic compounds have been studied in [1-3]. Observations on the e.p.r. spectra of the anions of benzene, toluene, and the xylols have been reported in [4].

We have studied the e.p.r. spectra of certain substituted benzene anions, and the problems involved in possible electron transfer over systems of conjugated and saturated bonds. Such data could be of interest to a study of the chemical properties of this type of ion-radical. The ion-radicals were prepared by interacting the corresponding aromatic compounds with metallic potassium in 1, 2-dimethoxyethane solution. Certain of the less-stable ions were prepared at reduced temperatures ranging down to -70°.

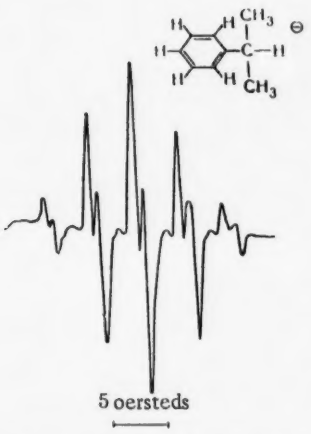

Fig.1. Spectrum of the cumene anion.

The spectra of the anions of the monoalkyl-substituted benzenes, cumene, cyclohexylbenzene, tertiary isobutylbenzene, toluene, and ethylbenzene each show a hyperfine structure containing 5 principal components with a binomial distribution of energy. These 5 lines could arise from interaction of the unpaired electron with 4 equivalent hydrogen atoms. These equivalent hydrogen atoms would occupy the ortho and meta positions in the investigated compounds. Each component of the quintuplet in the spectra of the anions of cumol (see Fig. 1) and cyclohexylbenzene is double. Such additional splitting is not observed in the spectrum of the tertiary isobutylbenzene anion, so that the additional doublet splitting in the spectra of the anions of cumol and cyclohexylbenzene could be presumed to arise through the α-protons of the substituent, with a considerably lower spin density in the para position.

The spectra of toluene and ethylbenzene both show additional splitting from the α-protons of the substituent and from the hydrogen in the para position. Figure 2 represents the spectrum of the toluene anion; this consists of 5 principal lines, each of which, as analysis proves, is further split into 8 components as the result of interaction between the unpaired electron, the 3 α-protons and the proton in the para-position. It is to be noted that this additional splitting was not detected in [4].

We have also studied the e.p.r. spectra of the anions of the ortho, meta, and para xylols. There are 5-components in the spectrum of the n-xylol anion, and 7, in the spectrum of the o-xylol. It would seem that the presence of 7 components in the spectrum of the o-xylol anion could be explained by the interaction of the unpaired electron with the 6 protons of the two methyl substituents. The higher complexity of the spectrum of the m-xylol anion indicates that the splitting involves not only the protons of the methyl substituents, but the protons of the ring as well. The authors of [4] could not give a unified treatment of the spectra of these three types of xylols since they observed only 5 lines in the spectra of the o-xylol and ascribed these to the hydrogens of the ring in analogy with the case of the n-xylol.

Fig. 2. Spectrum of the toluene anion.

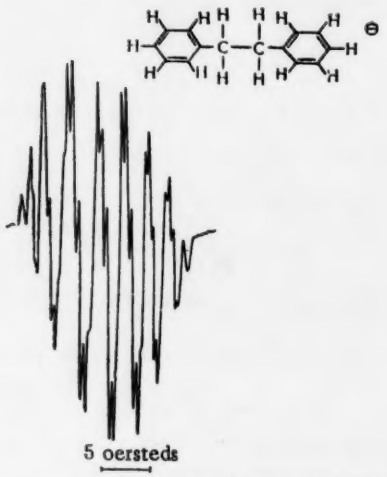

Fig. 3. Spectrum of the dibenzyl anion.

TABLE 1

e.p.r. Spectra of Negative Aromatic Ion-radicals

Negative ion-radical	Number of principle lines	Splitting in oersteds	Number of additional lines	Additional splitting	Density			
					ortho	meta	para	Σ
$(C_6H_6)^-$	7	3,75						
$(C_6H_5CH-(CH_3)_2)^-$	5	4,5	2	1 **	0,2	0,2	0	0,8
$(C_6H_5C_6H_{11})$	5	4,5	2	1 **	0,2	0,2	0	0,8
$(C_6H_5C(CH_3)_3)^-$	5	2,8			0,12	0,12	0	0,48
$(C_6H_5CH_3)^-$	5	4,0	8	1,5 **, 0,5 ***	0,18	0,18	0,02	0,74
$(C_6H_5C_6H_5)^-$	5	3,75	6	1,5 **, 0,5 ***	0,16	0,16	0,02	0,66
$(n\text{-}C_6H_4(CH_3)_2)^-$	5	4,0			0,18			0,72
$(o\text{-}C_6H_4(CH_3)_2)^-$	7	3,8						
$(C_6H_5-CH=CH-C_6H_5)^-$	3	5,65	14					
$(C_6H_5-CH_2-CH_2-C_6H_5)^-$	9	2,5	6	1	0,11	0,11		

* In each of the principle components.

** Splitting from the α-protons of the substituent.

*** Splitting from the protons in the para position.

All the results from the measurements on the line splitting are presented in Table 1, together with the spin densities of the unpaired electron calculated from the experimental data.

The e.p.r. spectra of stilbene, azoxybenzene, and dibenzyl were studied with a view to clearing up the possibility of electron transfer along a chain of conjugated and saturated bonds. An analysis of the stilbene spectrum points to the possibility of delocalization of the electron, both on the benzene ring and on the chain of conjugated bonds, the spin density being principally localized at the carbon atoms of the bridge group. Analysis of the spectrum of the azoxybenzene anion indicates that replacement of the $-\overset{H}{\underset{|}{C}}=\overset{H}{\underset{|}{C}}-$ bridge by $-\overset{O}{\uparrow}N=N-$

does not impede the delocalization of the electron over the entire molecule. A complete breakdown of the conjugation between the rings in the anion of dibenzyl could be anticipated because of saturation in the bond between the CH_2 groups. The spectrum of the negative dibenzyl ion shows 9 principal lines with a splitting of 2.5 oersteds, as is to be seen from Fig.3; these can best be interpreted by relating them to the 8 ortho and meta protons. The spectrum would be similar to that of ethylbenzene if the electron was localized on a single ring. The frequency of interchange between the rings can be estimated from the line splitting and proves to be equal to 10^7-10^8 sec^{-1}. The additional splitting indicates that the spin density is different from zero at the bridge carbon atoms.

The spectra of the anions of pyridine and quinoline were studied with a view to clearing up the effect of the heteroatoms on the spin-density distribution. Analysis of the spectrum of the pyridine anion shows that the spin density is different from zero at the nitrogen atom and at the α, β , and γ carbon atoms, the number of lines being close to the theoretical 54. This last fact indicates that the α, β, and γ protons are not equivalent.

LITERATURE CITED

[1] O. Lipkin and D. E. Paul, et al., Science, 117, 534 (1953).

[2] S. I. Weissman, J. Townsend, et al., J. Chem. Phys., 21, 2227 (1953).

[3] T. R. Tuttle Jr., K. L. Ward, and S. I. Weissman, J. Chem. Phys., 25, 189 (1956).

[4] T. R. Tuttle Jr., and S. I. Weissman, J. Am. Chem. Soc., 80, No.20, 5342 (1958).

Received August 31, 1959.

AN INFRARED ABSORPTION STUDY OF THE COMPLEXES OF OF ACETYLENE AND ITS DERIVATIVES

E. A. Gastilovich, D. N. Shigorin, E. P. Gracheva
and M. F. Shostakovskii

L. Ya. Karpov Physicochemical Institute and N. D. Zelinskii
Institute of Organic Chemistry, Academy of Sciences, USSR

(Presented by Academician A. N. Terenin July 6, 1959)

A study of the infrared absorption spectra of the complex derivatives of acetylene in the region from 3100 cm^{-1} to 2100 cm^{-1} has been used in [1] to prove the possibility of hydrogen bonding between the $\equiv C\text{-}H$ group and electronegative atoms ($O<$, $N\leqslant$) certain considerations being expressed there relative to the nature of the secondary chemical bonds which arise when complexes are formed between molecules of compounds.

The infrared absorption spectra of $H-C\equiv C-H$, $D-C\equiv CH$, $CH_3-C\equiv CH$ (I), $C_2H_5-C\equiv CH$ (II), $C_4H_9-O-\underset{\underset{C}{|}}{H}=\underset{\underset{H}{|}}{C}-C\equiv CH$ (III), and of solutions of these compounds in carbon tetrachloride, acetone, dioxane, ether, and pyridine have been studied over the 34000-3000 cm^{-1} interval in the present paper with the aim of further elucidating the nature of secondary chemical bonds [2].

The compounds $CH_3-C\equiv CH$, $C_2H_5-C\equiv CH$ and $C_4H_9O-CH=CH-C\equiv CH$ were specially synthesized by well-known methods; their constants agreed with values found in the literature. The acetylene for this study was taken from a tank, and was freed of acetone and moisture before use.

The study was carried out on a IKS-1 apparatus with a LiF prism. The intensity of the $\equiv CH$ absorption band was used in approximating the concentrations of acetylene and methylacetylene in solution. The accuracy of the determination of the absorption maxima was estimated to be $\pm$ 5 cm^{-1}. The results of the study are shown in Table 1.

An absorption band, ν, with a maximum at 3310-3313 cm^{-1} was observed in spectra of the test substances, $CH_3-C\equiv C-H$, $C_2H_5-C\equiv CH$ and $C_4H_9-O-CH=CH-C\equiv CH$ in CCl_4, a neutral solvent; this band was ascribed to the $\equiv C-H$ group of each of these molecules, its vibration being unperturbed by the hydrogen bonding. Association was observed between the test substance and the molecules of solvents containing the electronegative atoms $O<$, $N\leqslant$. Thus the spectra of I – III in ether and pyridine solutions showed an absorption band, ν', for hydrogen-bonded molecules, in addition to a free molecule band, the indication being that equilibrium was established between the associated and the free molecules in solution. The absorption band maximum for the associated molecules was at ν' = 3263-3270 cm^{-1} in ether and at ν' = 3225-3210 cm^{-1} in pyridine. This considerable difference in the position of the absorption maxima for the $\equiv C-H$ group of the associating molecules was consistent with ideas concerning the basicity of the solvent involved in the association [2] and its effect on the bond strength. The spectra of the test substances in acetone and dioxane showed a single absorption band for the $\equiv C-H$ group of the associating molecules; this was at ν' = 3260-3270 cm^{-1} and resembled the band for absorption in ether. A certain asymmetry here pointed to the presence of an unresolved band (ν) in the absorption of the free molecules (Fig. 1a).

TABLE 1

State	HC≡CH	HC≡CD	$CH_3C{\equiv}CH$	$C_2H_5C{\equiv}CH$	$C_4H_9{-}O{-}CH{=}HC{-}{-}C{\equiv}CH$	c
Vapor	3293 3285 3267 } 3280	3347 3305 } 3326	3337 3315 } 3326	3335 3325 } 3330	3330	
Liquid			3295	3295	3290	
					3305	1:4
			3313	3313	3310	1:40
					3310	1:400
Solution in CCl_4	3260 3260				3310	1:1000
					3290	1:4
Solution in ether					3310 3260	1:20
			3315 3270	3313 3265		1:40
					3268	1:4
Solution in acetone	3218					
			3273	3270	3263	1:40
Solution in dioxane					3263	1:4
	3210					
			3267	3265	3245	1:40
Solution in pyridine					3295 3305	1:4
			3300 3228	3298 3225	3300 3195	1:40

Decreasing the concentration of a test substance in solution (Fig.1b) was observed to displace the equilibrium toward increased association with the solvent, the absorption band ν' moving toward long wavelengths and increasing in relative intensity. An increase in the solution temperature led to displacement of the equilibrium in the opposite direction, the degree of association with the solvent diminishing while the absorption-band maxima for the free and associated molecules moved toward the short wavelengths: $\nu = 3293 \rightarrow 3298\ cm^{-1}$, $\nu' = 3195 \rightarrow 3205\ cm^{-1}$ (Fig. 2a).

A comparison of the spectra of the test substances in solutions of equal concentrations showed the absorption-band maximum, ν', in dioxane, a nonpolar solvent, to be displaced toward long wavelengths with respect to its position in acetone solution. The displacement of the associated molecules toward long wavelengths was somewhat greater in the spectra of ether, acetone, dioxane, and pyridine solutions of $C_4H_9-O-CH-C\equiv CH$ than in the spectra of methylacetylene and ethylacetylene solutions. Further study will be needed for an understanding of this effect, but it can be presumed that the π-electrons of the molecules play a considerable role here in strengthening the hydrogen bond; this presumption is consistent with results from certain special studies of this problem [3].

There was considerable variation in the position of the absorption maximum in the $\equiv C-H$ bond, and very little difference in the C−H frequency of the aliphatic group, in the spectra of the liquid and gaseous phases of the test substances, just as is the case with the more complex molecules of the acetylene derivatives [1]. Thus the displacement of the absorption maximum of the $\equiv C-H$ group in III (gas-liquid) was equal to $\Delta\nu = 40\ cm^{-1}$ (Fig. 2b) while the displacement of the C−H group frequency in C_4H_9 was $\Delta\nu = 5\ cm^{-1}$; it should be noted that the $\equiv C-H\ldots O\langle$ type of interaction is here lacking in the liquid phase. This fact is the basis for the postulated formation of the π-complexes according to the reaction

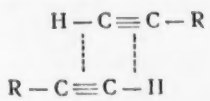

Conclusions concerning the fact that the band intensity for molecules in π-complexes was greater than the intensity for molecules in noninteracting vapor complexes (Fig. 2b) could be drawn from a comparison of the liquid and gaseous phase absorption spectra of $C_4H_9-O-CH=CH-C\equiv CH$. The same conclusions concerning the relatively higher band intensity for molecules involving participation of the $\equiv C-H$ group in the

formation of the hydrogen bond could be drawn from a comparison of absorption spectra at different temperatures; there was a marked alteration in the intensity of the absorption band of the associating molecules and an accompanying weak alteration in the intensity of the absorption band of the free molecules (Fig. 2a). Similar conclusions concerning the alteration in the band intensities for molecules in the free and in the associated state are known from the case of hydrogen bonding in O−H....O systems [3].

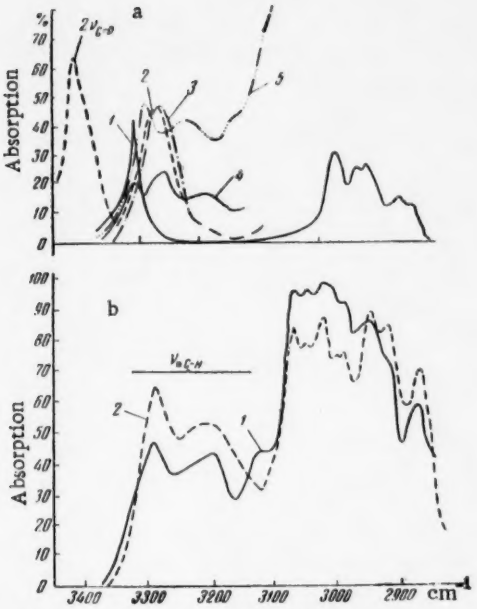

Fig. 1. Infrared spectra: a) Ethylacetylene in solutions, C = 1:40, d = 95 mμ. 1) In CCl_4; 2) in acetone; 3) in dioxane; (4) in pyridine; 5) in ether. b) $C_4H_9-O-CH=CH-C\equiv CH$ in pyridine: 1) C = 1:40 (d = 55 μ); 2) C = 1:4 (d = 95μ).

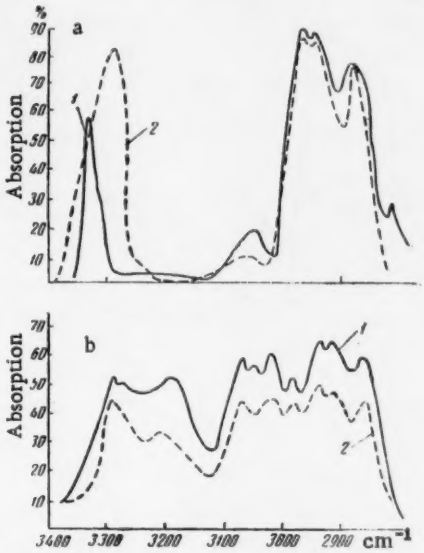

Fig. 2. Infrared spectra: a) $C_4H_9-O-CH=CH-C\equiv CH$; 1) Vapor; 2) liquid. b) $C_4H_9-O=CH-C\equiv CH$ in pyridine; C = 1:4; d = 50μ. 1) At -64°, 2) at + 22°.

It is interesting to note that the data on the displacement of the absorption band, $\Delta\nu$, and the band width, $\nu_{1/2}$, in the ≡C−H....O, and ≡C−H....N types of hydrogen bonding fit into the width, displacement relation, $\nu_{1/2} = 0.72 + 2.5\ \Delta\nu\ cm^{-1}$, which has been established for hydrogen bonds of the O−H....O and OH....N types [4]. With $C_4H_9-O-CH=CH-CH$. *

in pyridine	$\nu_{1/2}$=90 cm^{-1}	$\Delta\nu_{calc.}$=120 cm^{-1}	$\Delta\nu_{exp.}$ =110cm^{-1}
in ether	$\nu_{1/2}$=45 cm^{-1}	$\Delta\nu_{calc.}$=59 cm^{-1}	$\Delta\nu_{exp.}$ =55 cm^{-1}

Because of molecular symmetry, the frequency of vibration of the ≡C−H group in gaseous acetylene (ν = 3280 cm^{-1}), and in CCl_4, acetone, and dioxane solutions of acetylene (Fig. 3), differed from the frequency of vibration of ≡C−H group in derivatives of acetylene under the same conditions. This symmetry could be destroyed by replacing the hydrogen of the gaseous acetylene by deuterium, and the vibration frequency of the ≡C−H group in the resulting HC≡CD molecule then appeared in a region which is characteristic of the acetylene homologs (ν = 3326 cm^{-1}). The observed displacements of the absorption maximum for the ≡C−H band in the spectra of acetylene and its homologs in acetone and dioxane solutions with respect to its position

*No account was taken of the distortion of the ≡C−H absorption band in the determination of $\nu_{1/2}$.

in the spectra of these compounds in CCl_4 were approximately equal; this was clearly due to the participation of both hydrogen atoms in the formation of the acetylene complexes. The large difference between the frequency of vibration of the $\equiv C-H$ group in gaseous acetylene and in acetylene in CCl_4 solution ($\Delta = 20\ cm^{-1}$) requires further study.

An estimate of the energy of complex formation with participation of the $\equiv C-H$ group could be made on the basis of the experimental data. For this purpose the equilibrium between $R-C \equiv C-H$ and pyridine was studied over the temperature interval from 293 to 373°K by the method of infrared absorption spectra. A calculation based on the reaction isochor gave 2-2.5 kcal for the heat of reaction. The change in the integral intensity of the $\equiv C-H\ldots$ bond band during formation of the $\equiv C-H\ldots X$ complex was taken into account in this calculation. The ratio of intensity coefficients, $I_{\equiv C-H\cdots} / I_{\equiv C-H}$ was approximately equal to four in this case. The energy of formation of the $\equiv C-H\ldots O\langle$ system proved to be 1-1.5 kcal.

An evaluation of the energy of the $\equiv C-H\ldots X (X = O\langle, N\langle\!\langle)$ bonds from the equation of N. D. Sokolov [5] $\varepsilon = 4D\frac{a^2}{b^2}\frac{1}{f}\frac{\Delta\nu}{\nu}$, with allowance for the ionic character of the bond gave a result of the correct order of magnitude. The stability of the $\equiv C-H\ldots X$ complex is strongly dependent on the valence state of the atom.

The results obtained here have significance for an understanding of the nature of secondary chemical bonds and gives a scientific basis for processes of separating the acetylene hydrocarbons.

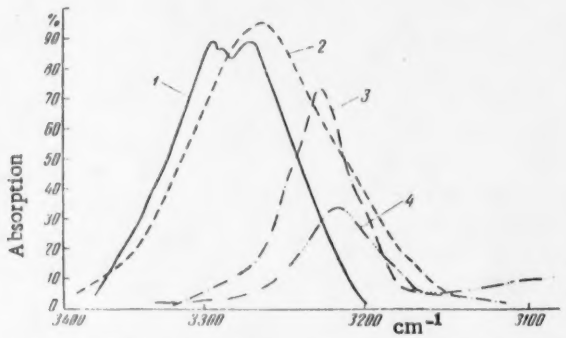

Fig. 3. Infrared spectra of acetylene: 1) Vapor; 2) in CCl_4 (d = 3.5 mm); 3) in acetone (d = 95 μ); 4) in dioxane (d = 55 μ).

LITERATURE CITED

[1] D. N. Shigorin, M. M. Shemyakin, et al, Izvest. Akad. Nauk SSSR, ser. khim., 9, 1133 (1958).*

[2] D. N. Shigorin, Problemy Fiz. Khim., 1, 173 (1955).

[3] D. N. Shigorin and N. S. Dokunikhin, Zhur. Fiz. Khim., 29, 1958 (1955).

[4] C. M. Higgins and G. C. Pimentel, J. Phys. Chem., 60, 1615 (1956),

[5] N. D. Sokolov, Doklady Akad. Nauk SSSR, 58, 4, 611 (1947).

Received June 2, 1959.

*Original Russian pagination. See C. B. translation.

A UNIVERSAL SCALE FOR THE EFFECT OF SOLVENTS ON THE ELECTRONIC SPECTRA OF ORGANIC COMPOUNDS

I. A. Zhmyreva, V. V. Zelinskii, V. P. Kolobkov and N. D. Krasnitskaya

(Presented by Academician A. N. Terenin July 15, 1959)

The effect of solvents in altering the absorption and fluorescence spectra of organic compounds can be due to various types of interaction, some chemical and some physical. It has recently become increasingly clear, however, that there is a common origin for certain well-defined changes which are observed in the spectra of radically different substances.

A. I. Kipriyanov [1] has noted the existence of a general ordering of the solvents according to their effect on the absorption spectra of various organic substances, the spectra of one group being displaced toward long wavelengths on passing from one solvent to another, while the spectra of another group are displaced toward short wavelengths. Lippert and Moll [2,3], studying the effect of an extensive group of solvents on the spectra of various organic compounds, have shown the spectra of all of their working substances to be similarly affected by interaction with a given solvent; thus it should be possible to construct a single scale ordering the solvents according to their action on the spectra of organic substances. Such a scale was not constructed by these authors, however.

V. V. Zelinskii, V. P. Kolobkov, and L. G. Pikulik [4] have directed attention to the uniformity of the effect of an extended group of solvents on the fluorescence spectra of various derivatives of phthalimide and have proposed that solvents be ordered according to their effect on the fluorescence spectrum of 4-amino-N-methylphthalimide. V. V. Zelinskii, V. P. Kolobkov, and I. I. Reznikova have noted in [5] that the ordering of the solvents with respect to their effect on the fluorescence spectra of the phthalimide derivatives holds with respect to other chemical classes as well. Kosaver [6] has also noted the uniform action of solvents on the absorption spectra of various organic compounds.

It is shown in the present work that a universal scale for the effect of solvents on the spectra of organic compounds can be constructed by using 4-amino-N-methylphthalimide as a reference substance.

A frequency scale has been plotted on the axis of ordinates in Fig.1. The various solvents have been located on the axis of abscissas in such a way that the distance between any two of them is equal to the length of segment on the axis of ordinates representing the difference in the frequencies of the spectral maxima in these solvents. Many of the points representing the position of the fluorescence spectra of other organic compounds in various solvents prove to be distributed along straight lines when the frequencies of the spectral maxima are plotted with respect to this ordering. Fig. 1 shows such lines for certain phthalimide derivatives.*

Values of ν_{fl}^{max} for other substances (o-methoxybenzoic acid, aminonaphtheurobin and its derivatives of maleinimide, acridine, and 2-aminoacridine) in various solvents have been plotted on the proposed scale in Fig. 2. It is clear that the ν_{fl}^{max} —solvent relations for these substances are also linear.** The absorption

*We have studied 21 phthalimide derivatives. On the proposed scale, each of these derivatives showed a linear relation between the frequency of the maximum in the fluorescence spectrum and the solvent.

**Instances of nonlinear ν_{fl}^{max} – solvent relations will be presented elsewhere.

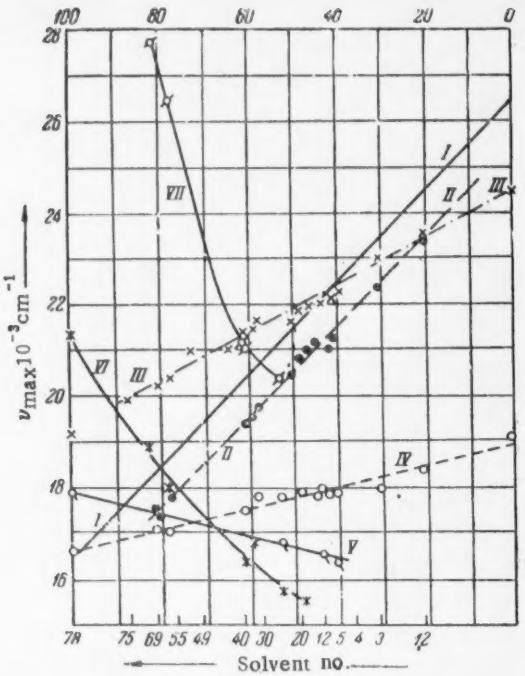

Fig. 1. The ν_{fl}^{max} -solvent relation. Fluorescence: I) 4-amino-N-methylphthalimide; II) 4-dimethylamino-N-methylphthalimide (Nos. 69, 66, 37, 31, 22, 19, 18, 14, 8, 7, 3, 2,1); III) 3-amino-N-methylphthalimide (Nos. 78, 75, 69, 66, 50, 45, 37, 35,31, 22, 19, 18, 16, 10, 8, 7, 6, 3, 2, 1); IV) 3, 6-tetramethyldiamino-N-methylphthalimide (Nos. 78, 69, 66, 37, 35, 25, 19, 16, 10, 8, 7, 3, 1); V) 3-hydroxy-N-methylphthalimide(Nos. 78, 69, 25, 10, 6); Absorption: VI) Dye 11 in McRae's nomenclature [7] (Nos. 78, 71, 66, 37,25, 19); VII) the iodide of 1-alkyl-4-carbomethoxy-pyridine [6] (Nos. 69,66, 39, 37, 25).

maxima in the spectra of two substances taken from Kosaver [6] and McRae [7] have been plotted in Fig.1. The results of these authors fit well into the proposed solvent scale. On the proposed scale, the variation in the position of the absorption spectra of the phthalimide derivatives are not represented by straight lines, but by curves which pass through minima. The ordering of the solvents in terms of their effect on spectra is maintained even here since all of these points fall nicely on a single curve.*

Thus, for an extended class of substances, the position assigned to a given solvent on the basis of its effect on the absorption spectra is the same as that assigned on the basis of its effect on the fluorescence spectra. This makes it possible to give a numerical expression to the relative intensity of the effect of a solvent on the spectrum of an organic substance. The zero point of this scale is naturally located at the position occupied by the spectrum of the vapor, the position of the fluorescence spectrum in water being chosen as 100. Tables 1 gives numerical expressions for the relative intensity of the action of solvents** on spectra, these being based on the alteration of the positions of certain solvents.

The reference substance for our scale, 4-amino-N-methylphthalimide, was studied in a great number of chemically different solvents. An ordering of the solvents in terms of the frequency of the maximum of the fluorescence spectra proved to be also an ordering in terms of chemical type. Thus, the hydroxyl-containing solvents occupy the spectral region from 16000 to 19000 cm^{-1}, or 0.25 of the above-proposed scale. The alcohols occupy a still more narrow interval within this region, ie., from 17600 to 19600 cm^{-1}, or 0.14 of the scale. The esters form the next large group. In these substances, ν_{fl}^{max} varies from 18800 to 21600 cm^{-1}, and they occupy 0.34 of the scale. Following these, come the ethers with ν_{fl}^{max} = 21700 -22050 cm^{-1}, or 0.035 of the scale, the aromatic hydrocarbons with ν_{fl}^{max} = 22000-22500 cm^{-1}, or ΔS = 0.05, and the saturated hydrocarbons with ν_{fl}^{max} = 24400 cm^{-1}.

It is to be noted that differences in the state of aggregation of solvents are of no significance in many cases. Thus the position of the fluorescence spectra in solid methanol is exactly the same as in the liquid alcohols. The fluorescence spectra in solid stearic acid occupy the same position as in the liquid acids. The fluorescence spectra in solid dimethyloxalate are almost identical with those in liquid diethyloxalate.

The generality of the effect of solvents on the spectra of highly dissimilar substances eliminates the possibility of explaining this effect in terms of certain specific bonds. In particular, Lippert and Moll [3] have shown, that hydrogen bonding cannot be responsible for the observed general relation between solvents and spectra.

---

*Causes for different solvent effects in absorption spectra and in fluorescence spectra have been treated in [2,4]. The present authors will deal with this problem in detail elsewhere.

**We did not have the opportunity of studying all of the test solvents in satisfactorily pure form. A check of the spectra of the reference substance in ideally pure solvents would undoubtedly show changes in the scale position of certain solvents.

Table 1

No.of compound	Solvent		S	No.of compound	Solvent		S
	Vapors	26.5	0	43	Formal	20.1	64
1	n-Hexame	24.4	21	44	Cyclohexanone	20.0	65
2	n-Octane	24.4	21	45	Quinoline	20.0	65
3	Carbon tetrachloride	23.4	31	46	Dibutyl ester of sebasic acid	20.0	65
4	Ethylene chloride	22.8	37	47	α-Bromonaphthalene	19.9	66
5	Isopropyl bromide	22.5	40	48	o-Formic ester	19.9	66
6	Toluene	22.5	40	49	Propyl formate	19.4	71
7	Benzene	22.4	41	50	Methyl formate	19.1	74
8	Chlorobenzene	22.3	42	51	Isobutyric aldehyde	19.0	75
9	Ethyl bromide	22.25	42.5	52	Thymol	19.0	75
10	Propyl bromide	22.15	43.5	53	Diethyl oxalate	18.9	76
11	Bromobenzene	22.05	44.5	54	Dimethyl oxalate	18.8	77
12	Diisoamyl ether	22.05	44.5	55	Benzaldehyde	18.8	77
13	Diisopropyl ether	22.0	45	56	Glycerine dichlorohydrin	18.8	77
14	Diethyl ether	22.0	45	57	Menthol	18.8	77
15	Ethylene bromide	21.9	46	58	Cyclohexanol	18.8	77
16	Anisole	21.9	46	59	Secondary octyl alcohol	18.8	77
17	Carbon disulfide	21.75	47.5	60	Primary octyl alcohol	18.8	77
18	Propyl chloride	21.75	47.5	61	Isobutyl alcohol	18.8	77
19	Dioxane	21.7	48	62	Butyl alcohol	18.8	77
20	Camphor	21.6	49	63	Isopropyl alcohol	18.8	77
21	Methyl ester of benzoic acid	21.6	49	64	Stearic acid	18.8	77
22	α-Chloronaphthalene	21.5	49	65	Monyl acid	18.8	77
23	Dibutylphthalate	21.45	50.5	66	Ethyl alcohol	18.7	78
24	Dimethylphthalate	21.4	51	67	Tertiary butyl alcohol	18.65	78.5
25	Chloroform	21.2	53	68	Monethyl ester of ethylene glycol	18.55	79.5
26	Triethylamine	21.0	55				
27	Diethyl ester of maleic acid	20.7	58	69	Methyl alcohol	18.4	81
28	Tributylphosphate	20.7	58	70	Butyric acid	18.25	82.5
29	Isoamyl acetate	20.7	58	71	Formamide	18.15	83.5
30	Butyl acetate	20.7	58	72	Benzyl alcohol	17.95	85.5
31	Propyl acetate	20.65	58.5	73	Phenol	17.75	85.5
32	Ethyl acetate	20.65	58.5	74	Glycol	17.75	87.5
33	Acetal	20.65	58.5	75	Acetic acid	17.75	87.5
34	Nitromethane	20.6	59	76	Glycerin	17.6	89
35	Acetone	20.55	59.5	77	Monochloroacetic acid	17.55	89.5
36	Diethyl malonate	20.5	60	78	Water	16.5	100
37	Pyridine	20.4	61	79	Trichloroacetic acid •		117.5
38	Benzyl acetate	20.4	61				
39	Acetonitrile	20.4	61				
40	Pinocoline	20.3	62				
41	Methylbutyl ketone	20.25	62.5				
42	Acetic anhydride	20.2	63				

•S was determined from the effect on the Spectrum of 4-acetylamino-N-methylphthalimide (see Fig. 2).

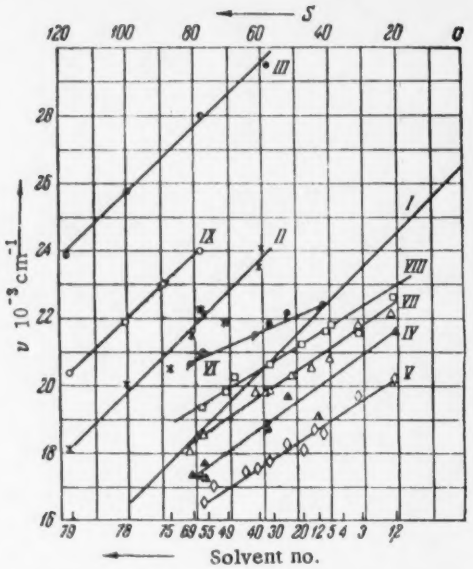

Fig. 2. The ν_{fl}^{max}, solvent relation. I) 4-amino-N-methylphthalimide; II) 4-acetylamino-N-methylphthalimide (Nos. 79, 78, 76, 75, 69, 66, 49, 37, 35); III) o-methoxybenzoic acid (Nos. 79, 78, 66, 32); IV) aminonaphtheurobin (Nos. 69, 67, 66, 32, 25, 2); V) dimethylaminonaphtheurobin (Nos. 66, 51, 44, 37, 32, 25, 19, 14, 7, 3, 2); VI) acetylaminonaphtheurobin (Nos. 69, 66, 37, 32, 25, 7); VII) aminochloromaleinimide (Nos. 69, 66, 40, 32, 29, 25, 16, 6, 2); VIII) cyclohexylaminomaleinimide (Nos. 66, 48, 31, 19, 8, 6, 3, 2); IX) acridine (Nos. 79, 78, 76, 66).

Bond formation could only result in departures from the general rule. On the other hand, the existence of a clearly expressed relation between the alteration of the spectra, the chemical nature of the solvent, and the presence of a functional group in the solvent molecule, as well as the almost complete invariance of the spectra under pronounced alteration in the macro properties of a solvent of given chemical type, all force one to seek the origin of this effect in the micro properties of the solvent [5]. Kosaver [6] has also concluded that the micro properties of the solvent fix the position of the spectra.

LITERATURE CITED

[1] A. I. Kipriyanov and B. E. Petrun'kin, Zhur. Obshchei Khim, 10, 613 (1940); A. I. Kipriyanov and E. S. Tinyushchenko, Zhur. Obshchei Khim., 17, 1468 (1947); Jubilee Collection. AN Ukr. SSR, (Kiev, 1950), p.287; A. I. Kipriyanov, Ukr. Khim. Zhur., 18, 339 (1952).

[2] E. Lippert, J. phys. et rad., 15, 627 (1954).

[3] E. Lippert and F. Moll. Zs.f.Electrochem.,58, 718 (1954).

[4] V. V. Zelinskii, V. P. Kolobkov, and L. G. Pikulik, Opt. i Spektr., 2, 402 (1957).

[5] B. B. Zelinskii, V. P. Kolobkov, and I. I. Reznikova, Transactions of a Conference on Thermodynamics and the Structure of Solutions, January 27-30, 1958, Acad. Sci. USSR Press, 1959, page 262[In Russian].

[6] E. M. Kosaver, J. Am. Chem. Soc., 80, 3253 (1958).

[7] E. G. McRae, Spectrochimica Acta 12, 192(1958).

Received July 6, 1959.

THE SOLUBILITY OF GRAFTED COPOLYMERS DERIVED FROM POLYSTYRENE AND ACRYLIC ACID

M. M. Iovleva, P. V. Kozlov, and Academician V. A. Kargin

M. V. Lomonosov Moscow State University

A close examination of the available data on the properties of double-strand grafted copolymers reveals that these systems exhibit peculiar properties. Thus, the thermomechanical data indicate that the grafted copolymers retain the transition temperatures of the initial components, meaning that they preserve the glass transition temperature (T_g) of the component with the lower T_g, and that the flow temperature (T_f) is determined by the flow temperature of the component with the highest T_f [1, 2]. This means that the grafted segments and the main chain segments exhibit a certain degree of individuality despite the fact that they are chemically bonded to each other. Structural characteristics exhibit similar effects [3].

These observations give rise to a certain ambiguity, in the sense that one does not know how the grafted copolymers should be treated from the standpoint of fundamental thermodynamic concepts, particularly in view of the usual definition for a component.

A component is defined as an independent constituent of a system, or in other words, as a substance which can be removed from the system and exist independently outside of it [4]. When the initial system before grafting includes a polymer and some monomer, there is no doubt that two components are present. The act of grafting involves a chemical reaction which results in the formation of a chemical bond between two polymers. The initial components cease to be independent since they can not anymore be extracted from the system. On this basis we are right in regarding the grafted copolymer as a one-component system. On the other hand, the well-known individual character still retained by the components constituting the grafted copolymer raises certain doubts concerning the above-mentioned formal deduction, and the latter, naturally, requires experimental verification.

According to Gibbs' phase rule the number of components in a system is rigidly controlled by the number of phases and degrees of freedom. The interdependence between these three parameters is usually used to determine the number of degrees of freedom from the known number of phases and components. It is quite obvious that the reverse problem can also be solved – from the number of phases and degrees of freedom, which can be be determined from phase diagrams, one can get the number of components in the system. The phase diagrams of two-component polymeric systems have been examined in great detail in several papers dealing with both homopolymers and copolymers [5-7].

Three-component polymeric systems have been analyzed theoretically by Scott [8], who also listed the principal types of phase diagrams. The three-component systems have also been studied experimentally by Brönsted [9] and Papkov [10, 11].

In our opinion, by studying the phase diagrams of grafted copolymers, and comparing them with the already-known types of diagrams, it should be possible to resolve the problem of the number of components in a grafted copolymer. We used for our study the grafted copolymers of polystyrene and acrylic acid; these were prepared and subjected to a preliminary study in an earlier work [2].

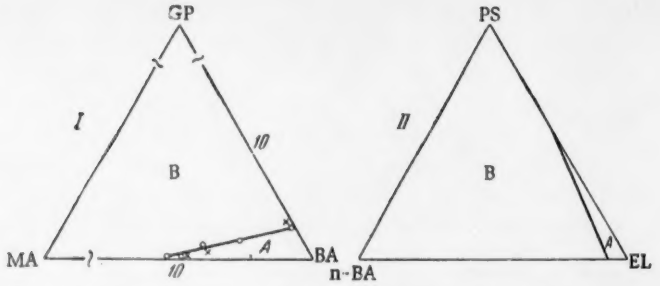

Fig. 1. Phase diagrams: I) grafted copolymer (GP) – benzyl alcohol (BA) – methyl alcohol (MA) system; II) polystyrene (PS) – ethyl laurate (EL) – n-butyl alcohol (n-BA) system. A) Solubility region; B) phase-separation region.

We found that the grafted copolymers were insoluble in the commonly used organic solvents and were only sparingly soluble in acetophenone, benzyl alcohol, and ethyl benzoate. Moreover, even then it took 24-48 hours of refluxing to achieve solution. The resulting solutions remained homogeneous upon cooling.

Due to this solubility behavior the phase diagrams of grafted copolymers could not be studied by means of the methods commonly used for studying two-component systems [5]. We therefore used a method involving the addition of a precipitating component to a solution maintained at a constant temperature [9].

Benzyl alcohol was used as solvent. The solutions were prepared by refluxing the grafted copolymer with benzyl alcohol for 24-48 hours. The resulting homogeneous solutions were cooled and kept at room temperature for 2-3 days, after which the precipitating agent (methyl alcohol) was added until turbidity appeared in solutions of various fixed concentrations. The appearance of turbidity was determined by using a photoelectric colorimeter to note the abrupt increase in optical density. It should be noted that upon standing the system containing the grafted copolymer, benzyl alcohol, and methyl alcohol separated into two phases – a solution of methyl alcohol in benzyl alcohol, and the swollen grafted copolymer dissolved in benzyl alcohol. From the known amounts of grafted copolymer, benzyl alcohol, and methyl alcohol we computed the critical concentrations of the system at this point (at room temperature, 25°).

The experimental critical concentrations in solutions of grafted copolymers with a 5 and 22% acrylic acid content are represented in the form of Gibbs triangles in Fig. 1, I. The figure shows that the critical concentrations of the investigated systems lie on a straight line which starts from the side representing the methyl and benzyl alcohol components and crosses the side representing the grafted copolymer and benzyl alcohol. Both grafted copolymers give practically the same critical concentration line, which is evidently connected with the fact that the component ratio in the two grafted copolymers is not very different.

Our phase diagrams for the grafted copolymer – benzyl alcohol – methyl alcohol system indicate that the given system has one degree of freedom and consists of two phases. Using the phase rule and assuming a constant temperature and pressure we can determine the number of components present:

$$k = f + p = 1 + 2 = 3,$$

where k is the number of components, f the number of degrees of freedom, and p the number of phases.

We thus find that the system containing the grafted copolymer, benzyl alcohol, and methyl alcohol consists of three components. Consequently the grafted copolymer should be regarded as a one-component system.

This result can also be confirmed by comparing our phase diagram with that for a distinct three-component system, namely polystyrene (PS) – ethyl laurate (EL) – n-butyl alcohol (n-BA), shown in Fig. 1,II [9]. In the latter the components interact in the same manner as do those in the previously discussed system: polystyrene is weakly soluble in ethyl laurate, just like the grafted copolymer in benzyl alcohol; polystyrene is immiscible with n-butyl alcohol, and the same was observed in the case of the grafted copolymer and methyl alcohol; n-butyl alcohol is completely miscible with ethyl laurate, and so is benzyl alcohol and methyl alcohol. This

similarity is apparent from the fact that both systems have very similar phase diagrams (Fig. 1). One should, however, note that the solubility region of the second system is greatly attenuated in comparison with that of the first, since the solubility of the grafted copolymer is limited to 2-3%.

The results obtained above and the thermomechanical and structural results mentioned earlier, are in no way contradictory. Apparently the thermomechanical and structural properties depend on fairly large segments of both the grafted polymer and the principal polymer chains. The peculiar thermomechanical and structural properties result from the fact that the formation of chemical bonds between these chain segments does not prevent their more or less independent motion. But in solution phenomena, where the heterogeneous chemically bonded microsegments can only act as a single entity, the grafted copolymer behaves like a one-component system.

From all this one would also conclude that two-strand grafted copolymers should, in general, exhibit very low solubility in solvents in which either one of the copolymer components is highly soluble. This was, in fact, confirmed in one of our earlier papers [2].

LITERATURE CITED

[1] V. A. Kargin, P. V. Kozlov, et al., Vysokomolek. Soed. 1, 114 (1959).

[2] P. V. Kozlov, M. M. Iovleva, and N. A. Platé, Vysokomolek. Soed. 1, 1100 (1959).

[3] H. C. Haas, S. J. Cohen, et al., J. Polimer. Sci., 15, 427 (1955).

[4] A. V. Rakovskii, Introduction to Physical Chemistry [in Russian] , Moscow, 1938.

[5] S. P. Papkov, V. A. Kargin, and Z. A. Rogovin, Zhur. Fiz. Khim. 10, 607 (1937).

[6] A. A. Tager and V. A. Kargin, Zhur. Fiz. Khim. 15, 1029 (1941).

[7] P. V. Kozlov, M.M. Iovleva, and L. L. Shiryaeva, Vysokomolek. Soed. 1, 1106 (1959).

[8] R. Scott, J. Chem. Phys., 17, 268 (1949).

[9] J. N. Brönsted and V. Volgvartz, Trans. Farad. Soc., 36, 619 (1940).

[10] S. Papkov and K. Korshunova, Zhur. Priklad. Khim. 11, 859 (1938).

[11] S. P. Papkov, Vysokomolek. Soed. 1, 395 (1959).

A STEADY-STATE THEORY FOR THE THERMAL EQUILIBRIUM IN THE CONDENSED PHASES OF POWDERS AND EXPLOSIVES

B. I. Plyukhin

Institute of Chemical Physics, Academy of Sciences USSR

(Presented by Academician V. N. Kondrat'ev, June 12, 1959)

In analyzing the thermal processes in the c-phase (condensed phase) of a burning powder or explosive, use is made of the equation [1]:

$$\lambda T'' + cmT' + W(x) + kq_r e^{-kx} = 0 \qquad (1)$$

with the boundary conditions: $T(0) = T_s$ [or $T'(0) = \varphi_s$] and $T(\infty) = T_0$, and where λ is the thermal conductivity coefficient, T the temperature (T_s the temperature at the burning surface, T_0 the initial temperature), c the specific heat at a constant pressure, m the mass combustion velocity, $W = Ae^{-E/RT} = \rho Q_{chem} Ze^{-E/RT}$ the specific rate of heat evolution in the c-phase, ρ the density, Q_{chem} the heat of the reaction, Z the frequency factor, k the absorption coefficient of the radiant energy flux, q_r the radiant energy flux from the g-phase (gas phase).

The c-phase of a burning material is partially decomposed and partially dispersed into the s-phase (smoke-gas phase) [2]. The percent decomposition ν and percent dispersion μ will determine the total heat evolved in the c-phase, $Q_{chem} = \nu Q_0 = (1-\mu)Q_0$, $\nu + \mu = 1$, where Q_0 is the heat for a complete decomposition of the c-phase and the dispersed particles (drops) in the s-phase [for nitroglycerin and pyroxylene powders in vacuo [2] $Q_{chem} \simeq 80$ cal/g; $\nu = 0.3$; $\mu \simeq 0.7$, i.e., $Q_0 = (Q_{chem}/\nu) \simeq 270$ cal/g].

The first integration of Eq. (1) yields the over-all thermal equilibrium in the c-phase:

$$cm(T_s - T_0) = \lambda\varphi_s + \int_0^\infty Ae^{-E/RT}dx + q_r, \quad q_0 = q_h + q_{chem} + q_r, \qquad (2)$$

where $q_0 = cm(T_s - T_0)$ is the heat absorption rate in the c-phase, $q_h = \lambda\varphi_s$ is the heat transmitted from outside by conduction and convection, $q_{chem} = mQ_{chem} = \int_0^\infty Ae^{-E/RT}dx \approx \int_{T_0}^{T_s} Ae^{-E/RT}\frac{dT_s}{\varphi_s} \simeq \frac{AT_s}{\varphi_s}\mathcal{E}_2\left(\frac{E}{RT_s}\right)$ the evolution rate of chemical heat ($E/RT_s \gg 1$), $q_r = \epsilon'\epsilon\sigma T_2^4$ the heat transmitted by radiation,

$\mathcal{E}_2(x) = \int_1^\infty \frac{e^{-xt}}{t^2}dt$ $\left(\text{for } x \geqslant 1 \quad \mathcal{E}_2 x \simeq \frac{e^{-x}}{x}\right)$; ϵ' the opacity coefficient of the powder, ϵ the opacity coefficient of the flame, σ the Stefan constant, T_2 the flame temperature.

After determining the width of the chemical reaction zone, $W(h_{chem}) = W_s/e$ we get $T_{chem} =$

$$= \frac{T_s}{1 + (RT_s/E)\ln(eA_{chem}/A_s)}, \quad h_{chem} \simeq \frac{T_s - T_{chem}}{\varphi_s} = \frac{RT_s^2}{E\varphi_s}\ln\left(e\frac{A_{chem}}{A_s}\right).$$

The heat evolution rate in the c-phase is $q_{chem} \simeq \frac{RT_s^2}{E\varphi_s} Ae^{-E/RT_s} f_s = h_{chem} W_s f_s$, $f_s = 1 - 2\frac{RT_s}{E} + 6\left(\frac{RT_s}{E}\right)^2 - \ldots \simeq 1$.

Thus from the thermal equilibrium Equation (2) we get:

$$m = \frac{q_h + q_{chem} + q_h}{c(T_s - T_0)} = \frac{\lambda\varphi_s + h_{chem} W_s + \varepsilon'\sigma_0 T_2^4}{c(T_s - T_0)}. \tag{3}$$

To get φ_s as a function of T_s it is convenient to first get the approximate solutions of Equation (1), neglecting for the time being the radiant-heat transfer which will be considered separately. Then Equation (1) can be transformed into a dimensionless form:

$$v'' + v' + \delta e^v = 0 \tag{4}$$

with the boundary conditions: $v(0) = 0$ or $v'(0) = v'_s$. $v(\infty) = E(T_0 - T_s)/RT_s^2$, where

$$v = \frac{E(T - T_s)}{RT_s^2}; \quad \xi = \frac{cmx}{\lambda}; \quad \delta = \frac{\lambda\rho Q_0(1-\mu)EZ}{c^2 m^2 RT_s^2} e^{-E/RT_s} = \frac{h_t^2}{\lambda}\left(\frac{dW}{dT}\right)_s. \tag{5}$$

The parameter δ is similar to that used by D. A. Frank-Kamenetskii for thermal detonation [3]; in our case the width of the thermal layer, $h_t = \lambda / cm$, replaces the width (diameter) of the reactant.

Solution of Equation (4), where $v = v(\delta, v_0, \xi)$, on the surface has the form $0 = v(\delta, v_0, 0)$, or in other words the following relationship exists [$\delta = \delta(v_0) = \text{&}\, E(T_0 - T_s)/RT_s^2$]. Consequently,

$$m = Be^{-E/2RT_s} = \sqrt{\frac{\lambda E\rho Q_0(1-\mu)Z}{cRT_s^2\delta(E(T_0 - T_s)/RT_s^2)}} e^{-E/2RT_s} = \sqrt{\frac{\lambda}{c^2\delta}\left(\frac{dW}{dT}\right)}, \tag{6}$$

is identical, except for the coefficient, with the expressions for m derived by Ya. B. Zel'dovich [1] and by A. N. Komogorov et al. [4].

A numerical integration indicates that the thermal contour of $v(\xi)$ depends on the following boundary conditions: a) $v''_s = -(v'_s + \delta) < 0$ (c-phase important), b) $v''_s = -(v'_s + \delta) = 0$ (c-phase unimportant), and c) $v''_s = -(v'_s + \delta) > 0$ (c-phase can be entirely neglected), where v''_s is the curvature of the thermal contour surface.

a) Combustion in vacuo ($-v'_s \ll |v''_s|$): $v'' + \delta e^v = 0$. Combining the solution of our equation with a Michelson solution (for the conservation of thermal flux) we will get:

$v \simeq -2\ln\text{ch}\left(\sqrt{\frac{\delta}{2}}\xi\right)$, $\delta \simeq D^2\frac{v_0^2}{2} = \frac{E^2(T_s - T_0)^2}{2R^2T_2^4}$, $m \simeq D^2\sqrt{\frac{2\lambda\rho ZRT_s^2(1-\mu)Q_0}{c^2(T_s - T_0)^2 E}} e^{-E/2RT_s}$. Since

$v(h_{chem}) = -1$, then $\xi_{chem} = \frac{h_{chem}}{h} \simeq \sqrt{\frac{2}{\delta}}\text{Ar ch}\sqrt{e} = \frac{1{,}54}{\sqrt{\delta}} = 2{,}18\frac{RT_s^2}{E(T_s - T_0)}$ and $\delta \simeq 0{,}422\left(\frac{h_T}{h_{chem}}\right)^2$.

The parameter δ has a simple physical interpretation— it gives the square of the ratio between two rates (in the thermal layer h_e and the chemical layer h_{chem}).

b) Combustion at high pressures ($-v'_s \gg |v''_s|$): $v'_s + \delta e^v = 0$. Again, by combining our solution with a Michelson solution we will get:

$$v \simeq -\ln(1 + \delta\xi), \quad \delta \simeq -v_0 = \frac{E(T_s - T_0)}{RT_s^2} \simeq -v'_s = \frac{h_t}{h_{chem}}, \quad m \simeq \sqrt{\frac{\lambda\rho Z(1-\mu)Q_0}{c^2(T_s - T_0)}} e^{-E/2RT_s}.$$

Since $\nu(h_{chem}) = -1$, then $\xi_{chem} \simeq \frac{h_{chem}}{h_t} = \frac{e-1}{\delta} = \frac{1{,}718}{\delta} = 1{,}718\frac{RT_s^2}{E(T_s - T_0)}$, $\delta \simeq 1{,}718\frac{h_t}{h_{chem}}$.

Again the parameter δ defines the ratio between two rates (h_t and h_{chem}).

The parameters of the c-phase can be related to T_s by means of the equations: $\frac{1}{\tau_{chem}} = Ze^{-E/RT_s}$, $h_{chem} = u\tau_{chem} = \frac{B}{\rho Z}e^{E/2RT_s}$, $h_t = \frac{\lambda}{cm} = \frac{\lambda}{cB}e^{E/2RT_s}$, $\frac{h_{chem}}{h_t} = \frac{cB^2}{\lambda\rho Z}$, $\varphi_s \simeq \frac{T_s - T_{chem}}{h_{chem}} \simeq \frac{\rho ZRT_s^2}{BE}e^{-E/2RT_s}$,

$$q_{chem} \simeq \frac{AT_s}{\varphi_s}\mathcal{O}_2\left(\frac{E}{RT_s}\right) = BQ_0(1-\mu)e^{-E/2RT_s}, \quad q_0 = cm(T_s - T_0) = c(T_s - T_0)Be^{-E/2RT_s}.$$

For a general case Equation (3) has the form:

$$m = \frac{q_h + q_{chem} + q_r}{c(T_s - T_0)} = \frac{[\text{const}(1-\mu)^{-1/3} + \text{const}(1-\mu)^{2/3}]e^{-E/2RT_s} + \varepsilon'\sigma_0 T_2^4}{c(T_s - T_0)}. \tag{7}$$

Let us introduce the thermal equilibrium parameters for the c-phase,

$$\alpha_{chem} = \frac{q_{chem}}{q_0}\cdot\frac{AT_s}{cm\varphi_s(T_s - T_0)}\mathcal{O}_2\left(\frac{E}{RT_s}\right) = \frac{Q_0(1-\mu)}{c(T_s - T_0)} \simeq \frac{h_{chem}}{h_t},$$
$$\alpha_t = \frac{q_h}{q_0} = \frac{\lambda\varphi_s}{cm(T_s - T_0)} = \frac{\lambda\rho ZRT_s^2}{cB^2E(T_s - T_0)}, \quad \alpha_r = \frac{q_r}{q_0} = \frac{\varepsilon'\sigma_0 T_2^4}{c(T_s - T_0)}. \tag{8}$$

In a steady-state approximation the combustion velocities are equal:

$$m = m_1 = m_2 = Be^{-E/2RT_s} = B_1P^{n_1/2}e^{-E_1/2RT_1} = B_2P^{n_2/2}e^{-E_2/2RT_2}, \tag{9}$$

where B_1 and B_2 are two proportionality constants calculated from the Ya. B. Zel'dovich equation [1]; E_1 and E_2 the effective activation energies for reactions in the s- and g-phases; T_1 and T_2 the temperatures in zones of maximum heat evolution in the s- and g-phases; n_1 and n_2 the effective reaction orders in the s- and g-phases, respectively. Whence,

$$\frac{P^{n_2}}{1-\mu} = \text{const}\cdot e^{-E/RT_s}, \quad \frac{dT_s}{dP} = \frac{n_2RT_s^2}{EP} + \frac{RT_s^2}{E(1-\mu)}\frac{d\mu}{dP}. \tag{10}$$

If the degree of dispersion does not vary with the pressure ($d\mu/dP = 0$), we will get an equation similar to the Clausius-Clapeyron equation for the boiling point. Consequently the effects of pressure on the surface temperature T_s are identical regardless of whether the c-phase reaction is exothermic or endothermic, or in other words the Ya. B. Zel'dovich equation for $m(T_s)$ is valid in both cases.

Under reduced pressure the flow of heat into c-phase from outside declines to almost zero, and at low enough pressures (at ~ 40 mm of Hg for nitroglycerin and pyroxylene powders [2]) the surface temperature and the combustion velocity cease decreasing. Thus the results of experiments on the combustion velocity in powders [2] confirm the validity of the Ya. B. Zel'dovich equation, in that, in general, the surface temperature T_s depends on pressure. Equation (10) was verified experimentally [2] and therefore proves a means of determining E and Z.

For the opaque zone (s-phase) temperature T_1 we get:

$$P^{n_2 - n_1} \simeq \text{const}\cdot e^{-E_1/RT_1}, \quad \frac{dT_1}{dP} = (n_2 - n_1)\frac{RT_1^2}{E_1P}. \tag{11}$$

According to Equations (10) and (11) as P is reduced the temperatures T_s and T_1 rapidly decline. However, at certain limiting values $T_{scr} > T_0$ and $T_{1cr} \gg T_{scr}$ the decline in temperature levels off. This constitutes a limiting case in which the effects of pressure have been entirely eliminated.

In the case of secondary explosives, where there is no possibility for the dispersion of solid particles or liquid drops, one only has to consider the relationship between the c-phase and s-phase characteristics, Eq.(9).

The $T_s(P,\mu)$ function derived here enabled us to determine the remaining c-phase characteristics as a function of pressure P and percent dispersion μ:

$$h_{chem} = \frac{B^2}{\rho Z B_2} P^{-n_2/2} e^{E_2/2RT_s} = \text{const} \cdot (1-\mu) Q_0 P^{-n_2/2} e^{E_2/2RT_s},$$

$$h_t = \frac{\lambda}{cB_2} P^{-n_2/2} e^{E_2/2RT_s}, \quad \varphi_s = \frac{\rho Z R T_s^2 B_2}{B^2 E} P^{n_2/2} e^{-E_2/2RT_s} = \text{const} \frac{P^{n_2/2} e^{-E_2/2RT_s}}{(1-\mu) Q_0},$$

$$q_{chem} = B_2 Q_0 (1-\mu) P^{n_2/2} e^{-E/2RT_s},$$

$$q_t = \frac{\lambda \rho Z R T_s^2 B^2}{B^2 E} P^{n_2/2} e^{-E_2/2RT_s} = \text{const} \frac{P^{n_2/2} e^{-E_2/2RT_s}}{(1-\mu) Q_0}.$$

In the range of pressures generated in rockets (100-200 atm) the thermal equilibrium parameters α_{chem} and α_h in Eq. (8) are constant to the first approximation (when μ is constant). Thus for nitroglycerin and pyroxylene powders $\alpha_{chem} \approx 0.70$, $\alpha_h \approx 0.15 - 0.20$ and $\alpha_t \approx 0.10$–0.15 [2]. However, at very high pressures ($P \to \infty$), due to an increase in T_s (P) [see Eq. (10)],

$$\alpha_{chem} = \frac{Q_0 (1-\mu)}{c (T_s - T_0)} \to 0, \quad \alpha_h = \frac{cRT_s^2}{E (1-\mu) Q_0} \to 1, \quad \alpha_r \to 0. \tag{12}$$

To evaluate $\alpha_r = q_r / q_0$ we calculated the radiant heat transfer $q_r = \varepsilon' \varepsilon \sigma T_2^4$ separately as a function of pressure. The opacity of powder $\varepsilon' = 1 - R'$ (where R' is the light-reflection coefficient of the powder surface) is approximately 0.9 [2]. The degree of flame darkness

$$\varepsilon = e^{-\tau_1} (1 - 2\mathcal{E}_3 \tau_2) = e^{-\alpha_1 P M_1 S_1(P)/RT_1} \left[1 - 2\mathcal{E}_3 \left(\frac{\alpha_2 P M_2 S_2(P)}{RT_2} \right) \right],$$

where τ_1 and τ_2 are the optical paths, α_1 and α_2 the absorptivities of the media, M_1 and M_2 the mean molecular weights of the media, S_1 and S_2 the dimensions of the s-phase and the g-phase; $\mathcal{E}_3 x = \int_1^\infty \frac{e^{-xt}}{t^3} dt$.

Calculations have shown that the relative magnitude of radiant heat transfer $\alpha_r = q_r / q_0$ remains practically zero until a flame appears in the g-phase, when it rapidly increases, attaining a maximum (0.07-0.20) at pressures which result in a complete combustion of powders ($\sim$ 50 atm) and then slowly begins to decline; at high pressures the decline is roughly inversely proportional to the pressure.

In regions where the thermal equilibrium parameters vary very little one of three possibilities exist: $\alpha_{chem} > \alpha_h$, $\alpha_{chem} = \alpha_h$, $\alpha_{chem} < \alpha_h$, depending on the heat of the reaction (Q_{chem}) in the c-phase. Thus for the boundary condition $v''_s = -(v'_s + \delta) = 0$ we get $\alpha_{chem} \approx \frac{h_{chem}}{h_t} \approx \frac{1}{\delta} \approx \frac{RT_s^2}{T_s - T_0} \approx 0.07$.

The theories analyzing the heating of the c-phase caused by the flow of heat from the g-phase cover just one limiting case of the thermal equilibrium equation: $\alpha_h \to 1$, $\alpha_{chem} \to 0$, $\alpha_r \to 0$, $Q_{chem} = Q_0 (1-\mu) \to 0$. Theories analyzing the heating of the c-phase caused by a chemical reaction on the combustion surface cover another limiting case: $\alpha_h \to 0$, $\alpha_{chem} \to 1$, $\alpha_r \to 0$, $Q_{chem} = Q_0 (1-\mu) \to c (T_s - T_0)$. Sanger's theory [5] leads to the third case where $\alpha_r \to 1$, which does not seem to be attainable in practice.

LITERATURE CITED

[1] Ya. B. Zel'dovich, Zhur. Eksper. Teoret. Fiz. 12, 498 (1942).

[2] P. F. Pokhil, Coll. Explosion Physics, 2, 1953; P. F. Pokhil, L. D. Romodanova, and M. M. Belov, Coll. Explosion Physics, 3, 1954.

[3] D. A. Frank-Kamenetskii, Zhur. Fiz. Khim. 13, 738 (1939).

[4] A.N. Kolmogorov, I. G. Petrovskii, and N. S. Piskunov, Byull. Mosk. Univ., Division A, 1, No.6 (1937).

[5] E. Sanger, Weltraumfahrt, 1, 4 (1954).

Received June 11, 1959.

THE EFFECTS OF INERT SOLVENTS ON THE PHYSICOCHEMICAL PROCESS IN SOLUTIONS

E. S. Rudakov

All-Union Scientific Research Institute of Petrochemical Processes

(Presented by Academician M. I. Kabachnik, July 15, 1959)

There exist a large number of processes which strongly depend on the medium (solvolysis of alkyl halides, solubilities of certain electrolytes and nonelectrolytes, etc.), and which could not possibly be connected with the formation of specific compounds between the solvent and solute molecules [1]. Let us see if it is possible to account for these effects within the framework of ideal-solution theory [2]. To do this we will use the following equation for the activity coefficient γ_1 of molecules in dilute solutions:

$$RT \ln \gamma_1 = \Delta E_1 = \left[E_1^{1/2} - E_s^{1/2} \left(\frac{V_1}{V_s} \right)^{1/2} \right]^2 = E_1 + E_s \left(\frac{V_1}{V_c} \right)^{2/3} - \\ - 2E_1^{1/2} \cdot E_s^{1/2} \left(\frac{V_1}{V_s} \right)^{1/2}, \quad (1)$$

where ΔE_1 is the potential energy in the given solvent relative to that of the pure solute, which is selected as the standard state; E_1, E_s, V_1, and V_s, are the molar energies and volumes of the solute and solvent respectively.

The activity coefficient is calculated from the equation $\gamma_1 = \frac{1}{P_{10}} \left(\frac{P_1}{N_1} \right)_{N_1 \to 0}$, where P_1 is the vapor pressure of the solute when its mole fraction in solution is N_1, and P_{10} is the vapor pressure of the pure solute.

Equation (1) can be derived in the following manner. Let us assume that $V_1 = V_s$. To transfer molecule 1 from liquid 1 into the solvent we have to: 1) provide energy E_1 to get it into the vapor phase; 2) provide energy E_s to form a "hole" of molecular dimensions in the solvent (it is assumed [4] that the energy of "hole" formation) without evaporation is equal to the energy of vaporization); 3) transfer molecule 1 from vacuum into this hole, gaining the energy $2E_{1s} = 2E_1^{1/2} E_s^{1/2}$. If the volumes V_1 and V_s are not equal, the energy required to form a "hole" of size V_1 in the solvent should be proportional to the "hole" surface, $E_s \left(\frac{V_1}{V_s} \right)^{2/3}$. The energy of interaction between the "hole" and molecule varies accordingly. Equation (1) differs from the usual equation for ideal solutions [2-4],

$$RT \ln \gamma_1 = V_1 \left[\left(\frac{E_1}{V_1} \right)^{1/2} - \left(\frac{E_s}{V_s} \right)^{1/2} \right]^2 = E_1 + E_s \left(\frac{V_1}{V_s} \right) - 2E_1^{1/2} E_s^{1/2} \left(\frac{V_1}{V_s} \right)^{1/2}, \quad (2)$$

in that in the latter the energy of "hole" formation $E_s \left(\frac{V_1}{V_s} \right)$ is taken as proportional to the volume V_1 and not to the surface of the "hole".

Since in the theory of ideal solutions it is assumed that there are no specific interactions between the solute and solvent molecules, we should introduce into Equation (1) the nonspecific interaction energies instead of heats of vaporization, which depend on the molecular association in the liquid and vapor phases. The former can be determined from the Van der Waals constants a_i ($E_i \approx a_i/V_i$) or from the boiling points of the liquids T_i ($E_i \approx cT_i$). Let us examine some of the applications of Equation (1).

1). The solvolysis of tertiary butyl chloride provides an example of a monomolecular reaction where the specific reaction rate decreases by 18 orders of magnitude in going from water to the gas phase [1]. This pronounced solvent effect is not related, however, to any chemical properties of the solvents: the reaction rate is independent of pH [5], and studies carried out in formic acid show that traces of water have no effect on the rate either [6,7]; the rate also remains practically the same in such a variety of chemically different solvents as CH_3NO_2, C_2H_5OH, NH_3, and CH_3COOH [1]. This unusual behavior indicates that the solvents are all inert (with respect to the given reaction), and therefore Equation (1) can be used to calculate the rates.

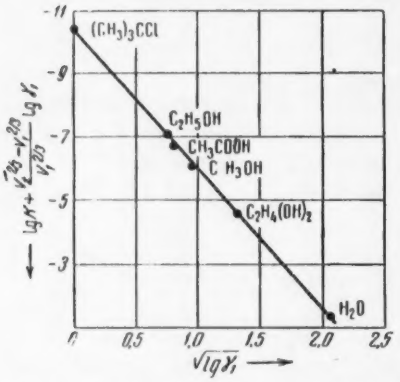

Fig. 1. Relationship between the specific solvolysis rate of $(CH_3)_3CCl$ and its activity coefficient, at 25°C.

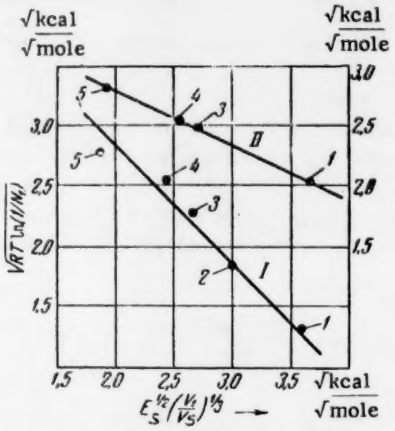

Fig.2. Solubility as a function of the activity parameter of the inert solvent $E_s^{1/2} V_s^{-1/3}$ $\frac{\text{kcal}^{1/2}}{\text{cm}\cdot\text{mole}^{1/6}}$ (Table 2).

I) Solubility of glycine ([14] at 25°) in water (1), formamide (2), methyl alcohol (3), ethyl alcohol (4), and acetone (5) (V_1 = 46.7 cm³/mole); II) solubility of silver acetate (at 25°C [15]) in water (1), methyl alcohol (3), ethyl alcohol (4), and acetone (5) (V_1 = 51.2 cm³/mole).

According to the theory of absolute reaction rates [4] the effects of medium on the specific rate k of a monomolecular reaction can be expressed by the equation:

$$k = k_0 \frac{\gamma_1}{\gamma_\pm}, \qquad (3)$$

where γ_1 and $\gamma_\pm$ are the activity coefficients of the reagent and the activated complex, respectively, while k_0 is independent of the medium. Replacing the activity coefficient γ_1 in Equation (3) by the corresponding function from Equation (1), and $\gamma_\pm$ by the expression:

$$RT \ln \gamma_\pm = \left[E_\pm^{1/2} - E_s^{1/2} \left(\frac{V_\pm}{V_s} \right)^{1/3} \right]^2, \qquad (4)$$

where $E_\pm$ and $V_\pm$ are the molar energy and volume of the activated complex, and by introducing the gas phase reaction rate k_g in place of K_0, we get:

$$RT \ln \frac{k}{k_g} = 2E_s^{1/2} V_s^{-1/3} (E_\pm^{1/2} V_\pm^{1/3} - E_1^{1/2} V_1^{1/3}) - E_s V_s^{-2/3} (V_\pm^{2/3} - V_1^{2/3}). \qquad (5)$$

Since the volume of an activated complex in a monomolecular reaction is not too different from that of

the initial molecule ($\Delta_{\neq} V = 2.8 cm^3/mole$ [13] when $V_1 = 111.1\ cm^3/mole$) we can assume as a first approximation that $V_1 = V_{\neq}$. Then Equation (5) can be simplified to:

$$RT \ln \frac{k}{k_g} = 2E_c^{1/3} \left(\frac{V_1}{V_s}\right)^{1/3} (E_{\neq}^{1/2} - E_1^{1/2}). \quad (6)$$

Using Eq.(6) we get the formula:

$$\lg k_g = \frac{\lambda \lg k_1 - \lg k}{\lambda - 1}, \quad \lambda = \left(\frac{E_s}{E_1}\right)^{1/3} \left(\frac{V_1}{V_s}\right)^{1/3}, \quad (7)$$

where k_1 is the specific reaction rate in pure $(CH_3)_3CCl$; with this rate constant we can compute the reaction rate in the gas phase using the experimental rate data in liquids (Table 1). In our calculations we replaced the E_s/E_1 ratio in Equation (7) with the ratio of boiling points at atmospheric pressure.

With the help of Equation (6) it is also possible to derive Winstein's empirical formula used for comparing the solvolysis rates of various alkyl halides [10-12]; it is also possible to account for the reaction-rate increase with pressure [13], and the peculiarities of reactions in 2-component and 3-component systems.

TABLE 1

Calculated Specific Solvolysis Rates of $(CH_3)_3CCl$ in the Gas Phase at 25°

Medium	V* in cm^3/mole	$\frac{T_c^*}{T_1}$	-log k** in sec^{-1}	-log k_g, in sec^{-1}
Water	18,0	1,152	1,50	19,6
Formic acid	37,9	1,155	3,00	24,0
Glycerin	73,3	1,740	4,10	22,6
Formamide	39,9	1,495	4,33	18,9
Ethylene-glycol	56,0	1,455	4,60	21,7
Methyl alcohol	40,7	1,042	6,17	20,5
Nitromethane	54,0	1,157	6,50	21,0
Acetic acid	57,5	1,208	6,67	20,3
Ethyl alcohol	58,7	1,085	7,05	21,9
Ammonia	28,2	0,742	7,26	19,4
tert-Butyl chloride	111,1	1,000	10,4	—
Measured in the gas phase [9] and extrapolated to 25°.				19,5±2

* Calculated from data given in [8].

** Taken from Ref. [1].

2. Interaction energies calculated from kinetic data. Neglecting the parameter $E_s V_s^{2/3}$, in Equations (1) and (5) we get a linear relationship between the functions for the reaction rate and the activity coefficient of $(CH_3)_3CCl$, which is in full agreement with the experimental results (Fig.1). The value of log γ_1 in ethyleneglycol was calculated from kinetic data taking into consideration the reagent distribution between the liquid and gas phases in the reaction vessel; log $\gamma_1 = 0$ in $(CH_3)CCl$ (standard state); the reamining values are from [12].

Making use of the linearity we find that $E_1 = 5.9$ kcal/mole and $E_{\neq} = 24.9$ kcal/mole. The great difference between these parameters is responsible for the great dependence of the reaction rates on medium.

In Table 2 we have compiled the interaction energies calculated from kinetic data E_i and from Van der Waals constants (a_i/V_i). In comparing these two functions one must remember that the constants a_i were calculated from critical data, and consequently involved the liquid association at the critical point. The method used for calculating the nonspecific interaction energies from the $(CH_3)_3CCl$ solvolysis rate data are free of this error. We have also listed in Table 2 the $E_s^{1/2} V_s^{-1/3}$ values characterizing the activity of the inert solvent. This parameter is in a way equivalent to Hildebrand's solubility parameter [2].

3. Solubility. The activity coefficient of a sparsely soluble compound in a saturated solution is equal to the reciprocal of its mole fraction, $\gamma_1 = 1/N_1$. According to Eq. (1) one would expect for nonelectrolytes the linear relationship between $\sqrt{RT \ln (1/N_1)}$ and $E_s^{1/2} (V_1/V_s)^{1/3}$ to hold, and the slope to be 45°. The solubility of glycine (Fig. 2) confirms this deduction. In the case of CH_3COOAg (Fig.2) and several other electrolytes there is also a distinct relationship between the solubility and parameter $E_s^{1/2} V_s^{-1/3}$.

We wish to thank Corresponding Member Acad. Sci. USSR V. V. Voevodskii for his comments on this work.

TABLE 2

Nonspecific Molecular Interaction Energies in Pure Liquids at 25°C.

Liquid	E_i kcal/mole	a_i/V_i kcal/mole	$E_i^{1/2} V_i^{-1/2}$ in $\frac{kcal^{1/2}}{cm \cdot mole^{1/6}}$	Liquid	E_i, kcal/mole	a_i/V_i, kcal/mole	$E_i^{1/2} V_i^{1/2}$ in $\frac{kcal^{1/2}}{cm \cdot mole^{1/6}}$
Water	6,80	7,42	0,994	Isopropyl alcohol	7,53	—	0,642
Formic acid	9,32	—	0,909	N-methyl propiona-mide	—	—	0,633
C_3F_7COOH	—	—	0,893				
Glycerin	12,60	—	0,848	tert-Butyl alcohol	7,85	—	0,615
Formamide	8,15	—	0,835	Acetic anhydride	7,86	5,12	0,614
Ethylene glycol	9,86	—	0,820	N, N-dimethyl forma	6,63	—	0,604
Methyl alcohol	6,43	5,72	0,737	Acetone	4,84	4,58	0,524
Nitromethane	7,29	—	0,715	tert-Butyl chloride	5,85	—	0,504
Acetic acid	7,39	7,47	0,705	Dioxane	4,48	—	0,476
Ethyl alcohol	7,06	5,00	0,684				
Ammonia	4,20	3,61	0,673				

LITERATURE CITED

[1] E. S. Rudakov, Doklady Akad. Nauk, 127, 1058 (1959).*

[2] J. H. Hildebrand and R. L. Scott, Solubility of Nonelectrolytes, N.Y., 1950.

[3] M. I. Sharparonov, Introduction to The Molecular Theory of Solutions [In Russian], Moscow, 1956.

[4] S. Glasstone, K. Laidler and H. Eyring, The Theory of Rate Processes [Russian Translation], Moscow, 1948.

[5] E. D. Hughes, J. Chem. Soc., 1935, 255.

[6] L. C. Bateman and E. D. Hughes, J. Chem. Soc., 1937, 1187.

[7] L. C. Bateman and E. D. Hughes, J. Chem. Soc., 1940, 935.

[8] A. Weissberger, E. Proskauer, J. Riddick, and E. Toops, Organic Solvents [Russian translation], Moscow, 1958.

[9] B. D. Brealey, G. B. Kistiakowsky and C. H. Stauffer, J. Am. Chem. Soc., 58, 43 (1936).

[10] E. A. Grunwald and S. Winstein, J. Am. Chem. Soc., 70, 846 (1948).

[11] A. H. Fainberg and S. Winstein, J. Am. Chem. Soc., 78, 2770 (1956).

[12] S. Winstein and A. H. Fainberg, J. Am. Chem.Soc., 79, 5937 (1957).

[13] J. Buchanan and S. D. Hamann, Trans. Farad. Soc., 49, 1425 (1953).

[14] T. L. McMeekin, E. J. Cohn and J. H. Weare, J. Am. Chem. Soc., 58, 2173 (1936).

[15] N. A. Izmailov and V. S. Chernyi, Trans. of the Committee on Analytical Chemistry, 9, 44 (1958).

Received July 15, 1959.

*Original Russian pagination. See C. B. translation.

ELECTRON DIFFRACTION STUDY OF THE STRUCTURE OF THE BORON SULFIDE MOLECULE

P. A. Akishin and V. P. Spiridonov

M. V. Lomonosov State University, Moscow

(Presented by Academician V. N. Kondrat'ev, July 16, 1959)

The aim of the present work was to determine the configuration and geometrical parameters of the molecules of boron sulfide B_2S_3 in the vapor state. The work was carried out using the electron diffraction apparatus which has been designed in the Moscow State University for studying the structure of the molecules of compounds which are difficult to volatilize: the apparatus has been described previously [1]. The boron sulfide specimen was prepared by the action of thoroughly purified, dry hydrogen sulfide on amorphous boron [2]. The material was purified by vacuum distillation . It was then loaded into an ampoule in a dry chamber. Before the electron diffraction patterns were recorded the boron sulfide in the molybdenum ampoule of the evaporator was remelted and degassed for a considerable time in a high vacuum directly inside the electron diffraction apparatus. The electron diffraction patterns of the B_2S_3 vapor were recorded at a temperature of ~ 800-900°, with and without the rotating sector, with varying exposures (from 10 seconds to 2 minutes), on diapositive photographic plates covered with a thin layer of black ink (to act as protection against the light radiated by the evaporator) which was washed off before development. 10 series of electron diffraction patterns (2 using the rotating sector) were obtained, at electron wavelengths varying from 0.0402 to 0.0573 A in the different experiments. The intensity of the scattered electrons was estimated visually. The electron diffraction patterns were studied by the version of the radial-distribution method described by Karle and Karle [3-5] and also by the method of successive approximations [6]. A detailed description of the method of working and the examination of the electron diffraction patterns has been given in previous papers from our laboratory [1, 7]. The curve for the radial distribution D(r) constructed from the experimental data (Fig. 1) has three clearly defined peaks at r = 1.73, 3.46 and 5.15 A, together with less well-defined peaks in the region of 2.70 and 4.10 A, which overlap the main peaks. The initial region of the intensity curve, which cannot be studied experimentally, was extrapolated by means of the theoretical curve for the structural element -S-B=S with values: r(B-S) = 1.81 A, r(B=S) = 1.65 A and r(S...S) = 3.46 A, since these three terms of the intensity function make the greatest contribution to the scattering of the B_2S_3 molecule.

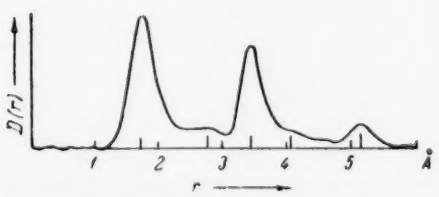

Fig.1. Radial distribution curve for the B_2S_3 molecule.

From structural chemical theory, the most probable configurations for B_2S_3 are: a bipyramid (the three sulfur atoms forming a regular triangle with the two boron atoms situated on either side of the plane of the triangle, at equal distances from it), and a planar angular molecule of the type

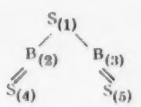

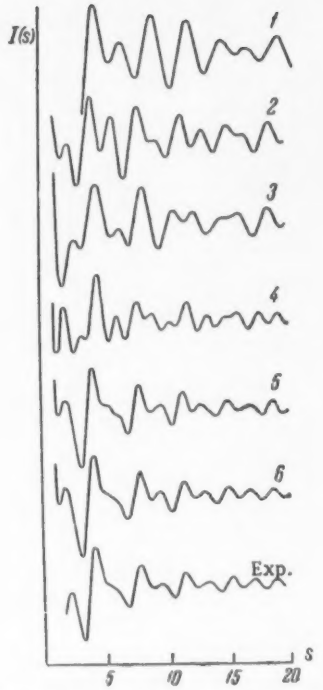

Fig. 2. Comparison of the theoretical intensity curves for various B_2S_3 models with the experimental curve.

Analysis of the D(r) curve shows clearly that the bipyramidal model for B_2S_3 is inapplicable. The two most distinct peaks on the radial-distribution curve would have to be interpreted as the distances B-S = 1.73 A and S-S = 3.46 A. It is impossible, however, to construct a bipyramid with these parameters, since the second distance is double the first. In addition, when the bipyramidal model is chosen, it is impossible to interpret the other peaks in the D(r) curve, and a considerable discrepancy is observed between the calculated and experimental values for the ratio of the peak areas.

In discussing the planar angular model, we have interpreted the radial-distribution curve as follows: the 1st peak at r = 1.73 A is due to the superposition of the two distances $B_{(2)}$-$S_{(1)}$ and $B_{(2)}$=$S_{(4)}$, which are similar in magnitude and cannot be separated; the 2nd peak at r = 3.46 A corresponds to the distance $S_{(1)}$...$S_{(4)}$ between the sulfur atoms linked to the same boron atom; the 3rd peak at r = 5.15 A correspond to the $S_{(4)}$...$S_{(5)}$ distance; and the peaks in the region of r~2.70 A and r ~ 4.10 A correspond to the interatomic distances $B_{(2)}$...$B_{(3)}$ and $B_{(3)}$...$S_{(4)}$, respectively. The ratio of the areas of the two peaks on the D(r) curve at r = 1.73 A and r = 3.46 A is equal to 1.5, while the theoretical ratio for the model under consideration is 1.3. This allocation of the peaks on the D(r) curve corresponds to a B-S-B angle of approximately 96°. Since the value r = 3.46 A for the peak corresponding to the S(1)...S(4) distance is double the value r = 1.73 A for the peak corresponding to the superposition of the similar $B_{(2)}$-$S_{(1)}$ and $B_{(2)}$=$S_{(4)}$* distances, the data from the D(r) curve show that the S-B=S group is linear. Thus the planar angular model for the B_2S_3 molecule shows good agreement with the radial distribution curve.

We shall next consider the results obtained by the method of successive approximations. Figure 2 gives the theoretical intensity curve 1, constructed for the bipyramidal B_2S_3 model with parameters: r(B-S)= 1.80 A, ∠S-B-S = 84° and ∠B-S-B = 78°; it can be seen that this curve does not agree with the experimental curve. The following B_2S_3 models were also rejected: a) a tetragonal pyramid with base formed by a quadrilateral of alternating boron and sulfur atoms, with a sulfur atom at the apex (Fig.2,2); b) planar models (Fig.2,3,4) of the

type 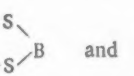 and . Figure 2 shows that curves 2-4 do not agree with the experimental

curve. We can also see that the interatomic distances for models of these types do not agree with the data obtained from the radial-distribution curve. Figure 2,(5) gives the theoretical I (s) curve for the planar angular B_2S_3 model with parameters: r[$B_{(2)}$ - $S_{(1)}$]= 1.81 A, r [$B_{(2)}$ = $S_{(4)}$] = 1.65 A and B-S-B angle equal to 96°. This curve shows satisfactory agreement with the experimental curve. The outer side of the second maximum on this curve, however, shows two intensity steps; the seventh maximum has an asymmetric contour, and the ninth maximum is smoothed out, which is not observed in the experimental curve. Complete agreement between the theoretical and experimental curves can be obtained if it is assumed that the contribution to the scattering from the interatomic distances $B_{(2)}$...$B_{(3)}$, $B_{(3)}$...$S_{(4)}$ and $S_{(4)}$...$S_{(5)}$ is less than expected for a rigid molecule. For the B_2S_3 model under consideration, it is natural to assume considerable deformational vibrations of the valence angle of the central sulfur atom. Unfortunately, exact calculation of the amplitudes of vibration of the atoms in the B_2S_3 molecule is at present impossible, since there are no experimental data on the vibrational frequencies of this molecule. We therefore used the D(r) curve to calculate the effective values, as described earlier [3]; these values are proportional to the mean squared amplitudes of vibration of the pairs of atoms under

*The number of interatomic distances of each of these types in the B_2S_3 model under consideration is the same, so that the value r = 1.73 A is equal to half the sum of the $B_{(2)}$-$S_{(1)}$ and $B_{(2)}$=$S_{(4)}$ distances.

consideration, which were then used to calculate the theoretical intensity curve (Fig. 2,6), and it can be seen that good agreement is obtained with the experimental curve. The values of $s_{theor.}$ for Curve 6 are compared with the values of $s_{exp.}$ in Table 1. The error in the value of the B-S-B angle was found by the method of successive approximations. Thus the electron diffraction data which we have obtained for the structure of the boron sulfide molecule are best satisfied by a planar angular molecule with linear arrangement of the bonds formed by the boron atoms, and the following values for the parameters: r(B-S) = 1.81 ± 0.02 A; r(B=S) = 1.65 ± 0.03 A; < B-S-B = 96 ± 5°.

It should be mentioned that the r(B=S) = 1.65 A which we have found for the B_2S_3 molecule is close to the interatomic distance in the diatomic BS molecule (1.62 A), calculated from the value of the constant B_e from spectroscopic data [8].

TABLE 1

Results of the Analysis of the Electron Diffraction Patterns for B_2S_3

Max.	Min.	l (s)	s_{theor}	s_{exp}	$\frac{s_{theor}}{s_{exp}}$
1		−2	1,83	(2,20)	(0,832)
	2	−25	3,03	(3,14)	(0,965)
2		+20	4,07	4,03	1,010
	3	—	—	(4,93)	—
3		—	—	(5,81)	—
	4	−10	6,82	6,76	1,009
4		+10	7,82	7,72	1,013
	5	−1	8,77	8,62	1,017
5		+1	9,51	9,54	0,997
	6	−6	10,44	10,44	1,000
6		+6	11,41	11,35	1,005
	7	−1,5	12,31	12,25	1,005
7		+1,5	13,03	13,23	0,985
	8	−4	14,03	14,21	0,987
8		+4	15,04	15,18	0,991
	9	−2	16,03	16,04	0,999
9		+2	16,83	16,95	0,993
	10	−3	17,77	17,87	0,994
10		+2	18,72	18,79	0,996
Mean value					1,000
Mean deviation					±0,006

LITERATURE CITED

[1] P. A. Akishin, M. I. Vinogradov, et al., Pribory i Tekhnika Eksperimenta, 3, 70 (1958).

[2] G. Brauer, Preparative Inorganic Chemistry (Russian translation), IL, 1956.

[3] I. L. Karle and J. Karle, J. Chem. Phys., 17, 1052 (1949).

[4] J. Karle and I. L. Karle, J. Chem. Phys., 18, 957 (1950).

[5] I. L. Karle and J. Karle, J. Chem. Phys., 18, 963 (1950).

[6] L. Pauling and L.O. Brockway, J. Chem. Phys., 2, 867 (1934).

[7] P. A. Akishin and V. P. Spiridonov, Kristallografiya, 2, 475 (1957).

[8] P.B. Zeeman, Phys. Rev., 80, 902 (1950).

Received July 15, 1959.

A STUDY OF ELECTRODE PROCESSES ON AN INDIUM AMALGAM USING RADIOACTIVE TRACERS

G. M. Budov and V. V. Losev

Institute of Electrochemistry Academy of Sciences, USSR
L. Ya. Karpov Physicochemical Scientific Research Institute

(Presented by Academician A. N. Frumkin, May 12, 1959)

Measurement of exchange currents and determination of transfer coefficients are at present used extensively as methods for examining the kinetics of the processes of anodic dissolution and the electrodeposition of metals. For the same purpose, use may also be made of a method based on a combination of electrochemical and radiochemical measurements. This method makes it possible to isolate one of the interconnected electrode processes and to study the relationship between its rate and the potential, in the equilibrium-potential range and under conditions where the corresponding reverse process predominates [1]. This method has been used to study the relationship between the rate of the anodic process of zinc amalgam dissolution and the potential [1,2]. * We have considered it of interest to use the method to examine the regular features governing the electrode processes at a metal amalgam, with as low an exchange current as possible, in order to avoid the necessity of adding a surface-active agent. We have chosen indium amalgam, since according to polarographic data [4,5], the discharge of indium ions (in the absence of activating anions) gives irreversible waves, and it may be assumed that the exchange currents are small.

The work was carried out using the method previously described [1-3], with several improvements: in particular, a magnetic stirrer was added to the cell to agitate the amalgam and solution (400 rev/min). The radioactive isotope In^{114} was used for the radiochemical measurements.

We have studied the relationship between the rate of the true anodic process (i_a) and the potential at 20.0 ± 0.1°, at indium amalgam concentrations of 0.002-0.9 M, in solutions of 0.0004-0.03 M $In(ClO_4)_3$ +0.01 M $HClO_4$ containing added $NaClO_4$ to give a constant ionic strength (3M). Figure 1 shows the relationship between the rate of the true anodic process i_a and the potential, together with the ordinary polarization curves recorded with respect to current. It is clear from Fig. 1 that a linear relationship is observed between the potential and log i_a. In addition to the curve for the anodic process, corresponding to constant $In(ClO_4)_3$ concentration (0.03 M), Fig. 1 also gives values for the exchange current i_0 at the equilibrium potentials φ_e for other $In(ClO_4)_3$ concentrations, at constant amalgam concentration (0.1 M). It can be seen that the values of i_0, measured at different indium ion concentrations in the solution, lie, with a fair degree of accuracy, on the straight line for the anodic process, recorded at the same amalgam concentration. Thus the rate of the anodic processs is independent of the $In(ClO_4)_3$ concentration. This result also shows that the gradient of the anodic (φ, log i_a) curve, from which the transfer coefficient β is determined as usual, using the relationship

*To eliminate the influence of concentration polarization, the exchange current was deliberately reduced by adding a surface-active agent – tetrabutyl ammonium sulfate. When this additive is not present, the exchange rate is so high that the exchange currents can only be measured at different concentrations of zinc in the amalgam and solution [3].

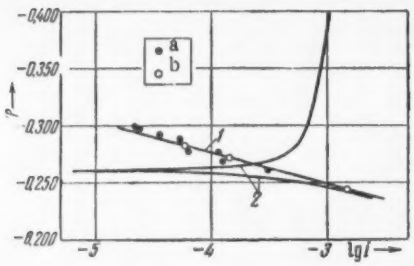

Fig.1. True anodic curve (1), polarization curves (2) for C_a = 0.1 M, C_s = 0.03 M, and exchange currents for various $In(ClO_4)_3$ concentrations (0.0004-0.03 M) and C_a = 0.1 M. a) Exchange current, b) rate of true anodic process i_a.

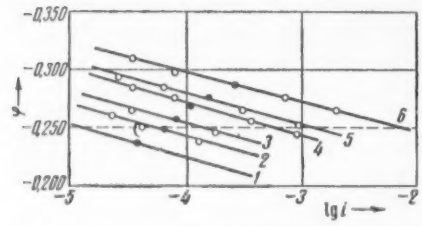

Fig. 2. True anodic curves for different amalgam concentrations 1) 0.002 M, 2) 0.0075 M, 3) 0.025 M, 4) 0.1 M, 5) 0.3 M, 6) 0.9 M In and C_s = 0.01 M $In(ClO_4)_3$.

$b_a = \partial\varphi/\partial \lg i_a = 2.3\,RT/\beta F_e$ coincides with the gradient of the curve with coordinates (φe, log i_0)*. Thus determination of the transfer coefficient by the two methods gives identical results, as was to be expected under conditions where the rate of the electrode process is determined by the discharge-ionization stage.

The relationship between the rate of the true anodic process and the potential, at different amalgam concentrations, is shown in Fig. 2. With increase in the amalgam concentration, the anodic curves are shifted towards more negative values while the gradient remains unchanged and amounts to b_a = = 0.0265 v, which corresponds to the transfer coefficient $\beta = 2.3RT/b_aF = 2.20 \pm 0.07$. The quantitative relationship between i_a and the amalgam concentration at constant potential may be estimated from the dotted line in Fig. 2 at φ =-0.250 v; the points of intersection of the anodic curves with this straight line give the values of i_a at constant potential. The relationship, found in this way, between the rate of the anodic process i_a and the amalgam concentration, is linear.

We have determined the transfer coefficient α using the data for the relationship between the exchange current and the equilibrium potential at different amalgam concentrations and constant indium concentration in the solution, which are shown in Fig. 3, together with the curve for the true anodic process and the corresponding polarization curves for the same solution and 0.3 M amalgam. The relationship between φ_e and log i_0 is linear, with gradient 0.064 v, so that $\alpha = 2.3RT/F(\partial\varphi_e/\partial \log i_o)_{C_s} = 0.91 \pm 0.02$. . The results of the measurement of the exchange current at different temperatures (6-60°) show that the relationship between log i_0 and $1/T$ is linear; the activation energy is 13.4 kcal.

Figure 1 shows that at a sufficient distance from the equilibrium potential in a positive direction, the values of i_a recorded by the radiochemical method coincide with the anodic polarization curve recorded with respect to current. Generally speaking, we should expect the same agreement between the true cathodic curve (recorded with respect to values of the exchange current at different values of C_a and constant C_s) and the cathodic polarization curve, recorded with respect to current, at a sufficient distance from the equilibrium potential in a negative direction. As can be seen from Fig. 3, however, these curves diverge considerably, and the gradient of the cathodic polarization curve is several times greater than the gradient of the true cathodic curve, and amounts to approximately 500 mv. It is evident that the polarization curve, recorded with respect to current at an appreciable distance in a negative direction from the equilibrium potential, does not correspond to the rate of the stage involving discharge of the indium cations. At the same time it can readily be seen that the nature of this curve is not determined by the process of indium ion transfer to the solution. In fact, when NaI (0.05 M) is added to the solution, the cathodic current increases sharply, and, in accordance with the literature data [4,5], a clearly defined cathodic-diffusion limiting current ($\sim 10^{-2}$ a/cm^2) is observed. At sufficiently high polarizations, the cathodic curve, recorded with respect to current, evidently reflects the presence of some chemical stage preceding the discharge of the indium ions.

*In the determination of the transfer coefficients from the gradient of the straight line (φ_e, log i_0), we may use the equations $(\partial\varphi_e/\partial \log i_0)_{C_a} = 2.3RT/\beta F$ and $(\partial\varphi_c/\log i_0)_{C_s} = 2.3RT/\alpha F$, which are readily obtained from the the relationship $i_0 = kC_a^{\alpha/n} C_s^{\beta/n}$ [3] (C_a and C_s are the concentrations of metal in the amalgam and solution) using the Nernst equation.

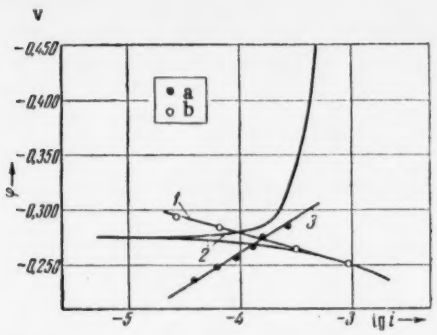

Fig. 3. True anodic curve (1) and polarization curves (2) for C_a = 0.3 M, C_s = 0.01 M, and the true cathodic curve (3), recorded with respect to the exchange current, for different amalgam concentrations (0.002-0.9 M). a) Exchange current, b) rate of true anodic process i_a.

The results which we have obtained may be expressed by the equation $i_a = k\,[In]e^{\beta F\varphi/RT}$, where β=2.2. Taking account of the fact that the relationship between the logarithm of the exchange current and the amalgam potential at constant C_s (Fig.3) is linear, and that the sum of α and β is close to 3, i.e. to the total number of electrons taking part in the electrode process, it may be concluded that under our conditions, the rate of the electrode process is determined by the stage involving the ionization and discharge of indium ions. As in the case of oxidation – reduction reactions in solution, the simultaneous removal of several electrons in electrode processes is less probable than the step-wise removal of electrons, where only one electron takes part in each unit stage [6,7]. Thus, for example, in the anodic dissolution of metals, where the final stable products are multi-charged cations, it is possible that cations of lower valence are produced as intermediate species. In particular, it may be assumed that the process of anodic dissolution of indium involves the three one-electron processes: $In \rightarrow In^+ + e$, $In^+ \rightarrow In^{2+} + e$, and $In^{2+} \rightarrow In^{3+} + e$.*

Since the (φ, log i_a) curve for the true anodic process remains linear in the equilibrium potential range, the value of the exchange current of one of the successive stages must be much less than the value of the exchange currents of the other stages [1,11], so that it may be assumed that one of the successive stages is a nonequilibrium process, and that its rate determines the rate of the total process, while the two remaining stages are equilibrium processes. The most probable assumption is that the stages involving the removal of the first and second electrons are equilibrium stages [12], and that the rate of the over-all process is determined by the rate of the last stage: $i_a = k'\,[In^{2+}]e^{\beta' F\varphi/RT}$. Taking account of the equilibrium conditions of the first two stages $[In^{2+}] = K\,[In]e^{2F\varphi/RT}$, we obtain $i_a = k''\,[In]e^{(2+\beta')F\varphi/RT} = k''\,[In]e^{\beta F\varphi/RT}$, where $\beta = 2 + \beta'$. For the cathodic process, we find that $i_c = k'''\,[In^{3+}]e^{-\alpha F\varphi/RT}$**. Consequently, if the rate of the over-all process is in fact determined by the rate of the stage $In^{2+} \rightarrow In^{3+} + e$, we should observe the conditions $\beta > \alpha$ and $\beta > 2$ (since $\alpha + \beta = 3$), which agrees with experiment. The assumption that the first stage is the limiting stage leads to the relationships $\alpha > \beta$ and $\alpha > 2$, while the second stage gives $\alpha > 1$ and $\beta > 1$, which are contradictory to the experimental data.

In the case of zinc amalgam, we have previously found the values $\alpha = 0.52$ and $\beta = 1.40$ [3], and on the basis of analogous arguments we have concluded that the rate of the over-all electrode process was determined by the stage $Zn^+ \rightarrow Zn^{2+} + e$ [1,2]. It is interesting to note that this large difference between the values of the transfer coefficients is also obtained for the majority of other electrode processes of the type $M \rightarrow M^{2+} + 2e$ at metal electrodes.*** The difference between the transfer coefficients in these cases is again evidently explained by the fact that the rate of the over-all process is determined by that of the stage $M^+ \rightarrow M^{2+} + e$, so that the experimental values of the coefficient β differ from the true values of the transfer coefficient corresponding to the limiting stage of the process, as a result of the influence of the preceding equilibrium stage $M \rightleftarrows M^+ + e$, as has been shown above in detail for the case of indium amalgam. This assumption is confirmed by the fact

*The results of the study of the oxidation – reduction potentials and the reducing properties of the system In–In^{3+} indicate that this system contains In^+ ions [8] and also, apparently, In^{2+} ions [9]. The anodic polishing of indium in perchlorate solutions containing C_2H_5OH or CH_3COOH is also accompanied by the formation of In^+ ions [10].

**It is clear from these relationships that, of the transfer coefficients α and β determined by experiment, in this case only α does in fact characterize the limiting stage of the electrode process, while the coefficient β' corresponding to the ionization stage, can be obtained from the experimental data only using the relationship $\beta' = \beta - 2$ [2].

***For cadmium amalgam [13], $\beta = 1.66$ and $\alpha = 0.42$; for nickel [14, 15], α varies between 0.32 and 0.70; for cobalt [16], $\alpha = 0.82$; and for copper [17], $\alpha = 0.50$ and $\beta = 1.40$ (the values of α and β have been recalculated in accordance with the normalization $\alpha + \beta = 2$).

that for one-electron oxidation – reduction electrode processes, the values of α and β, as a rule, are much closer to one another than for two-electron processes.* On the other hand, it has been proved in recent years that the anodic dissolution of a number of metals [8, 10, 19, 20] and the discharge of certain cations [21-23] lead to the formation of cations of intermediate valence. This is also in accordance with our conclusion regarding the step-wise nature of the processes of metal dissolution and ionization.

We have to express our gratitude to Academician A. N. Frumkin for valuable advice during discussion of the present work.

LITERATURE CITED

[1] V. V. Losev, Doklady Akad. Nauk SSSR,100, 111 (1955); V. V. Losev, Tr. Inst. Fiz. Khim. Akad. Nauk SSSR, No.6, 20 (1957).

[2] V. V. Losev and A. M. Khopin, Transactions of the 4th All-Union Electrochemical Conference, (Acad. Sci. USSR Press, 1959), p. 116.

[3] G. M. Budov and V. V. Losev, Doklady Akad. Nauk USSR, 122, 90 (1958).

[4] D. Cozzi and S. Vivarelli, Zs. Elektrochem., 57, 408 (1953).

[5] M. Bulovova, Collection Czech. Chem. Comm., 19, 1123 (1954).

[6] A. N. Frumkin, Problems of Chemical Kinetics (in Russian) (Acad. Sci. USSR Press, 1955), p. 402.

[7] D. C. Grahame, Ann. Rev. of Phys. Chem.,6, 337 (1955).

[8] W. Kangro and F. Weingärtner, Zs. Elektrochem., 58, 505 (1954).

[9] L. G. Hepler, Z. Z. Hugus, and W. M. Latimer, J. Am. Chem. Soc., 75, 5672 (1953).

[10] I. Epelboin, Zs. Elektrochem., 59, 689 (1955); I. Epelboin and M. Froment, Metaux (Corros. inds.), No.378, 3 (1957).

[11] K. I. Vetter, Zs. f. Naturforsch.,7a, 328 (1952); 8a, 832 (1953); Zs.Elektrochem., 56, 797 (1952).

[12] A. N. Frumkin et al., The Kinetics of Electrode Processes [in Russian], (Moscow, 1952), p. 231.

[13] H. Gerischer, Zs. Elektrochem, 57, 604 (1953); T. Berzins and P. Delahay, J. Am. Chem.Soc., 77, 6448 (1955).

[14] H. A. Laitinen, K. B. Oldham, and P. Kivalo, J. Am. Chem. Soc.,75, 4148 (1953).

[15] P. Delahay and J. E. Strassner, J. Am. Chem. Soc., 74, 6232 (1952).

[16] P. Delahay and C. C. Mattax, J. Am. Chem. Soc., 76, 874 (1954).

[17] L. I. Antropov and S. Ya. Popov, Zhur. Prikl. Khim., 27, 55 (1954);** E. Mattson and R. Lindström, Proc. 6th Meet. CITCE, 263 (1955); R. Audubert, C. R., 238, 1997 (1954); H. Fischer and R. Sroka, Zs. Elektrochem., 60, 109 (1956); J. O. M. Bockris and B. E. Conway, J. Chem. Phys., 28, 707 (1958).

[18] a) W. Mehl and J. O. M. Bockris, J. Chem. Phys., 27, 818 (1957). b) H. Gerischer, Zs. Elektrochem., 62, 256 (1958).

[19] J. Kleinberg, A. W. Davidson, et al., J. Am. Chem. Soc., 76, 363 (1954); 78, 556, 559 (1956).

[20] D. V. Kokoulina and B. N. Kabanov, Doklady Akad. Nauk SSSR, 112, 692 (1957).**

[21] R. H. Sanborn et al., J. Am. Chem. Soc., 78, 4852 (1956).

---

* Unfortunately, the literature contains almost no reliable data for the transfer coefficients of the type $M \rightleftarrows M^+ + e$, since the rate of these reactions is extremely high (for silver [18a] $\alpha = 0.55$, and, from other data [18b], $\beta = 0.68$). Preliminary data which we have obtained indicate that for the system Tl amalgam – $TlClO_4$, $\alpha = 0.4$ and $\beta = 0.6$.

** Original Russian pagination. See C. B. Translation.

[22] A. Vlcek, Chem. Listy, 50, 1072 (1956).

[23] H. Imai, J. Electrochem. Soc. Japan, 23, 583 (1955).

Received April 28, 1959.

THE DIELECTRIC PERMEABILITY AND DIPOLE MOMENTS OF CERTAIN ORGANOSILICON COMPOUNDS

A. A. Gundyrev, N. S. Nametkin, G. M. Panchenkov and Academician A. V. Topchiev

I. M. Gubkin Moscow Oil, Chemical, and Gas Industry Institute

Dielectric permeability. An apparatus operating by the beat method at a frequency of $7{,}95 \cdot 10^5$ cps was used to measure the dielectric permeability of fifteen organosilicon compounds: hexaalkyl derivatives of disilanemethane, disilaneethane, disiloxane and linear polyethylsiloxanes. All the measurements were carried out at a temperature of 25 ± 0.05°. The dielectric permeability was measured with an accuracy of 0.02%. The results of the measurements are given in Table 1.

From the data given in Table 1 it is evident that the dielectric constants of the hexaalkyl derivatives of disilylmethane and disilylethane increase within each series from the hexamethyl to the corresponding hexabutyl derivative, the greatest change taking place on passing from the hexamethyl to the hexaethyl derivative. Comparison of the dielectric constants of compounds of these two series, having identical alkyl radicals, shows that they are very nearly the same.

Table 1 also gives the value of the dielectric permeability of hexamethyldisiloxane obtained by us earlier [1]. This value shows good agreement with literature data [2]. The dielectric permeability of the hexaalkyl derivatives of disiloxane does not change regularly with increase in the molecular weight of the compounds. Hexamethyldisiloxane has the lowest value, after which, in order of increasing dielectric permeability, the compounds of this series are arranged in the sequence: hexabutyl-, hexapropyl- and hexaethyldisiloxane. It is interesting to note that the compounds of this series fall in the same sequence when arranged in order of increasing density d_4^{20} [3].

Dipole moments. The dipole moments of all the compounds listed in Table 1 were calculated by Hedestrand's method [4] from the measured values of the dielectric permeability, density and refractive index of dilute solutions of these compounds in n-hexane. The results of the measurements for different concentrations of dissolved substance are given in Table 2. The concentrations (C) are expressed in mole fractions.

The dipole moments were calculated using the formula:

$$\mu = 0{,}012813 \cdot 10^{-18} \sqrt{P_{or} \cdot T}, \qquad (1)$$

where μ is the dipole moment, P_{or} is the orientation polarization and T is the absolute temperature.

TABLE 1

Dielectric Permeability of Hexaalkyl Derivatives of Disilanemethane, Disilaneethane and Linear Polyethylsiloxanes at 25°

Compound	ε_{25}	Compound	ε_{25}
$(CH_3)_3SiCH_2Si(CH_3)_3$	2,1253	$(CH_3)_3SiOSi(CH_3)_3$	2,1719
$(C_2H_5)_3SiCH_2Si(C_2H_5)_3$	2,2173	$(C_2H_5)_3SiOSi(C_2H_5)_3$	2,2592
$(C_3H_7)_3SiCH_2Si(C_3H_7)_3$	2,2370	$(C_3H_7)_3SiOSi(C_3H_7)_3$	2,2685
$(C_4H_9)_3SiCH_2Si(C_4H_9)_3$	2,2412	$(C_4H_9)_3SiOSi(C_4H_9)_3$	2,1928
$(CH_3)_3SiCH_2CH_2Si(CH_3)_3$	2,1059	$(C_2H_5)_3SiO[(C_2H_5)_2SiO]_4Si(C_2H_5)_3$	2,4421
$(C_2H_5)_3SiCH_2CH_2Si(C_2H_5)_3$	2,2044	$(C_2H_5)_3SiO[(C_2H_5)_2SiO]_5Si(C_2H_5)_3$	2,4623
$(C_3H_7)_3SiCH_2CH_2Si(C_3H_7)_3$	2,2473	$(C_2H_5)_3SiO[(C_2H_5)_2SiO]_6Si(C_2H_5)_3$	2,4818
$(C_4H_9)_3SiCH_2CH_2Si(C_4H_9)_3$	2,2590	$(C_2H_5)_3SiO[(C_2H_5)_2SiO]_7Si(C_2H_5)_3$	2,5010

TABLE 2

The Dielectric Permeability ϵ, Density d and Refractive Index n_D of Solutions of Hexaalkyl Derivatives of Disilanemethane, Disilaneethane and Linear Polyethylsiloxanes in n-Hexane at 25°

Hexaalkyl derivatives of disilanemethane				Hexaalkyl derivatives of disilaneethane				Linear polyethylsiloxanes			
C	ϵ	d	n_D	C	ϵ	d	n_D	C	ϵ	d	n_D
Hexamethyldisilanemethane				Hexamethyldisilaneethane				Tetradecaethylhexasiloxane			
0	1,8854	0,6549	1,3724	0	1,8854	0,6549	1,3724	0	1,8854	0,6549	1,3724
0,0214	1,8963	0,6593	1,3745	0,0197	1,8948	0,6583	1,3741	0,0193	1,9381	0,6832	1,3798
0,0378	1,9021	0,6624	1,3761	0,0359	1,9012	0,6610	1,3755	0,0354	1,9763	0,7029	1,3851
0,0513	1,9061	0,6651	1,3774	0,0501	1,9066	0,6633	1,3765	0,0503	1,9981	0,7160	1,3886
Hexaethyldisilanemethane				Hexaethyldisilaneethane				Hexadecaethylheptasiloxane			
0	1,8854	0,6549	1,3724	0	1,8854	0,6549	1,3724	0	1,8854	0,6549	1,3724
0,0209	1,9050	0,6635	1,3768	0,0205	1,9075	0,6638	1,3769	0,0189	1,9455	0,6867	1,3808
0,0357	1,9164	0,6692	1,3797	0,0345	1,9140	0,6691	1,3798	0,0325	1,9944	0,7056	1,3853
0,0513	1,9247	0,6747	1,3825	0,0507	1,9297	0,6754	1,3829	0,0463	2,0229	0,7232	1,3900
Hexapropyldisilanemethane				Hexapropyldisilaneethane				Octadecylethyloctasiloxane			
0	1,8854	0,6549	1,3724	0	1,8854	0,6549	1,3724	0	1,8854	0,6549	1,3724
0,0203	1,9054	0,6657	1,3780	0,0201	1,9086	0,6657	1,3784	0,0193	1,9554	1,6916	1,3827
0,0361	1,9197	0,6730	1,3819	0,0355	1,9228	0,6733	1,3823	0,0332	1,9986	0,7135	1,3890
0,0509	1,9316	0,6797	1,3853	0,0497	1,9389	0,6801	1,3858	0,0482	2,0368	0,7338	1,3940
Hexabutyldisilanemethane				Hexabutyldisilaneethane				Eicosethylnonasiloxane			
0	1,8854	0,6549	1,3724	0	1,8854	0,6549	1,3724	0	1,8854	0,6549	1,3724
0,0197	1,9092	0,6681	1,3787	0,0199	1,9142	0,6685	1,3796	0,0188	1,9614	0,6948	1,3835
0,0351	1,9273	0,6772	1,3840	0,0350	1,9322	0,6777	1,3844	0,0320	2,0087	0,7187	1,3889
0,0497	1,9435	0,6854	1,3883	0,0486	1,9488	0,6853	1,3883	0,0457	2,0448	0,7384	1,3963

In the calculation of the dipole moments, the deformational polarization was taken as equal to the molar refraction.

Table 3 gives the values obtained for the dipole moments of the hexaalkyl derivatives of disilanemethane, disilaneethane and linear polyethylsiloxanes, together with the values for the dipole moments of hexaalkyl derivatives of disiloxane calculated by us earlier [1]. Of the compounds listed in Table 3, literature data on the dipole moments are available only for hexamethyl- and hexaethyldisiloxane. The dipole moment of hexamethyldisiloxane, measured in benzene, was found to be equal to 0.80 debye [5]. According to other data [6], the dipole moment for this compound, again measured in benzene, is equal to 0.79 debye. These values are in good agreement with the dipole moment of hexamethyldisiloxane as measured by us in n-hexane, namely 0.78 debye [1]. In order to obtain a more complete comparison of our data with the literature data, we have measured the dipole moment of hexamethyldisiloxane in benzene at 25°. The value found was 0.78 debye, i.e., the same as in n-hexane. The value given for the dipole moment of hexaethyldisiloxane, measured in carbon tetrachloride at 24.2°, is 0.63 ± 0.01 debye [7]. This value is also in good agreement with the value of the dipole moment which we have obtained, namely, 0.66 debye.

The values for the dipole moments given in Table 3 show that all the hexaalkyl derivatives of disilanemethane and disilaneethane have practically identical dipole moments, the average value being 0.57 debye. Thus the value of the dipole moment of these compounds is not affected by the length of the main chain of the molecule or by the nature of the alkyl radicals joined to the silicon atom. On the other hand, the hexaalkyl derivatives of disiloxane show a decrease in the value of the dipole moment for compounds containing ethyl, propyl and butyl radicals, compared with the compounds containing methyl radicals. In the series of polyethylsiloxanes $(C_2H_5)_3SiO[(C_2H_5)_2SiO]_nSi(C_2H_5)_3$, the dipole moments increase with increase in the molecular weight of the compounds. Examination of the relationship between the values of the dipole moment μ for the compounds of this series and the number of oxygen atoms in the molecule has shown that it is given by our empirical equation

$$\mu = 0{,}63\sqrt{n+1}, \qquad (2)$$

where n + 1 is the number of oxygen atoms in the molecule of the linear polyethylsiloxane. Table 3 gives the values of the dipole moments of the linear polyethylsiloxanes, calculated using Eq. (2). These values are in good agreement with the dipole moment values found from Eq. (1), with the exception of the dipole moment for hexaethyldisiloxane, which differs slightly from the value found by us from Eq. (1), but which agrees with the literature data [7].

TABLE 3

Dipole Moments of Hexaalkyl Derivatives of Disilanemethane, Disilaneethane, Disiloxane and Linear Polyethylsiloxanes

Compound	$m \cdot 10^{18}$, calc. from Eq. (1)	$m \cdot 10^{18}$, calc. from Eq. (2)	Compound	$m \cdot 10^{18}$ calc. from Eq. (1)	$m \cdot 10^{18}$ calc. from Eq. (2)
$(CH_3)_3SiCH_2Si(CH_3)_3$	0,60	—	$(CH_3)_3SiOSi(CH_3)_3$	0,78	—
$(C_2H_5)_3SiCH_2Si(C_2H_5)_3$	0,57	—	$(C_2H_5)_3SiOSi(C_2H_5)_3$	0,66	0,63
$(C_3H_7)_3SiCH_2Si(C_3H_7)_3$	0,56	—	$(C_3H_7)_3SiOSi(C_3H_7)_3$	0,67	—
$(C_4H_9)_3SiCH_2Si(C_4H_9)_3$	0,60	—	$(C_4H_9)_3SiOSi(C_4H_9)_3$	0,71	—
$(CH_3)_3SiC_2H_4Si(CH_3)_3$	0,56	—	$(C_2H_5)_3SiO[(C_2H_5)_2SiO]_4Si(C_2H_5)_3$	1,41	1,41
$(C_2H_5)_3SiC_2H_4Si(C_2H_5)_3$	0,59	—	$(C_2H_5)_3SiO[(C_2H_5)_2SiO]_5Si(C_2H_5)_3$	1,55	1,54
$(C_3H_7)_3SiC_2H_4Si(C_3H_7)_3$	0,55	—	$(C_2H_5)_3SiO[(C_2H_5)_2SiO]_6Si(C_2H_5)_3$	1,67	1,67
$(C_4H_9)_3SiC_2H_4Si(C_4H_9)_3$	0,56	—	$(C_2H_5)_3SiO[(C_2H_5)_2SiO]_7Si(C_2H_5)_3$	1,78	1,78

LITERATURE CITED

[1] A. A. Gundyrev, N. S. Nametkin and A.V. Topchiev, Doklady Akad. Nauk SSSR, 121, 1031 (1958).*

[2] R. O. Sauer and D. J. Mead, J. Am. Chem. Soc., 68, 1794 (1946).

[3] A. V. Topchiev, G. M. Panchenkov, et al., The Chemistry and Practical Application of Organosilicon Compounds [in Russian] (Leningrad, 1958), part 3, p. 84.

[4] G. Hedestrand, Zs. phys. Chem. (B), 2, 429 (1929).

[5] V. Kurita and M. Kondo, Bull. Chem. Soc. Japan, 27, 160 (1954).

[6] H. Freiser, M. Fagel and J. Speier, J. Am. Chem. Soc., 75, 2824 (1953).

[7] L. Malatesta, and R. Pinzotti, Gazz. chim. ital., 73, 143 (1944).

Received August 10, 1959.

*Original Russian pagination. See C. B. translation.

THE ROLE OF DIFFUSION IN ELEKTROKINETIC PHENOMENA
THE DIFFUSION THEORY OF THE DORN EFFECT
(THE POTENTIAL OF MOVING PARTICLES)

Corresponding Member Acad. Sci. USSR B. V. Deryagin
and S. S. Dukhin

Physical Chemistry Institute, Academy of Sciences, USSR

In the theory of electrokinetic phenomena for solid surfaces of separation, it is usual, when taking account of the viscosity and electrical conductivity, to ignore the diffusion of ions under the influence of the concentration gradients which may be produced. In a number of our works [1], however, it has been shown that the electrical field of a moving bubble or drop is due chiefly to the difference in the diffusion coefficients of the anions and cations, and is independent of the ζ-potential. These phenomena would rationally be called diffusion—electrokinetic phenomena, to distinguish them from electrokinetic phenomena at solid surfaces, if the mechanism of the latter phenomena were independent of diffusion processes.

In fact, however, this is not the case, and consideration of diffusion phenomena in the calculation of the values from the classical formulae often introduces corrections which are of the same order of magnitude as the values themselves.

In the present article we consider the role of diffusion in the Dorn effect. We shall consider the case of an immobile, solid, nonconducting sphere of radius a, washed by a flow of solution of a binary electrolyte with ions of charges z^+ and z^-, concentrations c^+ and c^-, and diffusion coefficients D^+ and D^-. Assuming as a first approximation the electrical neutrality condition

$$z^+c^+ - z^-c^- = 0 \tag{1}$$

in the bulk of the electrolyte (the justification for this assumption may be confirmed a posteriori), we can express c^+ and c^- in terms of the concentration of electrolyte, c mole/cc:

$$c^+ = z^-c, \quad c^- = z^+c. \tag{2}$$

The tangential stress which arises next to each point on the surface produces, in the boundary layer, a flow of definite rate gradient $(\partial v/\partial r) = w(\theta)$, which is a function of the polar angle θ in the system of polar coordinates with axis directed in the opposite direction to that of the current. This flow causes convective surface flow of ions equal to

$$I^+ = \int_0^\infty v_t(0, x)\,\gamma^+(x)\,dx, \qquad I^- = \int_0^\infty v_t(0, x)\,\gamma^-(x)dx, \tag{3}$$

where x is the distance from the "glide plane", $v_t(\theta, x)$ is the tangential component of the rate close to the latter, and $\gamma^+(x)$ and $\gamma^-(x)$ are the excess concentrations of the corresponding ions in the diffusion layer by comparison with the concentrations in the bulk, i.e., quantities which make up the adsorption increase in the concentration of these ions. We assume that the rates of liquid and ion flow are so small that we can use the equilibrium values of $\gamma^+(x)$ and $\gamma^-(x)$, i.e., we may assume that the structure of the diffusion layer remains intact. If we neglect the difference between the value of the viscosity in the double layer and its value in the

bulk, then $v_\xi(\theta, x)$ is equal to $xw(\theta)$, and since for Stokes flow, to which we restrict ourselves, $w(\theta) = \frac{3}{2}\frac{U_\infty}{a} \cdot \sin\theta$, we may, instead of (3), write:

$$I^{\pm} = \frac{3}{2}\frac{U_\infty}{a} c^{\pm} \xi^{\pm} \sin\theta, \tag{4}$$

where U is the flow rate at infinity,

$$\xi^{\pm} = \frac{1}{c^{\pm}} \int_0^\infty \gamma^{\pm}(x)\, x\, dx. \tag{5}$$

In the phenomenological discussion, the values of $\xi^{\pm}$ must be regarded as empirical constants related to the ζ-potential by the relationship

$$\xi = \frac{1}{4\pi} \int_0^\zeta \varepsilon\, d\psi = \frac{\bar{\varepsilon}\zeta}{4\pi} = F\, c\, z^+ z^- (\xi^+ - \xi^-) = \frac{\bar{\varepsilon}}{4\pi}(\zeta^+ - \zeta^-), \tag{6}$$

where F is the Faraday, ζ^+ and ζ^- are the cationic and anionic components of the zeta-potential, ξ is the moment of the double layer in "helmholtz" units (according to Guggenheim [2]), ϵ is the dielectric constant and $\varphi = \varphi(x)$ is the potential in the double layer. An important feature is that the constants $\xi^{\pm}$ may differ considerably in magnitude.

Since the surface ion currents are dependent on θ, their surface divergencies differ from zero, so that for stationary conditions the following continuity boundary conditions must be satisfied:

$$\operatorname{div}_s I^+ = \frac{3U_\infty}{a^2} c^+ \xi^+ \cos\theta = \left(D^+ \frac{\partial c^+}{\partial r} - \frac{F}{RT} D^+ z^+ c^+ E_r\right)_a; \tag{7}$$

$$\operatorname{div}_s I^- = \frac{3U_\infty}{a^2} c^- \xi^- \cos\theta = \left(D^- \frac{\partial c^-}{\partial r} + \frac{F}{RT} D^- z^- c^- E_r\right)_a, \tag{8}$$

where E_r is the radial component of the electrical field. From this, taking account of condition (1), we obtain, by eliminating $(E_r)_a$, the relationship

$$\frac{3U_\infty c}{a^2}(D^- z^- \xi^+ + D^+ z^+ \xi^-)\cos\theta = D^+ D^- (z^+ + z^-)\frac{\partial c}{\partial r}. \tag{9}$$

Neglecting the surface conductivity, and also the surface diffusion, we find the surface convection current from the formula

$$I = F(z^+ I^+ - z^- I^-) = \frac{3}{2}\frac{U_\infty F}{a} c z^+ z^- (\xi^+ - \xi^-)\sin\theta. \tag{10}$$

The boundary continuity equation for the charges will be

$$\operatorname{div}_s I = \frac{3FU_\infty}{a^2} c z^+ z^- (\xi^+ - \xi^-)\cos\theta = i_n, \tag{11}$$

where i_n is the component of the total current density in the bulk normal to the surface.

Our treatment differs from the usual treatment [4], which erroneously takes account only of the continuity equation for the charges, in that we have taken account of the continuity equations for the two types of ion separately [so that Eq. (11) is not now an independent condition – it follows from Eqs. (7) and (8)].

In the same way we also take account of the continuity equations separately for the two types of ion in the bulk:

$$D^+\Delta c^+ + \frac{F}{RT} D^+ z^+ \operatorname{div}(c^+\mathbf{E}) = \mathbf{v}\operatorname{grad} c^+, \tag{12}$$

$$D^-\Delta c^- - \frac{F}{RT} D^- z^- \operatorname{div}(c^-\mathbf{E}) = \mathbf{v}\operatorname{grad} c^-, \tag{13}$$

where E is the vector of the electrical field intensity in the bulk.

From this, taking account of Eq. (2), we have:

$$D_e \Delta c = \mathbf{v}\operatorname{grad} c, \tag{14}$$

where $D_e = \dfrac{D^+ D^- (z^+ + z^-)}{(z^+ D^+ + z^- D^-)}$ is the effective diffusion coefficient.

At the same time the continuity equation for the charges should be fulfilled; it follows from Eqs. (12) and (13):

$$\operatorname{div} \mathbf{i} = 0. \tag{15}$$

Eq. (15) together with the boundary condition (11) determines the current field. At the same time, as follows [1] from (12) and (13), the total current should have the form $i = c \operatorname{grad} \psi (r\,\theta)$. In our case, where the rates are low, we may take an approximation and regard $\underline{c}$ as a constant which is close to the concentration c_0 at infinity, so that $i = \operatorname{grad} \psi' (r\,\theta)$.

The "current potential" $\psi' (r, \theta)$ may be determined from the equation

$$\Delta\psi' = 0 \tag{16}$$

with the boundary condition

$$\frac{\partial\psi'}{\partial r} = \frac{-3FU_\infty}{a^2} c z^+ z^- (\xi^+ - \xi^-). \tag{17}$$

The equation for convective diffusion (14), together with the boundary condition (9), determines the concentration field.

The problem of finding $\underline{c}$ is simplified considerably when not only the Reynolds criterion, but also the Peclet criterion, are small, so that instead of Eq. (14) we may take the equation

$$\Delta c = 0. \tag{18}$$

In this case the concentration field has the form:

$$c - c_0 = -\frac{3}{2} \frac{U_\infty a}{r^2} \frac{c(D^- z^- \xi^+ + D^+ z^+ \xi^-)}{D^+ D^- (z^+ + z^-)} \cos\theta. \tag{19}$$

In analogous fashion, the potential field of the total current, φ', has the form:

$$\psi' = \frac{3FU_\infty a}{r^2} c(D^- z^- \xi^+ - \xi^-) \cos\theta. \tag{20}$$

Taking account of the fact that the ion transfer responsible for the total current results partly from migration in the electrical field E with potential φ, and partly from diffusion, we may write*

$$\frac{\operatorname{grad}\psi'}{Fz^+z^-} = \frac{F}{RT}(z^+ D^+ + z^- D^-)\, c \operatorname{grad}\varphi + (D^+ - D^-) \operatorname{grad} c,$$

from which, by integration, we obtain

$$\varphi = \frac{RT}{F^2} \frac{\psi'}{(z^+ D^+ + z^- D^-)\, z^+ z^- c_0} - \frac{RT}{F} \frac{(D^+ - D^-)}{(z^+ D^+ + z^- D^-)} \frac{(c - c_0)}{c_0}. \tag{21}$$

*This equation can also be derived [3] from Eqs. (12) and (13).

Substituting the values for $(c - c_0)$ and ψ' from (19) and (20), and introducing the specific conductance κ, we obtain, finally:

$$\varphi = \frac{3U_\infty a}{2\varkappa r^2} Fcz^+z^- \frac{(D^-\xi^+ - D^+\xi^-)}{D_{eff}}. \qquad (22)$$

Taking account of the relationship (6), we see that the expression obtained for φ coincides with the classical equation, first obtained by M. Smoluchowski *:

$$\varphi = \frac{3}{2} \frac{U_\infty a \varepsilon \zeta}{r^3 4\pi\varkappa} \cos\theta, \qquad (23)$$

when, and only when, $D^+ = D^- = D_{eff}$. Only in this case is it possible to find ζ from the observed value of φ. In the general case, the measured values of φ cannot be used to determine separately ζ or ξ^+ and ξ^-, but only to determine a combination of these, which also depends on the ratio of the cation and anion mobilities. The total information regarding ζ can be obtained in two ways.

Firstly, it may be assumed that the coefficient corresponding to the side ions – say ξ^- – is small by comparison with the other, ξ^+. With this assumption**, we obtain, from (22),

$$\varphi = \frac{3}{2} \frac{U_\infty a \cos\theta}{r^2} \frac{\varepsilon\zeta}{4\pi\varkappa} \left[1 - \frac{z^-(D^+ - D^-)}{(z^+ + z^-) D^+}\right]. \qquad (24)$$

Since the values of D^+/D^- and z^+/z^- are known for any ions, the formula obtained by correcting (23) can be used calculating ζ from a knowledge of φ, or vice versa. The "correction" introduced is particularly high in the case where the side ions are heavy ($D^- \ll D^+$) multi-charged ions ($z^- = 3$ or 4, $z^+ = 1$). In such cases, the uncorrected formula (23) obviously gives values of φ which are 4-5 times too high, and the calculation of ζ from experimental data gives values which are 4-5 times too low. Cases are also possible where $D^- \gg D^+$. In this case we have, from (24), the possibility of anomalous high values of φ at "normal" values of ζ. The calculation of ζ from (23) would give values which were much higher than the true values.

Secondly, we may express ξ^+ and ξ^- in terms of the potential of the glide plane, using the theory of the double layer, and by substituting in (23), relate it unambiguously to the values of the potential φ. The resultant calculations are cumbersome, and this procedure will be dealt with in another paper.

Since the streaming potential in porous dielectrics at $Pe \equiv ul/D \ll 1$, l, where u is the linear rate and is the length of the capillaries (after the stationary concentration field has been established) does not differ in principle from the potential of movement of a spherical nonconducting particle at low Peclet numbers, it can be seen that the formula for the first (without taking account *** of the surface conductivity)

$$\Delta\varphi = \frac{\Delta P}{\varkappa\eta} \frac{\varepsilon\zeta}{4\pi}$$

must be replaced by the following:

$$\Delta\varphi = \frac{\Delta P}{\varkappa\eta} Fcz^+z^- \frac{(D^-\xi^+ - D^+\xi^-)}{D_{eff}} = \frac{\Delta P}{\varkappa\eta} \frac{\varepsilon}{4\pi} \frac{(D^-\zeta^+ + D^+\zeta^-)}{D_{eff}}.$$

It can be seen that in this case all that has been said above regarding the significance and value of the corrections introduced into the classical formula are again applicable.

---

*M. Smoluchowski [4], however, did not take ϵ into account.

** In the case where $\xi^+ \ll \xi^-$, the superscripts $\pm$ in formula (24) must be interchanged.

***This will be taken into account in a subsequent paper.

LITERATURE CITED

[1] S. S. Dukhin and B. V. Deryagin, Kolloid. Zhur., 20, 705 (1958); Doklady Akad. Nauk SSSR, 121, 503 (1958)*.

[2] E. A. Guggenheim, Trans. Farad Soc., 36, 139 (1940).

[3] V. G. Levich, Physicochemical Hydrodynamics [in Russian] (Acad. Sci. USSR Press. 1952).

[4] M. Smoluchowski, Bull. de L'Acad. des Sci. de Cracovie Classe des Sci. Math.et Natur., 1, 182 (1903).

Received September 30, 1959.

*Original Russian pagination. See C. B. translation.

THE VISCOSITY OF CERTAIN BINARY HYDROCARBON MIXTURES AND GAS CONDENSATES IN THE SUPERCRITICAL RANGE

S. L. Zaks and V. I. Sergeevich

(Presented by Academician P. Ya. Kochina, March 31, 1959)

The present work is devoted to the study of the viscosity, density and compressibility of certain binary hydrocarbon systems whose components are present in the natural gases encountered in petroleum and gas condensate deposits. A knowledge of these properties is necessary for hydrodynamic calculations of the movement of the gas in a porous medium. The studies were carried out at 20° and 228 atm pressure with the systems methane–pentane, methane–hexane, methane–heptane and methane–isooctane, at different component ratios in each of the systems. In the systems studied, the second component (pentane, hexane, etc.) is a liquid at atmospheric pressure, but at the experimental pressure these systems exist in a single-phase, gaseous state.

Of the existing methods for measuring the viscosity, the one chosen was that involving a sphere rolling in an inclined tube. The viscosity was calculated from the empirical equation $\eta = k\tau(\rho_s - \rho_g)$ (η is the viscosity in poises, k is the viscometer constant, τ_s is the time of rolling of the ball in seconds, and ρ_s and ρ_g are the densities of the sphere and gas, respectively, in g/cm^3), which is applicable to the determination of the viscosity of liquids. The applicability of this formula is confirmed by the good agreement between our data for methane and the data of N.V. Meshcheryakov and I. F. Golubov [1] obtained in the determination of the viscosity of methane by the capillary method. The applicability of the formula to the study of highly compressed gases may be explained by the fact that at the high pressure, which brings about a considerable decrease in the distance between the molecules, the properties of the compressed gases approach the properties of liquids. To avoid large errors in the measurement of the time of rolling, the gap between the tube and the sphere should be narrower than in the determination of the viscosity of liquids, in order to increase the time of rolling. In our experiments, the gap was 40μ, for a tube diameter of 6.4 mm. The measurement of the viscosity was carried out with the tube inclined at angles of 15, 30 and 45°. The arithmetic mean of the three viscosity values obtained was then taken.

The dissolution of the liquid hydrocarbon in the methane was carried out in a PVT bomb. Inside the bomb, which consists of a high-pressure vessel, there are two pistons moved by means of glycerol, which is pumped into the space in the bomb behind the pistons. By decreasing the volume of the bomb, and hence increasing the pressure inside it, it is possible to bring the gas condensate mixture inside the bomb to a single-phase, gaseous state. This can be confirmed visually by observing the disappearance of the boundary of separation between liquid and gas, through the glass window provided. The density ρ_g of the gases, which appears in the equation for the viscosity calculation, was determined by a hydrostatic method in a densitometer, from the change in length of a spring, to the end of which was suspended a graduated glass float. The construction of the apparatus, its calibration, the experimental procedure and the density calculation have been described earlier [2, 3].

Figure 1 gives the viscosity curves for the systems studied. They show a systematic increase in the viscosity of the solution with increase in the concentration and molecular weight of the second component. The broken curve shows the position which Curve 4 would occupy if the experiments with pentane had been carried out using the same methane composition as the experiments with hexane, heptane and isooctane.

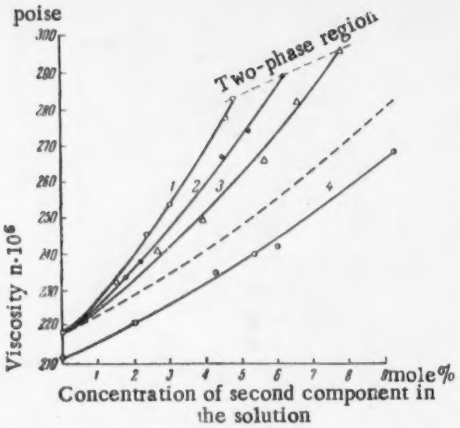

Fig. 1. The relationship between the viscosity of binary hydrocarbon systems and the concentration of the second component in the solution: 1) Methane—isooctane, 2) methane—heptane, 3) methane—hexane, 4) methane—pentane. (The significance of the broken line is explained in the text).

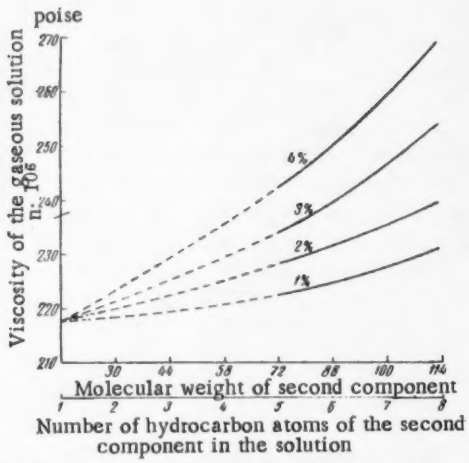

Fig. 2. The influence of the molecular weight of the second component on the influence of gaseous solutions of identical concentration at a pressure of 228 atm and 20°.

The influence of the number of hydrocarbon groups of the second component on the viscosity of the solutions studied is shown in Fig. 2. The curves show that the longer the hydrocarbon chain, the greater the viscosity of the solution. With increase in the concentration (Fig. 2 gives the curves corresponding to concentrations from 1% to 4%), the change in viscosity with change in molecular weight becomes sharper. The density data for the solutions studied were used to calculate the compressibility coefficients at 228 atm and 20°, and the relationships between these quantities and the concentration are shown in Fig. 3. The curves show that with increase in the concentration of the system, the compressibility coefficients at first decrease, and then gradually increase. The lower the molecular weight of the liquid component, the more marked are these changes.

Measurements were also made of the viscosity and density of the condenser gas obtained when methane and methane—propane mixtures were passed through oil-bearing rock, compressed to 300 atm at room temperature. The condensate gas is formed as a result of the phenomenon of reverse evaporation (dissolution in the moving gas) of some of the components of the oil; these components condense again when the pressure is lowered to form the so-called condensates [4,5]. For a concentration of 50-70 g condensate in 1 nm^3 gas, the viscosity is 0.031-0.037 cp, and the density 0.2710-0.2945 g/cc.

The data obtained show a considerable change in the viscosity and other properties of the systems studied, from which it follows that these changes must be taken into account in hydraulic calculations when planning the development of gas condensate deposits and deposits which are to be worked by the forced passage of high-pressure gases.

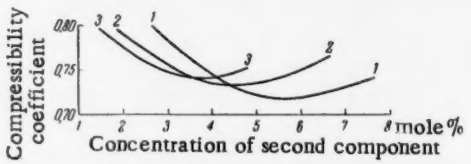

Fig.3. The relationship between the compressibility coefficients of gaseous solutions and the concentration of the second component in the solution at a pressure of 228 atm and 20°. 1) Methane—hexane, 2) methane—heptane, 3) methane—isooctane.

LITERATURE CITED

[1] N. V. Meshcheryakov and I. F. Golubov, Trudy GIAP, 4, 22 (1954).

[2] T. P. Zhuze and V. I. Sergeevich, Izvest. Akad. Nauk SSSR, Otdel. Tekh. Nauk, No.5, 156 (1956).

[3] V. I. Sergeevich, Thesis, Moscow, 1957.

[4] S. L. Zaks, Izvest. Akad. Nauk SSSR, Otdel. Tekh. Nauk, No.9, 3 (1955).

[5] M. A. Kapelyushnikov, S. L. Zaks and V. F. Burmistrova, Trudy Inst. Nefti Akad. Nauk SSSR, 11, 209 (1958).

Received March 4, 1959.

A STUDY OF THE OXIDATION MECHANISM OF SOME INORGANIC SUBSTANCES BY PERSULFATE

V. A. Lunenok-Burmakina and Academician A. I. Brodskii

Institute of Physical Chemistry Acad. Sci . USSR

The oxidation by peroxide compounds can be carried out via electron transfer as well as by the transfer of active oxygen atoms. Both mechanisms can be distinguished by the means of isotope-labeling of the oxygen. In the present work a number of oxidation reactions by persulfate are studied in this manner.

In our joint work with I. F. Franchuk [1] it has been shown that in the hydrolysis of persulfate the peroxide group is passed on without breakdown, forming consecutively, permonosulfuric acid and hydrogen peroxide, which evolves elementary oxygen on its decomposition (the stars show the labeled oxygen atoms):

$$-O_3S\overset{*}{O}\overset{*}{O}SO_3^- \rightarrow -SO_3\overset{*}{O}\overset{*}{O}H \rightarrow H\overset{*}{O}\overset{*}{O}H \rightarrow \overset{*}{O}_2, \qquad (1)$$

The preservation of the O—O peroxide group in the oxygen which was liberated on the decomposition of the water solution of hydrogen peroxide was also shown in several earlier studies (2-10).

On the other hand, Kolthoff and Miller (11) found that the thermal decomposition of persulfate solutions proceeded in two different ways, depending on the acidity of environment. In neutral and alkaline solutions oxygen was liberated from water; this was explained by the breakdown of the peroxide group, forming SO_4^- radical ions:

$$S_2O_8^{--} \rightarrow 2SO_4^-;\ 2SO_4^- + 2H_2\overset{*}{O} \rightarrow 2HSO_4^- + 2H\overset{*}{O}.$$
$$2H\overset{*}{O} \rightarrow H_2\overset{*}{O} + {}^1/_2\overset{*}{O}_2. \qquad (2)$$

In acidic solution a catalyzed H^+ reaction dominated, and the O—O group did not break down. Kolthoff and Miller [11] presumed that the reaction took place in stages via the intermediate formation of SO_4 radicals. However in our works [1,12] it was shown that to explain the reaction the hydrolytic splitting of the persulfate according to the mechanism described above [1], could be presumed with greater probability.

The interaction of persulfate with hydrogen peroxide. The reaction of $K_2S_2O_8 + H_2O_2 \rightarrow 2KHSO_4 + O_2$ was studied by Friend [14], who proposed, on the basis of kinetic investigations, that the process took place through the formation of the intermediate $(K_2S_3O_8)_y(H_2O_2)_x$ compound, the dissociation of which determined the reaction velocity. The course of decomposition of this intermediate product was not explained.

We studied this reaction in the three following systems, which differed in the placing of the isotope-label: $K_2S_2\overset{*}{O}_8 + H_2O_2 + H_2O$; $K_2S_2O_8 + H_2\overset{*}{O}_2 + H_2O$;. $K_2S_2O_8 + H_2O_2 + H_2\overset{*}{O}$;. Equimolar weights of hydrogen peroxide and aqueous solution of persulfate, and in certain experiments a weighed portion of acid or alkali, indispensable for the formation of their 0.1 N solution, were mixed in a vessel, which was then degasified with great care, hermetically sealed and left at room temperature for the time of the reaction. The liberated oxygen captured for mass spectrometric determination of its O^{18} content. The isotopic analysis of the remaining substances was carried out as described in [1]: the hydrogen peroxide and persulfate were decomposed and the liberated oxygen was analyzed either directly, or after burning to CO_2 with degasifier coal; to facilitate the mass spectrometric analysis, water had previously been exchanged with carbon dioxide [14]. The oxygen of the sulfate was transferred to CO_2 by roasting $PbSO_4$ with degasifier coal.

TABLE 1

Expt. No.	Time, days	The O^{18} content in % above the natural level.					Catalysts
		initial substances			reaction products		
		H_2O_2	$K_2S_2O_8$	H_2O	O_2	$KHSO_4$	
1	1	0,64	0	0	0,65	—	—
	40	0,64	0		0,61	0,01	
2	1	0	0,59	0	—0,01	—	—
	40	0	0,59	0	—0,01	0,59	
3	4	0	0,59	0	—0,01	—	0,1*N*
	7	0	0,59	0	0,01	0,56	$HClO_4$
4	2	0	0,59	0	0,02	—	0,1*N*
	15	0	0,59	0	—0,02	—	H_2SO_4
5	4	0	0	1,0	—0,01	—	
	7	0	0	1,0	—0,01	0	
6	2	0	0	1,0	—0,01	—	0,1*N*
	15	0	0	1,0	0,02	0,01	KOH

From the data in Table 1 it can be seen that the liberated oxygen has the same isotopic composition as the hydrogen peroxide, and that the isotopic composition of oxygen in the bisulfate corresponds to the isotopic composition of the persulfate. Oxygen from the water takes no part in the reaction and is liberated solely from the hydrogen peroxide. During the course of the reaction the peroxide bridge of persulfate breaks down, as the alteration in acidity – unlike the thermal decomposition of the aqueous solution of persulfate – does not change the mechanism.

Oxidation of silver nitrate by persulfate. The investigation of the oxidation of silver nitrate by persulfate $K_2S_2O_8 + 2AgNO_3 + 2H_2O \rightarrow Ag_2O_2 + 2KHSO_4 + 2HNO_3$ is interesting not only from the point of view of studying the course of decomposition of persulfate but also for the explanation of the debated question concerning the nature of silver oxide, formed in the course of the reaction. This combination is called silver peroxide and, according to some authors, it appears to be a true peroxide combination [15], while others regard it as the higher oxide of silver [16]. We added silver nitrate at 0° to the solution of labeled persulfate in "light" water, or to that of ordinary persulfate in water with heavy oxygen. The solution turned brown, and gradually a black residue of silver peroxide was precipitated from it; this was filtered, washed with a little ice-cold water and dried at room temperature.* The bisulfate found in the filtrate was deposited with the lead nitrate. The oxygen of the silver peroxide was liberated on heating the residue under vacuum to 140°. The O^{18} content in the sulfate was determined in the way described above.

In the series of experiments in which the O^{18} content of water was enriched to 0.98 % (here and further on, the heavy oxygen isotope content is understood to be above the natural level percentage the oxygen of silver peroxyde contained 0.99 to 0.93% of O^{18}. Bisulfate in these experiments turned out to be the same as the persulfate, i.e., light (0.03 to 0.01% of O^{18}). In the experiments with persulfate labeled with 0.60% of O^{18}, the oxygen of silver peroxide was found to be light (0.01 to 0.02% of O^{18}), while the bisulfate was heavy (0.60 to 0.54% of O^{18}).

It follows from the data presented that the oxidation of silver takes place via an electron mechanism, so that the peroxide bridge is not transferred to the silver during the course of the reaction. This fact refutes one of the arguments of those who regarded AgO as a true peroxide compound, and it is in greater accord with the evidence obtained by other methods [16] that the substance called silver peroxide is not a true peroxide compound.

The oxidation of bivalent manganous salts. On boiling the solution of bivalent manganous salts with persulfate, H_2MnO_3 residue precipitates: $MnCl_2 + K_2S_2O_8 + 3H_2O = H_2MnO_3 + 2KHSO_4 + 2HCl$. Hydrogen peroxide in alkaline solution also oxidizes the bivalent manganese to tetravalent.

*The analysis revealed that the residue obtained in this manner contained about 40% silver peroxide (the determination was carried out by the iodometric method) [17]. The rest of the residue consisted of silver oxide and sulfate.

Solutions of persulfate and manganous salt, containing either the persulfate or the water labeled with O^{18}, were mixed and boiled for 5 to 10 minutes. The precipitated residue was filtered, washed with light water and dried at 150°. The oxygen was liberated from it by heating to 600-700° under vacuum. In the filtrate lead sulfate was deposited.

In the experiments with labeled persulfate (0.60% of O^{18}) the resultant H_2MnO_3 contained the light isotopes (0.04 to 0.02% of O^{18}), while the bisulfate contained the heavy ones (from 0.60 to 0.55% of O^{18}). In the experiments with water, the O^{18} content of which had been enriched to 0.97%, the bisulfate contained the light isotopes (0.03 to 0.01% of O^{18}), and H_2MnO_3, the heavy ones (0.60 to 0.65% of O^{18}). The fact that the O^{18} content was found to be $^1/_3$ less than in the initial water, can be explained by the rapid exchange of one of the oxygen atoms of the hydrated manganese dioxide with water during the washing of the residue. The additional experiments showed that generally only one of the three oxygen atoms of H_2MnO_3 was exchanged. No more atoms were exchanged, even when the residue was boiled with water for several hours. When the hydrated manganese dioxide—which can be represented more correctly by the formula of $MnO_2 \cdot H_2O$ * — obtained in the experiment with labeled water was washed, not in ordinary, but in water with heavy oxygen isotope, then its isotopic composition (0.91 %) hardly differed from that of the initial water.

Thus, similarly to the previous reaction, the oxidation by persulfate proceeds, not by the transfer of oxygen from the peroxide group, but via an electron mechanism. The oxygen in the oxidized substance comes from the water.

The $MnO_2 \cdot H_2O$ residue was obtained with the natural isotopic composition of oxygen when the alkaline solution of the bivalent manganous sulfate in light water was oxidized by hydrogen peroxide containing heavy oxygen. Consequently, the oxidation of the bivalent manganese by hydrogen peroxide in alkaline solution proceeds via the same mechanism as the oxidation by persulfate, contrary to all other previously investigated reactions, where the oxidation by hydrogen peroxide takes place through the transfer of oxygen from hydrogen peroxide [11].

The oxidation of lead sulfide. Persulfate solution reacts with ground lead sulfide powder, slowly forming lead sulfate and precipitating sulfur: $K_2S_2O_8 + PbS \rightarrow PbSO_4 + K_2SO_4 + S$.

We treated the freshly prepared lead sulfide with light persulfate dissolved in water containing heavy oxygen. The solution with the residue was either kept at 60° for about 2 hours, or left at room temperature for a day. Then the developed lead sulfate was filtered, and the potassium sulfate found in the filtrate was precipitated by lead nitrate. The lead sulfate residue was decomposed and analyzed as described above. The isotopic composition both in the lead sulfate and in the potassium sulfate was found to be the same as in the initial persulfate, i.e., natural. The oxygen of the water does not enter into the reaction products. It follows from the data obtained that the persulfate oxidizes the lead sulfate to elemental sulfur **by an electron mechanism.

In order to confirm these interpretations, we carried out experiments with lead sulfide labeled with radioactive sulfur. To produce it, (PbS) H_2S^{35} was passed through lead nitrate solution which had been previously freed from oxygen.

The experiments were carried out under the same conditions as those with heavy oxygen isotopes. After the reaction the residue containing the resultant lead sulfate, sulfur, and the unreacted lead sulfide was filtered. The potassium sulfate found in the filtrate was precipitated by barium chloride. In order to separate it from the lead sulfide and sulfate, the elemental sulfur was dissolved in benzene and then recovered by the evaporation of the benzene solution. The lead sulfate was separated from the sulfide by dissolving the former in excess ammonium acetate at boiling temperature and precipitating it in the form of $BaSO_4$. The radioactivity of the residue was determined in the usual way with 10 milligram portions by the means of an end-type counter. It was found that the specific radioactivity of the sulfur which separated out was equal to the specific radioactivity of sulfur in the initial lead sulfide with ±5 % accuracy. The lead and the potassium sulfate formed as a result of the reaction, like the initial persulfate, are nonradioactive. These data show conclusively that the persulfate oxidizes lead sulfide only to elemental sulfur (and not to sulfate) by an electron mechanism, and the lead sulfate is formed entirely from the decomposing persulfate.

*The different values of oxygen atoms in hydrated manganese dioxide were established by other methods as well.

**We found that hydrogen peroxide oxidizes lead sulfide to sulfate by oxygen transfer — the opposite of this reaction.

Thus, oxidation by persulfate, contrary to the oxidation by hydrogen peroxide, is accompanied by the breakdown of the $-O-O-$ bond in all the investigated reactions, and proceeds by means of electron transfer, and not by the transfer of oxygen atoms from the oxidizing agent to the oxidized substance.

The authors express their gratitude to A. P. Potemskaya, E. G. Veselaya and T. A. Vovk for participating in the execution of certain parts of this study.

LITERATURE CITED

[1] A. I. Brodskii, I. F. Franchuk, and V. A. Lunenok-Burmakina, Proc. Acad. Sci. USSR 115 334 (1957).*

[2] H. S. Taylor and A. J. Gould, J. Am. Chem. Soc. 56, 1823 (1934).

[3] R. Bentley, Cold Spring Harbor Symposia Quant. Biol. 13, 11 (1948).

[4] E. R. S. Winter and H. V. A. Briscoe, J. Am. Chem. Soc. 73, 496 (1951).

[5] P. Baertschi, Experientia 7, 215 (1951).

[6] M. Dole, D. P. Rudd, et al., J. Chem. Phys., 20, 961 (1952).

[7] A. E. Cahill and H. Taube, J. Am. Chem. Soc. 74, 2312 (1952).

[8] C. A. Bunton and D. R. Llewellyn, Research 5, 142 (1952).

[9] J. P. Hunt and H. Taube, J. Am. Chem. Soc. 74, 5999 (1952).

[10] P. Baertschi quoted by J. K. Christiansen, Acta Chem. Scand. 6, 1056 (1952).

[11] J. M. Kolthoff and J. K. Miller, J. Am. Chem. Soc., 73, 3055 (1951).

[12] I. F. Franchuk and A. I. Brodskii, Proc. Acad. Sci. USSR 118 128 (1958).*

[13] J. A. N. Friend, J. Chem. Soc. Trans. 89, 1092 (1906).

[14] A. I. Brodskii, S. G. Demidenko, O. L. Strizhak and V. R. Lechekhleb, J. Anal. Chem. 10, 256 (1955).

[15] H. Marshall, J. Chem. Soc. 59, 775 (1891); W. Machu, Das Wasserstoffperoxyd und die Perverbindungen 11 A, (1951), 257.

[16] A. B. Neiding and I. A. Kazarnovskii, Proc. Acad. Sci. USSR 78, 713 (1951); R. L. Dutta, J. Ind. Chem. Soc. 32, 95 (1955); W. S. Graff and H. H. Stadelmaier, J. Electrochem. Soc., 105, 446 (1958).

[17] F. Jirsa, Zs. anorg. u. allgem. Chem. 158, 33 (1926).

[18] S. Ya. Rode, The Oxides of Manganese [In Russian] (Acad. Sci. USSR Press, 1952).

[19] J. Halperin and H. Taube, J. Am. Chem. Soc. 74, 380 (1952); M. Anbar and H. Taube, J. Am. Chem. Soc. 76, 6243 (1954).

Received September 5, 1959.

*Original Russian pagination. See C. B. translation.

THE SINGLE ELECTROCHEMICAL BOND IN A SOLID ELECTROLYTE

S. F. Pal'guev, S. V. Karpachev, and L. D. Yushina

Institute of Electrochemistry, Urals Branch of the Academy of Sciences, USSR

(Presented by Academician A. N. Frumkin July 16, 1959)

Solid silver bromide is almost an entirely ionic conductor [1]. However, in an atmosphere of bromine vapor its conductivity increases in a few cases, apparently due to the advent of electronic conductivity, based upon small structural gaps or holes. The degree of electronic conductivity increases with rising temperature, and at 200° it amounts to about 17% [3].

From the foregoing observations we have described points of interest in the study of the temperature dependence of emf in the bond Ag/AgBr (solid)/Br_2, C. We know of only one paper in this connection [4], where measurements were made over a comparatively narrow temperature range (203-407°), and in this case the results obtained were of poor reproducibility. We have measured the emf of the described bond carefully from room temperature up to 421°C.

The electrochemical cell itself consists of a cylinder pressed from silver bromide. A silver wire was pressed into one face to act as a silver electrode, while in the other was inserted a carbon pin to act as a bromine electrode. The cell was inserted into a hard glass U-tube. Contact with the carbon pin was effected externally by means of a platinum wire. During the time of measurement, gaseous bromine was fed to the cell from a special type of evaporator. Its temperature was approximately that of the cell. When working at temperatures above 60°C, the bromine pressure on the cell reached atmospheric. At lower temperatures it equaled the saturation pressure of bromine at room temperature. The results of these latter measurements were converted to atmospheric bromine pressure.

We prepared silver bromide from chemically pure reagents (silver nitrate and potassium bromide). The measurement of emf was made by the usual method of compensation.

The results of the measured emf of the cell Ag/AgBr (solid)/Br_2, C with the thermal emf corrections for the vapor, are set out in Fig. 1 for platinum-silver. It is apparent that over the temperature range 110° to 421°, the experimental results fit closely on a straight line, which may be expressed as the empirical equation

$$E = (1{,}1518 - 0{,}493 \cdot 10^{-3} T) \pm 0{,}0017 \text{ v}.$$

According to [5] the emf of our cell, but with molten silver bromide, amounts to 0.8056 v at the melting point, (434°), while at the same temperature the derived equation gives 0.8033 v. The satisfactory correspondence of these values confirms the accuracy of our measurements, while it also indicates that in every case for solid silver bromide near its melting point, the emf points clearly to the ionic nature of the conductivity.

Thermodynamic calculations based on certain data [6,7], give an emf of 0.9904 v at 25°. On extrapolating the straight line in Fig. 1 to 25°, the resulting voltage is found to be 1.0049. The agreement between these figures can be regarded as satisfactory, while the divergence of 14.5 mv can arise from the error in extrapolating through a narrow temperature interval (from 110 to 25°). All this indicates, that over the temperature range 420-110°, our emf measurements reveal that if there should be electronic conductivity in solid silver bromide, it is absent under these conditions, although as was pointed out earlier, even at 200° electronic conductivity still comprises 17% of the total conductivity.

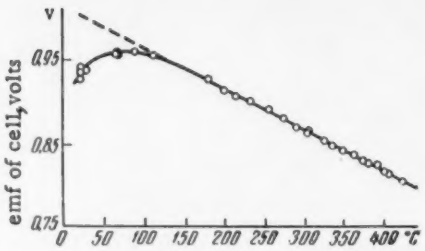

Fig. 1.

Our measurements at 25° gave an emf of 0.944 v while the thermodynamic figure was 0.9904 v. In an atmosphere saturated with bromine vapor at 25°, the conductivity of silver bromide exceeded approximately 10 times its conductivity in the absence of bromine vapor. In connection with this measurement at 25° in a bromine atmosphere, the emf of our cell would rightly be 0.1 against the corresponding thermodynamic figure of 0.099 volts.

From doubts concerning the increase in conductivity of silver bromide in an atmosphere of bromine vapor, the emergence of electronic conductivity was suggested, although we showed this to be impossible by our measurement of the transfer numbers in solid silver bromide surrounded by bromine vapor. The measurements were conducted by the usual method for solid electrolytes. The transport number of ionic bromine was shown to be equal to zero, while the transport number of silver ion lay in the range 0.03 to 0.05 (20°) and from 0.06 to 0.11 (93°).

In explaining the behavior of the emf of our cell let us consider its design. Evidently, inside the solid silver bromide there is a place where there will be a concentration gradient of dissolved bromine and consequently a concentration gradient of holes as well, which will result in the formation of an electropotential gradient. To calculate the latter, we use the thermodynamic methods of irreversible processes.

Under our conditions, the following components will exist in solid silver bromide; silver ions (Ag^+), bromine ions (Br^-), positively charged gaps or holes (0). Let I with the corresponding indexes be the current in the components indicated; I without an index is the total current; ψ the electric potential; μ the chemical potential of the different components; and F Faraday's constant.

Let us write down from the various phenomena, equations for the currents cited;

$$\begin{aligned} I_{Ag^+} &= -L_{11}\operatorname{grad}\mu_{Ag^+} - L_{12}\operatorname{grad}\mu_{Br^-} - L_{13}\operatorname{grad}\mu_0 - L_{14}\operatorname{grad}\phi, \\ I_{Br^-} &= -L_{21}\operatorname{grad}\mu_{Ag^+} - L_{22}\operatorname{grad}\mu_{Br^-} - L_{23}\operatorname{grad}\mu_0 - L_{24}\operatorname{grad}\phi, \\ I_0 &= -L_{31}\operatorname{grad}\mu_{Ag^+} - L_{32}\operatorname{grad}\mu_{Br^-} - L_{33}\operatorname{grad}\mu_0 - L_{34}\operatorname{grad}\phi, \\ I &= -L_{41}\operatorname{grad}\mu_{Ag^+} - L_{42}\operatorname{grad}\mu_{Br^-} - L_{43}\operatorname{grad}\mu_0 - L_{44}\operatorname{grad}\phi. \end{aligned} \tag{1}$$

In equation (1) ψ is expressed in volts, the current I_{Ag^+}, I_{Br^-} and I_0 in gram equivalents, and I in coulombs per square centimeter. For Onsager's coefficient L, it is possible to write down the following obvious relationships

$$L_{14} = L_{41} = \frac{t_{Ag^+}\varkappa}{F}; \quad L_{24} = L_{42} = -\frac{t_{Br^-}\varkappa}{F}; \quad L_{34} = L_{43} = \frac{t_0\varkappa}{F}; \quad L_{44} = \varkappa; \tag{2}$$

Here κ is the total specific conductivity of the solid salt.

Under conditions of equilibrium I = 0. In this case, neglecting the dependence of the chemical potential of silver and bromine ions on their solution in the bromine salt, we obtain

$$F\,d\phi = -t_0 d\mu_0, \tag{3}$$

where t_0 is the transport number of the holes. From the concentration of holes in each cross section of the solid electrolyte, it is possible to calculate the proportional concentration of dissolved bromine in this cross section. If the solution of bromine and holes in silver bromide is assumed to be ideal, then $d\mu_0 = d\mu_{Br}$. Hence

$$F\,d\phi = -t_0 d\mu_{Br}. \tag{4}$$

The emf of our cell E can be written in the following form:

$$EF = -\mu_{Br} - \mu_{Ag} + \mu_{AgBr} + F(\phi_{Ag} - \phi_{Br}). \quad (5)$$

Using (4) and (5) and having measured the chemical potential of dissolved bromine near the silver electrode from the equilibrium Ag + Br → AgBr we obtain

$$EF = (1 - \bar{t}_o)(-\mu_{Br} - \mu_{Ag} + \mu_{AgBr}); \quad (6)$$

here $\bar{t}_0$ is the average value of the transport number of the holes which we write in the form

$$\bar{t}_o = \frac{\int_C^{Ag} t_o \, d\mu_o}{\mu_o^{Ag} - \mu_o^C}; \quad (7)$$

The indexes Ag and C show that the values of the corresponding quantities are preserved in the vicinity of the silver or carbon electrode.

Evidently

$$t_o = \frac{v_o C_o}{v_o C_0 + \varkappa_i}; \quad (8)$$

here v_0 and C_0 are the mobility and concentration of the holes; $\varkappa_i$ is electrical conductivity, dependent on the mobility of silver and bromine ions.

From (7) and (8) we obtain, assuming dispersion of the holes in an ideal crystal and neglecting $v_0 C_0^{Ag}$ in comparison with $\varkappa_i$:

$$\bar{t}_o = \frac{\lg \frac{v_o C_o^C + \varkappa_i}{\varkappa_i}}{\lg \frac{C_o^C}{C_o^{Ag}}}. \quad (9)$$

At 200° [3].

$$\frac{v_o C_o^C + \varkappa_i}{\varkappa_i} \cong 2{,}21.$$

Hence

$$\bar{t}_o = \frac{0.08}{\lg \frac{C_o^C}{C_o^{Ag}}}. \quad (10)$$

Using thermodynamic data, it is possible to assess the pressure of gaseous bromine in equilibrium with silver. The concentration of bromine in solid silver bromide is proportional to the square root of the pressure of gaseous bromine [2], while the concentration of holes in pure silver bromide can be regarded as proportional to the concentration of dissolved bromine.

From these considerations there is derived $C_0^C / C_0^{Ag} = 10^n$, where $n \cong 20$-30. Hence $\bar{t}_0$ appears to be so small, that without incurring much error, it is possible to write $\bar{t}_0 = 0$.

A reading is made at this point and also at 100°. At temperatures higher than 200°, t_0 is also practically zero. In this case, over a temperature range of 100-434° our electrochemical bond behaves as if the conductivity of the electrolyte were entirely ionic in nature.

Weininger [8] prepared some tiny elements in which one of the electrodes was silver while the other was bromine or iodine. Therefore, the fact that similar elements function and correlate better with the thermodynamic values for emf is explained by the above considerations.

Evidently the regularities observed here can occur sequentially in other similar cases.

It is our pleasant duty to convey our thanks to Academician A. N. Frumkin for discussions on the results of the present work.

LITERATURE CITED

[1] C. Tubandt, Handb. der Experimentalphys. 12, T1, 1, 402 (1932).

[2] G. W. Luckey and W. West, J. Chem. Phys., 24, 879 (1956).

[3] C. Wagner, Zs. phys. Chem. 32, 447 (1936).

[4] H. Reinhold, Zs. anorg.,allgem. Chem. 171, 181 (1928).

[5] E. J. Salstrom and J. H. Hildebrand, J. Am. Chem. Soc. 52, 4650 (1930).

[6] A. F. Kapustinsky and E. V. Britzkei, Thermal Constants of Inorganic Compounds (Moscow-Leningrad, 1949). [In Russian].

[7] D. L. Hildebrand, W. R. Kramer, et al., J. Am. Chem. Soc. 80, 4129 (1958).

[8] J. L. Weininger, J. Electrochem. Soc. 105, 439 (1958).

Received July 15, 1959.

THE CHARACTERISTIC FEATURES OF CRYSTALLIZATION STRUCTURE FORMATION DURING THE HYDRATION HARDENING OF CALCIUM OXIDE

E. E. Segalova, S. I. Kontorovich and Academician P. A. Rebinder

Physical Chemistry Institute, Academy of Sciences, USSR

Colloid Chemistry Faculty, M. V. Lomonosov Moscow State University

Although the hydration properties of quicklime have been known for approximately 30 years [1], the mechanism of the purely hydration hardening of calcium oxide has not yet been sufficiently fully studied.

In the study of the kinetics of supersaturation in dilute suspensions of CaO it has been established that there exists a constant supersaturation level which may be regarded as the metastable solubility of calcium oxide [2]. The process of hydration of CaO, like that of other hydration-binding materials, involves the dissolution of the original CaO and crystallization of hydrated $Ca(OH)_2$ from the resultant supersaturated solution. A distinguishing feature of calcium oxide is its very high rate of dissolution, which is related to the very high specific surface of ordinary CaO, prepared by ignition of $CaCO_3$ under relatively mild temperature conditions. The study of the hydration hardening of pure calcium oxide presents considerable difficulty, as a result of the high thermal effect of the reaction. In the study of the hardening of lime–sand mixtures, however, the hydration hardening of the CaO is accompanied by the process of hydrosilicatization [3], which complicates the study of the hydration properties of the calcium oxide.

In the present work the process of structure formation has been studied using suspensions containing, in addition to pure calcium oxide, a large quantity of an inert filler, and this has made it possible, firstly, to increase the water–lime ratio without separation of the system into layers, and hence to reduce the rate of the process of structure-formation, and secondly, to reduce the rise in temperature of the specimens.

The inert filler used was pure calcium carbonate with a specific surface of 2000 cm^2/g, as determined using a Tovarov apparatus. This filler does not lead to hardening when mixed with calcium hydroxide in the absence of CO_2, and has practically no influence on the solubility of CaO and $Ca(OH)_2$, since its own solubility is low. The mechanical properties of concentrated suspensions were characterized by measuring the plastic strength using a cone plastometer [4]. The specimens were stored in a desiccator over saturated $Ca(OH)_2$ solution, and were not protected from the action of atmospheric carbon dioxide, since it was shown by means of special experiments that in the course of several hours, the CO_2 of the air has practically no effect on the strength of the hardening structure, if the measurements are carried out with the plastometer cone embedded to a depth of not less than 3-5 mm. The rate of hydration of the calcium oxide was determined using a calorimeter with an automatically controlled adiabatic jacket [5], which made it possible to follow the hydration of the calcium oxide over a period of several hours.

Figure 1 shows the characteristic kinetics of the crystallization structure formation in suspensions containing 25% CaO and 75% $CaCO_3$, together with the rate of hydration of the CaO in these suspensions, determined simultaneously (from the heat evolved). Immediately after the sharp increase in the plastic strength related to the crystallization of the greater part of the $Ca(OH)_2$, there is a decrease in strength, which starts even before the calcium oxide hydration is complete. At W/S = 0.4 (Fig. 1A), the decrease in strength gives way to an increase in strength, which is complete at the moment of complete hydration of the CaO.

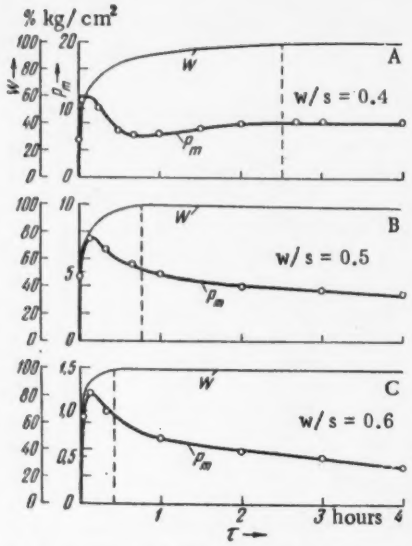

Fig. 1. Kinetics of the hydration (W) and crystallization structure-formation (P_m) in calcium oxide suspensions. Suspension composition 25% CaO + 75% $CaCO_3$.

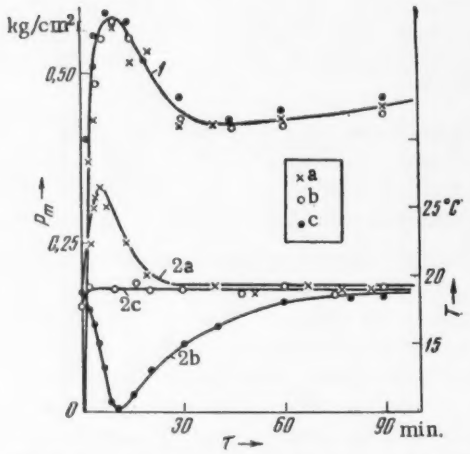

Fig.2. Relationship between the kinetics of structure formation and temperature in specimens containing 5% CaO + 95% $CaCO_3$, W/S = = 0.4. 1) Kinetics of structure-formation; 2) change in temperature in specimens (a) hardened under ordinary conditions, b) under the opposite conditions of temperature change, c) under isothermal conditions.

The decrease in strength during the hardening of pure CaO was noted earlier by G. I. Logginov [6], who related the phenomenon to an increase in the solubility of the $Ca(OH)_2$ with decrease in the temperature of the specimen immediately after the maximum value reached, as a result of the thermal effect of the reaction. Fig.2 shows the kinetics of the crystallization structure formation and the change in temperature of specimens hardened under different temperature conditions. The first series of specimens (a) was hardened under ordinary conditions, the second (b) under the opposite conditions of temperature change, and the third (c) under isothermal conditions. The figure shows that the decrease in strength is observed in all three cases, and is independent of change in the temperature of the specimens. There are several possible explanations for the decrease in the strength of the structure during the hardening process.

The decrease in the strength may be related to the dissolution of crystallization contacts in a state of thermodynamic nonequilibrium [7], or to the conversion of a less stable, and hence more soluble modification to a less soluble, more stable form [8], or, finally to the production of stresses in the process of growth of the crystals, which are joined to one another by growth contacts to form a compact crystallization structure which prevents their free movement.

The dissolution of the crystallization contacts can explain only that drop in strength which is observed after hydration is complete, and which is more clearly revealed at high values of W/S (Fig. 1, B and C). It should be noted that at W/S = 0.4, after the hydration is complete, there is again observed a certain decrease in the strength, but the drop is very slight. The decrease in strength which takes place during the hydration process, and which is particularly clearly shown at small values of W/S (Fig. 1A) cannot, however, be explained by dissolution of crystallization contacts, since it commences when a large quantity of the original binding material is still present in the suspension (approximately 25% in the case illustrated in Fig. 1,A), and this is able to maintain, in the suspension, the supersaturations preventing the recrystallization processes.

The decrease in the strength cannot be explained by the conversion of an unstable modification of the type $Ca(OH)_2 \cdot \frac{1}{2} H_2O$ and $Ca(OH)_2 \cdot H_2O$ [9] to the stable hydrate $Ca(OH)_2$ on hardening, since the thermograms and x-ray diagrams which we have recorded show unambiguously that under ordinary conditions (in our experiments), only one chemical compound, $Ca(OH)_2$, exists throughout the whole of the hardening process.

Thus the cause of the decrease in strength which takes place before hydration is complete can only be the production of tensile stresses in the structure during its

development. These tensile stresses result from overgrowth of the skeleton of the crystallization structure. This overgrowth leads, on the one hand, to an increase in the strength of the structure as a result of the increase in the size of the component crystallites, and, on the other hand, to a decrease in strength as a result of the formation of internal tensile stresses which lead to a breakdown of the structure at its weakest point. The dual nature of this process leads to the appearance of an inflection on the curve showing the increase in strength with time, as can be seen from Fig. 1, A. In this case, after the maximum value has been reached, the strength at first decreases as a result of the breakdown of the structure under the influence of the stresses, and afterwards increases again, since the removal of the stresses by partial breakdown of the structure means that the increase in strength predominates during the continuing crystallization of the new formations. The stresses produced during the growth of the skeleton of the crystallization structure will be greater, the lower the porosity of the structure, i.e., the lower the water–solid ratio (W/S). Consequently, the decrease in strength related to the internal stresses should should be smaller, the greater W/S. This feature makes it possible to distinguish readily the decrease in strength related to the production of internal stresses and partial breakdown of the structure at its weakest points from the decrease in strength resulting from the dissolution of crystallization contacts in thermodynamic nonequilibrium, which is more marked, the greater the total porosity of the specimen, i.e., the greater W/S [7].

TABLE 1

W/S	Plastic strength Pm, kg/cm²			Decrease in strength %	
	maximum $(Pm)_{max}$	at complete hydration, $(Pm)_H$	at τ = 4 hours after complete hydration $(Pm)_H$	$\frac{(P_m)_{max}-(P_m)_H}{(P_m)_{max}}$	$\frac{(P_m)_H-(P_m)_\tau}{(P_m)_H}$
0,4	12	9,0	9,0	25	0
0,5	7,5	6,0	3,8	20	36
0,6	1,2	1,05	0,45	12,5	57

When the data given in Fig. 1 are used to calculate the relative decrease in strength taking place during the process of development of the hardened structure before hydration is complete $[(P_m)_{max}(P_m)_H]/(P_m)_{max}$ and after complete hydration * as a result of recrystallization and dissolution of the crystallization contacts $(P_m)_{max}-(P_m)_\tau/(P_m)_H$, it is found that the first decreases, while the second increases, with increase in W/S (Table 1). This confirms that the decrease in strength during the process of CaO hydration is determined by the stresses produced in the structure during its development. The decrease in strength resulting from the dissolution of the crystallization contacts is observed only after hydration is complete, when the specimens are stored under moist conditions, and it can be seen clearly only at fairly high values of W/S. The decrease in strength resulting from the internal stresses becomes much more marked with increase in the CaO content of the mixture and decrease in W/S, and at very small values of W/S leads to complete breakdown of the crystallization structure, as takes place also when quicklime is slaked to produce slaked lime.

O. V. Pyasetskaya took part in the work.

LITERATURE CITED

[1] I. V. Smirnov, Quicklime [in Russian], 1950; The Preparation of Ground Quicklime and its Application in Building Construction [in Russian], 1950; B. V. Osin, Quicklime as a New Binding Material [in Russian] (Moscow, 1954).

[2] E. E. Segalova, S. I. Kontorovich and P. A. Rebinder, Doklady Akad. Nauk SSSR, 123, No.3 (1958).* *

[3] V. F. Abrosenkova, G. I. Logginov and P. A. Rebinder, Doklady Akad. Nauk SSSR, 115, No.3 (1957).* *

*For example, in the 4 hours following complete hydration τ = 4 hours.

* *Original Russian pagination. See C. B. translation.

[4] E. E. Segalova, P. A. Rebinder and O. I. Luk'yanova, Vest. Moskov. Univ., No.2, 1954; P. A. Rebinder and N. A. Semenenko, Doklady Akad. Nauk SSSR, 64, 835 (1949).

[5] O. I. Luk'yanova, E. E. Segalova and P. A. Rebinder, Kolloid. Zhur., 19, No.4 (1957); V. F. Kiselev, Proceedings of the Conference on the Chemistry of Cement [in Russian] (Moscow, 1956).

[6] G. I. Logginov, Vest. AN SSSR, No.7 (1954).

[7] E. E. Segalova and V. N. Izmailova, Kolloid. Zhur., 20, No.5 (1958).

[8] E. S. Solov'eva and E. E. Segalova, Kolloid. Zhur., 20, 5 (1958).

[9] F. F. Selivanov, Zhur. Russ. Fiz.-Khim. Obshch., 45, 252 (1913).

Received July 31, 1959.

DOUBLE BONDS IN POLYETHYLENE IRRADIATED WITH FAST ELECTRONS

N. A. Slovokhotova, A. T. Koritskii and N. Ya. Buben

L. Ya. Karpov Physicochemical Institute
Chemical Physics Institute, Academy of Sciences, USSR

(Presented by Academician V. A. Kargin, July 29, 1959)

In the present work, the method of infrared spectroscopy was used to study the formation of double bonds in polyethylene during its irradiation with fast electrons at different temperatures from -196° to +50° in a medium of nitrogen. The recording of the infrared spectra at low temperatures and all the operations involved in the transfer of the specimens were carried out in a stream of cold nitrogen. The temperature was varied by altering the rate of evaporation of the nitrogen.

The spectrum of polyethylene irradiated in liquid nitrogen, recorded (without intermediate heating) at a temperature below -100°, shows an absorption band in the region of 966 cm^{-1}. This confirms the accuracy of the suggestion made earlier, that double bonds of the trans-vinyl type are formed immediately in the polyethylene at the moment of irradiation, as a result of the removal of hydrogen atoms from two neighboring methylene groups.

The intensity of the band at 909 cm^{-1} corresponding to the vinyl group in the spectrum of low-pressure polyethylene irradiated at a temperature of +26°, decreases with increase in the radiation dose. The spectrum of the same polyethylene, irradiated at the temperature of liquid nitrogen, shows a very slight decrease in the intensity of this band only on irradiation with small doses; with irradiation by doses of more than 25 Mrad, there is almost no change in the intensity of this band.

The spectrum of high pressure polyethylene irradiated at a temperature below -100° (Fig. 1), however, shows the appearance of an absorption band in the region of 909 cm^{-1}, whose intensity increases with increase in the radiation dose; when the same polyethylene is irradiated at a temperature of + 26° and above, the band of the vinyl group is observed, but the intensity is very much less, and possibly for this reason it was not detected in earlier studies.

The appearance of vinyl unsaturation on irradiation of high-pressure polyethylene may be explained either by the end effect or by rupture of the main chain of the polymer. In order to solve this question it is necessary to carry out more precise quantitative measurements, taking account of the degree of branching of the specimens studied. The decrease in the vinyl unsaturation on irradiation of low pressure polyethylene may be explained by interaction between the vinyl groups and radicals formed during the irradiation; the more rapid decrease in the vinyl unsaturation during the irradiation of polyethylene at a high temperature is evidently related to the increase in the mobility of the polymer chains and polymeric radicals at this temperature.

The spectrum of polyethylene irradiated at a temperature below -100° with a dose of 206 Mrad (Fig. 2) shows, in addition to an intense absorption band at 966 cm^{-1}, two less-intense bands at 985 and 944 cm^{-1}, and the intensity of these bands is greatest when the spectrum is recorded at a temperature of approximately -100°, without preliminary heating of the specimen; on subsequent heating, the intensity of these bands decreases as the temperature is increased.

When the specimen is heated for several minutes in a medium of nitrogen at a temperature of approximately 100°, the band at 944 cm^{-1} disappears, while the band at 985 cm^{-1} becomes broader and appears as a

shoulder on the more-intense band at 966 cm^{-1}. When the same polyethylene specimen is again frozen, its spectrum at low temperature shows only a weak band at 944 cm^{-1}, while the band at 985 cm^{-1} is again observed just as clearly, and with the same intensity, as in the spectrum of the same specimen before heating. This region contains the absorption bands characteristic of two conjugated double bonds: one intense absorption band in the region of 988 cm^{-1} is characteristic of trans-trans conjugation, and two bands of average intensity at 982 and 948 cm^{-1} are characteristic of cis-trans conjugation. On this basis it is possible to explain the appearance of the bands at 985 and 944 cm^{-1} in the spectrum of irradiated polyethylene as due to the formation of pairs of conjugated double bonds. The disappearance of the band at 944 cm^{-1} when the specimen is heated, however, indicates that this band is related to the presence of some type of short-lived radicals in the irradiated polyethylene. The radical with structure most closely resembling that of a pair of conjugated double bonds is the allyl radical, whose presence in irradiated polyethylene has been shown by the electron paramagnetic resonance method [3]. It is possible that the band at 944 cm^{-1} is related to the vibrations of the CH-group in the allyl radical.

We have to express our deep gratitude to Academician V. A. Kargin for fruitful discussion and valuable advice.

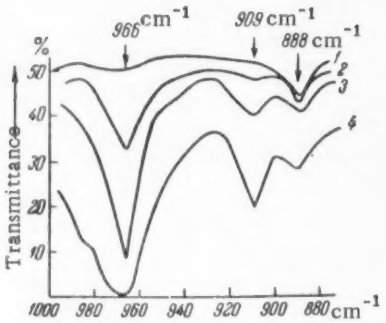

Fig. 1. Infrared spectrum of high-pressure polyethylene (d = 500μ) before irradiation (1) and after irradiation with fast electrons at -196° with a dose of 25 Mrad (2), 100 Mrad (3) and 300 Mrad (4). Spectrum recorded at a temperature of + 25°.

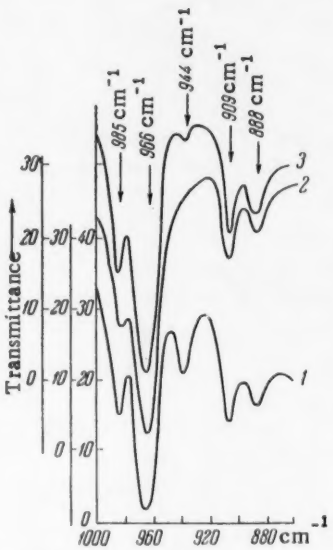

Fig.2. Infrared spectrum of high-pressure polyethylene irradiated with fast electrons at -100° with a dose of 206 Mrad, recorded at -100° (1), +25° (2) and after recooling to -100° (3).

LITERATURE CITED

[1] A. A. Miller, E. J. Lauton, and J. S. Balwit, J. Phys. Chem., 60, 599 (1956).

[2] D. Chapman and R. J. Taylor, Nature, 174, 1011 (1954).

[3] A. T. Koritskii, Yu. N. Molin, et al., Vysokomolekulyarnye Soedineniya, 1, No. 8 (1959).

Received July 13, 1959.

THE REACTION CAPACITY OF THE ANIONS OF CERTAIN CARBOXYLIC ACIDS IN THE ACID-CATALYZED ENOLIZATION OF ACETONE

A. I. Tal'vik and V. A. Pal'm

Tartar State University

(Presented by Academician V. N. Kondrat'ev, July 17, 1959)

The enolization of acetone serves as a general example of acid-base catalysis [1]. Most of the work on the study of the kinetics of this reaction also was done by Dawson and collaborators [2, 3]and others at 25°,but they paid little attention to the chemical nature of the phenomena studied [4], and their catalytic constants are not completely reliable and do not possess an appropriate physical meaning.

Proceeding from our [4] established reaction mechanism on the enolization of acetone, for the observed monomolecular constant of the speed of general acid-base catalysis in real solution (assuming $a_{H^+} = h_0 \ll K_{aB}$, where h_0 is the acidity of the medium and K_{aB} is the basicity constant of acetone) we derive the expression

$$k_I = \frac{k_{OH^-}}{K_{a_B}} a_{H^+} [OH^-] \frac{f_{BH^+} f_{OH^-}}{f_{(BH^+ \ldots OH^-)_{\neq}}} + \frac{k_{H_2O}}{K_{a_B}} a_{H^+} [H_2O] \frac{f_{BH^+} f_{H_2O}}{f_{(BH^+, \ldots H_2O)_{\neq}}} +$$

$$+ \frac{k_{A^-}}{K_{a_B}} a_{H^+} [A^-] \frac{f_{BH^+} f_{A^-}}{f_{(BH^+ \ldots A^-)_{\neq}}} + k^*_{OH^-} [OH^-] \frac{f_B f_{OH^-}}{f_{(B \ldots OH^-)_{\neq}}} + k^*_{A^-} [A^-] \frac{f_B f_{A^-}}{f_{(B \ldots A^-)_{\neq}}}. \quad (1)$$

The activity coefficients of the appropriate molecules, ions, and active complexes are designated by f, B is acetone, the asterisks indicate velocity constants in the case of base catalysis.

Substitution of experimental data in formula (1) allows the determination of the actual bimolecular velocity constant for the simple reaction between an acetone ion and different bases, as well as acid anions, if the value of K_{aB} is known.

EXPERIMENTAL

We investigated the reaction of iodoacetone in the presence of buffered acetic, propionic, bromoacetic, and iodoacetic acids with their corresponding salts. The buffered mixtures were made from KOH, solutions of the corresponding acids, and aqueous iodine (the concentration of I_2 had been previously determined spectrophotometrically). The concentration of hydrogen ion in solution was determined from the equation $[H^+] = K_{HA} [HA] / \gamma^2 \pm [A^-]$; $\gamma \pm$ was calculated from the formula $-\log \gamma \pm = Z_+ Z_- A \sqrt{\mu} (1 + \alpha_0 B \sqrt{\mu})^{-1}$, assuming $\alpha_0 = 5A$ [5].

The reaction velocity was measured spectrophotometrically by the loss of iodine. Since the constant for iodine consumed depends largely on the concentration of salts present, therefore the value of ϵ_{I_2} is determined separately in each case from experimental values of the original optical density.

The experimental details were reported similarly in [6] except that an ampoule of carefully weighed acetone was broken in a closed flask under a layer of solution. Kinetic measurements were made at three temperatures

(15, 25 and 35°) at wavelengths 465 or 350 mμ. Examples of the kinetic curves obtained are shown in Fig. 1.

The values of k_A / K_{aB} (in so far as K_{aB} can be estimated somewhat approximately [4], the value of K_{A^-} not being calculated separately) are determined in the following manner. It is possible to neglect the first and penultimate terms in (1) since under the experimental conditions they become negligibly small. Furthermore we have

$$a_{H^+}[A^-]\frac{K_{HA}[HA]}{\gamma_\pm}, \quad \frac{a_{H^+}}{\gamma_\pm} = [H_3O^+];$$

$$\frac{f_{BH^+} f_{H_2O}}{f_{(BH^+\ldots H_2O)^+}} \approx 1; \quad \frac{f_{BH^+} f_{A^-}}{f_{(BH^+\ldots A^-)^+}} \approx \gamma_\pm^2.$$

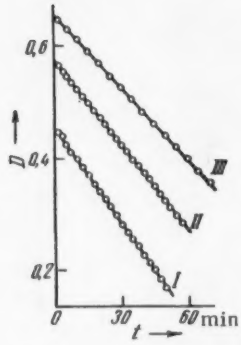

Fig. 1. Kinetic curves from buffered solutions of acetic acid at wavelength 350 mμ; $[A^-]$ = 0.040 mol/liter; [KI]= = 0.005 mol/liter; I) [HA] = 0.205 mol/liter, ϵ_{I_2} = 16500; II) [HA] = = 0.153 mole/liter; ϵ_{I_2} = 17000; III) [HA] = 0.058 mol/liter, ϵ_{I_2} = = 16300.

Hence, in a given concrete case, expression (1) may be written in the following way:

$$k_I = \frac{k_{H_2O}}{K_{aB}}[H_2O][H_3O^+]\gamma_\pm + \frac{k_{A^-}}{K_{aB}} K_{HA}[HA]\gamma_\pm + + k^*_{A^-}[A^-]. \qquad (2)$$

The quantity $\frac{k_{H_2O}}{K_{aB}}[H_2O]$ equals the described catalytic constant for hydrogen ion and it is known from the literature [7-9] $\frac{k_{H_2O}}{K_{aB}}[H_2O] = 4.27 \cdot 10^{10}\ e^{-20700/RT}$. In the case of the halogenoacetic acids it is also possible to neglect the last term in expression (2). Therefore, from the various measured ratios [HA]/ /$[A^-]$, values for k_I are constructed graphically

$$\frac{k_I}{\gamma_\pm} - \frac{k_{H_2O}}{K_{aB}}[H_2O][H_3O^+] = y, \quad [HA] = x. \qquad (3)$$

From the slope of the derived straight line, which goes through the origin, the quantity $\frac{k_{A^-}}{K_{aB}} K_{HA}$ is calculated.

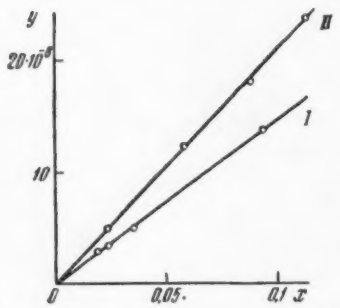

Fig. 2. I) ICH_2COOH, II) $BrCH_2COOH$.

In the case of acetic and propionic acids, the values of k_I employed are obtained from a different [HA] and a constant $[A^-]$. From the slope of the straight line and the coordinates in (3) the quantity $\frac{k_{A^-}}{K_{aB}} K_{HA}$ is calculated. The value of y when [HA] = 0 equals the quantity $\frac{k^*_{A^-}}{\gamma_\pm}[A^-]$. Employing data from [9] a similar calculation was made for chloroacetic acid.

Examples of interrelationship of the functions of (3) are given in Figs. 2 and 3 (t = 25°).

Our results and the values of the acid dissociation constants in [10, 11] are given in Table 1. (ΔS_B and ΔH_B are the entropy and thermal effect of the acid dissociation of acetone ion; ΔS_0 and ΔH_0 are the entropy and thermal dissociation of the corresponding acids.

TABLE 1

Acid	$\frac{k_{A^-}}{K_{a_B}} \cdot 10^4$ (25°)	$K_{HA} \cdot 10^4$ (25°)	ΔS_0, entr.	$\log A_0 - \frac{\Delta S_B}{2,3R}$	ΔH_0, eff	$E_0 - \Delta H_B$, cal
Acetic	68,5	0,175	−21,7	12,29	0	19700
Propionic	92,5	0,134	−22,3	12,49	0	19800
Iodoacetic	22,4	6,68	−19,3	13,62	−1400	22200
Bromoacetic	16,5	12,5	−17,4	13,06	−1200	21600
Chloroacetic	15,1	13,8	−15,3	12,12	− 700	20400

DISCUSSION

As indicated earlier, our determinations of the values for k_{A^-}/K_{aB} are characterized from so-called catalytic constants for the corresponding acids as much by their numerical values, as by their physical significance. In connection with this it is interesting to check the possibility of linking them with the dissociation constants of the corresponding acids correlated by Bronsted [12].

Calculation shows that for the highest accuracy ± 10%

$$\frac{k_{A^-}}{K_{a_B}} = aK_{HA}^{\alpha}, \tag{4}$$

where $a = 10^{13,63} \cdot 10^{-5200/T}$ and $\alpha = 0.243 - 178/T$. Both parameters a and α include "energy" as well as "entropy" components, so that the values of the latter are commensurable. In the same way it is necessary to point out that a and α possess the essentials of neutral parameters. In going from acetic acid to propionic, only log A and ΔS_0 change. In the series of halogen-substituted acetic acids consistent change occurs as log A and ΔS_0, as well as E and ΔH_0. On comparing the dissociation constants of halogenated acids and the velocity constants of corresponding anions, we see that the strength of the acids increases and the nucleophilic nature of the anions decreases in the order ICH_2COOOH-$BrCH_2COO$ H-$ClCH_2COOH$. Such regularity can be interpreted in the usual manner, from the view point of increased intensity of inductive effects in the halogen series I < Br < Cl.

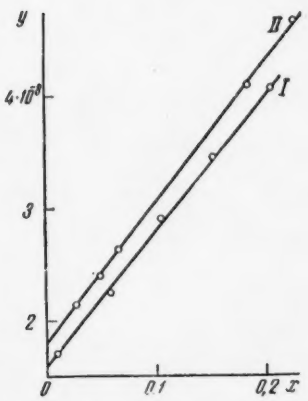

Fig. 3. I) CH_3COOH, II) C_2H_5COOH.

However, further available data show that such a sequence results solely from corresponding changes in the values ΔS_0 and log A. Changes in the value of ΔH_0 and E act directly in opposite ways. It is interesting to note that in the series of halogen hydrides, the acidity increases with increase in molecular weight, with a simultaneous decrease in dissociation energy [13]. This is apparent in Table 1 and clearly corresponds to the changes $E_0 - \Delta H_B$ and ΔH_0 of the halogen-substituted acids. From what has been said, it is clear that in the case of organic acids there are major factors which define existing differences in thermodynamic and kinetic strength of the acids, appearing as a nonthermal effect and activation energy, while corresponding entropy and frequency coefficients operate. Proceeding from the physical nature of the induction effect, the latter must influence the reaction capacity only by way of its effect on the energy factor.

Expression (4) is correlated in an equivalent way with the equation of Taft [14, 15]

$$\log \frac{k_{A^-}}{k_{A_0^-}} = \rho^*_{A^-}\sigma^*, \quad \log \frac{K_{HA}}{K_{HA_0}} = \rho^*_{HA}\sigma^*, \tag{5}$$

since $\alpha = \rho^*_{A^-}/\rho^*_{HA}$. $k_{A^-_0}$ and K_{HA_0} are characteristic values for acetic acid, which is taken as a standard (for CH_3-$\sigma^* = 0$).

The quantity $\rho^*\sigma^*$ is interpreted as a quantitative measure of the action of the inductive effect of a substituting group on the reaction capacity of a given compound in a given reaction [16, 17]. According to this interpretation, the quantity $\rho^*\sigma^*$ must be entirely one of entering into the activation energy or the thermal effect [17]. In the example under study, this is not the case. Values of $\rho^*\sigma^*$ can be presented in the condition $\rho^*\sigma^* = W - \epsilon/2.3\,RT$.

Values of W and ϵ are brought together in Table 2, as well as values of σ^* at 25°, determined from $\log (k_A/k_{A_0}) = \rho^*_A\sigma^*$ (assuming $\rho^*_{A^-} = -0.613$) and from Taft's data.

TABLE 2

Group R in Acid R-COOH	W_{A^-}	ϵ_{A^-}, kcal	W_{HA}	ϵ_{HA}, kcal	σ^* from $\log \frac{k_{A^-}}{K_{A^-_0}}$	σ^* according to Taft (16)
CH_3—	0	0	0	0	0	0
C_2H_5—	+0,13	0	−0,13	0	−0,21	−0,1; −0,24[15]
ICH_2—	+1,33	+2,5	+0,52	−1,4	+0,79	—
$BrCH_2$—	+0,77	+1,9	+0,96	−1,2	+1,01	+1,03
$ClCH_2$—	−9,17	+0,7	+1,40	−0,7	+1,07	+1,05

The data of Table 2 offer good support for Taft's equation in the case of the reaction considered, but the electronic interpretation of this correlated formula is contradicted.

It is curious to record the following regularities which are observed by the halogen-substituted acetic acids, but not by acetic and propionic. Between the values $\log A = \log A_0 - \Delta S_B/2.3R$ and $E = E_0 - \Delta H_B$ there is a linear relationship, $\log A = -4.73 + 0.835 \cdot 10^{-3} E$. An approximate linear relationship $\log A = 6.23 + 0.382\ \Delta S_0$ can also be seen. This suggests that between the halogenoacetic acids on the one hand, and acetic and propionic acids on the other, essential differences in mechanism occur, distinguished by the dependence of the reaction capacity of a given compound on its structure.

LITERATURE CITED

[1] R. P. Bell, Acid-Base Catalysis, Oxford, 1941.

[2] H. M. Dawson, M. Leslie, J. Chem., Soc., 1909, 1860.

[3] H. M. Dawson and E. Spivey, J. Chem. Soc., 1930, 4578.

[4] Yu. L. Khaldna, A. I. Tal'vik, and V. A. Pal'm, Doklady Akad. Nauk. 126, No.1 (1959).*

[5] M. Kh. Karapet'yants: "Chemical Thermodynamics" 1953, p.404 [In Russian].

[6] A. I. Tal'vik and V. A. Pal'm, Zhur. Fiz. Khim. 33, B, 6 (1959).

[7] F. O. Rice and M. Kilpatrick, J. Am. Chem. Soc., 45, 1401 (1923).

[8] F. O. Rice and W. Lemkin, J. Am. Chem. Soc., 45, 1893 (1923).

[9] G. F. Smith, Trans. Chem. Soc., 1774 (1934).

[10] D. J. G. Ives and J. H. Pryor, J. Chem. Soc., 1955, 2104.

[11] Handb. Chem. and Phys., 37th ed., Cleveland, Ohio, 1955-1956.

[12] J. N. Brönsted and K. Pedersen, Zs. phys. Chem., 108, 185 (1924).

*Original Russian pagination. See C. B. translation.

[13] R. P. Bell, Acids and Bases, their Quantitative Behavior, London-New York, 1956.

[14] R. W. Taft, Jr.,J. Am. Chem. Soc., 74, 3120 (1952).

[15] R. W. Taft, Jr.,J. Am. Chem. Soc., 75, 4231 (1953).

[16] R. W. Taft,Jr., J. C. Lewis, J. Am. Chem. Soc., 80, 2436 (1958).

[17] R. W. Taft,Jr., J. Am. Chem. Soc., 75, 4534 (1953).

Received July 16, 1959.

THE ELECTROMAGNETIC PROPERTIES AND STRUCTURAL DIAGRAM OF THE $FeO-SiO_2-ZnO$ SYSTEM

Corresponding Member Acad. Sci. USSR, D. M. Chizhikov,
V. P. Schastlivyi, and L. I. Blokhina
A. A. Baikov Institute of Metallurgy Acad. Sci. USSR

In the literature, data concerning the threefold diagram of the phase structure of the $FeO-SiO_2-ZnO$ system are absent. In the present work, on the basis of actual measurements of the electromagnetic properties and petrographic analysis, the structural diagram of the $FeO-SiO_2-ZnO$ system has been partly constructed, which has great importance for the metallurgy of nonferrous metals.

Melts were prepared by fusing oxides together in corundum crucibles in a furnace with a graphite heater. The ferrous oxide was obtained by heating ferrous oxalate in nitrogen in covered iron glasses with slow raising of temperature up to 700-800° and with subsequent slow cooling.

Measurements of specific electrical conductivity were carried out by the voltmeter-ammeter method; magnetic susceptibility was measured by Gouy-Faraday's method. Petrographic analysis of melts was carried out on the basis of the investigation of transparent sections utilizing immersion fluids and Fedorov's table.

Petrographic investigation was carried out on melts containing from 26 to 64% of SiO_2; from 0 to 52% of ZnO; from 4 to 76% of FeO. Note should be taken that the structural diagram of the $FeO-SiO_2-ZnO$ system is a pseudoequilibrium, since at high temperatures a reaction proceeds between ferrous oxide and zinc oxide which results in the liberation of zinc vapors and disproportionation of trivalent iron [1].

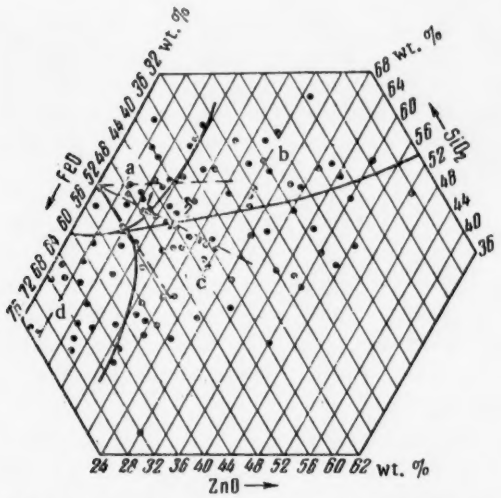

Fig. 1. The structural diagram of the $FeO-SiO_2-ZnO$ pseudoequilibrium system.

In $FeO-SiO_2-ZnO$ melts the trivalent iron is always present, and its concentration rises by the decrease of silica content and the increase of zinc oxide concentration. In Fig. 1 the points of investigated melts of the system are shown according to the data of chemical analysis.

Within the investigated field of the diagram there are four areas of phase equilibrium. Area A is characterized by the presence of fayalite, tridymite and magnetite in the melt. Area B is distinguished by the presence of fayalite, willemite, tridymite and magnetite in the melt. In Area C the melt contains phases of fayalite, willemite and magnetite. Area D is characterized by the fayalite and magnetite content of the melt. It has been observed that willemite and magnetite crystallize first from the melt, and fayalite follows next. The optical properties of the mineral phases are presented in Table 1.

TABLE 1

The Optical Properties of the Mineral Phases in the $FeO-SiO_2-ZnO$ System

Area	Mineral phases	Axes	Optical sign	$2V$	N_g	N_p	N_g-N_p
A	Fayalite	Biaxial	—	52—55	1,858—1,873	1,836—1,851	0,022
	Tridymite	"	+	68	1,475		
B	Fayalite	"	—	59—61	1,858—1,873	1,836—1,851	0,022
	Willemite	Monoaxial	+		1,719	1,692	0,027
	Tridymite	Biaxial	+	70	1,475		
C	Fayalite	"	—	52—54	1,855—1,871	1,807—1,834	0,048—0,037
	Willemite	Monoaxial	+		1,720	1,690	0,030
D	Fayalite	Biaxial	—	50	1,864—1,871	1,825—1,834	0,037—0,039

TABLE 2

The Size of Grains of Mineral Phases at the Quenching of the Melts in Water

Temperature	Fayalite	Willemite	Magnetite
	size of grains, mm		
1300	0,08—0,1	0,008—0,016	0,02—0,08
1200	0,8 —1,0	0,008—0,016	0,04—0,1
1000	1,8 —2,0	0,06 —0,2	0,1 —0,2
800	2,0 —2,5	0,1 —0,15	0,1 —0,2
600	1,5 —2,5	0,1 —0,4	0,2 —0,4

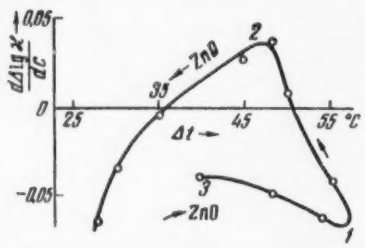

Fig. 2. The curve of change of the intervals of specific electrical conductivity during smelting, as a function of compositions and the interval of smelting Δt.

As can be seen from the diagram, the solubility of zinc oxide in the $FeO-SiO_2$ melts amounts to 9-12% in Area a. Within the investigated part of the diagram triple compound of $xFeO \cdot ySiO_2 \cdot nZnO$ type has not been found. It can be assumed that in this area of the diagram zinc has displaced isomorphously the bivalent iron ion in the fayalite without being precipitated as a separate phase.

In order to determine the development rate of individual mineral phases in the $FeO-SiO_2-ZnO$ system, quenching was carried out after heating the oxide melts to the temperatures of 1300, 1200, 1000, 800 and 600°. The liquid melt was mixed in a corundum crucible, heated to the given temperature, which was maintained for 10 minutes, then the crucible was submerged in a vessel with running water. The test pieces were cooled down to 20° within 3 to 4 minutes. Sections were prepared from the congealed melts, in which the size of the grains was determined. Melts of Area C were investigated. In Table 2B shown the size of the grains present in the mineral phases in the melt containing 43.5% of FeO, 38.4% of SiO_2, 18.05% of ZnO. In melts tempered at a temperature of 1300°, a willemite phase was observed in the form of tiny crystals measuring 0.008-0.016 mm; fayalite crystallizes sufficiently well at these temperatures and forms grains as large as 0.1 mm. By reducing the initial quenching temperature of the test pieces to 600°, the relative development rate of fayalite and willemite (crystals) remained unaffected.

Measurements of specific electrical conductivity and magnetic susceptibility of the melts of $FeO-SiO_2-ZnO$ system were carried out in the interval of 1450-1000°. The composition of the investigated melts varied in three ways: (a) the ratio of $SiO_2/FeO = 0.9$, or the concentration of (b) silica, or (c) ferrous oxide were taken as constants, respectively. The zinc oxide content of the investigated melts varied between 0.0 and 30.0%. In the melts with a constant proportion of $SiO_2/FeO = 0.9$ the increase of the ZnO concentration from 0.0 to 30.0% led to the increase of specific electrical conductivity from 2.4 to 6.8 $ohm^{-1} \cdot cm^{-1}$ at 1450°. The isotherms of specific electrical conductivity had an extreme value at 17% of ZnO. In melts in which silica was replaced by zinc oxide the specific electrical conductivity increased proportionally to the zinc oxide content. So, by raising the zinc oxide concentration to 30.0%, specific electrical conductivity was increased from 1.37 to 7.4 $ohm^{-1} \cdot cm^{-1}$ at 1450°. The isotherms of specific electrical conductivity had an extreme value at about 12% of ZnO concentra-

tion. When the ferrous oxide was replaced by zinc oxide in the melts, specific electrical conductivity decreased, dropping from 1.37 to 0.45 $ohm^{-1} \cdot cm^{-1}$ at 1450°. The isotherms of specific electrical conductivity of these melts had an extreme value at 9-12% of ZnO.

The absolute magnitude value of specific electrical conductivity as a function of temperature obeys an exponential theorem, described by the equation: $\kappa = A_{\kappa} \cdot e^{Ex/RT}$. The experimental data of specific electrical conductivity, obtained in the field of melting, were treated on the coordinates of $\frac{d\Delta \lg \kappa}{dc} - \Delta t$, this showed clearly defined extreme values in the curves of the change in the character of specific electrical conductivity ($d\Delta \lg \kappa$) depending on the zinc oxide concentration (dc) and the interval of smelting (Δt).

Thus, in Table 2 for $SiO_2/FeO = 0.9$ melts in the curve, two extreme values are exposed: (point 1) at 9.0% of ZnO and (point 2) at 16.0% of ZnO. Plotting these points against the structural diagram of the $FeO-SiO_2-ZnO$ system shows that the extreme value at 9.0% of ZnO corresponds to the appearance of free mineral combinations of willemite type ($2ZnO \cdot SiO_2$) in the melts, while the extreme value at 16.0% of ZnO corresponds to the disappearance of the structurally free tridymite. In melts with constant concentration of ferrous oxide the extreme value at these coordinates corresponds to the appearance of willemite phase. For melts in which ferrous oxide was replaced by zinc oxide, the extreme value at the coordinates of $\frac{d\Delta \lg \kappa - \Delta t}{dc}$ corresponds to the disappearance of tridymite and the appearance of willemite.

The measurements of magnetic susceptibility of the melts in the investigated system showed that all of them were paramagnetic; the magnetic susceptibility of melts was determined by the concentration of ferric oxide present in the melts. The absolute magnitude of paramagnetism of the investigated melts varied to an insignificant degree according to the temperature. The isotherms of magnetic susceptibility of melts of the $FeO-SiO_2-ZnO$ system had extreme values at the points corresponding to the borderline of Areas A and B, i.e., at the transition of melts into the willemite-containing area. The disappearance of the tridymite phase was not found in the isotherms of magnetic susceptibility, inasmuch as tridymite is diamagnetic, and the changes in the general susceptibility of the system are insignificant.

Thus, on the basis of measurements of electromagnetic properties and petrographic analysis, a part of the pseudoequilibrium diagram of the ternary $FeO-SiO_2-ZnO$ system has been constructed.

The investigated diagram is not an equilibrium owing to the reduction and volatilization of zinc when the ferriferrous melts are held in high temperature ranges.

The measurements of specific electrical conductivity and magnetic susceptibility of melts, obtained in the field of smelting, and the treatment of the data on the coordinates of $\frac{d\Delta \lg \kappa}{dc} - \Delta t$ allow us to draw the borderline of fields in the investigated structural diagram.

LITERATURE CITED

[1] D. M. Chizhikov and V. P. Schastlivyi, Proc. Acad. Sci. USSR 127, 2, 356 (1959).*

[2] A. N. Winchell and G. Winchell, Optical Mineralogy [Russian translation] 1953.

Received September 11, 1959.

*Original Russian pagination. See C. B. translation.

MISSING PAGES ARE INDEX PAGES
WHICH HAVE BEEN PHOTOGRAPHED
AT THE BEGINNING OF THE VOLUME(S)

ERRATUM

Vol. 128, September-October, 1960

Page	Line	Reads	Should read
888	Ref. [2]	M. Yamazaki, J. Chem. Phys. 24, 1260 (1956)	M. Yamazaki, J. Phys. Chem. 24, 1260 (1956)

SIGNIFICANCE OF ABBREVIATIONS MOST FREQUENTLY ENCOUNTERED IN SOVIET PERIODICALS

FIAN	Phys. Inst. Acad. Sci. USSR.
GDI	Water Power Inst.
GITI	State Sci.-Tech. Press
GITTL	State Tech. and Theor. Lit. Press
GONTI	State United Sci.-Tech. Press
Gosenergoizdat	State Power Press
Goskhimizdat	State Chem. Press
GOST	All-Union State Standard
GTTI	State Tech. and Theor. Lit. Press
IL	Foreign Lit. Press
ISN (Izd. Sov. Nauk)	Soviet Science Press
Izd. AN SSSR	Acad. Sci. USSR Press
Izd. MGU	Moscow State Univ. Press
LEIIZhT	Leningrad Power Inst. of Railroad Engineering
LET	Leningrad Elec. Engr. School
LETI	Leningrad Electrotechnical Inst.
LETIIZhT	Leningrad Electrical Engineering Research Inst. of Railroad Engr.
Mashgiz	State Sci.-Tech. Press for Machine Construction Lit.
MEP	Ministry of Electrical Industry
MES	Ministry of Electrical Power Plants
MESEP	Ministry of Electrical Power Plants and the Electrical Industry
MGU	Moscow State Univ.
MKhTI	Moscow Inst. Chem. Tech.
MOPI	Moscow Regional Pedagogical Inst.
MSP	Ministry of Industrial Construction
NII ZVUKSZAPIOI	Scientific Research Inst. of Sound Recording
NIKFI	Sci. Inst. of Modern Motion Picture Photography
ONTI	United Sci.-Tech. Press
OTI	Division of Technical Information
OTN	Div. Tech. Sci.
Stroiizdat	Construction Press
TOE	Association of Power Engineers
TsKTI	Central Research Inst. for Boilers and Turbines
TsNIEL	Central Scientific Research Elec. Engr. Lab.
TsNIEL-MES	Central Scientific Research Elec. Engr. Lab.- Ministry of Electric Power Plants
TsVTI	Central Office of Economic Information
UF	Ural Branch
VIESKh	All-Union Inst. of Rural Elec. Power Stations
VNIIM	All-Union Scientific Research Inst. of Meteorology
VNIIZhDT	All-Union Scientific Research Inst. of Railroad Engineering
VTI	All-Union Thermotech. Inst.
VZEI	All-Union Power Correspondence Inst.

Note: Abbreviations not on this list and not explained in the translation have been transliterated, no further information about their significance being available to us. – Publisher.